DOCTOR OF PHILOSOPHY

The Global Riverine Hydrokinetic Resource

Ridgill, Michael

Award date:
2023

Awarding institution:
Bangor University

DOCTOR OF PHILOSOPHY

The Global Riverine Hydrokinetic Resource

Ridgill, Michael

Award date:
2023

Awarding institution:
Bangor University

PRIFYSGOL
BANGOR
UNIVERSITY

THE GLOBAL RIVERINE HYDROKINETIC RESOURCE

Michael Ridgill

A thesis submitted for the degree of Doctor of Philosophy

April 2023

Title	**The global riverine hydrokinetic resource**
Candidate	**Michael Ridgill**
Principle Supervisor	**Prof. Simon Neill** School of Ocean Sciences, Bangor University
Co-Supervisors	**Dr. Matt J. Lewis** School of Ocean Sciences, Bangor University
	Dr. Peter E. Robins School of Ocean Sciences, Bangor University
Financial Support	**Repetitive Energy Company** Sunderland House, The Dockyard, Pembroke Dock SA72 6TD
	Knowledge Economy Skills Scholarships (KESS 2)
Assessment Committee	**Dr. Martin Austin** (Chair) School of Ocean Sciences, Bangor University
	Prof. Mattias Green (Internal Examiner) School of Ocean Sciences, Bangor University
	Dr. Athanasios Angeloudis (External Examiner) Institute of Infrastructure and Environment, Edinburgh University

Abstract

A large and under-developed source of renewable energy exists, due to the properties and associated processes attributable to the substantial and ubiquitous presence of water, globally. Hydrokinetic energy conversion refers to the conversion of kinetic energy in moving water to electricity. It offers an alternative to conventional hydropower, with benefits of modularity and scalability, in addition to being environmentally and socially less impactful. Hydrokinetic energy conversion can benefit isolated communities currently without access to electricity.

This study aims to determine the global theoretical riverine hydrokinetic resource. A 35 year modelled daily discharge data set and vectorised representation of rivers, with near-global coverage and suitable spatiotemporal resolution, is used to determine the mean annual energy yield of 2.94 million river reaches. Two methodologies are applied, considering the hydrokinetic resource as: a *conversion* from gravitational potential energy to kinetic energy; and, directly, as the *transfer* of kinetic energy.

Using the former method, and aligning to the convention of previous large-scale hydrokinetic resource assessments, the mean global resource (excluding Greenland and Antarctica) is estimated to be 58,000 ± 11,000 TWh yr^{-1} (6.7 ± 1.2 TW). Consideration of global spatial distribution, by river reach, illustrates regional variation and shows a tendency for potential to be concentrated along major rivers and in areas of significant elevation change. China, Russia and Brazil are found to be the countries with the greatest potential. After normalisation by total river length, Bhutan, Nepal and Tajikistan also show great potential.

With the latter method, a novel approach is proposed, and an argument is presented to suggest that there are pragmatic advantages to the perspective this provides. In this case, the mean hydrokinetic energy of global rivers (excluding Greenland and Antarctica) is estimated to be 1.642 ± 0.003 TWh (5.911 ± 0.009 PJ). In contrast, this time the overall resource is quantified as a measurement of hydrokinetic energy, rather than power. The two approaches differ in their perspective, with the former giving a Lagrangian description and the latter a Eulerian description. With this latter approach, the resource is shown to have great potential on the continents of South America, Asia and Africa. Hydrokinetic power within individual reaches is considered, as before, and comparable with the earlier method. Yet, due to the Eularian view, in this case, global power cannot be quantified, reflecting an alternative perspective of the global riverine hydrokinetic resource. This novel perspective concludes that major rivers, and particularly the lower-courses of major-rivers, are found to offer the most potential for hydrokinetic energy conversion. Areas with large elevation change are not found to be as significant, using this method. Recognising the importance of major rivers, basin-scale resource assessment of prominent rivers identifies the Amazon, Ganges and River Plate as those offering the greatest potential for hydrokinetic energy conversion.

Comparison with a field-scale study in Lithuania, that used a hydraulic model at 3 locations,

demonstrates the extent to which the conventional method results in significant over-estimation, with a percentage bias of +11,000 ± 5,435 %. In contrast, the novel method proposed is found to have a percentage bias of $+40^{+7994}_{-139}$%. Large uncertainties in the parameters used in the estimation of channel form and flow velocities in this method certainly affect precision, but potentially offer a more accurate perspective. The limitations of this imprecision are improved by application at large-scale and the use of a Monte Carlo approach. For this reason, this methodology is more appropriately applied in this context, rather than at reach-scale. Improvements in large-scale determination of hydraulic geometry parameters offer a promising way to improve this methodology, potentially providing a more precise and accurate perspective of the global distribution of riverine hydrokinetic resource.

Contents

List of Figures

List of Tables

别推河，它自己流。

Don’t push the river, it flows by itself.

Acknowledgements

Thank you to my supervisors Simon, Matt and Peter. My project was certainly wet, but not from water of the density and salinity you are used to. I appreciate you making the effort to operate 'upstream' of your usual ~~fields~~ pools of expertise and for your patience and wisdom. I hope the freshwater was a welcome change from the salty stuff and an opportunity to utilise your substantial skill in a similar, but slightly different, context and gain some 'extra-curricular experience'. The discipline of oceanography has long exemplified the spirit of a multi-disciplinary approach and, at the end of the day, it's all just water.

Thank you to Dr. Sopan Patil, of the School of Natural Sciences, for his legitimate and significant hydrological expertise, and willingness to spend time assisting a student from across the Menai Strait.

Frank Moloney, of Repetitive Energy Company, has the worthy intention of helping the people of the world — of whom, there are unfortunately many — that are living in energy poverty, despite living right next to an abundance of free-flowing energy. Good on you, Frank. Your witty Irish charm has blessed many a (long) phone call, not to mention the occasional enjoyable (and well lubricated) meal. Thank you Frank.

Thank you to Dr. Martin Austin and Prof. Mattias Green, who offered sagely support, holding me to account and ensuring that things stayed on track. Thank you to Penny Dowdney, Brian Murcutt and Dawn Davies, of KESS 2, for administrative support and for keeping π and me fed and warm.

Thank you Mum. Thank you Dad.

Declaration

I hereby declare that this thesis is the results of my own investigations, except where otherwise stated. All other sources are acknowledged by bibliographic references. This work has not previously been accepted in substance for any degree and is not being concurrently submitted in candidature for any degree unless, as agreed by the University, for approved dual awards. I confirm that I am submitting this work with the agreement of my Supervisors.

Signed:

Date: 24 September 2022

Abbreviations

Abbreviation	Description
ADCP	Acoustic Doppler Current Profiler
AEP	Annual Energy Production
AHG	At-a-station Hydraulic Geometry
AMG	At-Many-stations Hydraulic Geometry
ASTER	Advanced Spaceborne Thermal Emission and Reflection Radiometer
CAMELS	Catchment Attributes and MEteorology for Large-Sample Studies
CAS	Canadian Space Agency
CCGT	Combined Cycle Gas Turbine
CE90	Circular Error at the 90th percentile
CNES	Centre National d'Études Spatiales
DAG	Directed Acyclic Graph
DCW	Digital Chart of the World
DECIPHeR	Dynamic fluxEs and ConnectIvity for Predictions of HydRology
DEM	Digital Elevation Model
DHG	Downstream Hydraulic Geometry
DSM	Digital Surface Model
DTM	Digital Terrain Model
EEP	Energy Extraction Plane
FDC	Flow Duration Curve
FRA	Free-flowing River Assessment
GEE	Google Earth Engine
GIS	Graphical Information System
GRADES	Global Reach-level A priori Discharge Estimates for Surface water and ocean topography
GRDC	Global Runoff Data Centre
HEC	Hydrokinetic Energy Conversion
HEC-RAC	Hydraulic Engineering Center's River Analysis System
IEA	International Energy Agency
IEC	International Electrotechnical Commission
IRENA	International REnewable Energy Agency
ISO	International Organisation for Standardisation[1]
KGE	Klinga-Gupta Efficiency
LCOE	Levelised Cost of Electricity/Energy
LE90	Linear Error at the 90th percentile

Continued on next page

Continued from previous page

Abbreviation	Description
LSM	Land Surface Model
MAE	Mean Absolute Error
MERIT	Multi-Error-Removed-Improved-Terrain
MHK	Marine and HydroKinetic
MMSS	Mean Maximum Spring Speed
MUS	Multiple Use of Space
NARWidth	North American River Width
NASA	National Aeronautics and Space Administration
NH	Northern Hemisphere
NHDPlus	National Hydrograph Dataset Plus
NPV	Net Present Value
OECD	Organisation for Economic Co-operation and Development
PAS	Publicly Available Specification
PBIAS	Percentage BIAS
RAPID	Route Application for Parallel Computation of Discharge
RCECS	River Current Energy Conversion System
RCT	River Current Turbine
RHG	Reach-averaged Hydraulic Geometry
RISEC	River In-Stream Energy Converter
RMSE	Root Mean Square Error
RSSA	River and Stream Surface Area
SAR	Synthetic Aperture radar
SDA	Spatial Data Analysis
SEM	Standard Error of the Mean
SH	Southern Hemisphere
SIF	Significant Impact Factor
SRTM	Shuttle Radar Topography Mission
SWOT	Surface Water Ocean Topography
TISEC	Tidal In-Stream Energy Converter
UKSA	Unit Kingdom Space Agency
USGS	United States Geological Survey
VDC	Velocity Duration Curve
VIC	Variable Infiltration Capacity
VLH	Very Low Head
WCT	Water Current Turbine
WGHM	WaterGAP Global Hydrology Model

[1]Because ‘International Organisation for Standardisation’ would have different acronyms in different languages (IOS in English, OIN in French for ‘Organisation internationale de normalisation’, etc.), it was decided to give it the short form ISO. ISO, derived from the Greek ’isos’ and meaning equal, is used whatever the language.

Symbols

Symbol	Description
a	Coefficient of power law for estimating w
A	Cross-sectional area of river section
A_D	Cross-sectional area of sweep of turbine
α	Number of days in data set
b	Exponent of power law for estimating w
β	Number of river reaches in data set
c	Coefficient of power law for estimating d
C_P	Power coefficient
γ	Specific weight of water
d	River depth
E	Energy
E_k	Kinetic energy
E_p	Gravitational potential energy
$\mathbf{E}_{\mathrm{MC}}$	Matrix containing daily values of hydrokinetic energy for each reach (calculated using randomly applied hydraulic parameters and Monte Carlo approach)
$\vec{E}_{\mathrm{MC}}$	Vector of daily hydrokinetic energy (calculated using randomly applied hydraulic parameters and Monte Carlo approach)
$\overline{\vec{E}}_{\mathrm{MC}}$	Vector with mean values of $\vec{E}_{\mathrm{MC}}$ after a number of Monte Carlo runs
$\overline{\overline{E}}_{\mathrm{MC}}$	Global mean hydrokinetic energy of all river reaches (calculated using randomly applied hydraulic parameters and Monte Carlo approach)
$\hat{E}_{MC}$	Least squares polynomial fit of hydrokinetic energy time series (calculated using randomly applied hydraulic parameters and Monte Carlo approach)
$\Delta\hat{E}_{MC}$	Uncertainty in least squares polynomial fit of hydrokinetic energy time series (calculated using randomly applied hydraulic parameters and Monte Carlo approach)
$\mathbf{E}_{\mathrm{MP}}$	Matrix containing daily values of hydrokinetic energy for each reach (calculated using globally applicable mean hydraulic parameters)
$\vec{E}_{\mathrm{MP}}$	Vector of daily hydrokinetic energy (calculated using globally applicable mean hydraulic parameters)
$\overline{E}_{\mathrm{MP}}$	Global mean hydrokinetic energy of all river reaches (calculated using globally applicable mean hydraulic parameters)
ϵ	Blockage coefficient
f	Exponent of power law for estimating d

Continued on next page

Continued from previous page

Symbol	Description
g	Acceleration due to gravity
H	Static head height
ΔH	Absolute error for measurements of H
k	Coefficient of power law for estimating v
L	Length of a river reach or body of water
m	Exponent of power law for estimating v
M	Mass of water
n	Manning roughness coefficient
N	Number of Monte Carlo runs
p	Pressure
P	Power
$\mathbf{P}$	Matrix containing daily values of hydrokinetic power for each reach
$\vec{P}$	Vector of daily values of for hydrokinetic power
$\Delta\vec{P}$	Uncertainty in daily values for hydrokinetic power
$\hat{P}$	Least squares polynomial fit for hydrokinetic power time series
$\Delta\hat{P}$	Uncertainty in least squares polynomial fit for hydrokinetic power time series
Q	Discharge (volumetric flow rate)
ΔQ	Absolute error for measurements of Q
$\mathbf{Q}$	Matrix containing daily values of discharge for each reach
R	Hydraulic radius
ρ	Fluid density
s	River slope
σ	Standard deviation
t	Time
v	Flow speed
w	River width
W	Wetted perimeter of river cross-section
ω	Stream order
z	Elevation

Chapter 1

Introduction

1.1 Research background and rationale

1.1.1 The global riverine context

Referred to descriptively as the 'blue planet' [1, 2] and poetically as the 'pale blue dot' [3], Earth's association with the colour blue reflects the predominance of water found here. Approximately 71 % of the surface is covered by water, with the ocean comprising 96.5 % of Earth's total water [4]. Of the remaining fresh water, one-fifth is in liquid form, with nearly 99 % groundwater, 1 % stored in lakes, 0.2 % stored as soil moisture, 0.1 % free-flowing rivers and 0.005 % stored in plants [5].

Water is constantly circulating between Earth's surface and the atmosphere, as part of the hydrological cycle. According to Walling [6], the total energy input required to drive the hydrological cycle is estimated to be equivalent to 40 million major power stations[1], with a value of 1.3×10^{24} J yr^{-1} (3.6×10^{8} TWh yr^{-1}). Though free-flowing rivers constitute a fraction of Earth's water, by volume, they represent a significant component of the hydrological cycle. Rivers are open channels resulting from streamflow, as water flows from higher to lower elevation. Driven by gravity, rivers always flow downhill and end their journey at the ocean. The ocean, as a whole, is defined as a body of water extending landwards from the deep ocean, to include the shelf seas, coastlines and estuaries that serve as an interface between the oceanic and terrestrial domains. The global river network comprises many independent and disconnected basins, but when considered collectively constitute a whole that is the sum of these parts. In considering the entire global network of rivers, with a combined length of 2.7×10^7 km (according to the GRADES data set, introduced in Subsection 3.1.3), this study considers a key component of Earth's processes, integral to an understanding of the interaction of oceanic, atmospheric and

[1] This calculation corresponds to a 'major power station' converting energy at a rate of 3.3×10^{16} J yr^{-1} (9.0 TWh yr^{-1}), or a capacity of 1 GW. This provides a useful reference which can be applied to other similar values, which might otherwise be difficult to conceptualise. This unit of measure will be referred to as a *standard power station*, i.e. 40×10^6 standard power stations. The World Nuclear Asscociation [7] states that there are 440 nuclear power plants, worldwide, with a combined capacity of 390 GW, giving an average of 0.9 GW. Therefore, the neat value of 1 GW for this 'yardstick' would appear to be reasonable.

terrestrial dynamics.

Although ubiquitous, water is a relatively under-developed renewable energy resource. Given that hydropower accounts for 16 % of global electricity production, generating more electricity than any other renewable energy technology [8], and the Three Gorges Dam is the largest power station of any type in the world [9], this statement may seem unjustified. Yet, the true potential of this resource is hinted at by the substantial energy evident in the numerous oceanic and riverine processes observable throughout nature, and accentuated by the fact that the total energy conversion associated with the vast ocean accounts for <0.1 % of all renewable energy conversion [10]. The energy in water is apparent as the propagation of gravity waves, density gradients, the gravitational potential energy attained through elevation change, or as kinetic energy due to its movement.

1.1.2 The importance of energy

A foundational concept within physics and a fundamental property at the root of all events within the universe, *energy* is present in all processes, from the very big to the very small. Smil [11] offered this comment:

> Energy is the only universal currency: one of its many forms must be transformed to get anything done. Universal manifestations of these transformations range from the enormous rotations of galaxies to thermonuclear reactions on stars.

Energy, from the perspective of mechanics, is defined as 'the capacity to do work' [12]. Whether considering an individual, the collective global population, or the biosphere as a whole, energy is of central importance to everything that takes place on planet Earth. It shapes the dynamics of the systems all life operates within and has been recognised as an important driver of species evolution [13–15]. From the food we eat to support our bodily processes, to the light that enables the process of photosynthesis as crops grow to produce that food, to the production of fertiliser to aid growing those crops, to the fuelling of machines to help in the farming process, to the transportation of this food within global distribution networks, to cooking that food, onward and onward, and in any number of a multitude of systems we care to consider, energy is involved and crucial. Every product and service within our economy comes into being via a process initiated by an input of energy and probably a number more subsequent steps that require the same. Our ability to source, harness and make use of energy dictates the extent to which we are able to live and prosper, with a direct correlation observed between economic output and energy consumption [16–18]. For this reason, Bose [19] believes energy to be the life-blood for continual progress of human civilisation, stating that per capita energy consumption has served as a 'baromter of a nation's economic prosperity'.

White [20] proposed that, if other factors remain constant, culture evolves as the amount of energy harnessed per capita per year is increased, or as the efficiency of the instrumental means of putting the energy to work is increased. In summary, describing White's law, the degree of cultural development C is given by

$$C = ET \tag{1.1}$$

where E is the annual energy consumption per capita and T is a measure of the efficiency of the energy use. Instead of a consideration of the many *cultures* of the world, the focus here is upon

culture as a general human phenomenon [21]. For White, the primary function of culture is to harness and control energy. The subsequent theory that developed from White's law identified three components to the concept of culture: technological, sociological and ideological [22]. Reflecting a materialist approach, perhaps, the technological component was deemed the most important, acting as the primary determining factor responsible for cultural evolution.

The Industrial Revolution of the late 18th century saw a massive increase in energy usage and corresponding rise in productive output, moving beyond a dependence upon the annual cycle of plant photosynthesis which limited societies previously [23]. An important element of the Second Industrial Revolution of the late 19th century was the widespread availability of electricity [24]. It was communication, not power transmission, that was the first application of this new technology; which serves as a reminder that electricity is not a source of energy, but a medium of transfer. Though more technically difficult, the use of electricity as a prime means of transmitting and using energy was to follow, initiating a corresponding push to develop the means for converting other forms of energy into electricity and ways of efficiently transmitting this electrical energy over large distances [25]. This movement of electrical energy continued to develop and evolve, culminating in the Third Industrial Revolution of the late 20th century, marking the beginning of the Information Age, with increased use of electronics and information technology [26]. This increase in the use and consumption of electronic goods, in addition to the emergence of a 'world wide web' of interconnected computers [27] and associated 'stack' of hardware components, coincided with a complementary increase in manufacturing capacity [28]. Common to all of these civilisational 'jumps' is the importance and increased requirement for energy.

Schwab [29], of the World Economic Forum and epitome of the 'Davos Man' [30], has predicted an imminent Fourth Industrial Revolution. Though his particular vision for this next iteration is 'somewhat' dystopian (and hopefully incorrect), it lists a number of bleeding edge technologies, promising revolutionary improvements in productivity and potency, such as: artificial intelligence, robotics, the internet of things, autonomous vehicles, 3D printing, nanotechnology, biotechnology, material science, energy storage and quantum computing. Not on this list, but also relevant in any discussion about current paradigm-shifting technology, is cryptocurrency, blockchain and distributed ledger technology. Indeed, Su et al. [31] consider this technology a key driver behind the accelerating pace towards the Fourth Industrial Revolution, in the domain of finance, promising the benefits of a reduction in international transaction fees and liquidity costs.

The law of conservation of energy [32] states that, since the total energy of an isolated system remains constant, energy can be neither created nor destroyed. Therefore, energy *consumption* refers to the *conversion* of existing energy. This will generally refer to the conversion of *primary energy* to an energy source that provides some use, such as providing light in a dark room, in addition to the accompanying forms of wasted energy that arises from inefficiencies associated with the energy conversion, such as heat. Primary energy is energy from a naturally occurring source, where no conversion process has been applied. Examples from non-renewable sources include fossil fuels and the mineral fuels used in nuclear energy, such as uranium and thorium. Renewable sources predominately include bioenergy, wind, solar, hydro, marine and geothermal. *Global energy consumption* is a measure of the total energy conversion from primary energy sources and is typically measured per year. In 2017, global energy consumption was 163,226 $\mathrm{TWh\,yr^{-1}}$ (18,631 standard power stations)[33]. This was a

2.2 % increase from 2016 and driven by an increase of 1,396 TWh yr^{-1} (159 standard power stations) from coal and oil. In 2018, global energy consumption had risen to 166,100 TWh yr^{-1} (18,959 standard power stations) [8], with contributions from a variety of energy sources (Fig. 1.1). It is worth noting that the International Energy Agency (IEA) counts the use of 'biofuels and waste' — which includes charcoal, animal dung and a variety of other 'less than optimal' fuels, indicative of energy poverty (see Subsection 1.1.3) — in this calculation and that this is the largest contributor outside of the fossil fuels; larger than the contribution from hydro.

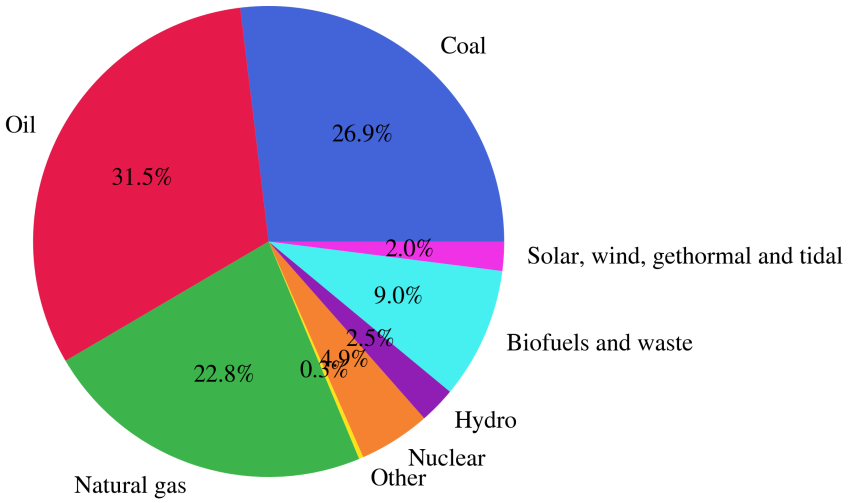

Figure 1.1: The contributions of different energy sources to the global energy consumption of 2018.

Global energy consumption is predicted to rise 30 % from 2016 to 2040 [34]. This is driven by growth in global economy (3.4 % yr^{-1}), population (7.4×10^9 to 9.0×10^9) and urbanisation at the rate of a population approximately that of Shanghai every four months. The largest contribution is expected from India and China, with Asia as a whole contributing two-thirds of global energy growth [34]. Other predictions see global energy consumption rising to approximately 1 ZJ yr^{-1} (1×10^{21} J yr^{-1}, or 30,303 standard power stations) by 2050, if economic growth continues the course shown in previous decades [35–39].

In accepting the importance of energy to human civilisation, we provide a 'slow layer' context against which other issues can be evaluated and judged, acknowledging that there may exist contrary points of view, dependent upon the relevant timescales of those perspectives. In fact, given this framework, it is entirely possible that completely opposite points of view can both be correct, simultaneously, according to the chosen criteria of evaluation. Ahuja and Tatsutani [40] highlight the difficulty of 'squaring the circle', when considering how to solve the problem of providing access to basic, modern energy services to the billions of people who are currently without, while simultaneously participating in a global transition to clean, low-carbon energy systems. Yet, as they point out, with roughly a quarter of the world's population currently living without access to electricity, the electricity required for these people to be able

to read at night, pump a minimal amount of drinking water and listen to radio broadcasts would amount to <1 % of overall global energy demand. The convenience afforded by even small quantities of electricity, that enable seemingly trivial actions to be carried out, are often taken for granted by those of us living in the developed world. The ability to simply charge a mobile phone, for example, is seen to offer significant socio-economic benefits to many living in energy poverty [41, 42].

1.1.3 Energy poverty

Energy poverty has been defined by the IEA as a lack of access to electricity and clean cooking facilities [43]. This widespread problem is seen to cause several detrimental effects: decrease in public health, degradation of the natural environment due to deforestation and changes in land use, reduction of educational opportunities, gender disempowerment and increased emission of per capita green house gases [44]. Households living in energy poverty also lack the choice of which energy sources to use. This results in many people in poorer countries having no choice but to cook on unventilated and inefficient wood, charcoal, and dung cooking stoves. This type of energy use has a substantial impact on health due to indoor air pollution, caused by the emission of carbon monoxide, aromatic compounds and suspended particles. For this reason, energy poverty is said to cause more deaths than from malaria, or tuberculosis [45]. In addition to this risk from using such fuels, people can suffer physical injury when carrying out the chores that their usage necessitates, such as wood collection. Again, the perspectives of someone in the developed world may downplay this risk, when subjective experience is used as a reference. Yet, compounded on top of this hazard is the fact that lack of sufficient energy means that such tasks are often carried out by children or the elderly, as the responsibilities of a community, or family, are stretched [46]. Further, the extra challenges of providing medical care, without the energy needed for medical applications and refrigeration, underscore an often under-appreciated reality of the inequality between the day-to-day challenges of the developed and undeveloped worlds.

According to the *energy ladder model*, as incomes increase, low-quality fuels such as biomass tend to be replaced by higher-quality fuels such as kerosene, oil and ultimately electricity [47]. This concept allows a measurement of energy poverty, by providing a quantification according to a person's position on a 'ladder'. The lowest rungs represent traditional fuels such as animal power, candles and wood. The highest rungs represent advanced fuels such as electricity and refined gasoline. This has been defined by one study as a measure of the percentage of population along a spectrum running from simple biomass fuels (dung, crop residues, wood, charcoal) and coal (or soft coke) to liquid and gaseous fossil fuels (kerosene, liquefied petroleum gas, and natural gas) to electricity [48]. Barnes and Floor [49] have defined the energy ladder in terms of the efficiencies of the fuels used.

The model assumes that people will look to rise up the ladder, as their circumstances improve. In fact, it has been found that fuel is chosen for many reasons, with many richer people in Botswana, India, Mozambique, South Africa, Zimbabwe, Tanzania and Nigeria choosing to use a variety of different fuels, due to low cost, availability, or preference [50]. In addition to these factors, fuel choices have been shown to be influenced by tradition and social expectations, in a study spanning 34 cities across Africa, Asia, the Caribbean, Latin America and the Middle East [51].

The number of people affected by energy poverty, globally, can be measured by three ap-

proaches, focused on energy access, according to a technological, physical, or economic threshold. The technological threshold approach recognises the problem of accessing modern energy sources as the main problem. Therefore, either a determination of the number of people who do not have access to electricity, or the number of people who rely upon biomass for cooking, could be used as a measure. In this case, as of 2017, 1.1 billion people do not have access to electricity and 2.5 billion people rely on biomass for cooking [34]. The physical threshold sets a minimum level of basic necessity. The problem here lies in determining what this level is. Chakravarty and Tavoni [52] considered 100 kWh and 150 L of gasoline per person per year to serve an appropriate level, which is equivalent to 5 GJ. With this threshold, 1.8 billion people were living in energy poverty in 2009 (27 % of the world's population). It may be argued that an economic threshold is more applicable for a measurement of *fuel poverty*, which is defined in economic terms and results from a problem of affordability, rather than availability.

The idea of fuel poverty grew from political concern in the UK, during the 1970s and 1980s, first formally defined as an inability to afford adequate warmth in the home [53]. DEFRA and DTI [54] refined this definition further, to provide an official interpretation of fuel poverty as a household needing to spend more than 10 % of its income on all fuel use and to heat its home to an adequate standard of warmth. Hills [55] offered a new definition which, in contrast to this absolute measure, would provide a relative measure by determining the numbers of households that would be put under the official poverty line due to their spending on fuel. Adoption of this new definition was shown to result (conveniently?) in a reduction of the number of people in fuel poverty, in England, from 3.2 million to 2.6 million people [56]. Price et al. [57] proposed a further measure of fuel poverty, based upon a person's subjective feeling of whether they were living in fuel poverty, or not. This study provided results that differed greatly from objective determinations.

Fuel poverty remains a term that is mostly applied in cold climates and predominately in the UK, Ireland and New Zealand [58]. These are countries where energy is widely available. Reiterating what was said before, in contrast to energy poverty, fuel poverty tends to result from a problem of affordability, rather than availability. In some circumstances, people may experience both energy poverty and fuel poverty. For example, low income households in cold climates and developing countries, such as China, Nepal and India.

Access to electricity provides positive socio-economic impacts for disadvantaged, isolated communities, in developing nations [59, 60]. This access can be improved by grid-extension, the use of diesel generators, or small-scale renewable energy systems. Let us consider each of these in turn. Grid-extension can be slow to help these communities, due to low consumption and poor capacity factors causing utility companies to view such endeavours as uneconomic [44, 61, 62]. Capacity factor is a measure of actual power output relative to potential power output, given by

$$\text{Capacity factor } \% = \frac{\text{Actual output}}{\text{Potential output}} \times 100 \tag{1.2}$$

For wind turbines, capacity factor has been shown to be a proxy for average wind speed [63], but has also been shown to decrease, as global wind energy production increases [64, 65]. This is because it is not just a measure of efficiency and can be affected by variations in demand. For example, a period of high output coinciding with low demand will see a fall in capacity factor, causing an increase in the levelised cost of electricity (LCOE). LCOE provides

a means for comparing the unit costs of different technologies over the period of their operation and is defined as the ratio of total lifetime expenses versus total expected outputs, expressed in terms of the present value equivalent. For example, the units used might be \$/kWh, or \$/MWh (see Subsection 1.1.4 for a more thorough description). Running diesel generators is challenging for isolated communities due to high LCOE rates, rising diesel prices, the constant requirement for fuel and associated transportation difficulties. Renewable energy technologies use energy obtained from the continuous or repetitive currents of energy recurring in the natural environment to provide a conversion to electrical energy [66]. We shall consider this in more detail in the next subsection.

1.1.4 Renewable energy technologies

Sørensen [67] defines renewable energy as 'energy flows which are replenished at the same rate as they are "used".' Various reasons are commonly given to explain the increased interest in renewable energy.

- Growing concerns on the impacts of climate change, due to anthropogenic addition of CO_2 to the atmosphere caused by the use of fossil fuels [68–71].
- Reduction in the finite availability of fossil fuel [71–73].
- Increased desire for energy independence, due to political policy and individual preference [74–77].

IRENA [10] classifies renewable energy technology according to one of the following categories: bioenergy, wind, solar, marine, hydro and geothermal. They report that the total installed capacity for these technologies in 2018 was 2.5 TW (Table 1.1). This represents the maximum net generating capacity of power plants and other installations that convert renewable energy sources to electricity. There has been an increase in the installed capacity of these technologies from 2009 to 2018 (Fig. 1.2).

Table 1.1: Installed capacity of renewable energy technologies for 2018 [10].

RE technology	Installed capacity (MW)
Hydro	1,292,595
Wind	563,726
Solar	485,826
Bioenergy	115,731
Geothermal	13,329
Marine	532
Total	2,471,739

All forms of renewable energy technology require an input of supplementary energy to allow the intended conversion of the renewable source of energy to electricity. This input is the sum of energy related to the manufacture, operation, maintenance and decommissioning of the device and associated infrastructure. The net energy provided by a device used to convert energy from one source to another (e.g. from the kinetic energy in moving water into electrical energy via a turbine) is given by

$$\text{net energy} = \text{gross energy output} - \text{energy input} \tag{1.3}$$

where the gross energy output is the conversion of energy by the device over its lifetime. Net energy is the energy which is used by the non-energy producing sectors of the economy. The useful energy conversion of a device, over its lifetime, can be measured by its energy ratio E_r, given by

$$E_r = \frac{\text{gross energy output}}{\text{energy input}} \tag{1.4}$$

For a renewable energy technology to be viable, $E_r > 1$ is a minimum requirement and, according to Moriarty and Honnery [38], $E_r \approx 5$ is probably necessary. Moriarty and Honnery [39] state that it is inevitable that as renewable energy technologies progressively dominate global energy supply, E_r will reduce due to higher-quality resources being exploited; and, due to their being intermittent sources, E_r will fall as storage, or conversion into other forms of energy other than electricity (e.g. hydrogen), becomes necessary to balance production with demand.

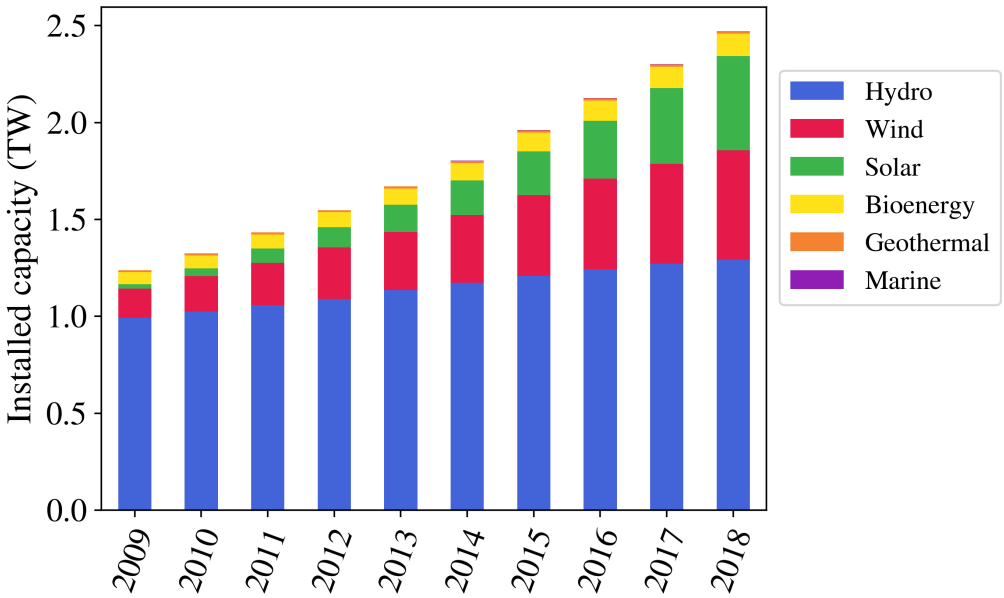

Figure 1.2: The development of installed capacity, for different renewable energy technologies, from 2009–2018.

Renewable energy technologies differ in many regards, meaning that deployment is context-specific, in addition to their being suitable for the conversion of different primary energy sources. It is desirable for an energy source to be predictable, reliable and dispatchable[2] [78]. The application of *any* technology to address an identified need, problem, or issue, such as the conversion of one form of energy to another more desirable form of energy, requires considera-

[2]The term *dispatchable*, relating to a source of electrical energy production, means that output can be switched off, on, or otherwise moderated, according to demand.

tion of the implications, from different perspectives and according to different factors: ethically, morally, socially, economically, politically, culturally and environmentally. An evaluation of the benefits and limitations should be made to justify the appropriateness of using a given technology within a given context. All energy conversion technologies, including from 'green' renewable energy sources, generate unwanted impacts, such as pollution to the air, water, or soil; greenhouse gas emissions; or, biodiversity loss. For renewable energy technology, the true extent of theses affects are uncertain, due to the relatively low levels of output, at present. Even at this early stage, deployment of renewable energy technologies has faced local opposition [79–81]. This opposition could escalate as efforts to increase the energy output from renewable energy progresses. Along with the much touted benefits offered by renewable energy technologies — including overall reduction of greenhouse gas emission, a reduced reliance on finite energy sources and opportunities for energy independence — there remains a responsibility to balance this against a full consideration of all limitations. Table 1.2 summarises adverse impacts resulting from renewable energy technologies.

A key challenge for renewable energy technologies being integrated into an electrical grid is the need to ensure that the supply of electrical energy meets the demand [82, 83]. We have already discussed the relevance of the capacity factor of a device (Eq. (1.2)), in this regard. Many renewable energy technologies exhibit variable power output over a range of timescales, with low predictability compared to traditional sources of electricity (e.g. fossil fuels and nuclear) [84]. Without an ability to store excess converted energy, variable renewable energy technologies need to continuously balance supply and demand. This can be resolved, to some extent, by using 'smart metering' and 'smart grids' to provide responsive demand. Otherwise, an inability to productively use excess converted energy will result in a decrease in capacity factor and therefore an increase in LCOE (as mentioned in Subsection 1.1.3). Development of storage solutions could allow increased system flexibility and better integrate variable renewable energy sources. Unfortunately, storage and system control measures to aid overcoming these problems are expensive [85–87]. In addition to economic challenges, Castillo and Gayme [88] identify a number of further technical and regulatory barriers, including technological maturity, cycle efficiency and a lack of coherence in modelling approaches.

A number of technologies are available to store energy at a grid-scale. For example, pumped-storage hydroelectricity is a mature grid-scale energy storage technology and is the largest-capacity option currently in use [89]. The method involves storing energy in the form of gravitational potential energy, pumped from a lower elevation reservoir to a higher elevation. The production of hydrogen can also be an option for excess electrical energy and is considered suitable for off-grid applications [90, 91]. Once produced, the hydrogen can then be used to fuel an energy conversion device, such as a fuel cell or an internal combustion engine. A hydrogen fuel cell converts the chemical energy potential in oxygen and hydrogen molecules into heat and electricity, using electrolysis. The fuel can be formed directly from a device *in situ*, thus allowing isolated communities to have access to energy and storage options, without grid connection. Other technologies include: compressed-air energy storage [92, 93], cryogenic energy storage [94, 95], batteries [96], flywheel energy storage [97], superconducting magnetic energy storage [98], thermal energy storage [99], gravitational potential energy storage with solid masses [100] and deep sea pumped storage [101].

In an electrical grid, the *baseload* is the minimum level of demand over a given period. Since the storage of electrical energy is limited and relatively expensive, it is preferable to keep

Table 1.2: Summary of adverse impacts from renewable energy technologies.

Renewable energy technology	Limitations and adverse impacts
Hydro	Loss of homes and livelihoods from displacement; loss of freshwater biodiversity; flooding of farmland or natural forests; possible increase in microseismicity; slope instability; loss of heritage sites; increased downstream erosion; coastal land retreat and declining soil fertility from loss of sediment deposition; and, greenhouse gas emissions from submerged biomass [103–107].
Wind	Bird and bat deaths; habitat loss; noise and vibration pollution; adverse effects on visual amenity; adverse effects on marine mammals from offshore sites; and, possible climate change effects from large-scale implementation [103, 108–116].
Solar	Pollution from photovoltaics production; adverse effects on semi-arid land ecosystems; competition for fresh water; depletion of scarce materials; and, albedo reduction [103, 111, 117].
Bioenergy	Competition with other bioenergy uses (e.g. food production) for fertile land and water; loss of existing uses for bioenergy; and, loss of biodiversity [107, 118, 119].
Geothermal	Land subsidence; increase in microseismicity; and, potential air and water pollution [103, 104, 116].
Marine	Disruption to marine ecosystems from pumping vast amounts of water (for ocean thermal energy conversion); possible adverse effects on marine mammals; and, disruption to marine vessels [103, 120, 121].

primary production closely linked to demand. There are inevitably fluctuations in demand and, within the diverse energy portfolio of a national grid, generation technologies vary in how predictable, reliable and dispatchable they are. Therefore, generation technologies that easily regulate output, despite often being more expensive, are used to accommodate the peak loads. More efficient and cheaper generation technologies, that lack flexibility in output, are used to provide the baseload. Natural gas-fired combined cycle gas turbines, coal and nuclear are commonly used to provide baseload power generation [102]. An *intermediate baseload* can serve to represent the range of differences in the full spectrum of generation technologies and reflect that a combination of approaches are used to deal with variable supply and demand.

Many policy discussions over the costs of different technologies for electricity generation are based on the concept of levelised costs of electricity (LCOE), defined as the ratio of total lifetime expenses versus total expected outputs and expressed in terms of the present value equivalent [102], summarised as

$$\text{LCOE} = \frac{\text{costs over lifetime}}{\text{electrical energy produced over lifetime}} \tag{1.5}$$

The LCOE is calculated using the *discounted cash flow* method and achieved using

$$\text{LCOE} = \frac{\sum_{t=1}^{n} \left[\frac{I_t + O_t + M_t + F_t + C_t + D_t}{(1+r)^t} \right]}{\sum_{t=1}^{n} \left[\frac{E_t}{(1+r)^t} \right]} \tag{1.6}$$

which uses factors related to costs incurred and the energy yield expected over the lifetime of a project (Table 1.3). The units used tend to be \$/kWh, \$/MWh, or similar, with different currencies and energy units applied, as deemed appropriate. LCOE is determined by market structure, the policy environment and resource endowments. It can be seen as the average price that the converted electricity must be sold for to break even over a project's lifetime.

Table 1.3: Factors considered in calculating the levelised costs of electricity (LCOE) using Eq. (1.6).

Variable	Description
I_t	Investment costs over year t.
O_t	Operation costs over year t.
M_t	Maintenance costs over year t.
F_t	Fuel costs over year t.
C_t	Carbon emission costs over year t.
D_t	Decommissioning and waste management costs over year t
E_t	Energy converted over year t expressed in MW h.
r	Discount rate. Weighted average cost of capital (WACC) over year t.
n	Expected number of years of operation.

With regards to this study, and as an example, the reduction of the LCOE of hydrokinetic energy conversion (HEC) has been identified as one of the main challenges facing the development of the HEC industry [122, 123]. Here, the elements to be considered are: capital cost, operations and maintenance costs, design simplicity, diversity of applications, modularity, scalability, material and labour engagement, and availability of off-the-shelf components

[122]. Factors that have an indirect impact, are: system reliability, societal acceptance and system performance.

In Eq. (1.6), it looks as if E_t is being discounted. This is not the case and is due to the revenue being discounted, which is more apparent from considering the equation rearranged as

$$\sum_{t=1}^{n}\left[\frac{\text{LCOE}\cdot E_t}{(1+r)^t}\right]=\sum_{t=1}^{n}\left[\frac{I_t+O_t+M_t+F_t+C_t+D_t}{(1+r)^t}\right] \tag{1.7}$$

where the left-hand side represents the discounted sum of benefits and the right-hand side represents the discounted sum of costs. Since LCOE is constant over time, it can be removed from the summation, as in Eq. 1.6.

The discount rate r is used to define a discount factor D_n, using

$$D_n=\frac{1}{(1+r)^n} \tag{1.8}$$

which provides a measure of how cheaply money can be borrowed against a project to finance it. Three discount rates can be considered relevant: a 3 % rate corresponds approximately to the 'social cost of capital'; a 7 % rate corresponds approximately to the market rate in deregulated, or restructured, markets; and, a 10 % rate corresponds to an investment in a high-risk environment [102]. The discount rate can have a significant effect on costs [124], depending upon the technology considered. For example, the technologies of natural gas-fired combined cycle gas turbine (CCGT), coal and nuclear each have an LCOE that varies according to the discount rate applied. At a low discount rate (3 %), nuclear is the cheapest option of the three, due to nuclear technology being capital intensive relative to coal and natural gas. At a high discount rate (10 %), though, the LCOE of nuclear becomes more expensive, relative to the other two technologies [102]. This effect is less pronounced for renewable energy technologies.

There are limits to the effectiveness of LCOE as a metric. LCOE is calculated at the plant level and therefore does not include costs related to transmission, distribution, or other systematic costs, or externalities beyond CO_2 emissions. Furthermore, the LCOE methodology reflects generic technology risks. Therefore, it is less appropriate for calculating specific project risks in specific markets. The methodology is also more relevant in regulated markets and since there is a recent divergence from this, in electricity markets, the methodology becomes less accurate of a measurement [102]. For this reason, the LCOE methodology is less useful in OECD[3] countries, where liberalised electricity markets were introduced in the 1990s. In this case, electricity prices are an input rather than an output of investors' profitability calculations. This requires that calculations of net present value (NPV) are made, based on expected exogenous electricity prices and include an assessment of their variation and associated uncertainty over time. The LCOE provides an endogenously determined electricty price, effectively rendering the NPV equal to zero. Also, with the increased reliance upon variable renewable energy, it is *system cost* which concerns planners, rather than LCOE [125]. LCOE ignores the increasingly complex network of interactions that exists between generation technologies and the rest of the electricity system.

[3]The Organisation for Economic Co-operation and Development (OECD) is an intergovernmental economic organisation that aims to simulate economic progress and world trade, on the behalf of its 36 member countries.

1.1.5 Water as an energy resource

As stated previously, the energy within water is apparent in the propagation of gravity waves, density gradients, the gravitational potential energy attained through elevation change, or as kinetic energy due to its movement. Renewable energy technologies that convert the energy that exists in water, include: hydropower, various technologies that fall under the umbrella of 'marine energy' and HEC. It is desirable for an energy source to be predictable, reliable and dispatchable [78]. Compared to other sources of renewable energy technologies (e.g. solar and wind), hydropower along with tidal power best demonstrate these characteristics.

In conventional hydropower plants, a storage of gravitational potential energy is obtained due to the impoundment of water behind a dam, allowing a head to develop. The energy converted to electricity by a dammed hydroelectric plant is as a result of the conversion of gravitational potential energy into kinetic energy, which is used to drive the rotation of a hydraulic turbine. Run-of-the-river hydropower involves diverting a portion of the water flowing in a river, through a canal or penstock, to a turbine. In contrast to conventional hydropower, such power plants have a limited, or lack of, storage.

With a global installed capacity estimated to be 1.3 TW [10] (Fig. 1.3), hydropower accounted for 16.2 % of global electricity production in 2018, generating more electricity than any other renewable energy technology [8].

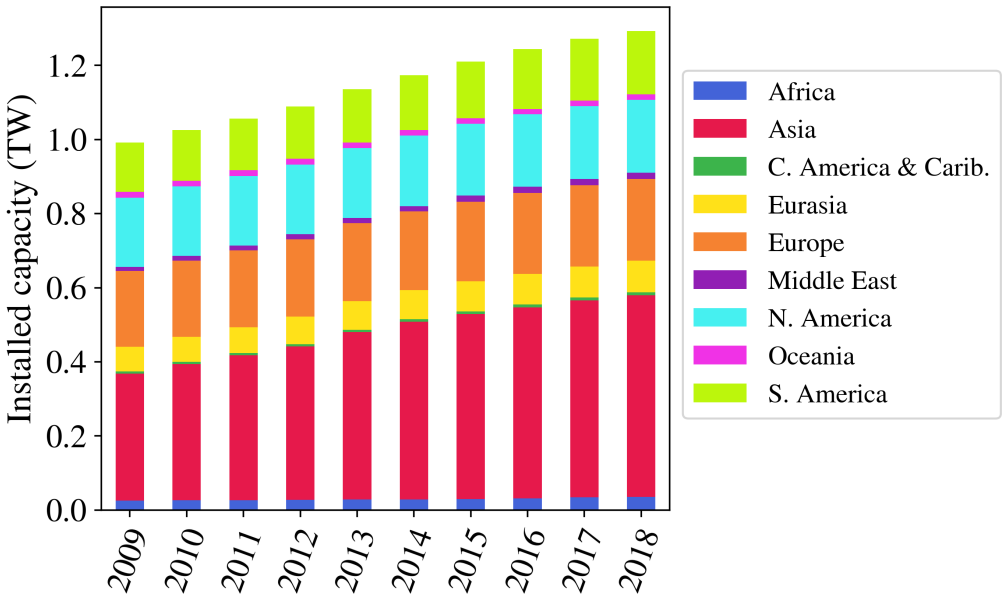

Figure 1.3: The development of installed capacity for hydropower from 2009–2018.

The ability to build large-scale hydropower plants, through the creation of a large static pressure impounded behind the construction of a dam, has been enabled in line with improvements in engineering and design. In combination with the promise of a large quantity of cheap electricity, for countries with the appropriate resources, this has made the development of larger hydropower plants an attractive option. Conventional hydropower plants have a comparatively long life, in relation to other renewable energy technologies (typically 20 to 25 years), of up to

100 years [126].

Despite providing large amounts of electricity, the development of hydropower has raised serious socio-economic and environmental concerns (Table 1.2) that question the justification for continued development [104, 106, 107]. Further, from a political, practical and economic perspective, future hydropower plant constructions may be either technically or economically, infeasible [103, 127]. As a specific example, Punys et al. [128] state that a limit on the growth of such plants, in Lithuania, has arisen due to environmental constraints, bans on the damming of rivers, the introduction of laws aimed at reducing the incentives offered for development of such projects and a change in administrative preferences towards less impactful renewable energy technologies, including HEC. Ansar et al. [127] suggest that in most countries, future large-scale projects will be too costly in absolute terms. They emphasise that this is particularly the case for developing countries. If we also consider the increasing sensitivity to environmental impacts, which is most apparent in developed countries, we might conclude that this is a global issue, if not always for the same reasons. Though criticism is predominately directed at large-scale hydropower plants, Abbasi and Abbasi [105] point out that a move to the development of more mini- and micro-scale hydropower plants, as what they describe as a decentralisation of hydropower production, causes problems no less serious, when considered per kilowatt generated.

Small-scale hydropower plants offer some benefits over large-scale plants, in relation to environmental and social impact, simply for the obvious reason of their being smaller. For isolated communities, with little or no access to electricity, they can offer a cost-effective solution to energy needs. Small-scale hydropower plants have proven effective in rural mountainous communities to provide access to electricity [129, 130].

The response to a perceived challenge, due to anthropogenic-induced climate change [131–133], has affected the development of hydropower, both positively and negatively. A commitment to reducing greenhouse gas emission has caused some countries to include an increased reliance upon this form of power generation in their plans, thereby allowing a reduction upon reliance on other green house gas emitting forms, such as the burning of fossil fuels. Unfortunately, carbon dioxide and methane may result from the construction of hydropower plants, when accompanied by the creation of a reservoir which leads to the rotting of vegetation covered by the water. This is particularly prevalent in tropical regions and may even result in greenhouse gas emissions, per kilowatt-hour of electricity produced, that are greater than that from a fossil fuel power plant [134]. This may be another reason that small-scale hydropower development is becoming more attractive.

Marine energy[4] includes the conversion from tidal energy, wave energy, ocean thermal energy and ocean current energy. IRENA [10] report that the global installed capacity for this technology, in 2018, was estimated to be 532 MW; largely constant in the years previous, following a marked overall increase from 2009–2010 (Fig. 1.4).

[4]Marine energy is also referred to as ocean energy.

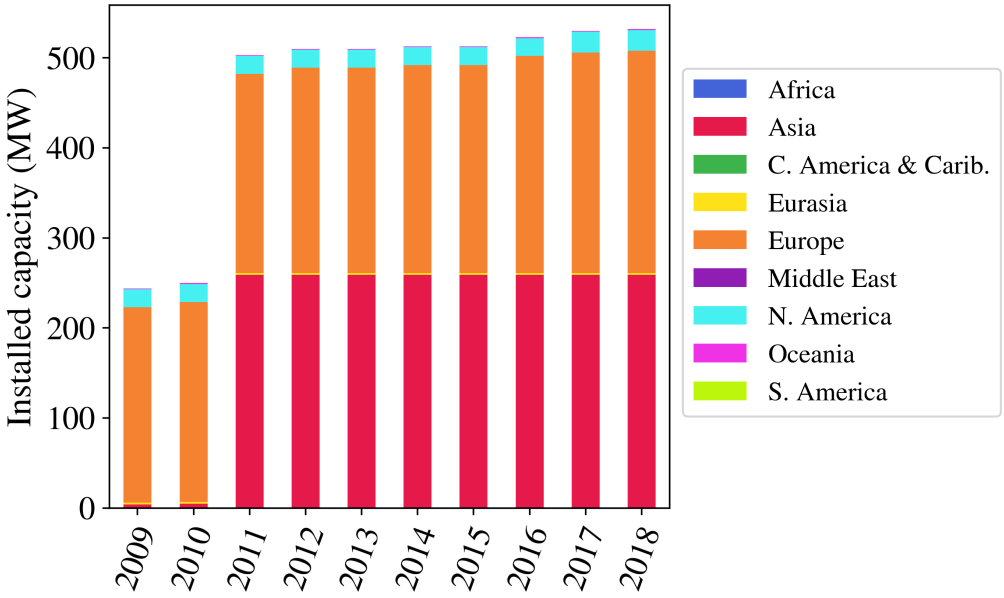

Figure 1.4: The development of installed capacity for marine power from 2009–2018.

Marine and hydrokinetic (MHK) resources refers to a combination of what is generally referred to as marine energy and a subset of hydro energy [135], according to the classification set by IRENA [10] . Following their proposed means of grouping, according to renewable energy technology type, it is common for such technologies to be classified as either bioenergy, wind, solar, marine, hydro, or geothermal. Since HEC refers to the conversion of the kinetic energy contained in river streams, tidal currents, or man-made waterways, it sits in an uncomfortable position, when attempting to fit it into these existing renewable energy technology classifications, straddling both marine and hydro. Being referred to as an MHK resource makes more sense, perhaps. Such a classification is particularly useful when considering estuaries, since they contain energy that can be considered both marine and hydro energy. As a topic of fundamental importance within this study, HEC will be considered, in full, in Chapter 2.

1.2 Aims and objectives

Free-flowing rivers are a globally abundant yet under-developed source of energy. Hydrokinetic energy conversion is relatively immature when compared with other renewable energy technologies and resource assessment has been identified as one of the main challenges hindering its development [122, 123]. A theoretical resource assessment, in contrast to technical or practical resource assessments which typically follow, quantifies the total energy that is hypothetically available for conversion, without consideration of feedbacks between extraction and the resource [78]. Therefore, in support of the development of a technology which promises to contribute to our civilisation's desire and responsibility to harness and control energy, supporting technological advancement, human flourishing and the reduction of energy poverty, this study aims to provide a perspective of the global theoretical riverine hydrokinetic resource. The global tidal resource is estimated to be in excess of 25,880 TWh yr^{-1} (2954 standard power stations) [136]. Gaining an understanding of the hydrokinetic resource within a riverine context,

when combined with existing understanding within a tidal context, provides a more complete assessment of the global potential for hydrokinetic energy conversion.

Objectives considered appropriate to support meeting these aims are listed.

- Review the fields of hydrokinetic energy conversion, resource assessment, fluvial geomorphology and hydrological modelling to gain a thorough understanding of the topics relevant in determining how to best carry out a hydrokinetic resource assessment.
- Evaluate existing hydrokinetic resource assessments, comparing and contrasting the methodologies used.
- Determine a methodology for resource assessment that aligns with the combined efforts of previous contributors to relevant topics and the informed advice of earlier related studies and resource assessments.
- Identify data sets potentially suitable for a global-scale resource assessment of the world's rivers, analysing their elements and accuracy to determine the most appropriate, according to the stated aims and objectives.
- Estimate the global theoretical riverine hydrokinetic resource, providing both a quantitative and qualitative description.
- Justify the results of the resource assessment, giving valid reasons or evidence in support.
- Interpret the results of the resource assessment, drawing relevant conclusions.

1.3 Thesis outline

Chapter 1 Summary of the wider-context topics that underpin this research and a statement of the aims and objectives of this study.

Chapter 2 Detailed description of hydrokinetic energy conversion and associated topics relevant to undertaking an assessment of the hydrokinetic resource.

Chapter 3 Presentation of a global riverine theoretical resource assessment, applying the conventional approach used in previous regional-scale studies. This resource assessment represents the first such hydrokinetic resource assessment at the global-scale. Through the unfolding of the narrative of this thesis, an argument is made that this approach provides a *hydrostatic* perspective.

Chapter 4 An evaluation of the conventional approach to hydrokinetic resource assessment and argument in support of the merits of using a truly *hydrokinetic* methodology. The derivation of an equation suitable for achieving this is proposed. Results of this alternative and novel approach are presented.

Chapter 5 The hydrokinetic resource assessment, proposed in Chapter 4, reveals the disproportionate importance of major rivers. Prominent rivers are further investigated and the basin-scale perspective examined.

Chapter 6 Conclusions and future work.

Chapter 3 is based upon an article published as Ridgill et al. [137] and Chapter 4 upon Ridgill et al. [138].

Chapter 2

Riverine hydrokinetic resource assessment

2.1 Hydrokinetic energy conversion

2.1.1 Harnessing the energy in free-flowing water

Hydrokinetic energy conversion (HEC) refers to the conversion of the kinetic energy contained in tidal currents, river streams, or man-made waterways, for the generation of electricity. This is in contrast to the conversion of the potential energy stored in conventional impoundment hydropower plants, tidal barrages, or tidal lagoons (see Subsection 1.1.5). It is HEC within a riverine context that this study is focused upon and therefore it is fluvial processes which are pertinent. While Sections 2.3, 4.1, 4.2 and 5.1 will address a thorough exploration of these processes, a number of general points are worth consideration, if we compare and contrast HEC within freshwater rivers and marine tidal currents, related to flow dynamics, the timescale of fluctuations, forces of influence and water properties (Table 2.1). As we transition from marine to riverine, it seems appropriate to first discuss estuaries, where a literal transition occurs and there exists an overlapping of these differences. With dynamics that are influenced by two driving agents, freshwater and marine, could they potentially be an important source of significant hydrokinetic energy?

Estuaries act as an interface between freshwater rivers and saltwater seas. Therefore, estuarine dynamics involve the interaction of a river current and a tidal current, with intermittency occurring due to both of these drivers, but at different scales of frequency. These environments undoubtedly present opportunities for HEC, but what is the net result of the interaction of a stochastically fluctuating river discharge and the regular oscillation of the tide? Since the power generated by a turbine is proportional to the flow velocity cubed (as will be described below in Subsection 2.1.2), does the inevitable, but short-lived, high-flow velocity event of the semi-diurnal occurrence of an ebbing tide, combined with the downstream flow of the river, compensate for the periods of an opposing flooding tide and river flow, in addition to the lack of water due to periods of low tide? Studies appear to be sparse, related to these questions. Fouz et al. [139], in their study of the affect upon HEC under combined river and tidal flow, find that river discharge is dominant and results in a pronounced seasonal variability, but do

not adequately answer the questions posed above. Zarzuelo et al. [140] suggest that constricted tidally-influenced areas, such as estuaries, experience a significant amplification of tidal currents. So, this would seem to be worthy of future investigation.

Table 2.1: Characteristics of river streams and tidal currents.

River streams	Tidal currents
Strong stochastic variation (seasonal to daily)	Semi-diurnal or diurnal
Unidirectional flow	Bi- or multi-directional flow
Density $\rho = 1{,}000\,\mathrm{kg\,m^{-3}}$	$\rho = 1{,}020$–$1{,}030\,\mathrm{kg\,m^{-3}}$
Forecasting flow conditions difficult	Predictable

The power available from HEC is modest compared to that from conventional hydropower. In Section 4.1, it will be demonstrated that the flow velocity v of water released from behind an impoundment, such as a dam, when the gravitational potential energy of falling water is converted into kinetic energy, is a function of static head height H of the water above a point of release, such that

$$v = \sqrt{2gH} \tag{2.1}$$

where the acceleration due to gravity $g = 9.81\,\mathrm{m\,s^{-2}}$. A flow speed of $v = 1.5\,\mathrm{m\,s^{-1}}$ (which we will see in Subsection 4.3.2 is globally significant) would correspond to a static head height of only $H = 11\,\mathrm{cm}$, as shown:

$$H = \frac{1.5^2}{2g} = 0.114\,\mathrm{m} = 11\,\mathrm{cm} \tag{2.2}$$

Therefore, even a modestly-sized conventional impoundment hydropower plant can theoretically provide a significant flow speed (Fig. 2.1). Despite this, advantages of HEC over hydropower include: modularity and scalability; less environmental and social impact; and, ease of construction due to being lower cost, quicker to construct and requiring less planning consent [122, 128, 141]. While HEC cannot generally compete with conventional hydropower, in terms of levelised cost of electricity (LCOE) (see Subsection 1.1.4) [142], apart from in some extreme cases, it can compete in absolute terms. Thus the bar is lowered for communities without access to electricity, yet living close to running water. In this situation, HEC offers a cost-effective solution for moving beyond having *no* electrity to the life-changing scenario of having *some* electricity.

In addition to extending access to electricity for isolated communities, HEC constructively benefits the current desire to transition away from fossil fuel based energy resources that contribute to greenhouse gas emissions [143–146]. HEC can be a significant contributor to a portfolio of renewable energy technologies used by communities directly, or via a grid, since energy from HEC is largely predictable, reliable and dispatchable [141, 147]. This is certainly true with respect to tidal currents, the dynamics of which are well understood, but also for river flow to some extent, with variations tending to be seasonal, or due to episodic events. With the exception of particularly flashy catchments[1], river discharge flows continuously over a given

[1]The flashiness of a catchment indicates the speed of response to a large influx of water to the system. A flashy catchment will show a fast response and is characterised by a small area, steep slopes and impermeable geology.

day, or a series of days. Changes to the flow tend to be more gradual, as the seasons change. For this reason, though not strictly true, HEC can often be considered a baseload power source (see Subsection 1.1.4), for periods when confidence of high flow can be assumed. Reducing intermittency and unpredictability means that power is made accessible for critical applications, such as refrigeration, or medical care. This may profoundly benefit communities currently without reliable power. Communities relying on diesel generators can reduce their fuel costs, or even eliminate them, by combining solar and/or wind power with HEC.

After a comparison of the relative advantages and disadvantages of HEC and conventional hydropower, as well as a consideration of the synergistic opportunities offered by combining different renewable energy technologies, mention should be made of how mutual benefit can be achieved for both of these riverine technologies, when deployed together. The tailrace water exiting a dam, after having been used to rotate a turbine and generate electrical power, still has significant energy and high flow speeds suitable for HEC [148, 149]. This results in an increase in capacity for a hydropower plant, with the additional energy conversion of a HEC turbine, or array of such turbines. Given that this could be repeated at any of the existing hydropower plants world-wide, this offers an opportunity to raise the global installed capacity of hydropower, without need of further dam construction. Also, a significant problem for HEC deployment is the effects from debris, sediment, frazil [2] and surface ice [150, 151]. Location in the tailrace, downstream of a hydropower installation, has been seen to reduce this problem by filtering much of this out [149].

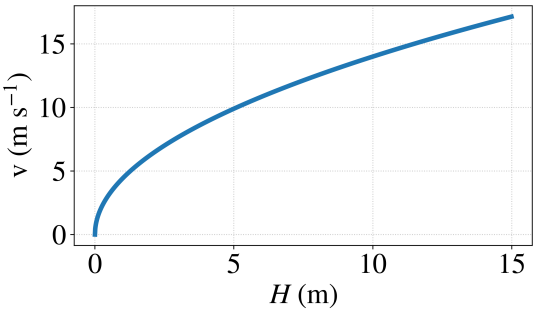

Figure 2.1: The conversion of gravitational potential energy to kinetic energy implies that flow velocity $v = \sqrt{2gH}$, when considered using Bernoulli's principle.

2.1.2 Hydrokinetic systems

There are broadly two types of system that can be used to convert the kinetic energy of moving water into electrical energy: turbine (Fig. 2.2) and non-turbine systems (Fig. 2.3). Non-turbine systems include: flutter vane [152], piozolectric [153], vortex (or flow) induced vibration [154], oscillating hydrofoil [155] and sails [156]. With the exception of the oscillating hydrofoil system, these non-turbine systems are mostly at the proof-of-concept stage.

[2] Frazil grows within the water column during freeze-up of rivers and open oceans and can accumulate on the components of a device.

Figure 2.2: Examples of hydrokinetic turbine systems: (a) axial; (b) vertical; (c) cross-flow; (d) Venturi; (e) gravitational vortex [157].

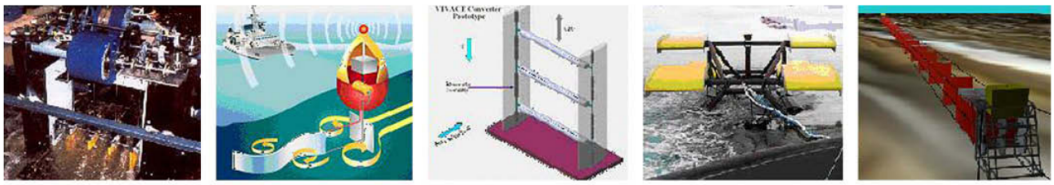

Figure 2.3: Examples of hydrokinetic non-turbine systems: (a) flutter vane; (b) piezoelectric; (c) vortex induced vibration; (d) oscillating hydrofoil; (e) sails. [157].

Generally, turbine systems are used to convert both gravitational potential energy and kinetic energy in falling, or moving, water to rotational mechanical energy. There are broadly three categories of turbine: impulse, reaction and very low head (VLH). Impulse and reaction turbines are used when a significant head of water has been created behind a barrier, therefore being more relevant to conventional hydropower. VLH is typically determined as having a head $H < 3.2\,\mathrm{m}$ [158, 159] and includes turbines which are *in-stream* and effectively 'zero head'. The theoretical power P available for a hydraulic turbine that benefits from a head is given by

$$P = \gamma Q H \tag{2.3}$$

where γ is the specific weight of water ($9{,}800\,\mathrm{N\,m^{-3}}$) and Q is the discharge (volumetric flow rate). As will be shown in Section 4.1, this relationship is derived from a consideration of gravitational potential energy E_p, using the classical equation

$$E_p = MgH \tag{2.4}$$

where M is the mass of water. Given the low head associated with these turbines, it would seem that they offer a less attractive option, when compared to impulse and reaction turbines, and their application in conventional hydropower, as we discussed above. Building upon the general points made in Subsection 2.1.1, though, VLH turbines do offer specific benefits, resulting in distinct advantages, environmentally and financially. For example, Pandey and Karki [130] list reasons why VLH turbines minimise detrimental effects on fish:

- relatively large diameter runner;
- lower speed of the runner;
- smaller pressure gradient between inlet and outlet of the runner;

- lower incidence of cavitation; and,
- smaller sheer stress.

A challenge with VLH projects, dependent upon the site, is that the cost to develop can be too great relative to the power generated [122]. Therefore, design and installation costs must be carefully managed to allow profitability.

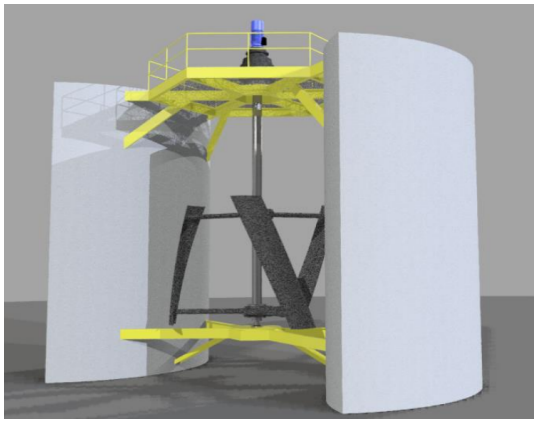

Figure 2.4: Repetitive Energy's 300 kW HEC Large Tidal Turbine can be deployed in a suitably-sized river, or in a tidal stream environment.

Turbines intended for free-flow HEC (e.g. Fig. 2.4) are strictly a subset of VLH turbines and, as such, it is appropriate to class them so. Yet, to be precise, we are interested in this study with turbines specifically intended to be deployed in-stream for the purpose of converting the kinetic energy of free-flowing rivers. The term 'hydrokinetic turbine' is deemed synonymous with many other terms which may be encountered, such as: water current turbine (WCT), ultra-low-head hydro turbine, free flow/stream turbine, zero head hydro turbine, in-stream hydro turbine, tidal in-stream energy converter (TISEC), tidal current turbine, river current turbine (RCT), river current energy conversion system (RCECS), river in-stream energy converter (RISEC), or river turbine. The length of this list demonstrates the usefulness of a catch-all term. Kirke [160] warns of the danger of referring to hydrokinetic turbines as 'zero head' hydro turbines, in what he refers to as the 'zero head myth'. He points out, as others have [161–163], that there is indeed no change in water level, or need for a head, with the use of such turbines. Yet, of course, any movement of water must involve a gradient, strictly speaking, whether river flow or tidal current.

These turbines can be aligned vertically (Fig. 2.5), or horizontally (Fig. 2.6). Although the wind energy industry has effectively discarded vertical axis systems, many hydrokinetic turbines employ this arrangement. There are benefits and limitations associated with vertically aligned turbines and horizontally aligned turbines (Table 2.2), meaning that either may be appropriate according to the criteria stipulated by different scenarios.

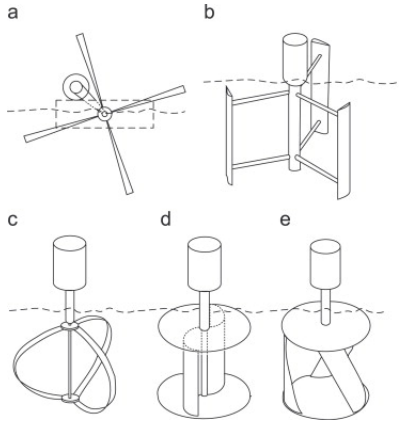

Figure 2.5: Types of vertically-aligned hydrokinetic turbines: (a) in-plane, (b) H–Darrieus, (c) Darrieus, (d) Savonious and (e) helical [122].

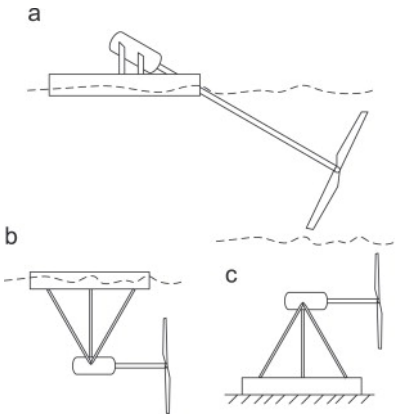

Figure 2.6: Types of horizontal axially-aligned hydrokinetic turbines: (a) inclined axis, (b) float mooring and (c) rigid mooring [122].

Table 2.2: Benefits and limitations of vertically- and axially-aligned hydrokinetic turbines.

Alignment	Benefits	Limitations
Vertical	Design simplicity. Generator coupling. Ease of flotation and augmentation arrangement. Less noise. Suitability for variable vertical velocity profile.	Low starting torque. Torque ripple. Lower efficiency. Poor starting performance.
Axial	Knowledge base. Performance due to taper and twist. Performance with high speed flow. Self-starting.	Difficult blade design. Underwater generator. Underwater cabling.

Hydrokinetic turbine efficiency varies with flow speed. If P is plotted against v (Fig. 2.7), there are three distinct regions.

- Region I: Zero to cut-in speed. The turbine will not rotate. No power is generated. This represents the minimum flow speed required to overcome friction within the turbine and rotate the generator sufficiently to generate power.
- Region II: Cut-in speed to rated speed. Power is generated according to a chain of 'water to wire' conversion factors.
- Region III: Greater than rated speed. The flow speed exceeds the rated speed of the turbine. Power output is constant and corresponds to the turbine's maximum capacity. Since an increase in power will not result from a further increase in the rate of rotation, but may risk damage to the turbine, a method of for preventing the turbines rotation can be employed, e.g. adjusting the pitch of the blades.

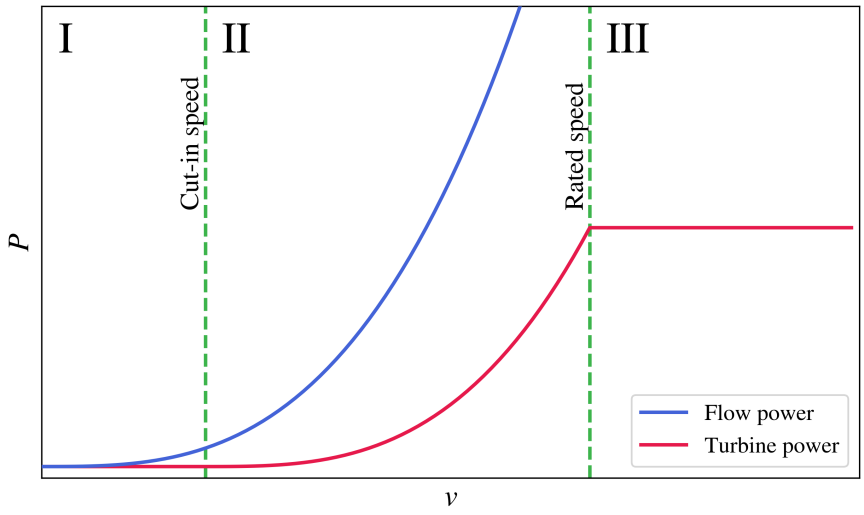

Figure 2.7: Approximate and relative comparison of the power P of flowing water and output by a turbine at different flow speeds v.

A *power curve* (Fig. 2.8) is plotted using empirical measurements of extracted power P_e generated by a turbine, at different flow velocities of the fluid passing across it. The power coefficient C_P is defined as the ratio of P_e to the theoretical power P, as

$$C_P = \frac{P_e}{P} \tag{2.5}$$

Betz's law states that the maximum value for an in-stream turbine's power coefficient is $C_P = 0.593$ [164]. This principle can be applied to all Newtonian fluids, which includes air and water. Therefore, this is relevant for both HEC and wind turbines and dictates an upper limit of efficiency for such devices of ~50 %, when all related factors are accounted for. This is an important limitation of these renewable energy technologies, relative to other forms. Radkey and Hibbs [165] claim that the use of a duct can allow a power coefficient of up to $c_p = 1.69$

to be achieved, with an axial turbine, suggesting this upper limit can potentially be exceeded. This view has been supported by subsequent studies [157, 166].

To derive a means for calculating HEC power, let's first consider that power P is defined as the rate of doing work W in time t,

$$P = \frac{dW}{dt} \tag{2.6}$$

In this case, the work done is by kinetic energy E_k, which is defined, according to the classical equation, as

$$E_k = \frac{1}{2}Mv^2 \tag{2.7}$$

So,

$$P = \frac{\frac{1}{2}Mv^2}{t} \tag{2.8}$$

If considering the mass of fluid that is travelling past the turbine,

$$M = \rho A_D L \tag{2.9}$$

where ρ is the fluid's density, A_D is the cross-sectional area of the sweep of the turbine and L is the length of fluid that moves past the turbine in time t. Substituting for M in Eq. 2.8 gives

$$P = \frac{\frac{1}{2}\rho A_D L v^2}{t} \tag{2.10}$$

Since $\frac{L}{t}$ is equivalent to the flow velocity of the fluid, this means

$$P = \frac{1}{2}\rho A_D v^3 \tag{2.11}$$

This can also be expressed as power density

$$\frac{P}{A_D} = \frac{1}{2}\rho v^3 \tag{2.12}$$

Technical limitations, that result in a turbine generating power below this theoretical calculation, are influenced by the efficiencies of the turbine, the drivetrain, the generator and power conditioning components (e.g. a voltage regulator). The effective power of a turbine, with these efficiency factors taken into account, therefore includes C_P (Eq. (2.5)), becoming

$$P = C_P \frac{1}{2}\rho A_D v^3 \tag{2.13}$$

After this, the cut-in and cut-out speed need to be considered (Fig. 2.7) and, before long, in practice, empirical measurements and the plotting of a power curve (Fig. 2.8) are often more pragmatically useful than a theoretical calculation.

Wind turbines and hydro turbines are similar, in that they are caused to rotate due to a passing fluid, meaning that that they can be compared and contrasted. The technology is essentially the same, though HEC technology is said to be 15–20 years behind the technology of wind power generation [150]. Since the densities of air and water are $\rho_{\text{air}} \approx 1.225\,\text{kg}\,\text{m}^{-3}$ and $\rho_{\text{water}} \approx 1{,}000\,\text{kg}\,\text{m}^{-3}$, the power generated by a hydro turbine would be $\sim$ 800 times that of a wind turbine, given the same flow velocity. For this reason, hydro turbines can produce significant power at relatively low flow velocity, relative to wind turbines. Consequentially, wind turbines are designed to work with flow velocities of $11-13\,\text{m}\,\text{s}^{-1}$, compared to $\sim 2\,\text{m}\,\text{s}^{-1}$ for hydro turbines [122, 167]. This also explains why the area required by a hydro turbine is considerably less than that required for a wind turbine. Yet, Fraenkel [168] highlights how this fact presents a challenge for hydrokinetic turbines, which he believes is limiting development. He states that due to the relatively slow rotation of these types of turbines, to generate comparable power relative to other types of turbine, they must be engineered to withstand substantial torque τ, because

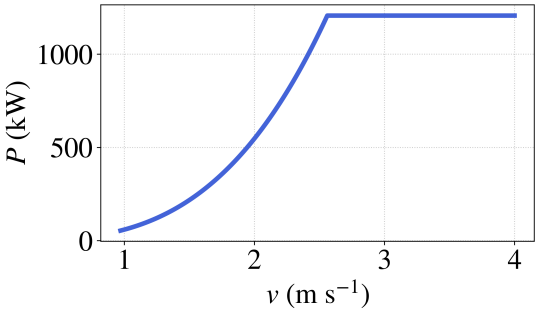

Figure 2.8: An example of a power curve, which plots power P against flow velocity v, using empirical measurements from a turbine. The example is plotted using arbitrary, but representative, data.

$$P = \tau\omega \tag{2.14}$$

where the rate of rotation is represented by the angular frequency ω. Therefore, a low ω means a high τ is needed. This increased engineering requirement causes an associated increase in costs, relative to wind turbines, for example.

Figure 2.9: Repetitive Energy's 100 kW HEC River Array, comprising an array of Smart Stream turbines.

Compared to wind, river flow and particularly tidal stream flow are more predictable, with flow variation in the interval of hours, or days. Flow is unidirectional in a river and bidirectional in a tidal stream (Table 2.1), compared to a much greater variation for wind.

The deployment of more than a single HEC device is known as an *array* (Fig. 2.9). The effect on overall energy production, when deploying turbines in arrays, is more pronounced in hydro turbines than wind turbines [169]. Wind turbines extract energy from a lower boundary layer of the atmosphere and though energy extraction reduces the wind speed immediately behind the turbine, the wind speed re-establishes itself a relatively short distance downwind, with energy replenished from boundary layers above. In contrast, hydro turbines are constrained between the water surface and a river bed, or seabed. Depths are generally far less than the height of the atmosphere. Thus,

energy is more spatially constrained and significant extraction results in a relatively greater affect.

Since each device causes a *backwater effect*, the spacing between each device in the array is an important consideration, which should be optimised to achieve maximum conversion. Two perspectives are relevant: macro- and micro-arrangement [170]. The macro-arrangement considers the total number of devices and the overall layout. The micro-arrangement deals with the factors between pairs of individual devices and rows. Vennell [171] states that the parameters responsible for the performance of an array are: the free-surface effect (clearance ratio), the duct augmentation and the blockage coefficient. The free-surface effect depends upon the affect of the fluid (air) above the surface of the flowing water. Bathymetry may also affect the layout of an array [172]. The blockage coefficient ϵ of a HEC device, or an array of devices, is given by

$$\epsilon = \frac{A_T}{A} \tag{2.15}$$

where A_T is the sum total of the flow-facing area of the moving and non-moving parts of all devices and A is the channel cross-sectional area. If considering an array of devices, the average cross-sectional area is calculated by dividing the volume of the fluid at the site, determined from bathymetry subject to the lowest operational flow, by the length of the project site along the direction of flow. According to the International Electrotechnical Commission (IEC) guidelines [173], a project is considered 'small' if $\epsilon < 0.05$, or 'large' if $\epsilon > 0.05$. The standards proposed by the IEC are discussed further in Subsection 2.2.3.

Without deployment of a device in a channel, this is referred to as the *baseline condition*. Once a device is deployed, this is then defined a *turbine-operated condition*. With the introduction of an obstruction into a channel, the resulting drag force will cause variations in the flow of water and may also lead to sediment deposition and scouring. Changes in flow velocity produce a backwater effect, with a rise in water level observed upstream of the device and a drop in water level downstream. The pattern seen downstream of the device may be referred to as the *wake*. The distance taken by the flow, before the effects from passing a turbine are no longer observed, is known as the *wake-recovery distance*. Knowledge of this parameter is important for determining appropriate spacing of an array of turbines. Other observations which can be relevant include the width of the wake, the profile of the velocity and the turbulence intensity.

With regards to the effect on power extraction from channel blockage, Garrett and Cummins [174, 175] state the ratio of power extraction P_e to power dissipation P_d is given by

$$\frac{P_e}{P_d} = \frac{2}{3(1+\epsilon)} \tag{2.16}$$

2.2 Resource assessment

2.2.1 Site selection

Site selection, for the deployment of renewable energy technology, is determined by a *resource assessment*. This generally includes an assessment of a resource according to three perspectives: theoretical, technical and practical [78, 135, 176, 177]. The first question to address is if

there is enough energy to extract in a cost-effective way. A theoretical resource assessment is a determination of the total annual energy that is hypothetically available. After this, a technical resource assessment calculates the portion of the theoretical amount of energy that can be converted, by a specific technology of interest, into electricity, or other useful form of energy, such as hydrogen (see Subsection 1.1.4).

Following a theoretical and technical resource assessment, a practical resource assessment assesses additional considerations and constraints, including economic, environmental and regulatory. With regards to HEC, the practical factors that may affect, or influence, site selection may include:

- proximity to important infrastructure, such as grid lines, road networks and settlements;
- environmental and socio-economic factors, such as water quality (presence of silt and debris);
- accessibility of the site depending on the terrain characteristics, land ownership, etc.;
- existing electricity availability and price;
- energy demand;
- economic constraints;
- availability of other energy sources; and,
- a host of many other lesser factors.

The interaction of fish and marine mammals has been highlighted as an issue of some importance in previous resource assessments [150], and linked to ecological stewardship, economics, culture and lifestyle factors. Copping et al. [178] considered environmental factors related to the marine environment: blade strikes, noise and effects that result from the extraction of energy affecting the flow. They found, along with other studies [179–182], that HEC has little affect on marine life. Avoidance predominates, but in the few occasions fish have passed through the turbine swept area, survival rates have been >98 % [178, 181, 182].

Installation in some scenarios will require careful review of the effects from debris, sediment, frazil and surface ice. Additional economic factors may include power plant design, size, efficiency and maintenance requirements. The inclusion of any combination of these factors when defining feasibility criteria may further refine the approach. Relevant factors here can be broad, overlapping and open to interpretation.

Considering just the theoretical and technical perspectives, the suitability of a site for HEC depends upon a number of factors, such as fluid dynamics, bathymetry and the stability of high-velocity zones. In rivers, the fluid dynamic factors will include discharge, flow velocity distribution, power density, turbulence and the Froude number. Ideally, these will need considering as a function of position, to allow the determination of local power variations, the total practical power and the available space for placing individual, or arrays of, devices. Beyond this, towards encompassing all practical considerations, it must be remembered that the physical features listed above, that describe a hydrodynamic system, must be accompanied with a consideration of features that describe this system's interaction with external and overlapping systems, which will not be only physical.

In general and stated simply, with regards to rivers, HEC devices are ideally located at locations with relatively steady flow throughout the year, that are not prone to serious flood events, too much turbulence, or extended periods of low water level. Neary and Gunawan [183] identified variables that could influence conditions along the length of a river reach:

- bed sediment, grain and form roughness;
- secondary circulation caused by channel form;
- wind shear on the water surface; and,
- the presence of structures that could create surface wakes, vortex shedding and increased turbulence in the wake.

Varying velocities and water levels mean that the data needed for an assessment of a HEC site is highly site-specific [161]. Pandey and Karki [130] consider description of the following hydrology features relevant as part of a feasibility study for a typical small hydropower plant: the river basin, the catchment area, precipitation, estimate of river discharges and derivation of a flow duration curve (FDC). Apart from the last point, this list contains items that need no further description, for now, but will be further expanded upon in Sections 2.3 and 5.1. To address the last point, an FDC shows the frequency with which discharges of different magnitudes are equalled, or exceeded.

The different values for discharge at a given location, represented by an FDC, show that different discharges vary in frequency. This frequency is a function of the watershed and its hydrologic and physical characteristics. These FDCs provide important information, when determining the feasibility of a location, giving a clear indication of the potential power generation throughout the year. Mean annual discharge generally has a frequency of ~25 % and magnitude of ~40 % of the bankfull[3] cross-sectional area [184].

The shape of the FDC gives an indication of a catchment area's response to precipitation. A steeply sloping curve results from a very variable flow and is usually associated with a small catchment, having much quickflow and little baseflow. In contrast, a very flat curve means that there is little variation in flow, due to damping effects of infilltration and groundwater storage. The FDC for three different locations (Fig. 2.10), using data from the National River Flow Archive [185], can illustrate these differences. Though the FDC of Fig. 2.10(a) shows a higher flow rate than in Fig. 2.10(b), they both show a steep drop from the maximum, with relatively low flow rates for the majority of the period recorded. In contrast, the FDC for Fig. 2.10(c), though having a much larger flow rate anyway, also shows a less steep drop off from the maximum, meaning there will be more consistent power generation throughout the year. In addition, FDC plots can provide developers with information to make informed decisions about whether to select a reduced installed capacity to take advantage of simpler licensing requirements, if doing so can be seen to have little impact on overall power generation.

[3]Bankfull discharge occurs when river flow fills the entire channel. A further increase in discharge will result in flooding.

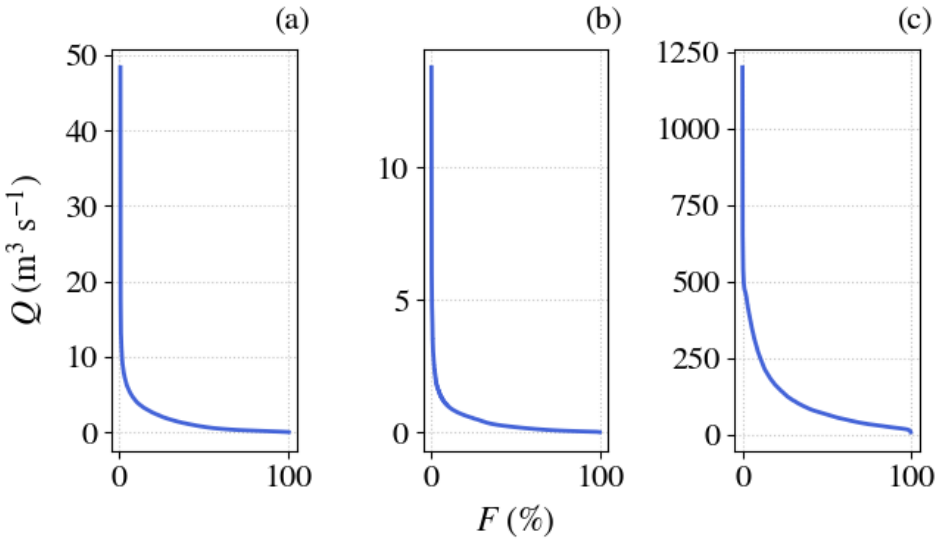

Figure 2.10: Flow duration curves (FDC), until 30 September 2017, for the rivers (a) Abhainn a' Bhealaich, at Braevallich, from 1 October 1981; (b) Cefni, at Bodffordd, from 10 October 1988; and, (c) Severn, at Haw Bridge, from 1 July 1971. In each case, discharge Q is plotted against the exceedence probability F, representing the proportion of time that Q is equalled, or exceeded. Data from the National River Flow Archive [185].

Seasonal variability, or intra-annual variability, is quantified by plotting an FDC for each month. Inter-annual variability is quantified with an FDC for each year. The IEC stipulate that this is the standard when focusing on a theoretical resource assessment, for a particular location [173] (see Subsection 2.2.3).

The steps to compute a FDC:

- Sort and rank-order the discharge data, labelling each position i. Assign 1 to the highest discharge and n to the lowest discharge, assuming n measurements in the record.
- Calculate exceedence probability F for each discharge:

$$F = \frac{i}{n+1} \times 100 \tag{2.17}$$

For a complete resource assessment, thorough and detailed study is required to estimate the theoretical, technical and practical resource, and to select candidates for hydrokinetic project development. Ideally, for an accurate technical resource assessment, the deployment of a single HEC device, or an array of devices, requires characterisation of spatial and temporal variation of the current speed and the turbulence acting on the proposed energy extraction plane (EEP) [4]. This is necessary to determine hydrodynamic forces, array configuration and resulting power estimates over a representative period of record. In addition, this influences design, providing information to aid the determination of structural loading and power capacity.

[4]For a hydrokinetic turbine, this would be the height of the hub.

Increasing the scale of a resource assessment, as is the aim of this study, reduces the extent to which such detail can be realistically considered. This necessitates a requirement to evaluate the cost of this loss of detail, in relation to the potential value that is provided by considering a larger perspective.

2.2.2 Previous hydrokinetic resource assessments

According to Lalander [186], HEC resource assessments have mainly been performed for tidal areas, such studies are minimal and have involved using point measurements. Jacobson et al. [187] state that though there are a number of studies that address the recoverable HEC resource in tidal settings, at the time of their own study (discussed below), they knew of no definitive study published on the recoverable riverine HEC resource other than by Miller et al. [188]. With this focus towards tidal areas, the methodology used in these studies have been geared towards tidal movements of water, using the two criteria of mean maximum spring speed (MMSS) and cross-sectional area of a channel. MMSS is the average maximum velocity during spring tide flow. Velocity is assumed to be sinusoidal and allows a time-series to be created. Using this time-series for velocity v and the equation for theoretical power (Eq. (2.11)) or power density (Eq. (2.12)) provides the means of assessing the theoretical resource by summing the power generated over a year, giving the raw flux of energy over one year through one cross-section.

Gunawan et al. [189] claim that the best practices for tidal energy resource assessments are not well-established and that universal adoption of consistent methods is yet to be realised. Such practices would require consideration of the instruments needed for collecting current speed and turbulence measurements, deployment strategies and methods for post-processing.

Some regional-scale, riverine hydrokinetic resource assessments have relied on gauged river segments alone [187, 188, 190, 191]. Later developments allowed estimation of ungauged river segments, using regionalisation and discharge modelling [137, 192].

A riverine hydrokinetic resource assessment of the continental United States[5], carried out by Jacobson et al. [187], determined that there was a theoretical resource of 1,381 TWh yr^{-1} and a technically recoverable potential for 120 TWh yr^{-1}, which at this time, represented 3 % of the country's usage. This study used $P = \gamma QH$ (Eq. (2.3)) to determine power and described this as the 'standard hydrological equation for determining theoretical hydraulic power'. Only river reaches with a mean discharge $Q > 28\,m^3\,s^{-1}$(1,000 cfs) were included in the assessment. Given these disharge restrictions, intended to exclude reaches which were clearly unfeasible for HEC deployment, it could be argued that this causes the distinction between a theoretical and technical resource assessment to be blurred, somewhat, and that such restrictions might be best left to a purely technical resource assessment.

The HEC-REC hydrologic model [193, 194] (see Subsection 3.1.1) was used to calculate technically recoverable power for a representative range of values for river slope s and Q, according to criteria determined by an expert panel, incorporating constraints based on depth d, v and device spacing. In this way they developed a formula to estimate the recovery factor RF, using

[5]To be clear, the authors state that this resource assessment covered the contiguous 48 states and Alaska, excluding tidal waters.

$$RF = \begin{cases} \frac{0.002647(Q-200)^{0.3426}}{\sqrt{62.4277s^2}} e^{\frac{-(\log(s)-1.498)^2}{19.87}} & \text{if } Q > 200\,\mathrm{m^3\,s^{-1}} \\ 0 & \text{if } Q \leq 200\,\mathrm{m^3\,s^{-1}} \end{cases} \tag{2.18}$$

The product of RF and the theoretical resource provided the technical resource for each reach. The expert panel advised that minimum values of $v \geq 0.5\,\mathrm{m\,s^{-1}}$ and $d \geq 2\,\mathrm{m}$ be set, for $Q = Q_5$ (5th percentile). A simplified 'V' shaped cross-section geometry was assumed. Device efficiency was considered by assuming a power coefficient $C_P = 0.30$.

A rule-of-thumb device spacing was used, based upon a deployment in rows. If D is the device diameter, then the rows would be $10D$ apart, with a separation of $2D$ within the rows. It was determined that $D = 0.8d$ at Q_5.

To represent HEC devices within HEC-RAS, in place of the Manning roughness factor n (see Subsection 4.2.1), an effective roughness n_t was calculated to account for the backwater effects of device deployment. Based on research by Kartezhnikova and Ravens [195], this was calculated using

$$n_t = n(b^{1/3} - 0.28263b^{-1/3} + 0.139296)^{5/3} \tag{2.19}$$

where

$$b = 0.46088a + \sqrt{(0.46088a + 0.68368)^2 + 0.022578} + 0.68368 \tag{2.20}$$

and

$$a = \frac{3}{4} \cdot \frac{C_p(1+\epsilon)}{n^2 g} \cdot \frac{NA_D}{wL} \cdot d^{1/3} \tag{2.21}$$

where N is the number of devices in the section of river under consideration and w is the width of the river. An initial value of $n = 0.03\,\mathrm{s\,m^{-1/3}}$ was universally applied, before calculating n_t. The recovery factor was seen to decrease with increasing discharge.

Jacobson et al. [187] state that validation of their hydrokinetic resource assessment was difficult, due to the lack of empirical data from existing HEC deployments. In fact they stated that they knew of no direct measurements of in-stream energy that could be used to validate their model, at that time. This can be attributed to both a lack of projects and also a reluctance to publish device data. Unfortunately, this state of affairs has not improved at the time of writing and has provided a challenge to this study.

Miller et al. [188] carried out an earlier study to assess the riverine hydrokinetic resource of the United States. The study determined the river reaches with the most potential, in 12 of 16 hydraulic regions, chosen using a criteria for including the region if mean discharge $Q > 113\,\mathrm{m^3\,s^{-1}}$(4,000 cfs) and mean flow velocity $v > 1.3\,\mathrm{m\,s^{-1}}$(4.3 fps). An inconsistent criteria was used across these regions, but river reaches identified as having the greatest potential were assessed for recoverable power. An estimate was achieved by:

- assuming turbine array deployment over 25 % of the width and 25 % of the length that met a minimum discharge criteria;
- with a turbine spacing of half a turbine diameter in each row and 5 turbine diameters spacing between the rows;

- where the turbine diameter is 80 % of the mean depth; and,
- the power coefficient $C_p = 0.40$.

This method resulted in an aggregate mean annual power of 12,500 MW, yielding 110 TWh yr^{-1}.

Studies have also been carried out in Canada [190, 196]. UMA Group [190] only assessed the hydrokinetic potential of certain rivers in Canada, that met the minimum criteria of $Q > 450\,m^3\,s^{-1}$, $v > 1.5\,m\,s^{-1}$, $w > 50\,m$ and $d > 3\,m$. This study included assumptions of uniformity along very long reaches (100s of kilometers). Both studies used the Manning formula (Eq. (4.17), defined in Subsection 4.2.1). Data was obtained from topographic maps and HYDAT, an archival database of daily and monthly means of flow, water levels and sediment concentrations across Canada [197].

2.2.3 Resource assessment standards

In their review of riverine hydrokinetic resource assessments, Kirby et al. [177] found that the methodology applied to site-specific assessments were not entirely consistent, with the most common discrepancies being the characterisation of discharge variability, calculation of uncertainty and the quantity of data collected to derive results. Further, they state that these issues are amplified for regional-scale, or larger-scale, resource assessments. Generally, smaller-scale resource assessments will involve either:

- a single potential deployment location;
- a single reach with several potential deployment locations; or,
- the assessment of several reaches, in close proximity.

Due to this reduced scale, there is more of an opportunity to collect high resolution spatial and temporal data, which contributes to the possibility of more precise and accurate results. The aim of this study is to assess the hydrokinetic resource on a global-scale. This implies an acceptance of reduced resolution, as scale is increased. In acceptance of the differences between these extremes, with site-specific at one end of the spectrum and global-scale at the other, and in acknowledging the constraints imposed by an effort to attain a larger-scale perspective, it is still useful to consider the efforts to standardise hydrokinetic resource assessment at the site-specific scale. It is important to state, as is confirmed by Kirby et al. [177], that there are no published standards, specifications, or rules-of-thumb for large-scale riverine hydrokinetic resource assessment (apart from, now, the proposed methodology of Ridgill et al. [137, 138], which forms part of this study and is described in Chapters 3 and 4) and that site-specific methods cannot feasibly be replicated in large-scale assessments.

The IEC is a worldwide organisation for standardisation, comprising all national electrotechnical committees (IEC National Committees). Their stated aim is to promote international co-operation on all questions concerning standardisation in the electrical and electronic fields [173]. The IEC publishes International Standards, Technical Specifications, Technical Reports, Publicly Available Specifications (PAS) and Guides, that are collectively referred to as 'IEC Publication(s)'. The preparation of IEC Publications is carried out by technical committees, who collaborate with any IEC National Committees interested in the subject dealt with

and liaise with international, governmental and non-governmental organisations. IEC collaborates closely with the International Organisation for Standardisation (ISO) in accordance with conditions determined by agreement between the two organisations.

The IEC has produced guidance and a model for standardisation in carrying out a theoretical resource assessment for HEC [173]. The purpose of this technical report is to provide a uniform methodology that will ensure consistency and accuracy in the estimation, measurement, characterisation and analysis of HEC in a riverine context (Fig. 2.11). Furthermore, it defines a standardised methodology with which the resource can be described and reported. This can be undertaken as part of a feasibility study, or a full study: the difference is based upon the amount of information that is available for the devices to be employed. In a comment on the inconsistencies of site-specific hydrokinetic resource assessments, with specific reference to how they differ from the IEC standards, Kirby et al. [177] determine that the most common aspects of divergence are the capturing of the variability of discharge, calibration of models used and validation of these models.

Specifically, for a full study, as informed by the IEC, it is required that the information for a HEC device includes:

- dimensions including position in the water column and swept area;
- a power curve with specified free-stream measurement location;
- operational range; and,
- thrust coefficient, for projects that include modelling energy extraction by the device.

For the feasibility study, they state, a generic HEC device is chosen and all supporting device data shall be presented with justification in any report. The power and thrust coefficient shall be defined as a range and therefore the feasibility study will result in an annual energy production (AEP) range, as described below.

The technical report explicitly excludes:

- practical resource assessment;
- resource characterisation;
- power performance assessment of devices; and,
- environmental impact studies, or similar assessments.

According to this guidance, an energy resource should be defined by velocity duration curves (VDCs), which can be used to determine the AEPs for individual, or arrays of, energy conversion devices.

There is no required methodology for identifying particular project locations. The technical specifications assume that a project location has already been identified (arguably, defining the gap in knowledge that this study aims to fill). However, it is stated that some or all of the methods outlined may be used to assist with project-location identification.

A VDC, similar to a FDC (see Subsection 2.2.1), quantifies the percentage of time that v exceeds a particular value. A key difference between the two is that an FDC is representative of

a river reach, whereas a VDC is location-specific, within a reach or cross-section. This accounts for the greater spatial variability of v within a river reach, compared to Q.

The method for developing a VDC is similar to that described earlier for a FDC, if sufficient data for v is available for a given location. Acceptable methods are applicable, in a scenario where there is sufficient data for Q but not for v, that use measurements of v taken over a shorter period. These methods will differ according to whether values for v were obtained by a direct-measurement, or measurements-only, technique. Either way, this involves a transfer function that relates Q to v, for a given exceedance probability.

If using the direct-measurement technique, corresponding values for v and Q can be paired according to time of measurement. This allows v to be plotted against Q such that a relationship can be determined by regression. It is recommended that at least 5 pairs are used and that, rather than equally spaced, pairings should provide increased resolution for higher values of Q [173]. Further, measurements of v should be representative of the full operational range of a potential device, from cut-in to cut-out speeds (Fig. 2.7).

The measurements-only technique is derived from the *index velocity method*, which provides a way to determine Q based upon the assumption that there is a relationship between the mean velocity of a cross-section and the local velocity at a specific location within this cross-section, using

$$Q(d, v_i) = A(d)v(v_i) \tag{2.22}$$

where Q, A and v are shown to be functions of the mean depth d and v_i. Indicative of the name of this method, v_i is the flow velocity of the i^{th} bin of the VDC. The index velocity method for computing Q has become increasingly common since the emergence of low-cost acoustic Doppler current profilers (ADCPs). In this case, the method is inverted to allow a calculation of a local velocity. This has the advantage of being applicable to many locations, once relationships are established.

According to the IEC, a hydrological model-based VDC can be produced for a specific location, but should be validated using direct measurements. Also, a river energy resource should be defined by a VDC, which can be used to determine the AEP for individual, or arrays of, energy conversion devices [173].

The AEP of an energy conversion device quantifies the average energy yield that is predicted over the period of a year. This is usually expressed with the units $\text{MWh}\,\text{yr}^{-1}$, or $\text{GWh}\,\text{yr}^{-1}$. Since it is a measure of energy conversion over a given time, it can also be considered the average annual power and can therefore be converted and expressed using kW,MW, or GW.

For HEC devices, AEP is calculated by combining VDC and device-specific performance power curves (Fig. 2.8). In accordance with standardised guidelines for resource assessment [173], the energy production EP of a device is estimated using

$$EP = N_h \sum_{i=1}^{N_B} P_i(v_i)B_i \tag{2.23}$$

where N_h is the number of hours in a year, or other period of interest; N_B is the total number of flow velocity bins in the VDC; $P_i(v_i)$ is the power provided by the device-specific performance power curve, associated with the i^{th} flow velocity bin of the VDC; and, B_i is the width of the i^{th} bin for the VDC, given as a decimal probability.

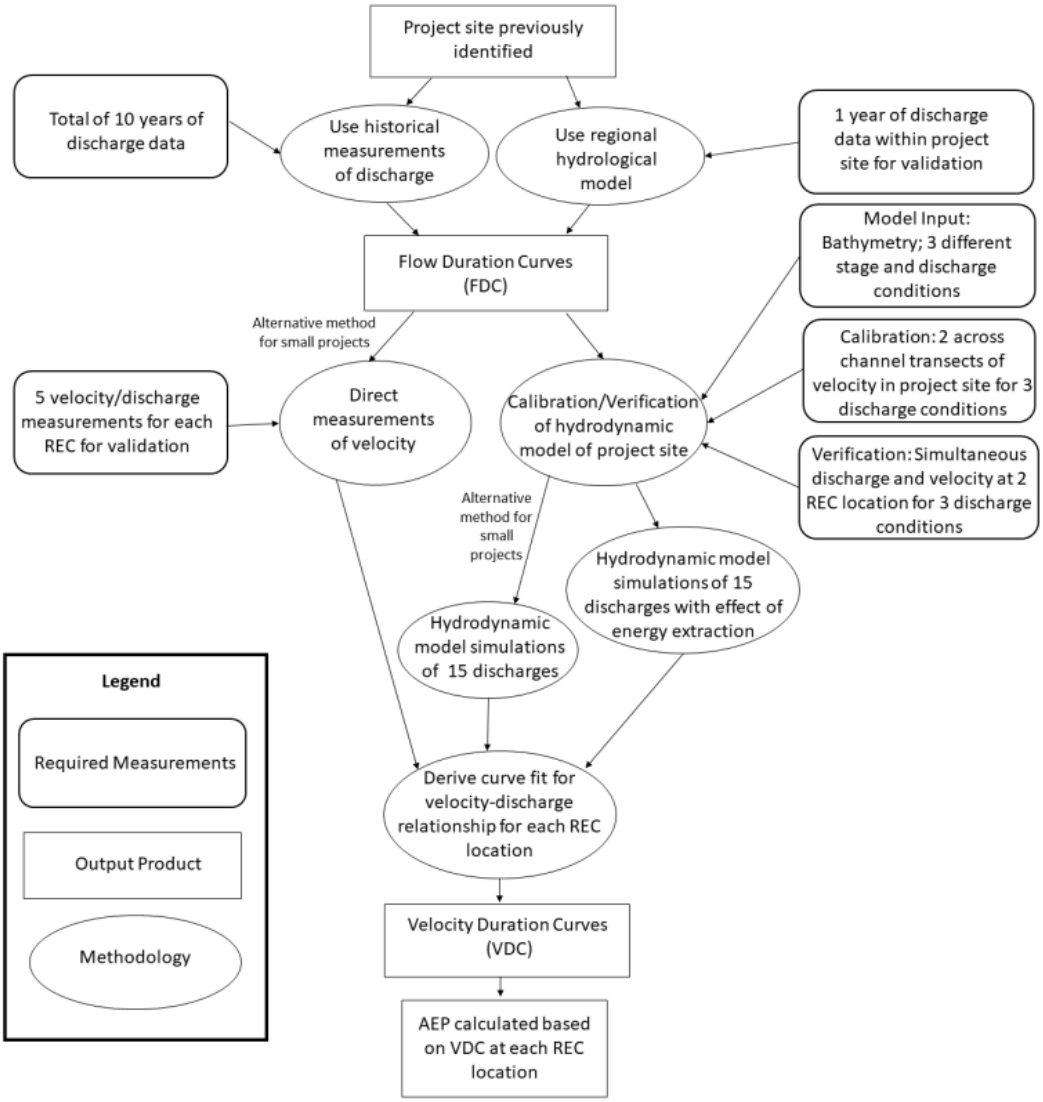

Figure 2.11: Flowchart outlining the methodology for a resource assessment, according to the International Electrotechnical Commission [173]. Here, REC refers to river energy conversion and is synonymous with hydrokinetic energy conversion (HEC).

To ensure adequate reliability and stationarity[6] of the FDC, which is also required (Fig. 2.11), a significant quantity of either measured, or model-generated, discharge data is required. Neary and Gunawan [183] developed a manual of best practice, outlining methods for the collection of field measurment data, specifically for the assessment of site-specific hydrokinetic resource assessment. It is stipulated that at least 10 of the previous 15 years of discharge data should be used to form an FDC. If this is not available, regional hydrological modelling provides an alternative. In this case, at least 10 years of data should be developed and validated with at least 1 year of discharge measurements. The period of 10 years is said to be sufficient to take into account impacts such as the El Niño Southern Oscillation.

In relation to the Froude number (see Subsection 2.3.2), the technical report states that

[6]A stationarity time series is one whose statistical properties are all constant over time.

installation in super-critical flow ($Fr > 1$) is feasible, but would be most feasible for 'small-scale' devices. This is due to the implication that such conditions are shallow, highly localised and having a high-velocity flow.

Again, though the IEC provides guidelines for location-specific hydrokinetic resource assessment, they state that there is no required methodology for identifying particular project locations. In this regard, remote sensing may offer the means to assess many locations, over a large area.

2.2.4 Remote sensing

Remote sensing refers to the use of satellite sensors, aircraft sensors and sensors mounted on land-, or sea-based platforms. If the sensor emits a signal which is reflected and then measured, this is categorised as *active* remote sensing. Otherwise, the sensor measures externally sourced signals, such as solar radiation reflected from the area of investigation and is referred to as *passive* remote sensing. Advances over the past two decades have permitted fast, precise and effective acquisition of topographic information of high quality [198].

Spatial data analysis (SDA) can be defined as a set of techniques devised for the manipulation of data whose outcomes are not invariant under relocation of the objects of interest in some space [199]. This definition purposely includes the possibility to apply SDA to data arrayed in any space, but it is geographical space that is most common. Geographical information systems (GIS) utilise the storage of databases and geospatial data to represent and characterise the earth's surface, enabling an understanding of geomorphology. This reveals the spatial, temporal and thematic relationships between processes, materials, landforms and controlling factors: both natural and anthropologic. SDA and GIS techniques can be combined to provide representation, visualisation, analysis and comprehension of geomorphological phenomena [200].

Advantages of using SDA, GIS, remote sensing or modelled data (see Section 3.1.1), compared to *in situ* surveys, include:

- a reduction in costs and time per location assessed;
- an increase in the number of potential locations that can be assessed; and,
- ease with which locations within challenging terrain and remote regions can be assessed.

This last point is particularly relevant, since high potential sites are often located in remote, inaccessible mountainous areas with rough terrain.

Though expensive and logistically challenging, true characterisation of a resource and validation of numerical simulations requires direct observation, to allow accurate quantification at high temporal and spatial resolution [78]. This can be achieved *in situ* or remotely, but consideration must be made of the difference in accuracy that may result between these methods. For example, an *in situ* resource assessment of the East River tidal strait, near Roosevelt Island, in New York, Gunawan et al. [189] determined a theoretical power density, derived from direct current speed measurements. When compared with values reported by previous national resource assessments [201, 202], arrived at through remote methods, the *in situ* values were found to be one order of magnitude greater. Though national-, regional-, or global-scale resource assessments are useful for identifying potential locations, it is necessary to remember that this may miss small 'hot spots' that could be viable. For this reason, remote methods are

suitable for the inception phase of a project, or as part of a feasibility study. This does not remove the necessity for field work. The aim is to identify potential sites that may justify further, more focused, investigation.

Remote sensing data can be used to obtain almost any information that is typically available from maps [5]. With regards to hydrology, which is relevant in this study, this traditionally included low resolution and coarse data related to drainage basin area and the drainage network. Recent advancements in theory and algorithms have enhanced the ability to measure the hydraulic parameters of rivers from space. A better understanding of rivers at the continental- and global-scale has followed from studies that have used remote sensing data:

- to trace river networks [203–207];
- extract basin and floodplain parameters and features [208, 209];
- map the extent of flooding and flood risk [210–212];
- estimate discharge [213–219];
- estimate river channel parameters [206, 220, 221]; and,
- describe the relationship between width, slope catchment area, meander wavelength, sinuosity and discharge [222].

Such studies have contributed to the creation of data sets describing these features at a large-scale (see Subsection 3.1.2). To understand natural river flow requires an understanding of the complex, spatiotemporal fluctuations of a number of variables. This implies an acceptance of reduced resolution as scale increases. The usefulness of global river databases for the purpose of large-scale hydrokinetic resource assessment has been questioned by some, highlighting the need for a development of methods for database analysis [122, 161]. Prior to the Surface Water Ocean Topography (SWOT) mission (originally expected to launch in 2021 [223], but now delayed), large-scale hydrological models are currently considered the best method for understanding continental- to global-scale hydrological features, at sub-monthly time-steps [224]. Though the direct measurements of SWOT will provide an improvement in observations, there will still remain spatiotemporal gaps. Therefore, an integration of SWOT measurements with existing models offers an opportunity to better develop our understanding of large-scale hydrological systems; and *vice versa*, since the SWOT mission uncertainties and river detection limits are often defined as functions of channel width [225–227].

The SWOT mission is jointly developed by the National Aeronautics and Space Administration (NASA) and Centre National d'Études Spatiales (CNES), in partnership with Canadian Space Agency (CSA) and UK Space Agency (UKSA) [223]. Included within the mission's scientific objectives is the intention to collect data to enable the production of a water mask able to resolve 100 m wide rivers and 250 m^2 lakes and reservoirs. This mask will include water level elevations of an accuracy of 0.10 m and a slope accuracy of 0.01 m km^{-1}.

A number of methods for determining river width using remote sensing have been developed [205, 221, 228–239]. RivWidthCloud is a Google Earth Engine (GEE)-based river width algorithm that extracts river centerlines and widths from remotely sensed images [221]. It has thus far been implemented using products from the Landsat program, but will work, in principle, with any remote sensing product capable of providing classifications of water and

visual obstructions, such as cloud, snow and ice. Clouds cover ~67 % of the earth's surface at any given time [240]. RivWidthCloud addresses the limitations of previous attempts to extract river widths, using remote sensing, that have suffered from the problem of this cloud coverage [205, 228, 234–239]. The ability to identify visual obstructions and having access to the vast number of images (for every location and over a number of years) made possible by using GEE, provides RivWidthCloud with the ability to overcome this problem of cloud cover. Another advantage over previous river width measuring algorithms is that it runs on GEE itself, which is a popular cloud computing environment. There are three steps in RivWidthCloud's process:

1. extract a river mask from a satellite image;

2. derive a river centerline from the river mask; and,

3. measure river width along the centerline.

Validation of river widths calculated by RivWidthCloud was carried out against *in situ* measurments by the United States Geological Survey and the Water Survey of Canada [221]. The period of 1984–2018 was considered and 1,514 widths from Landsat images were compared with an equal number of same-day *in situ* measurements, from 519 stations located across the US and Canada. Calculated widths were found to closely match *in situ* measurments (root mean square error (RMSE) = 99.2 m; mean absolute error (MAE) = 43.1 m; mean bias = −20 m).

Sampson et al. [241] have highlighted the difficulties of remotely determining river depth and state that it is not yet possible to measure this remotely on large scales. In the future, the SWOT mission may enable estimates of river depth by satellite [177, 223]. Since $Q = wdv$ (Eq. (2.30)), and given the progress made in remotely measuring w, a corresponding improvement of techniques to determine d, in combination with data sets for Q, such as the one used in this study (see Chapter 3), would permit a better estimate of v, which is probably the most challenging of these variables to determine remotely. Development of techniques for estimation of the bathymetry in cross-sections, that require less data, could also be applied [242].

The geometry of unsurveyed rivers can be approximated using historical stage-discharge data, if available, or with bankfull width, as determined by remote sensing, in combination with hydraulic geometry relationships (see Section 4.2). As will be explained in Subsection 2.3.2, the measurement of Q is considered of fundamental importance and usefulness in fluvial geomorphology. Though satellite-based measurements of Q will never achieve the accuracy, or precision, of ground-based gauge measurements, Smith and Pavelsky [243] suggest that the real power of such measurements is in allowing a consideration of remote river systems, or in providing a spatial view between existing point-based measurements. In contrast to the sparse spatial coverage of river gauge measurements — which for much of the world are rare, non-existent, or propriety — satellites provide spatially dense coverage, globally. Gleason and Smith [217] have demonstrated that useful estimates of Q may be derived solely from satellite images, with no *in situ* measurements, calibrated hydrological models, or other a priori information. Their method uses what they have defined at-many-stations hydraulic geometry, after finding that the paired coefficients and exponents of at-a-station hydraulic geometry relationships along a river exhibit very strong semi-log relationships. They demonstrate that this approach effectively halves the number of parameters required by traditional hydraulic geometry. These concepts will be described more thoroughly in Subsection 4.2.2.

2.2.5 Digital elevation models

Using laser and wavelengths corresponding to ultraviolet, visible, or near infrared, Lidar is a surveying method that allows the construction of 3D representations by measuring reflected pulses. It can target a wide range of materials and, in the extreme, can be operated with a high enough resolution to distinguish single molecules [244]. Mounted on an aircraft, narrow laser beams can be used to map terrain with a resolution of 0.30 m [245]. Lidar is considered highly accurate in measuring elevation, with a typical spatial resolution of 2 m and an average RMSE of 0.5 m, in the horizontal and vertical direction [246]. Lidar delivers a massive point cloud filled of varying elevation values, after the transmitted light is reflected by the ground. The height can come from the top of buildings, tree canopies, power lines, or many other features, and the signal will be reflected by both the tree canopy and the floor below. Multiple reflections can be used to aid constructing a digital surface model (DSM), or digital terrain model (DTM). A DSM captures the natural and built features on a planet's surface (Fig. 2.12). In this way, it measures the earth's surface height, including any surface objects (e.g. buildings, tree canopies, etc.). Therefore, DSMs do not represent the bare surface, as a DTM does.

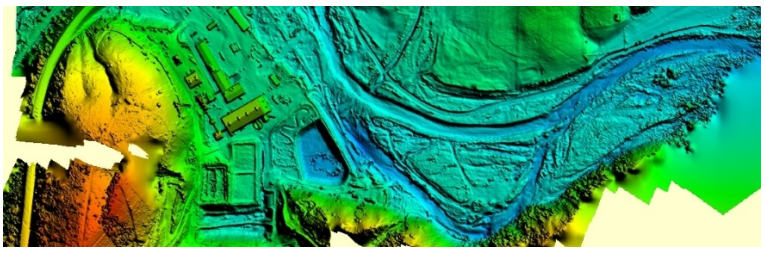

Figure 2.12: Digital surface model of the West Fork Mine, Missouri [247].

A DTM is a model in which terrain data has been further enhanced with an interpretation of the features on the ground, creating greater accuracy as it contains additional information, defining terrain in areas where Lidar data alone is unable to do the job effectively (Fig. 2.13).

Sofia et al. [233] consider the application of Lidar in obtaining topographical features to allow the automatic characterisation of reach-scale river widths. They point out that previous studies have demonstrated that physical processes and anthropogenic activities can leave important signatures in the statistics of morphological parameters derived from DTMs [248–257].

DTMs and DSMs are a subset of what is more broadly termed digital elevation models (DEMs). As a definition, DEMs provide an approximation of the true terrain surface that provides a 3D representation of a planet's topography. Weibel and Heller [258] consider DEMs to be '2.5D', rather than truly 3D, since they usually assign a single height value to each 2D point and cannot describe vertical terrain features, such as a cliff. They also suggest that they can be classified into two types: raster-based, or vector-based.

There are three sources of DEM data: ground survey techniques, topographic maps and remote sensing [259]. For remote sensing, three different methods are used: radar interferometry, stereophotogrammetry and Lidar. Radar interferometry describes various forms of spaceborne measurement, with the other two being airborne measurements. More accurate airborne measurements (<10 m horizontal resolution) are often available for developed regions of the world, with the rest of the globe covered by spaceborne measurements, which include non-negligible

vertical height errors. Freely available airborne DEMs are only available for ~0.005 % of the Earth's land surface [260].

Figure 2.13: Digital terrain model of Mina, in Saudi Arabia, illustrating road and building interpretation [261].

In relation to methods of measuring w, Allen and Pavelsky [206] found that conventional DEM-derived width data sets underestimate the abundance of wide rivers. DEMs suffers from systematic and random errors caused by the processes involved in digital terrain modelling and DEM uncertainty analysis is a field of study that has been identified as providing many challenges. Some have stated that these challenges are often under-considered [246, 262]. Errors associated with DEMs are caused by absolute bias [263], stripe noise [264–266], speckled noise [263, 267] and tree height bias [268]. Each of these errors, apart from tree height bias, can be classified by spatial scale (Table 2.3). Vertical height errors can be as large as 10 m [207]. Others have classified these errors into three groups: artefacts, blunders or gross errors; random errors, or noise; and, systematic errors [269, 270].

Table 2.3: Classification of DEM errors according to spatial scale.

Error	Wavelength	Approximate Scale
Absolute bias	Long	Few pixels
Stripe noise	Medium	0.5 km to 50 km
Speckled noise	Short	>20 km

Hebeler and Purves [271], based on a model of uncertainty coupled with a Monte Carlo simulation, found that watershed related features can vary significantly due to uncertainty and listed a number of topographical variables as a cause for this, including roughness, aspect, minimum extremity and mean extremity.

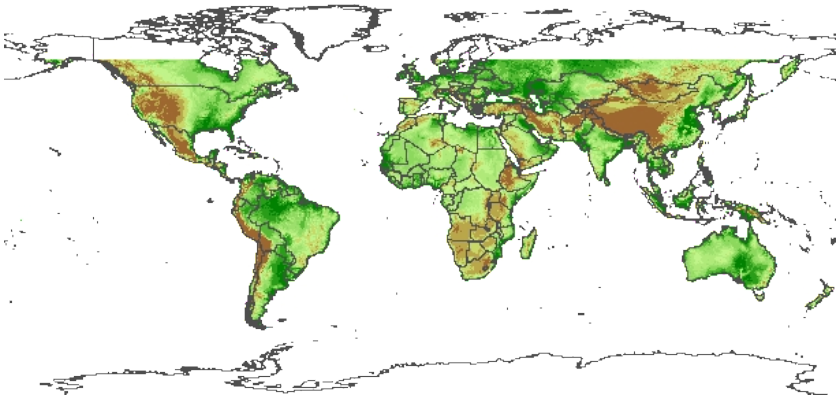

Figure 2.14: Extent of the Shuttle Radar Topography Mission (SRTM) elevation data [272].

The Shuttle Radar Topography Mission (SRTM) was the primary objective of Space Shuttle Endeavour's 11 day mission (STS-99) of February 2000 [273]. Elevation data for 80 % of the earth's surface was obtained, from 56°S to 60°N (Fig. 2.14), by reflecting interferometric synthetic aperture radar (SAR) off of the earth and measuring the reception of a back-scattered radar signal at the shuttle [274]. Fig. 2.15 illustrates an example of a high resolution topographic map that can be created from this data. NASA's initial release of data, in 2003, provided high resolution of 30 m (1 ″) for the United States and a lower resolution of 90 m (3 ″) for the rest of the world, within the region measured [272]. In 2014, it was announced that the high resolution data for the rest of the world be released [272].

The Advanced Spaceborne Thermal Emission and Reflection Radiometer Global Digital Elevation Model (ASTER GDEM) was intended to be an improvement on SRTM. The first version (GDEMv1) was released in June 2009 [275]. It covered the planet from 83°N to 83°S, surpassing SRTM's coverage of 56°S to 60°N, encompassing 99 % of the earth's landmass (Fig 2.16), becoming the first global-scale mapping system that provided comprehensive coverage of the polar regions. The second version (GDEMv2) was released in October 2011 [275], with the intention of enhancing coverage. Refined algorithms provided increased spatial resolution and higher accuracy in the horizontal and vertical planes. Water body coverage and detection was also improved. Chirico et al. [275] report that there are inconsistencies in the supposed improvement from version 1 to 2, revealing complex interactions between terrain and land cover characteristics. Consensus seems to be split upon the relative merits of SRTM and ASTER GDEM, with each appearing to offer benefits and limitations in different contexts and scenarios. ASTER GDEM has received unfavourable assessments of accuracy [276, 277].

Figure 2.15: High resloution topographic map of Africa from the Shuttle Radar Topography Mission (SRTM) [278].

Multi-Error-Removed-Improved-Terrain Digital Elevation Model (MERIT DEM) is also based upon improvements to the elevation measurements made by the SRTM. It increased the percentage of land areas mapped with a vertical accuracy of ±2 m from 39 % to 58 %, after the application of a global-scale algorithm to remove absolute bias, stripe noise, speckled noise and tree height bias [279]. This allowed clearer representations of hill and valley structure and therefore river networks. Flat regions, where errors were previously greater than topographical variability, saw significant improvement, providing a reduction in the distortions of many major floodplains (e.g., Ganges, Nile, Niger and Mekong) and swamp forests (e.g., Amazon, Congo and Vasyugan). A number of studies have found MERIT DEM to be a significant improvement over SRTM [280–282].

Analysis by Yamazaki et al. [279] suggests that the accuracy of MERIT DEM is relatively low in mountainous areas, where sub-pixel topography variability is large. SRTM accuracy had previously been identified to be low in mountainous areas [283].

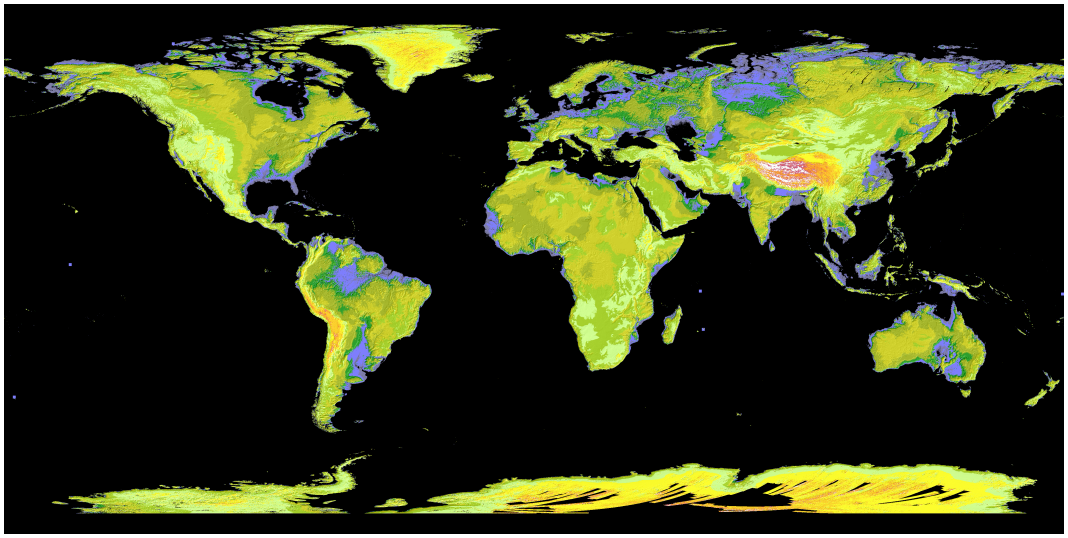

Figure 2.16: Coverage of 99 % of the Earth's landmass, using GDEMv1 [284].

Comparable to MERIT DEM, TerraSAR-X add-on for Digital Elevation Measurements at 90 m resolution (TanDEM-X 90) was made freely available following the TanDEM-X mission [285–287] and created from averaging the more accurate, commercially available TerraSAR-X add-on for Digital Elevation Measurements at 12 m resolution (TanDEM-X 12 DEM). The stated 90 m resolution of TanDEM-X 90 is an approximation and more easily understood description of the actual resolution of 3″. In contrast, TanDEM-X 12 has a resolution of 0.4″ (~12 m).

The mission had the goal of giving a vertical accuracy such that the absolute geolocation accuracy would give a linear error at the 90th percentile (LE90) of 10 m and a 2 m relative vertical accuracy for slopes <20 %, or 4 m for slopes >40 % [288]. Absolute geolocation accuracy is a measure of the determination of a target object, as provided by a model or instrument, relative to its true location. Geolocation accuracy is specified according to the circular error at the 90th percentile (CE90) and LE90 standards. In an assessment following the mission, the LE90 has been reported as 3.49 m globally, or 0.88 m if forested or ice areas are not considered [287]. For the relative vertical accuracy, Wessel et al. [289] report a global RMSE of 1.29 m, or values for areas of short vegetation, developed vegetation and forests of 1.1 m, 1.4 m and 1.8 m, respectively. Gonzalez and Rizzoli [290] used height error maps and reported a global value of 1.25 m.

Hawker et al. [282] characterised the vertical height errors of MERIT DEM and TanDEM-X 90 by comparison against a high resolution Lidar DEM for 32 floodplain locations, in 6 continents. The authors state that these two global-scale DEMs were considered due to them being regarded as the most accurate of the freely available DEMs, of this type. Each were found to be similarly accurate and a significant improvement on the SRTM DEM that had previously been considered the benchmark.

Hawker et al. [282] found TanDEM-X 90 to be the most accurate freely available global DEM for all of the land cover categories they tested[7], apart from short vegetation and tree-covered areas, where MERIT DEM was more accurate. They suggest that TanDEM-X 90,

[7]Land cover categories tested included bare, short vegetation, shrub-covered, sparse vegetation, tree-covered and urban.

alongside MERIT DEM, could be considered the benchmark global DEM in floodplains, for flood-risk application. Previous to this study, error assessment of TanDEM-X had only been carried out on non-freely available TanDEM-X 12 [285, 287].

In their review of TanDEM-X 90 and MERIT DEM, Hawker et al. [282] identify the problems with SRTM as: lack of coverage at high latitudes, presence of voids and non-negligible vertical areas. They conclude that both TanDEM-X 90 and MERIT DEM demonstrate a similar accuracy and significant improvement on SRTM with regards to these problems.

2.3 Fluvial processes

2.3.1 Fluvial geomorphology

Huggett [291] states that the field of geomorphology aims to investigate the interrelationship between form and processes, where form is considered according to constitution, configuration, or mass flow. Processes are carried out and observed through measurement of physical variables, such as energy, or power. In turn, this geomorphic *system* interacts, in the long-term, with geological forms and processes; and, in the short-term, with the biosphere (including humans) and the fluid systems of the atmosphere and the hydrosphere. Therefore, this summarises the full spectrum of available features for consideration, in attempting to develop a methodology for large-scale hydrokinetic resource assessment. The next task will be to identify which of these are most useful.

Viewing geomorpholgy in terms of it acting as a system means that a *systems approach* [292] might be appropriate for consideration. This idea, in relation to geomorphology, was first proposed by Chorley and Kennedy [293] and later adopted and adapted by Strahler [294]. There are three types of system: open, closed and isolated (Table 2.4). Geomorphic systems are open, since both mass and energy may be transferred between the system and surroundings. Furthermore, they are dissipative systems, because they involve irreversible processes that result in the dissipation of energy. For this reason, external sources of energy, such as from solar radiation, are required to maintain them. If treated as an open system, consideration can then be given to internal and external variables. For example, a drainage basin will be influenced by external variables, such as precipitation, and possess internal variables, such as volumetric flow.

Table 2.4: Description of the three types of system.

System	Description
Open	Mass and energy both may be transferred between the system and surroundings.
Closed	Energy may be transferred between the system and surroundings, but not mass.
Isolated	Neither mass, nor energy may be transferred between the system and the surroundings.

As we move to focus more upon the geomorphological elements related to rivers, we are now operating within the subdomain of *fluvial* geomorphology. Water is constantly circulating between Earth's surface and the atmosphere, as part of the water cycle. Conveying water from

land to the ocean, rivers are an important component of the hydrologic cycle. As a result of this process, groundwater storage is replenished, fresh water is made available for human use and a means for transport is provided.

Free-flowing rivers are considered to be the freshwater equivalent of wilderness areas and are defined by being unaffected by anthropogenic impact, such as from the construction of dams within the river, or roads, buildings and agricultural development alongside. When free-flowing, the movement of water, silt and river life can move unobstructed and hydrokinetic energy is available for conversion. The Free-flowing River Assessment (FRA) indicates a global view of the world's rivers and an indication of their status as a free-flowing river [295].

The removal of water from a river is known as *abstraction*. This water may be required for drinking, irrigation, or industrial use. Other human impacts, include:

- removal of sand and gravel for building materials;
- discharging sewage, wastewater or unwanted industrial material;
- recreation;
- fishing;
- transportation; and,
- extraction of energy.

Aside from defining *what* rivers are and *why* they are important, fluvial geomorphologists are concerned with *how* rivers respond to this throughput of water. Fluvial environments arise due to the movement of water as surface runoff and streamflow. Surface runoff is the flow of water over the ground that does not infiltrate the soil and is due to an influx of water generated either by rainfall, snowfall or by the melting of snow, or glaciers. Streamflow describes the flow of water in streams, rivers and other channels. Streamflow can be considered according to a variety of temporal resolutions: geological, yearly, monthly, daily, hourly and so on. This is important, because different affects can influence the flow over all of these resolutions, such as rainfall, snow-melt, monsoons, drought, man-made constructions in addition to many others. Thorough understanding of a river system may be lacking due to inappropriate temporal resolution. For example, daily mean river flow measurements do not resolve higher frequency discharge events, such as 'flash' floods, with a period <12 h [296]. This may cause errors and uncertainties in the determination of FDCs, or cause incomplete resource assessment.

Surface runoff will tend to join with streamflow and together they are referred to as *runoff* and considered a component of a land-surface water balance, being the difference between precipitation and evaporation. This is the quantity of water discharged in surface streams and includes water that travels through channels and water that infiltrates the soil surface and travels by means of gravity. Therefore, a fluvial environment results from an exceedance of precipitation over evaporation, assuming the temperature regime does not favour persistent ice formation [291]. The seasonal fluctuation of this balance means a corresponding fluctuation in surface runoff and therefore streamflow. Table 2.5 describes the nomenclature assigned to different streamflow regimes, which are a consequence of different climatic conditions. In a fluvial system, an equilibrium develops to produce an approximate equilibrium between a channel and the water and sediment it must transport [297].

Table 2.5: Streamflow types that result from different climatic conditions.

Streamflow type	Description
Perennial	Year round flow
Intermittent	Flowing for at least one month, but not year round
Ephemeral	After occasional storms, but otherwise dry

Hydrologists make use of a measurement of runoff to enable water supply forecasting, flood predictions and warnings, navigation, water quality management and estimating hydropower production. In this case, the objective is to use models, with equations describing hydraulic geometry and data from stream gauging stations, for providing accurate and timely predictions for a given point in a basin [5].

Though remote sensing cannot directly measure runoff, it is able to provide input data to supplement empirical methods. Equations for describing hydraulic geometry have been shown to have limitations in effectiveness and do not work well in all conditions [298]. We will evaluate the benefits and limitations of hydraulic geometry in Section 4.2.

2.3.2 River flow

Discharge Q is a measure of the volumetric flow rate of a fluid in a channel and therefore, in the field of fluvial geomorphology, of fundamental importance. With regards to a river, it is a function of meteorological runoff[8], drainage basin area and river channel form. Knowledge of Q is important in many domains and its measurement is required for:

- flood hazard management;
- water resource management;
- climate and ecological studies; and
- compliance with transboundary water agreements.

In an open channel, in simple terms, Q is given by

$$Q = Av \tag{2.24}$$

Flow velocity v will be discussed in detail in Section 4.2. The area of a river cross-section A (Fig. 2.17) can be calculated using

$$A = \sum_{i=1}^{n} d_i \delta w \tag{2.25}$$

where $n = \frac{w}{\delta w}$ is the number of segments of width δw that make up the cross-section of width w.

[8]Meteorological runoff is precipitation minus evaporation.

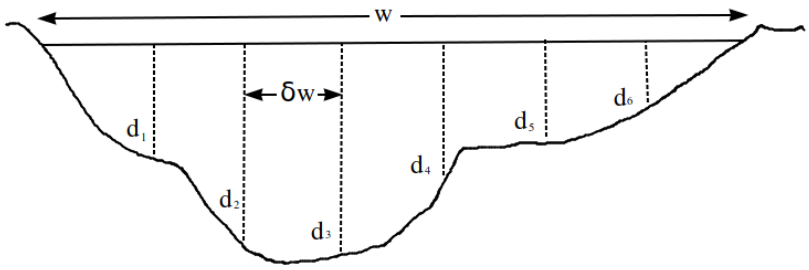

Figure 2.17: River cross-section of width w, divided up into n segments, each with an equal width δw and individual depth of d_i.

Chorley [299] and Pandey and Karki [130] identify various methods that may be employed to measure Q empirically: with a current meter, with a conductivity meter, using the float method, or measuring the change in dye-dilution between two points.

Current meters can be used to measure Q by integration of the velocity distribution across the river cross-section (Fig. 2.17). Average velocity is located at a depth of $0.6d$ or, more precisely, as an average of the velocities at $0.2d$ and $0.8d$. So, for a given cross-section,

$$Q = \sum_{i=1}^{n} \frac{v_{0.2d_i} + v_{0.8d_i}}{2} \cdot d_i \cdot \frac{w}{n} \tag{2.26}$$

Pandey and Karki [130] state that this method is suitable for $Q > 2\,\mathrm{m^3\,s^{-1}}$, a velocity range $0.2\,\mathrm{m\,s^{-1}} \leq v \leq 5\,\mathrm{m\,s^{-1}}$ and provides an accuracy as high as 98 %. They advise that if $d < 0.75\,\mathrm{m}$, the measurement should be taken at $0.6d$ and if $d \geq 0.75\,\mathrm{m}$, the measurement should be taken at $0.2d$ and $0.8d$.

Also known as the salt dilution method, measuring Q using a conductivity meter involves adding salt upstream and determining the change of conductivity, using

$$Q = \frac{k_s m_s}{(\sum_{i=1}^{n}[C_i] - nC_0)\Delta t} \tag{2.27}$$

where k_s is a salt constant, m_s is the mass of the salt, C_i represents an individual conductivity reading, n is the number of readings, C_0 is the base conductivity and Δt is the time interval between readings. Pandey and Karki [130] state that this method is suitable for $Q < 2\,\mathrm{m^3\,s^{-1}}$ and has the advantage of being simple and fairly accurate (within ~ 7 %).

The float method can also be used to measure Q. This simple method uses the observation of a float released into the river and

$$Q = Ak_f v_f \tag{2.28}$$

where v_f is the velocity of the float along the surface of the river, determined by measurement of the length travelled and the time taken. The coefficient to correct the surface velocity k_f is assigned a value dictated by the average depth of the channel (Table 2.6).

Table 2.6: Values for k_f to enable determination of mean channel velocity, from measurement of surface float velocity [130].

Average depth (ft)	Average depth (m)	k_f
1	0.3048	0.66
2	0.6096	0.68
3	0.9144	0.70
4	1.2192	0.72
5	1.5240	0.74
6	1.8288	0.76
9	2.7432	0.77
12	3.6576	0.78
15	4.5720	0.79
>20	>6.0960	0.80

The dye-dilution method uses

$$Q = Q' \frac{C_1}{C_2} \tag{2.29}$$

where Q' is the discharge at the point where the dye is injected, C_1 is the concentration of the dye in the injected flow and C_2 is the concentration of the dye in the unknown discharge Q.

Gauging stations are commonly relied upon for *in situ* measurements of Q. This is generally determined by empirical rating curves that relate occasional measurements of true discharge to another variable, such as river stage, or inundation area, which is more easily measured. River stage, defined as the elevation of the water surface above some arbitrary datum (usually near the river bed), is most common and uses a hydraulic geometry relationship that exists between discharge and depth $d = cQ^f$ (see Section 4.2). Sufficient measurements of Q and d allows the determination of the parameters c and f by regression. Regular measurements provide calibration for temporal variation. Being site-specific, these rating curves cannot be applied elsewhere [300]. Therefore, this site-specific approach to determining Q hinders more extensive ground-based river gauging.

Discharge can be defined in a number of ways (Table 2.7). Consideration of this may be important to ensure appropriate utilisation of this measurement, in different contexts. For example, when using hydraulic geometry relationships, the parameters are not independent of this choice [297, 301, 302]. This will be discussed further in Section 4.2.

Leopold and Maddock [297] postulate that Q is independent of stream channel, instead dependent upon the nature of the drainage basin. Variations in Q, over time, are particular to location and to the nature of a river. We will build upon this idea, too, when we discuss hydraulic geometry in Section 4.2.

If the cross-sectional area is assumed to be approximately rectangular, Eq. (2.24) can be expressed as

$$Q = wdv \tag{2.30}$$

A change in Q will therefore be accompanied by a change in w, d and v. Lalander [186] reports

that a change in Q will affect v primarily, with w and d less so. Except with an unusually low Q (droughts), or high Q (floods), d tends to remain fairly constant. A variation in d will influence v, due to friction. Therefore, there exists a non-linear relationship between v and d.

Table 2.7: Summary of definitions used to describe different forms of discharge.

Symbol	Definition of discharge
Q	stream discharge
Q_b	bankfull discharge
Q_d	dominant discharge
Q_e	most effective discharge
Q_m	mean annual discharge
Q_{ma}	mean annual flood
Q_p	peak discharge
Q_r	discharge ratio ($= \frac{Q_t}{Q_m}$)
Q_s	suspended sediment load
Q_t	threshold discharge
Q_2	discharge with a return period of 2 yr
$Q_{2.33}$	discharge with a return period of 2.33 yr

Variation of Q can be dependent upon upstream conditions, if the flow is super-critical; or downstream conditions, if the flow is sub-critical. This can be determined by calculating the Froude number. The Froude number Fr is a dimensionless value that describes different flow regimes of open channel flow and is based on a speed-length ratio. If considering a river channel and assuming an approximately rectangular cross-section with uniform d and v,

$$Fr = \frac{v}{\sqrt{gd}} \tag{2.31}$$

Celerity c is the speed at which a signal is transmitted through a medium. For an ideal wave,

$$c = f\lambda \tag{2.32}$$

where f is the frequency of the wave and λ is the wavelength.

In fluids, c is the measure of speed with which gravity waves travel. A gravity wave propagates along the interface between two fluids of different density, when gravity and buoyancy attempts to restore equilibrium. These mediums might be air and water, but could also be both water, or air. For example, subsurface waves propagate along a pycnocline, marking a transition from less dense to more dense water within the water column. The value of c for a gravity wave propagating along the surface in deep water, where there is no friction from a boundary below, is given by

$$c = \sqrt{\frac{g\lambda}{2\pi}} \tag{2.33}$$

In shallow water, when c is affected by the friction of a bottom boundary layer,

$$c = \sqrt{gd} \tag{2.34}$$

With reference to Eq. (2.31), this demonstrates how the Froude number can also be described as the ratio of v and c, in this context. When considering a river, the shallow water context is most relevant, meaning that v and c dictate the speed with which perturbations are transmitted along a river. Therefore, it is this speed which controls the hydrograph[9] of a river. Downstream information propagates at $v + c$ and upstream information at $v - c$. Therefore, if $v \geq c$, the upstream propagation of information will cease. The condition $v = c$ is known as *critical flow*, which corresponds with a wave trying to move upstream on the surface of the water at exactly the same speed as the water is advecting the wave downstream. Under such a condition, any wave disturbance stands in place. *Supercritical flow* occurs when $v > c$ and *subcritical flow* when $v < c$. The Froude number Fr, being a measure of the ratio of v to c, thus describes these conditions, such that $Fr = 1$, $Fr < 1$ and $Fr > 1$ correspond to flows which are critical, subcritical and supercritical, respectively. Further, if $Fr > 1$, Q is dependent upon upstream water level. Alternatively, if $Fr < 1$, Q is dependent upon downstream water level. Huggett [291] claims that in natural channels, the mean Froude number is rarely higher than $Fr = 0.5$ and that super-critical flow is only temporary, because this will cause erosion of the channel, causing enlargement and resulting in a reduction of flow velocity.

2.3.3 The development of fluvial geomorphology

In parallel with the trends in general geomorphology, different approaches to fluvial geomorphology have been prevalent throughout its development, leaning towards either field measurement-based empiricism and statistical analysis, or the more rational and theoretical. The latter is more deductive and built upon principles that are usually adopted from other fields, such as hydraulic engineering. This can be further separated into approaches that are either deterministic, or probabilistic. Using deterministic reasoning, these natural systems may be explained via an attempt to better understand the physical laws that dictate their behaviour. Critics of the deterministic perspective suggest that the complexity and interconnectedness of the natural world make this too demanding, arguing that a probabilistic approach, which takes account of this randomness, might better reflect the world as it is, rather than what we might like it to be [303].

Strahler [304] attempted to unify this diverse set of opinions in fluvial geomorphology, but the response for the following years was predominately empirical [305–309]. The power law equations proposed by Leopold and Maddock [297] used to describe hydraulic geometry, as functions of Q — which represent a fundamental foundation of this thesis and will be introduced shortly — and the relationship between meander wavelength and channel width [310], are classic examples. Yet, it is clear that they offer no explanation for *why* these relationships exist. Lane and Richards [311] suggest, in fact, that such empirical relationships risk being the product of the sampling and experimental design, rather than intrinsic to nature. Mackin [312] went further, arguing that 'shotgun empiricism', grounded in engineering practice, should not replace rational thought on landscape evolution. Though not a direct condemnation of Leopold and Maddock's ideas, Leopold responded to this criticism [313] by stating that an empirical and probabilistic approach may better represent variations in natural systems. In fact, he goes on, this variation may even become more important in this context than physical laws and that such empirical investigation may generate hypotheses of landscape processes, impossible from rational observation alone.

[9] A hydrograph is a time series of Q. This is fully defined in Section 5.1.

Leopold and Maddock [297] proved to be seminal work and as we consider the overall development of fluvial geomorphology, it is worth pointing out how perceptions and application of the resulting hydraulic relationships has varied. We shall briefly discuss this here, before consideration in more detail in Section 4.2. These relationships are:

$$w = aQ^b \tag{2.35}$$

$$d = cQ^f \tag{2.36}$$

$$v = kQ^m \tag{2.37}$$

where w, d , and v represent water-surface width, mean depth, and mean velocity, respectively. The parameters b, f, m, a, c, and k are numerical constants that vary with location, climate and discharge conditions. Park [314] states that there is significant variability in these parameters and Smith and Pavelsky [243] suggest that hydraulic relationships are most applicable in stable, single-channel rivers, but also point out that they have been widely used in many environments. These relationships are applicable for $Q < Q_b$, because beyond this the water is no longer contained within the channel and w increases rapidly.

The implication of Eqs. (2.35) and (2.36) is that channel size is influenced by Q, but consideration must be made of how the hydraulic regime can also have an effect on channel size [315]. The publication of these relationships inspired many further studies. Initially, most studies aimed to identify similarities in b, f and m among different rivers and attributing them to differences in climatic, geologic, or physiographic regime [314]. Growing numbers of cross-section studies revealed high variation in the local complexity of river channels and redirected interest towards the physical processes responsible for these deviations [302, 316, 317]. Going full circle, interest returned to generalised hydraulic geometry relationships, via reach-averaging of cross-sections [318], multi-scaling techniques [319] and the determination of reach-scale hydraulic geometry relationships by spatial studies of variability [320].

The progress of fluvial geomorpholgy, as a whole, echoed this. Through the 1980s and 1990s, an emphasis towards smaller temporal and spatial resolution emerged. This necessitated a move away from statistical generalisations, in the direction of a more detailed understanding of physical mechanisms involved in processes [321–335]. Ferguson [336] provided a key paper — considered so authoritative by Gleason [337], in a review of hydraulic geometry, that it caused research into the causes of at-a-station hydraulic geometry (AHG) to cease — that used a rational approach and existing flow equations (see Section 4.2) to derive AHG for different channel geometries. Still, it must be remembered that different scales of form and processes are not independent of each other. Lane and Richards [311] supported this view by providing evidence that short timescale and small space-scale processes have an influence over longer timescales and larger space-scales.

Despite challenges to Ferguson's formulation of AHG [317, 338, 339], it appears to have endured and by the 2000s, echoing the inclination of the 1960s, empirical studies became more common again [340–345]. Data-driven methods for determining channel geometry [228, 346–351] have resulted from increased application of high-resolution surveying technologies [352–356].

After reviewing 60 years of hydraulic geometry research, Gleason [337] concluded that the power law relationships (Eqs. (2.35), (2.36) and (2.37)), proposed by Leopold and Maddock [297], remain an important idea for monitoring river systems worldwide. These relationships, and the broader topic of hydraulic geometry, will be further elaborated upon in Chapter 4.

2.4 Summary

A summary of the salient points from Chapters 1 and 2 is given, to take forward to the subsequent chapters.

- Providing a means for generating useful energy from free-flowing water, hydrokinetic energy conversion is a renewable energy technology which offers benefits that complement other renewable energy technologies; having characteristics that make it appropriate to support isolated communities and those living in energy poverty.
- When compared with conventional hydropower, in a riverine context, HEC offers the advantages of modularity and scalability; less environmental and social impact; and, ease of construction due to being lower cost, quicker to construct and requiring less planning consent.
- Previous large-scale hydrokinetic resource assessments have measured the rate of energy conversion from gravitational potential energy to kinetic energy, using $P = \gamma QH$ (Eq. (2.3)), or the Manning formula (Eq. (4.17), defined in Subsection 4.2.1).
- Though the International Electrotechnical Commission (IEC) has provided standards for hydrokinetic resource assessment, for site-specific contexts, there are no published standards, specifications, or rules-of-thumb for large-scale riverine hydrokinetic resource assessment.
- To be feasible, a global riverine hydrokinetic resource assessment will rely upon what can be inferred by remote sensing and the development of digital elevation models (DEMs).
- Discharge Q is a much-used and important measure within rivers, with which methods have been developed to estimate other riverine characteristics.

Chapter 3

A hydrostatic perspective

This chapter is based upon the article *Global riverine theoretical hydrokinetic resource assessment* [137].

3.1 Modelling and data

3.1.1 Hydrological and hydraulic modelling

To understand natural water flow requires understanding of the variation, in space and time, of a number of variables, including flow velocity, water depth and elevations of the bed and water surface. Bridge [357] states that measurement of spatial and temporal variations of water flow in natural environments is extremely difficult, because of limitations of measuring equipment and the ability to deploy them effectively. Simplified fluid dynamics can be understood and simulated using integral and partial differential equations for conservation of mass, momentum, energy and entropy (see Subsection 4.2.1). Real-world understanding of the dynamics involved is too complex for these equations to be solved analytically, thus requiring the application of numerical models.

There are three types of energy present in a fluid: kinetic, potential and thermal. Aside from the kinetic energy of the flowing fluid and the gravitational potential energy due to its elevation, this energy takes various other forms:

- work done against viscous shear and turbulence (internal friction);
- work done against friction at a boundary;
- work done in eroding a boundary; or,
- work done in transporting suspended matter.

There is a hierarchy to the order in which energy input into a fluid will be used, with reference to the list above, overcoming friction internally and at the boundary, takes precedence over erosion, or transportation. For example, in a river, a critical energy level must be reached

before it can perform erosion at the channel boundaries, or transport a sediment load. It is these forms of energy that are responsible for the network of channels that develops.

River networks are mostly simple tree structures, with upstream tributary branches joining downstream main-stem channels, displaying a classic root branch pattern (Fig. 5.4). Water flows downhill due to a potential energy difference between higher and lower elevations, causing water to seek a lower energy state. Since water must flow downhill, river networks are inherently acyclic. Thus, at the most basic level, river networks can be treated as a directed acyclic graph (DAG) which connects tributary junctions with differential equations, representing the change of water surface elevation and flow rate.

Given that a river network can be considered a DAG, it might be thought that this permits a thorough understanding to be gained by simply identifying the appropriate equations along branches and between nodes. This is yet to be realised and the failure to do so can be explained by acknowledging the difficulties associated with quantifying boundary conditions, the uncertainties caused by non-linear interactions of a number of complex physical processes and the general chaotic randomness present in natural systems.

It is increasingly common for hydrological studies to use a reach-scale frame of reference [358–360]. A reach is a length of a river, between points of confluence, bifurcation, or channel initiation. It usually suggests a level, uninterrupted stretch. This definition allows hydrological characteristics to be considered at an intermediate scale, between catchment- and field-scale. The growth of 'big data' in geosciences allows higher fidelity data than can be achieved at the catchment-scale. Yet, a better understanding can be achieved at the reach-scale than for field-scale, as the numerous assumptions and approaches used in hydrological modeling still work reasonably well at this scale.

To consider another interesting perspective, Hodges et al. [361] describe the similarities between river networks and electric circuits, in both their network structure and derivation from conservation principals. They argue that, although the disciplines which have traditionally investigated these two areas have evolved separately, numerical methods developed to describe electric circuits can be used to significantly improve the understanding of river networks. They make an interesting observation, noting that at the end of the 19th century, models developed to explain hydraulics were used to explain electric phenomena, implying that this was the order of learning and an indication of the relative complexity. This has now reversed and electric theory is covered in high schools, while hydraulics is generally not encountered until university.

A comparison between electric circuits and fluid dynamics can be made, and these two areas considered analogous, because they both evolved from conservation laws: charge and magnetic flux for the former, mass and momentum for the latter. The similarities continue beyond basic conservation laws, when modelling the behaviour of both. Typically, the complex three-dimensional physics is simplified, in both cases, to describe the dominant one-dimensional behaviour (see Subsection 4.2.1). *Down-scaling* is any procedure to infer high-resolution information from low-resolution variables. The term usually refers to spatial resolution, but can also be used for temporal resolution. The uncertainty and non-linear nature observed, with increased spatiotemporal resolution, must be dealt with when *up-scaling* to produce practical models.

Here, we will discuss both *hydrological* and *hydraulic* models, which are the two types of models used for describing river flow. So, what is the difference? Hydrological modelling can be defined as the characterisation of real hydrologic features and systems, by the use of

small-scale physical models, mathematical analogues and computer simulations. Hydrological modelling helps in understanding, predicting and managing water resources. A hydraulic model (also referred to as a hydrodynamic model) is a mathematical model of a fluid flow system and used to analyse hydraulic behaviour, dealing with the physical properties of water, such as depth-velocity relationships in a pipe, or open channel. Hydraulic models are also commonly used in channel flooding studies.

In comparison, a hydrological model can be considered a derivative of a hydraulic model, where the gradient of momentum change is disregarded, with an assumption that this does does not contribute as much as mass flux. Instruments and gauges provide measurements of discharge Q, depth d, slope s and flow velocity v, with the hydrological approach. The hydraulic approach requires information on Q, bathymetry and the geospatial measurements from digital elevation models (DEMs). This approach permits the modelling of the conditions within a given reach, or section, of a river; in contrast to the single-site limitations of the hydrological approach.

A hydrological model is a simplification of a real-world system (e.g., surface water, soil water, wetland, groundwater, estuary, etc.) that aids in understanding, predicting and managing water resources. Commonly, hydrologists desire knowledge of Q within a river system. Use of gauges is the most accurate method for determining this, but for large-scale consideration, spatial coverage is limited and decreasing over time [362, 363]. Hydrological modelling can be used to fill in the gaps. Substantial investments have been made by the hydrological community, over the past 50 years, across multiple scales, to produce simulations and predictions of surface and groundwater flows, evaporation and soil management [364]. Both the flow and quality of water are commonly studied using hydrological models. There are two general categories of hydrological models: deterministic and stochastic. These are also referred to as conceptual models and statistical models, respectively.

Deterministic models simulate flows by modelling various physical processes in a catchment. This category can be further divided as a physically based model (also referred to as distributed models), or a lumped conceptual type model. The difference being that physically based models are based upon a host of different physical features associated with a catchment and meteorological data as forcing functions, whereas a lumped conceptual type model conceptualises the entire catchment as a single, homogeneous unit and characterises all physical processes using a single set of parameters, according to a conceptual framework. Although lumped conceptual type models are more simple to develop, continuity and water-balance constraints must be rigorously applied and require parameter calibration [365].

Stochastic models use statistics to describe these processes, acknowledging that there is an element of randomness present. Such models will likely produce different results each time the model is run. Hybrid deterministic and stochastic models, as one might imagine, are combinations of both of these approaches [366].

A land surface model (LSM) provides atmospheric models with bottom boundary conditions, based on a water and energy balance. For hydrological modelling these models serve as the land base and were developed to provide water inflow to river routing models that calculate Q (e.g. [367–377]). Early efforts predominately used gridded river networks, that best suited a computational domain. With the advent of vector-based representations of river networks, such as HydroSHEDS [378], different methods for calculating water inflow were developed, such as the Routing Application for Parallel ComputatIon of Discharge (RAPID) [379, 380]. Both of

these will feature prominently in the methodology laid out below.

Challenges to the performance of hydrological models include the lack of high-quality global data sets for modelling inputs [381], optimal combination of physical parameterisation schemes [382], reliable approaches to estimating model parameters [383] and access to sufficient computational power to represent physical realism at sufficiently high resolutions [384]. Also, since streamflow modelling relies on the upstream results of atmospheric forcing, LSMs and a river routing model, uncertainties can depend upon these upstream uncertainties.

Previous studies have attempted to determine hydrological model parameters from catchment attributes, thus permitting the application of models within ungauged basins [383, 385–388]. Others have gone further, using these attributes to also influence the choice of model structure [389–391]. This can aid the use of models in larger-scale contexts.

There is now a recognition that the use of hydrological models is an exercise in constraining prediction uncertainty [392]. This recognition holds for both global- and catchment-scale models [393, 394]. McDonnell and Beven [392] suggest that this situation can be improved upon by obtaining better data sets that are more informative in differentiating process representations at appropriate scales and improving observation methods to enable more effective model evaluation.

Hydraulic modelling requires topographical data, a stage-discharge relation for the model terminus and parameter values. One-dimensional hydraulic models have been used to derive hydraulic geometry relationships [395], but it is postulated that two-dimensional models perform better and are necessary for determining reach-scale hydraulic properties [396].

Given the stated aims of this project, with an intention to carry out a global-scale hydrokinetic resource assessment, the descriptions of hydrological and hydraulic modelling would suggest that the former is most suitable to serve this end. Below is a summary of some relevant hydrological models.

The Variable Infiltration Capacity (VIC) macroscale hydrologic model solves full water and energy balances that has been has been applied to most of the major river basins around the world, as well as globally [397, 398]. It is integral to the methodology used to produce the data set used in this study, as will be explained below.

Dynamic fluxEs and ConnectIvity for Predictions of HydRology (DECIPHeR) is a model framework that simulates and predicts hydrological flows from spatial scales of small headwater catchments, to continental-scale [364]. The framework is based on the key concepts of the Dynamic TOPMODEL [399], which has been applied widely [400–404]. Though it is yet to be applied at a continental-scale, Coxon et al. [364] have demonstrated its application for Great Britain and claim that this highlights the potential to be used for larger domains, implying what improvements can be achieved by making use of available big data sets, advances in flexible modelling frameworks and increasing computing power.

Hydrologic Engineering Center's River Analysis System (HEC-RAS) [193, 194] is a hydrologic model that performs one-dimensional hydraulic calculations, using three analysis components:

1. steady flow water surface profile computations;

2. unsteady flow simulation; and,

3. moveable boundary sediment transport computations.

This model was used to provide data suitable for validation of the estimates of reach-scale hydrokinetic power in Chapter 4 and Ridgill et al. [138].

Models can be improved by combining data obtained by remote sensing (see Subsection 2.2.4) with conventional empirical data. With at least one gauging station for calibration, Smith and Pavelsky [243] showed that multi-temporal satellite data can contribute effectively to an understanding of water discharge and flow conveyance in remote river systems.

David et al. [224] point out that the data collected from the Surface Water Ocean Topography (SWOT) mission (see Subsection 2.2.4), provides an opportunity for integration with the continental- to global-scale hydrologic and hydraulic models that have been developed over the past 20 years.

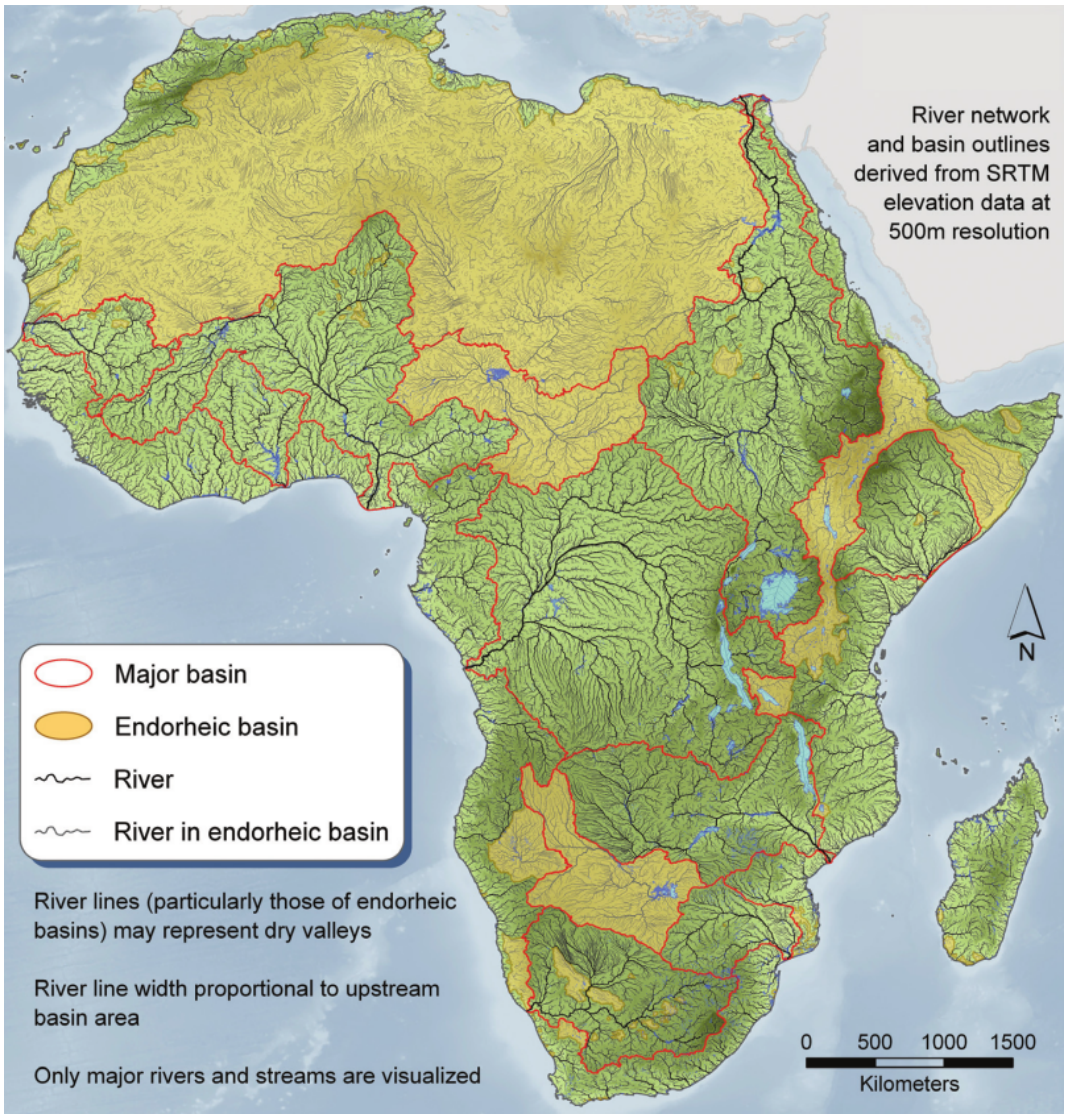

Figure 3.1: River network of Africa, produced from HydroSHEDS data set [203].

3.1.2 Data sets

Detailed, riverine-focused data sets exist, providing high resolution information for understanding some regional-scale river systems. Unfortunately, they do not provide the necessary coverage for a global-scale resource assessment and are therefore not suitable for use in this study. For example, the Catchment Attributes and MEteorology for Large-Sample Studies (CAMELS) is a data set of attributes for 671 catchments in the contiguous United States, which have been chosen because they are minimally impacted by human activities. Six main classes of attributes are described: topography, climate, streamflow, land cover, soil and geology. CAMELS extends a previous data set [405], covering the same 671 catchments, but extending the number of attributes.

Also, the North American river width (NARWidth) is a data set of 6.7×10^6 georeferenced measurements that contains continental-scale river centerlines and width measurements for $>2.4 \times 10^5$ km of rivers of width >30 m, at mean annual discharge [206].

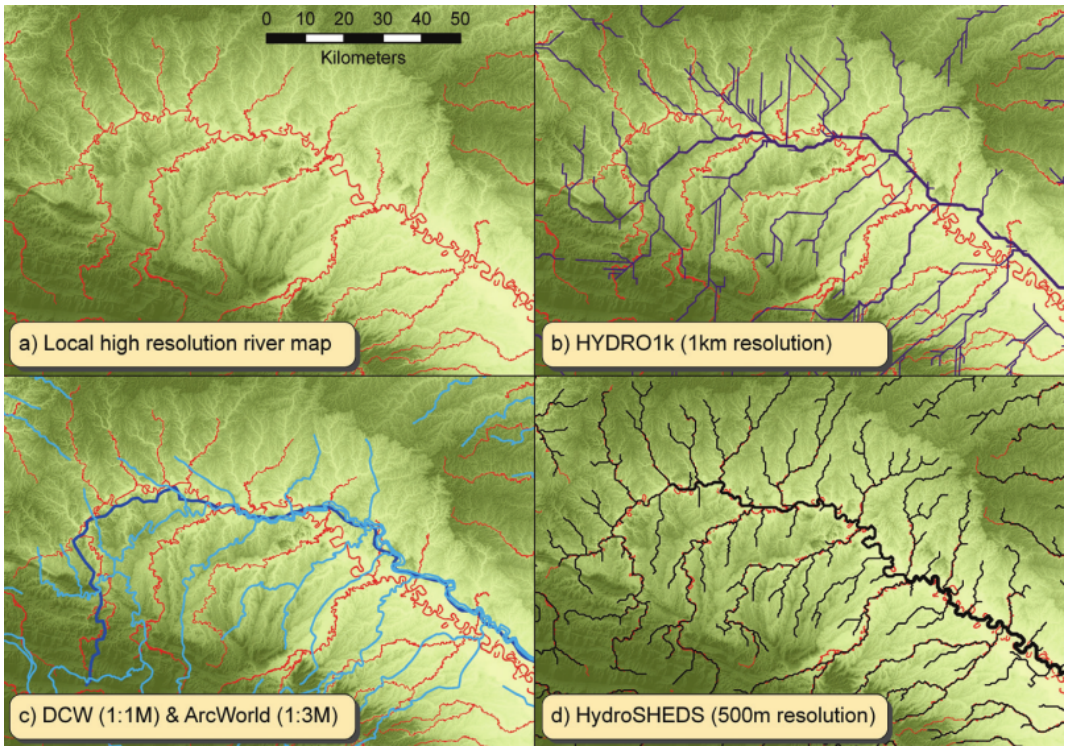

Figure 3.2: Portion of the Amazon basin, with green background provided by SRTM. The river network is represented according to: a) a locally produced high-resolution stream network; b) the HYDRO1k network; c) the Digital Chart of the World (DCW) network in light blue and ArcWorld network in dark blue; and, d) the HydroSHEDS network at a resolution of 450 m (15″) [203].

More suitable is a near-global data set, developed by the Conservation Science Program of World Wildlife Fund [406]: HydroSHEDS (Fig. 3.1) comprises hydrological data and maps based on shuttle elevation derivatives, at multiple scales, informed by the measurements of the Shuttle Radar Topography Mission (SRTM) (see Subsection 2.2.4). It provides reliable information about where streams and watersheds occur and how water drains the landscape.

Lehner et al. [203] state that the information is of a quality that supersedes previous, similar data sets. In all, HydroSHEDS offers a suite of geo-referenced data sets (vectors and raster), including stream networks, watershed boundaries and drainage directions. Ancillary data offers layers such as flow accumulations, distances and river topology information [378].

Though the SRTM DEM provides the majority of the data used in its construction, HydroSHEDS benefits from other sources, including: the SRTM Water Body Data, the Global Lakes and Wetlands Database and the river networks of the Digital Chart of the World (DCW) and ArcWorld.

Fig. 3.2 demonstrates that the HydroSHEDS database is better able to determine the position of stream networks, compared to other DEMs, such as Hydro1k and the Digital Chart of the World.

Table 3.1: Summary of the levels used in the HydroBASINS data set.

Level	Description
1	9 continental-level divisions
2	Division of continental-level into 9 large sub-units
3	The largest river basins of each continent
4-12	Further breakdown following the traditional Pfafstetter system

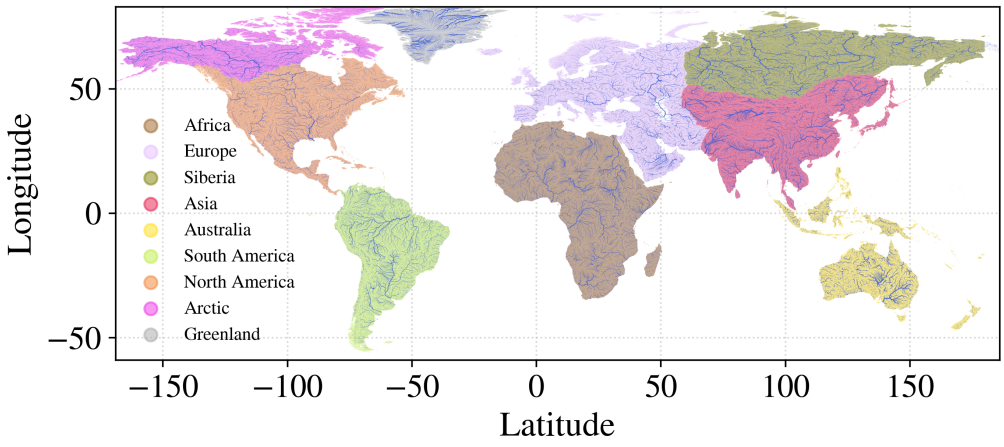

Figure 3.3: Level 1 continental-level divisions, as defined by the Pfafstetter coding system.

Two formats of the data set are available: Format 1, considered ‘standard’, without lakes; and Format 2, considered ‘customised’, with lakes. There are 9 continental-level divisions (Fig. 3.3).

The HydroSHEDS database allows for the derivation of watershed boundaries [406], thus giving rise to HydroBASINS. This data set set represents a subset of the HydroSHEDS database, providing a series of polygon layers that depict these watersheds, as basins and sub-basins, at

a global scale [204]. A coding scheme, developed from the Pfafstetter coding system [407], allows for analysis of watershed topography and identifications of neighbouring basin connectivity. The HydroBASINS data set provides scales of resolution, from Level 1 to Level 12 (Table 3.1).

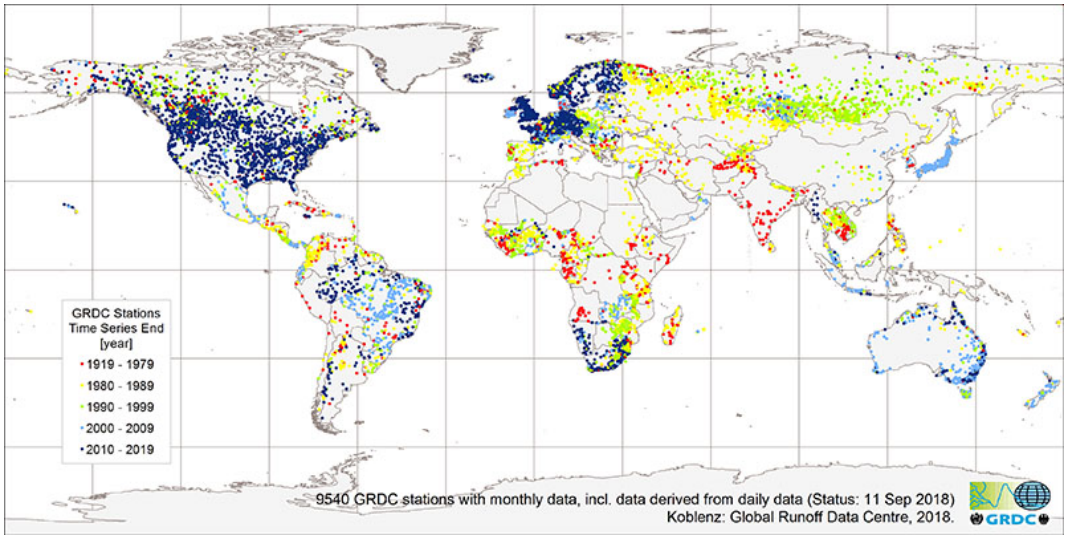

Figure 3.4: Distribution of Global Runoff Data Centre (GRDC) stations [408].

Based upon concepts proposed by the Brazilian engineer Otto Pfafstetter, Verdin and Verdin [407] developed the Pfafstetter system to delineate and code hierarchically nested catchments, using a simple coding system that enables the description of stream network position without need for a graphical information system (GIS).

Verdin and Verdin [407] had intended the Pfafstetter system to be used for describing the topological relationships of a connected river network. For this reason, Stein [409] has pointed out it is not well-suited for describing many endorheic basins[1], or complex drainage systems, such as groundwater connections, non-riverine surface water features (such as palustrine wetlands), or water infrastructure that are not dependent upon topographically driven flow. He goes on to state, as others have [410, 411], that another inadequacy is how the system relates to the variable level of decomposition of basins and the uneven size of the sub-basins that it may produce.

Over the past 30 years, the Global Runoff Data Centre (GRDC) has compiled a vast quantity of hydrological data [408]. The earliest data is from 1807 and now with 9,500 stations worldwide includes 415,000 station years of data (Fig. 3.4). The database they have built contains time series of daily and monthly river discharge, with access being free and unrestricted. Many stations have collected sufficient measurements to enable the construction of long time series (Fig. 3.5). Fig. 3.6 shows the number of stations providing daily measurements versus monthly measurements and indicates that there was a steady increase in the number of stations providing measurements, until a period in the 1980s when this appears to decline. GRDC [408] suggests that this can be explained by two factors. Primarily, this is due to the lag between the observation and the time it takes to get it in the GRDC database. Secondly, there is a decline of *in situ* measurements, that can be attributed to the collapse of the Soviet Union and civil wars in

[1]Endorheic basins are a class of basin that do not drain to the ocean.

developing countries, as well as cutbacks in monitoring programs, due to budgetary constraints on operating agencies, in developed countries.

Andreadis et al. [412] constructed a global database containing estimates and corresponding 95 % confidence intervals to allow the determination of bankfull widths and depths on a global scale. The database was based upon the hydraulic geometry equations of Leopold and Maddock [297] (described in detail in Section 4.2), the HydroSHEDS database and discharge data obtained from the GRDC.

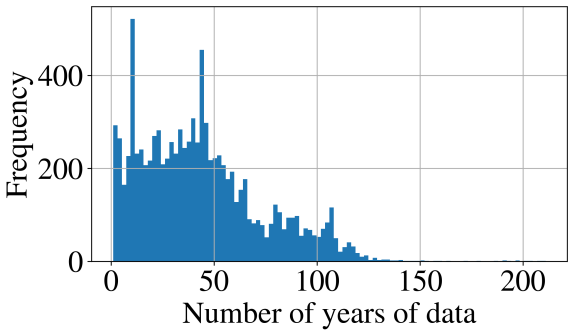

Figure 3.5: Histogram to show the length of time series available in the GRDC data set.

Fig. 3.7 provides a map of the global distribution of rivers and an indication of river width w. Andreadis et al. [412] used Landsat-derived measurements of w to validate a subset of their database of estimates. Though some errors are high, the Landsat-derived widths were always found to be within the 95% confidence error. The correlation coefficient across all sites was 0.88, indicating a strong overall agreement. In justifying their approach and motivation for constructing this database, they state that using satellite imagery, like Landsat, to directly determine river width on a global-scale is unlikely to happen in the foreseeable future.

This study by Andreadis et al. [412] is of particular interest, because the approach is similar to that used in the methodology developed and described in this thesis, as shall be covered below.

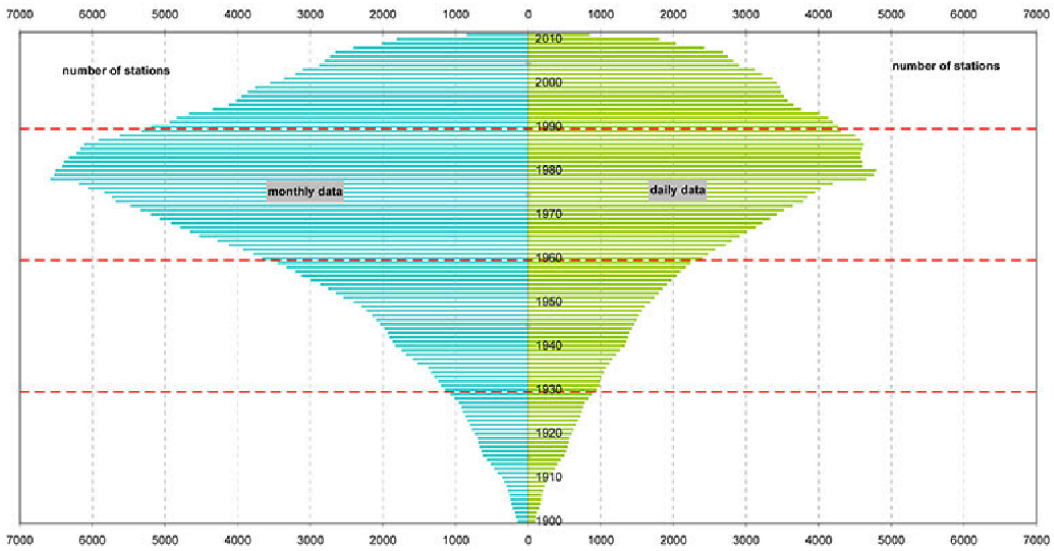

Figure 3.6: Number of stations providing monthly and daily measurements in the GRDC data set [408].

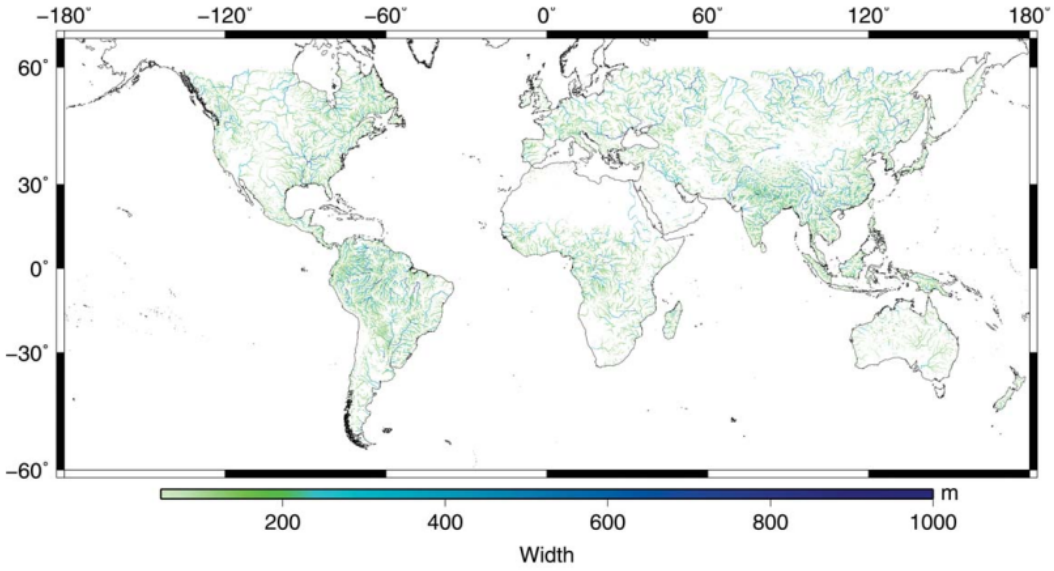

Figure 3.7: Global representation of river widths (not showing $w > 50$ m and $w > 1$ km restricted to this value) as proposed by Andreadis et al. [412].

3.1.3 GRADES data set

Global Reach-level A priori Discharge Estimates for Surface Water and Ocean Topography (GRADES) [359] is a 35 year reconstructed Q record, from the beginning of 1979 to the end of 2013, that incorporates the Variable Infiltration Capacity (VIC) macroscale hydrologic model [397, 398] and the Routing Application for Parallel computatIon of Discharge (RAPID) river routing model [379, 380]. Vectorisation of the river network and separation of the individual catchments was achieved using the Multi-Error-Removed-Improved-Terrain (MERIT) Hydro global hydrography data set, which provides high-resolution, vectorised, global flow direction maps at 3-arc sec resolution (~90 m at the equator) [207]. MERIT Hydro is based on MERIT DEM [279], as introduced in Subsection 2.2.5. An advantage that this global hydrography data set has over preexisting data sets [378, 413], in addition to the more realistic depiction of river flowlines, is coverage above 60°N. The GRADES data set includes additional information for each river reach, including elevation change H, length L and slope s.

To use MERIT Hydro in GRADES, the data set was first separated into basins, as defined within HydroBASINS (see Subsection 3.1.2). This is a subset of the HydroSHEDS DEM [406], that provides a series of polygon layers depicting watersheds, as basins and sub-basins, at a global scale [204]. Lin et al. [359] found that the basin boundaries defined by MERIT Hydro and HydroBASINS differed globally by <1 %. Further division of each continental-level basin into 9 large sub-units provides Level 2 basins. This process continues down to Level 12. The process to merge the HydroSHEDS definition of basin boundaries to MERIT Hydro involved first identifying 61 Level 2 basins, before being grouped into Level 1 continental-levels. The median (mean) length of each river reach in the data set is 6.8 km (9.2 km).

The atmospheric forcing which contributes to the LSM is from a 0.1° and 3-hourly precipitation data set [381]. Parameter calibration and bias calibration for the LSM was performed against machine learning derived global runoff characteristic maps [414]. There is an increasing recognition that machine learning is a powerful approach to understanding hydrology in

ungauged basins [359, 415].

Flow routing (also referred to as flood routing) predicts the downstream hydrograph[2] that results from an upstream hydrograph. Generally, a hydrograph downstream will show attenuation and a time delay. This can be considered from hydrologic, or hydraulic, principles. The former is concerned with the conservation of mass and the latter with conservation of mass *and* momentum.

If considering a single reach river and regarding the channel as a linear store, the continuity equation expresses the rate of change in storage S, as the difference between the input I and the output O from the reach, over time t,

$$\frac{\mathrm{d}S}{\mathrm{d}t} = I(t) - O(t) \tag{3.1}$$

Given that the aim is to gain knowledge of the downstream hydrograph, the problem consists of finding $O(t)$, given $I(t)$ and suitable assumptions about the form of S. The Muskingum method [416] is applied here, which provides a first-order approximation of the kinematic and diffusive wave equation. Though this method was later improved upon by Cunge [417], to give the Muskingum-Cunge method and a means to determine a second-order approximation of the kinematic and diffusion wave equation, David et al. [379] outline computational complications in applying this within the RAPID river routing model. The Muskingum method applies this continuity equation at time t_1 and t_2, aiming to determine $O(t_2)$ using

$$O(t_2) = c_1 I(t_1) + c_2 I(t_2) + c_3 O(t_1) \qquad \text{where } \Sigma c_i = 1 \tag{3.2}$$

The RAPID flow routing model provides flexibility in dealing with vector river networks in a range of regional- to continental-scale applications, as demonstrated in earlier studies [418–421]. Previous vector-based representations of river networks [204, 379, 422] provide realistic channel representations, but have only been applied regionally. GRADES builds upon these previous efforts by providing global coverage, using an unprecedented 2.94 million reaches.

Unfortunately, GRADES does not include Q data for the Greenland continental-level basin, at this time, due to a lack of sufficient training and validation data (M. Pan, coauthor of Lin et al. [359]; Pers. Comm.). Greenland accounts for 1.4 % of the total reaches in the global river network data set, or 2.5 % of the total length of all rivers. Information regarding the rivers of Antarctica does not feature in the data set. The Antarctic hydrological system consists of superglacial lakes, subsurface lakes, surface streams and rivers that function quite differently to the terrestrial hydrological systems that make up the vast majority of the global network of rivers [423].

RAPID uses the Muskingum method, in the form

$$(\mathbf{I} - \mathbf{C_1} \cdot \mathbf{N}) \cdot \vec{Q}(t + \Delta t) = \mathbf{C_1} \cdot \vec{Q}^e(t) + \mathbf{C_2} \cdot [\mathbf{N} \cdot \vec{Q}(t) + \vec{Q}^e(t)] + \mathbf{C_3} \cdot \vec{Q}(t) \tag{3.3}$$

where t is time and Δt is the river routing time step; $\mathbf{I}$ is the identity matrix; $\mathbf{N}$ is the river network matrix; $\mathbf{C_1}$, $\mathbf{C_2}$ and $\mathbf{C_3}$ are parameter matrices; $\vec{Q}$ is a vector of outflows from each reach and $\vec{Q}^e$ is a vector of lateral inflows for each reach. The lateral inflows include runoff, groundwater, or any type of forced inflow, such as a dam, etc. River network routing can be determined from Eq. (3.3) and solved using a linear system method. The use of vectors and

[2] A hydrograph is a time series of Q, which is defined in Section 5.1.

matrices allows a representation of the entire river network and removes the need of spatial iterations. A river network of β river reaches gives dimensions

$$\vec{Q}, \vec{Q}^e \in \mathbb{R}^\beta \tag{3.4}$$

and

$$\mathbf{I}, \mathbf{N}, \mathbf{C_1}, \mathbf{C_2}, \mathbf{C_3} \in \mathbb{R}^{\beta \times \beta} \tag{3.5}$$

The outlflows of all rivers within a network are thus

$$\vec{Q}(t) = \begin{bmatrix} Q_1(t) \\ Q_2(t) \\ \vdots \\ Q_\beta(t) \end{bmatrix} \tag{3.6}$$

and the lateral inflows

$$\vec{Q}^e(t) = \begin{bmatrix} Q_1^e(t) \\ Q_2^e(t) \\ \vdots \\ Q_\beta^e(t) \end{bmatrix} \tag{3.7}$$

Network connectivity is mapped using $\mathbf{N}$, which is comprised of ones and zeros. A value of one at row i and column j signifies that reach j flows into reach i. For example,

$$\mathbf{N} = \begin{bmatrix} 0 & 0 & 0 & \cdots & 0 & 0 \\ 0 & 1 & 1 & \cdots & 0 & 0 \\ 0 & 0 & 0 & \cdots & 0 & 0 \\ \vdots & \vdots & \vdots & \ddots & \vdots & \vdots \\ 0 & 0 & 0 & \cdots & 1 & 1 \\ 0 & 0 & 0 & \cdots & 0 & 0 \end{bmatrix} \tag{3.8}$$

The coefficients used in the Muskingum method are represented by $\mathbf{C_1}$, $\mathbf{C_2}$ and $\mathbf{C_3}$, such that

$$\mathbf{C_z} = \begin{bmatrix} C_{z1} & 0 & \cdots & 0 \\ 0 & C_{z2} & \cdots & 0 \\ \vdots & \vdots & \ddots & \vdots \\ 0 & 0 & \cdots & C_{z\beta} \end{bmatrix} \tag{3.9}$$

where z represents 1, 2 and 3. Then

$$C_{1j} = \frac{\frac{\Delta t}{2} - k_j x_j}{k_j(1 - x_j) + \frac{\Delta t}{2}}, \tag{3.10}$$

$$C_{2j} = \frac{\frac{\Delta t}{2} + k_j x_j}{k_j(1 - x_j) + \frac{\Delta t}{2}} \tag{3.11}$$

and

$$C_{3j} = \frac{k_j(1 - x_j) - \frac{\Delta t}{2}}{k_j(1 - x_j) + \frac{\Delta t}{2}} \tag{3.12}$$

The parameter k_j represents the travel time of a flow wave through the reach and the parameter x_j is a dimensionless weighting factor that represents the attenuation of this flow wave. In this case, in accordance with the published methodologies of both Lin et al. [359] and David et al. [379], x_j is set to 0.3, globally. Fread [424] states that this parameter has a value of 0.1 to 0.3 in most streams and Koussis [425] found that the Muskingum method is relatively insensitive to this parameter. To determine k_j, for each of the 2.94 million reaches, the travel time of a flow wave was determined using

$$k_j = \frac{L_j}{c_j} \tag{3.13}$$

where L_j is the length of the reach and c_j is the flow celerity. The Manning formula (see Subsection 4.2.1) can be used to calculate flow velocity v with

$$v = \frac{R^{\frac{2}{3}} s^{\frac{1}{2}}}{n} \tag{3.14}$$

where R is the hydraulic radius, s is the slope and n is the Manning roughness coefficient. Lin et al. [359] do not explicitly state how they were able to estimate flow celerity from flow velocity, but feasibly an explanation can be arrived at by the fact that an estimate can be made by calculating the flow celerity c with the Kleitz-Seddon law [426, 427], which uses conservation of mass to give

$$c = \frac{dQ}{dA} \tag{3.15}$$

where A is cross-sectional area.

If assuming a rectangular channel of width w and depth d, this becomes

$$c = \frac{1}{w} \cdot \frac{dQ}{dd} \tag{3.16}$$

Hydraulic radius R is a measurement related to A and wetted perimeter W as

$$R = \frac{A}{W} \tag{3.17}$$

Knighton [428] suggests that when a channel is much wider than it is deep, the wetted perimeter approximates the channel width. Therefore,

$$R \approx \frac{A}{w} \tag{3.18}$$

Since $A = wd$,

$$R \approx d \tag{3.19}$$

Now, substituting for R in Eq. (3.14),

$$v = \frac{d^{\frac{2}{3}} s^{\frac{1}{2}}}{n} \tag{3.20}$$

Since $Q = vA$, multiplying this by A gives

$$Q = \frac{A d^{\frac{2}{3}} s^{\frac{1}{2}}}{n} \tag{3.21}$$

Using $A = wd$ again

$$Q = \frac{w d^{\frac{5}{3}} s^{\frac{1}{2}}}{n} \tag{3.22}$$

Differentiating this with respect to d gives

$$\frac{dQ}{dd} = \frac{5}{3} \cdot \frac{w d^{\frac{2}{3}} s^{\frac{1}{2}}}{n} \tag{3.23}$$

Using Eqs. (3.16) and (3.20)

$$\frac{dQ}{dd} = \frac{5}{3} wv = cw \tag{3.24}$$

So,

$$c = \frac{5}{3} v \tag{3.25}$$

Therefore, bearing in mind the approximations made, monoclinal waves travel at approximately five-thirds the flow speed.

The main objective of GRADES is to provide *a priori* information for the Surface Water and Ocean Topography (SWOT) satellite mission (see Subsection 2.2.4), to aid measurements of Q. It is also intended for other hydrologic applications that require spatially explicit estimates of global river flows.

The simulated discharge, modelled by GRADES, was evaluated against >17,000 gauges (Fig. 3.8), from multiple sources (Table 3.2).

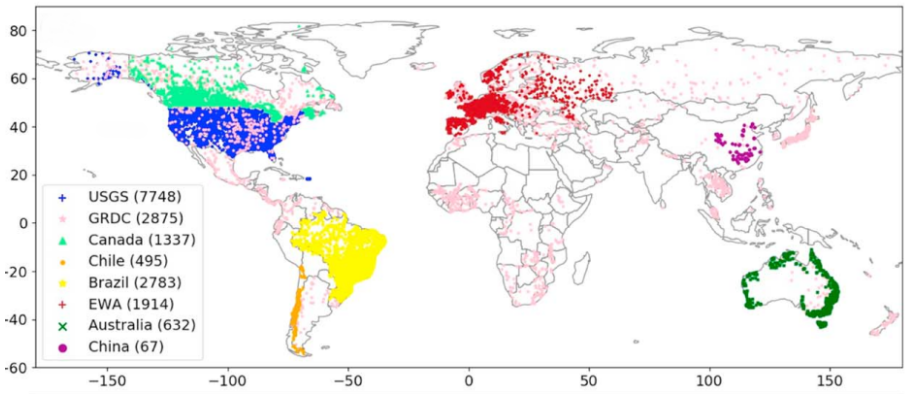

Figure 3.8: Stream gauges used to evaluate GRADES (Table 3.2).

Table 3.2: Organisations from which gauge data was used in evaluating GRADES. The numbers in parentheses refer to the number of gauges.

Organisation	Shorthand in Fig. 3.8
U.S. Gelogical Survey	USGS
Global Runoff Data Centre	GRDC
Water Survey of Canada	Canada
Chilean Centro de Ciencia del Clima y la Resiliencia	Chile
Brazilian Agência Nacional de Águas	Brazil
European Water Agency	EWA
Australian Bureau of Meteorology	Australia
Chinese Hydrology Bureau	China

Aware of inconsistent data collection, challenging sharing policies, differences of record lengths and data quality, Lin et al. [359] looked to make the most of the gauge data, to evaluate the model performance over the largest spatial extent possible. After assessment of the data set, ~14,000 gauges with more than 3 years of data were used.

The evaluation involved daily and monthly calculations of statistical values, including the correlation coefficient (CC)

$$CC = \frac{\mathrm{COV}(Q_m, Q_o)}{\sigma_{Q_m} \cdot \sigma_{Q_o}} \tag{3.26}$$

the percentage bias ($PBIAS$)

$$PBIAS = \frac{\overline{Q_m} - \overline{Q_o}}{\overline{Q_o}} \times 100\% \tag{3.27}$$

the bias ratio (BR)

$$BR = \overline{Q_m} / \overline{Q_o} \tag{3.28}$$

and the relative variability (RV)

$$RV = \left(\sigma_{Q_m}/\overline{Q_m}\right) / \left(\sigma_{Q_o}/\overline{Q_o}\right) \tag{3.29}$$

where, for Eqs. (3.26), (3.27), (3.28) and (3.29), Q_m and Q_o denote modelled and observed discharge, respectively.

The Klinga-Gupta Efficiency (KGE) determines the Euclidean distance between a point and the optimal point, where $CC, BR, RV = 1$ [429, 430], using

$$KGE = 1 - \sqrt{(CC-1)^2 + (BR-1)^2 + (RV-1)^2} \tag{3.30}$$

In terms of CC, better performance for humid regions than dry methods was revealed from this statistical evaluation (Fig. 3.9). Evaluation against monthly measurements is seen to be better than against daily measurements. With a CC of 0.6 to 1.0 (monthly) and 0.4 to 0.8 (daily), evaluation of this model is favourable, when compared with ten state-of-the-art hydrological models of Q [431].

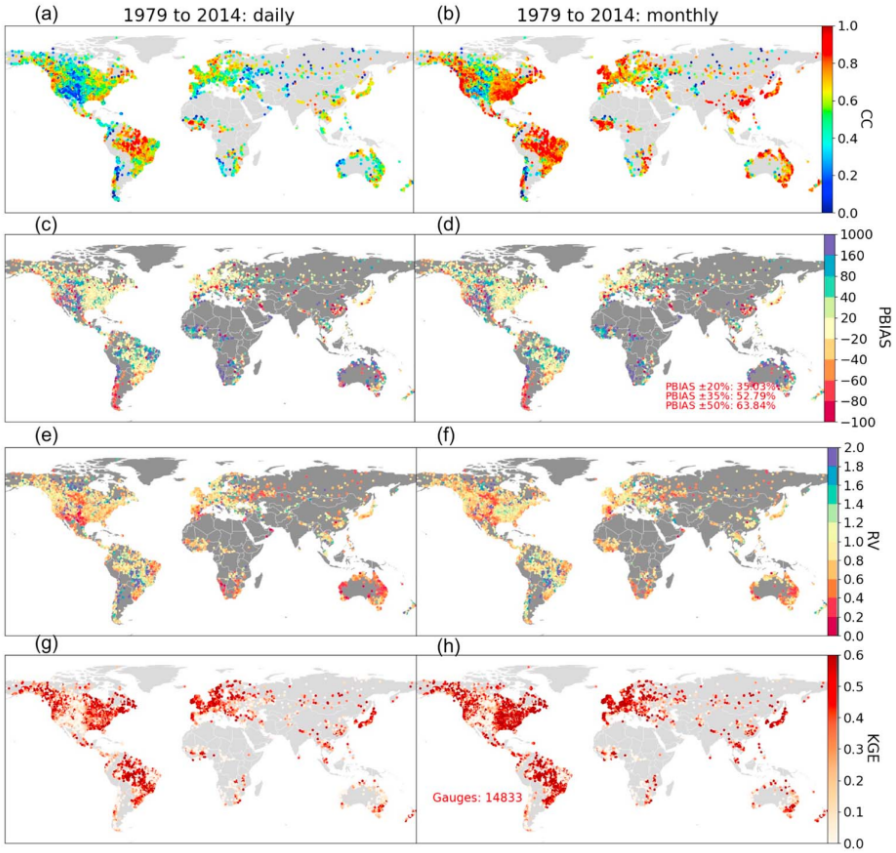

Figure 3.9: Evaluation of GRADES modelled streamflow against ~14,000 gauges [359].

3.2 Theoretical hydrokinetic resource assessment

A theoretical hydrokinetic resource assessment of global rivers was undertaken using

$$P = \gamma Q H \tag{3.31}$$

where γ is the specific weight of water (9,800 N m^{-3}). This equation is derived from a consideration of gravitational potential energy E_p, using the classical equation

$$E_p = MgH \tag{3.32}$$

where M is the mass of water and g is the acceleration due to gravity. Since M is the product of density ρ and volume V,

$$E_p = \rho VgH \tag{3.33}$$

P is the rate of energy conversion and $Q = V/t$ is the volumetric flow rate. Therefore, dividing by time t gives

$$P = \rho QgH \tag{3.34}$$

Given that $\gamma = \rho g$, this demonstrates the derivation of Eq. (3.31).

GRADES provides H and daily values of Q, from 1979–2013, for 2.94 million river reaches representative of the global river network, apart from Greenland and Antarctica. With this data expressed as a matrix $\mathbf{Q}$, a vector $\vec{H}$ and using Eq. (3.31), a matrix $\mathbf{P}$ representing values for P over α days and for β river reaches can be written as

$$\mathbf{P} = \gamma\mathbf{Q} \circ (\vec{H} \cdot \vec{1}_{\alpha}^{T})^{T} \qquad \text{where } \mathbf{P}, \mathbf{Q} \in \mathbb{R}^{\alpha\times\beta} \text{ and } \vec{H} \in \mathbb{R}^{\beta} \tag{3.35}$$

A vector of α ones is represented by $\vec{1}_{\alpha}$ and the operation $\circ$ describes a Hadamard (element-wise) product. With $\mathbf{P}$ we now have values that represent the theoretical conversion of gravitational potential energy to kinetic energy that occurs along each reach, for each day of the record.

A vector $\vec{P}$ of daily values of P, representing temporal variation of total power in the area for which $\mathbf{Q}$ and $\vec{H}$ are relevant, is given by

$$\vec{P}_i = \sum_{j=1}^{\beta} P_{ij} \qquad \text{where } \vec{P} \in \mathbb{R}^{\alpha} \tag{3.36}$$

The mean total power $\overline{P}$ of the area considered is given by

$$\overline{P} = \frac{1}{\alpha} \sum_{i=1}^{\alpha} \sum_{j=1}^{\beta} P_{ij} \qquad \text{where } \overline{P} \in \mathbb{R} \tag{3.37}$$

With this calculation, we are effectively summing the power for β reaches on a given day (Eq. (3.36)) and then calculating the mean of α daily values. Therefore, this represents the collective power of all reaches of a continental-level basin, or globally (if considered collectively), as a mean of all daily values within the period considered.

The uncertainty stated with the estimated value of the theoretcial riverine hydrokinetic resource, globally and for each continental basin, is the standard error of the mean (SEM). This is calculated using

$$\text{SEM} = \frac{\sigma}{\sqrt{\alpha}} \tag{3.38}$$

where the standard deviation σ is given by

$$\sigma = \sqrt{\frac{1}{\alpha - 1} \sum_{i=1}^{\alpha} (\vec{P}_i - \overline{P})^2} \tag{3.39}$$

The uncertainty in daily values for power $\Delta\vec{P}$ requires consideration of the terms in Eq. (3.31). The uncertainty of γ has been assumed to be negligible and therefore not considered. The change in elevation of each river reach H is derived from the measurements of MERIT DEM. This model is based upon improvements to the elevation measurements from the SRTM, in February 2000 [273]. As outlined in Subsection 2.2.5, these improvements increased the percentage of land areas mapped with a vertical accuracy of ±2 m from 39 % to 58 % after the application of a global-scale algorithm to remove absolute bias, stripe noise, speckled noise and tree height bias [279]. In this study, a linear absolute error that holds for 90 % of measurements (LE90) is stated as ±5 m, with a suggestion that the accuracy of MERIT DEM is relatively low in mountainous areas, where sub-pixel topography variability is large. A more recent evaluation of the accuracy of MERIT DEM for floodplains provided a more favourable assessment, with mean error, mean absolute error (MAE) and root mean square error (RMSE) of ±1.09 m, ±1.69 m and ±2.32 m, respectively [282]. Given the global perspective of this resource assessment, the more conservative value of ±5 m is assumed. Since the change in elevation is determined from measurements at either end of a river reach, an absolute error for H is given by

$$\Delta H = \sqrt{5^2 + 5^2} = 7\,\text{m} \tag{3.40}$$

The uncertainty in Q is based upon an analysis of the accuracy of GRADES [359]. After evaluation of the modelled data against ~14,000 gauges, the authors report that 35 % (64 %) have a percent bias within ±20 % (±50 %). PBIAS (Eq. (3.27)) measures the average tendency of the modelled discharge Q_m to be greater or smaller than observed discharge Q_o, with an optimal value of PBIAS = 0 % and low-magnitude values indicating accurate model simulation. It can be determined from the results published by Lin et al. [359] that ~85 % of evaluated modelled data have a PBIAS ≤ ±100 %, with a slight skew towards negative values, representative of an underestimation bias. The remaining ~15 % have a PBIAS > +100 %, which is representative of an overestimation bias. For this study, the fractional error for Q is considered to be

$$\frac{\Delta Q}{Q} = 1 \tag{3.41}$$

where ΔQ represents the absolute error for Q. The absolute error for $\vec{P}$ (Eq. (3.36)) is therefore given by

$$\Delta\vec{P} = \sqrt{\sum_{j=1}^{\beta} P_{ij}\left(\left(\frac{\Delta Q}{Q}\right)^2 + \left(\frac{\Delta H}{H_j}\right)^2\right)^2} \tag{3.42}$$

Given Eq. (3.41), this can be simplified to

$$\Delta\vec{P} = \sqrt{\sum_{j=1}^{\beta} P_{ij}\left(1 + \left(\frac{\Delta H}{H_j}\right)^2\right)^2} \tag{3.43}$$

and can be computed using data from GRADES with

$$\Delta\vec{P} = \left(\left(\gamma[\mathbf{Q} \circ (\vec{H} \cdot \vec{1}_{\alpha}^{T})^{T}]\right) \cdot \left(\vec{1}_{\beta} + \left((\Delta H \cdot \vec{1}_{\beta}) \oslash \vec{H}\right)^{\circ 2}\right)^{\circ 2}\right)^{\circ \frac{1}{2}} \tag{3.44}$$

where Hadamard (element-wise) operations for division and power are described using $\oslash$ and $^{\circ}$, respectively.

3.3 Estimate of the global riverine hydrokinetic resource

Global values for the theoretical riverine hydrokinetic resource were determined by summing the results of calculations on each continental-level basin (Fig. 3.3), excluding Greenland and Antarctica, for which data is unavailable in GRADES. Having calculated the theoretical riverine hydrokinetic resource for each continental-level basin (Fig. 3.10), the global resource (excluding Greenland and Antarctica) is estimated to be 58,400 ± 109 TWh yr^{-1} (Eqs. (3.37) and (3.38)).

Expressing a resource with units of TWh yr^{-1} describes the average hydrokinetic resource, but since it is a measure of energy conversion over a given time it can also be considered the average annual power. It is instructive to consider how power varies daily over the period 1979–2013, globally (Fig. 3.11) and for each continental-level basin (Fig. 3.12). The mean power of global rivers $\overline{P}$ over the period 1979–2013 can also be expressed as 6.660 ± 0.012 TW (6,660 standard power stations).

A clear intra-annual oscillation of power is observed for $\vec{P}$ (Figs. 3.11 and 3.12) and very pronounced for the continental-level basin of Asia. For all continental-level basins and globally, this oscillation of power is asymmetrical, with annual periods of maximum power being further from the average than for periods of annual minimum power. This is clearly seen in the box plots (Fig. 3.13). A least squares polynomial fit $\hat{P}$ has been applied to determine the trend described within the oscillations. The potential range of this fit $\Delta\hat{P}$ was established by applying a least squares polynomial fit to the maximum and minimum values for $\vec{P}$, as calculated by Eq. (3.42) or Eq. (3.44), using the range of potential values for H (Eq. (3.40)) and Q (Eq. (3.41)).

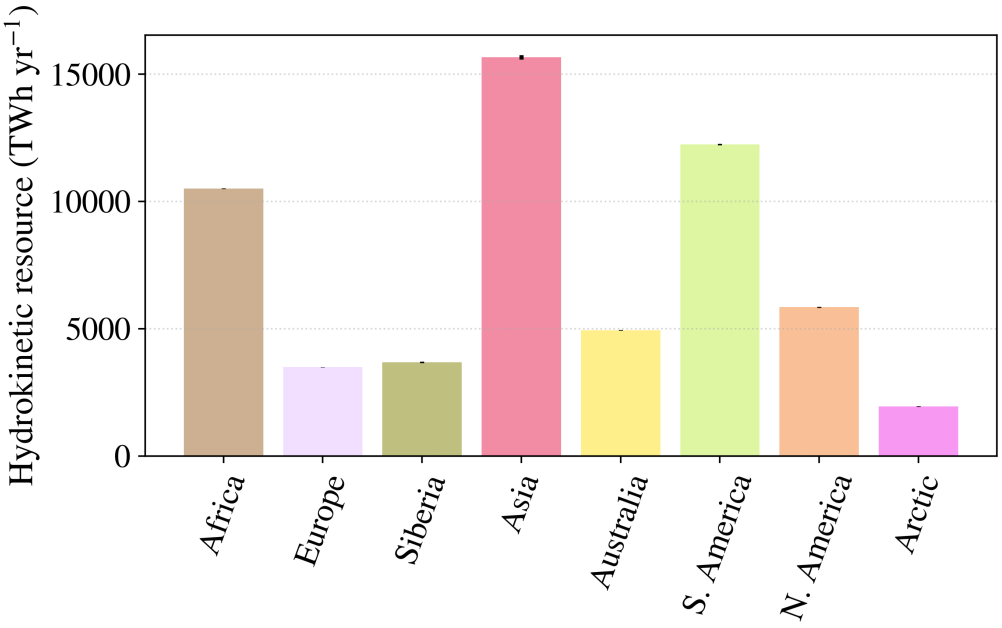

Figure 3.10: Mean hydrokinetic resource, by continental-level basin, averaged over the period 1979–2013.

A rising trend in inter-annual power of $1.49 \pm 1.38\,\mathrm{MWh\,d^{-1}}$ is seen globally, with similar rising trends present for all continental-level basins. It must be noted that significant uncertainty in the gradient of $\hat{P}$, as determined by $\Delta\hat{P}$, means that the trend may be neutral or, for some continental-level basins, could be falling (Fig. 3.14). Again, with due regard given to the uncertainty, it is seen that the rising trend is most significant for Africa, Australia and South America. In contrast, Europe, North America and the Arctic barely show a rising trend. This division would imply a difference between the Southern Hemisphere (SH) and the Northern Hemisphere (NH).

The calculation of P is dependent upon the product of γ, Q and H (Eq. (3.31)). For each reach, γ and H are constant. Therefore, we can say that $P \propto Q$ and that any fluctuations in P are directly as a result of changes in Q. Reasons for this may be attributed to changes in factors such as rainfall, or the rate of snowmelt and icemelt. The visible intra-annual oscillation can be explained by the expected seasonal variations of these factors. Inter-annual change may be attributed to changes in these factors due to a change in the climate. The rate of snowmelt and icemelt would be expected to correlate with a rise in global temperature. A rising global temperature has been linked to an increase in the intensity of the hydrological cycle [432], but Held and Soden [433] advise against a simple assumption that global systems become more energetic as they warm and conclude that the complexity of such systems should guard against over-confidence in simple arguments. Studies that have investigated an asymmetry between the climate change effects and affects of the NH and SH may be relevant in exploring further the observed differences in our results [434–436]. This trend is further explored in Section 4.4, with the benefit of a different perspective.

The theoretical riverine hydrokinetic resource can be determined by river reach, thus permitting a representation of spatial distribution and identification of areas with high concentrations of hydrokinetic energy (Fig. 3.15). A general description of areas which are prominent,

would include: the Himalayas, Tibetan Plateau and surrounding areas; the large, mountainous islands of Borneo, Indonesia and New Guinea; New Zealand; the Andes; the Pacific Northwest; Scandinavia; the Congo Basin and Equatorial Africa; Madagascar; and many of the major rivers of the world. This attempt to qualitatively describe areas of Earth identified as having potential for HEC, apart from including major rivers as might be expected, highlights the predominance of areas that have rivers with significant elevation change.

3.4 Distribution of hydrokinetic energy by country

The theoretical riverine hydrokinetic resource is considered by country (Fig. 3.16). The countries assessed to have the greatest total hydrokinetic resource are China, Russia and Brazil (Fig. 3.17).

Determining the theoretical riverine hydrokinetic resource by country is useful, but favours larger countries, which tend to have a greater combined length of rivers. Therefore, it may be instructive to consider the resource relative to the total length of the rivers in a country, providing a normalised perspective, which is referred to here as hydrokinetic resource density (Fig. 3.18). The river length of each river reach is also provided by GRADES, so the total length is a simple summation. In this case, the countries assessed to have the greatest total hydrokinetic resource, relative to total river length, are Bhutan, Nepal and Tajikistan (Fig. 3.19).

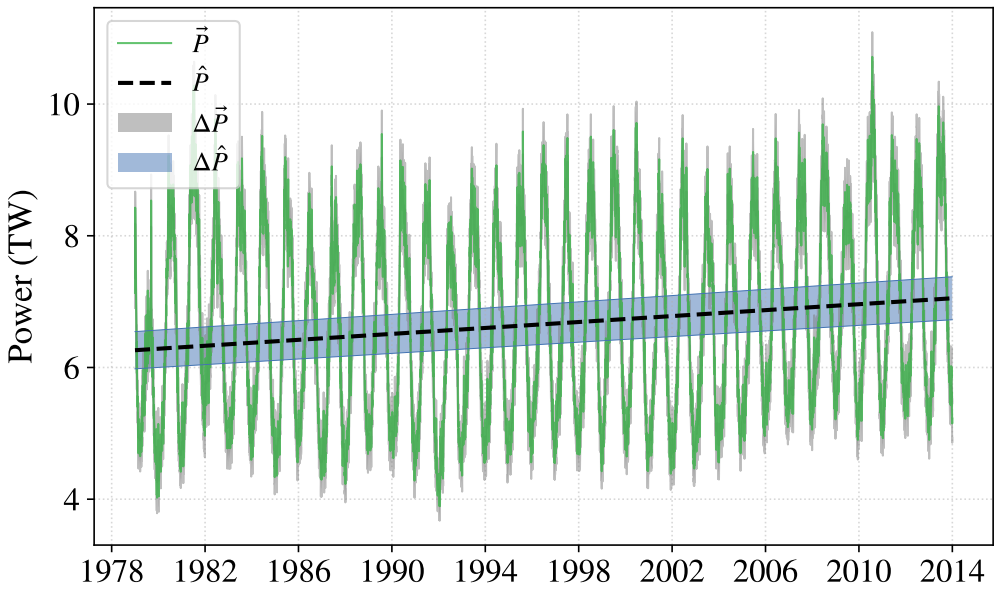

Figure 3.11: Total daily power $\vec{P}$ of global rivers (excluding Greenland and Antarctica) between 1979–2013, including the uncertainty in daily values $\Delta\vec{P}$, a least squares polynomial fit $\hat{P}$ and corresponding uncertainty $\Delta\hat{P}$.

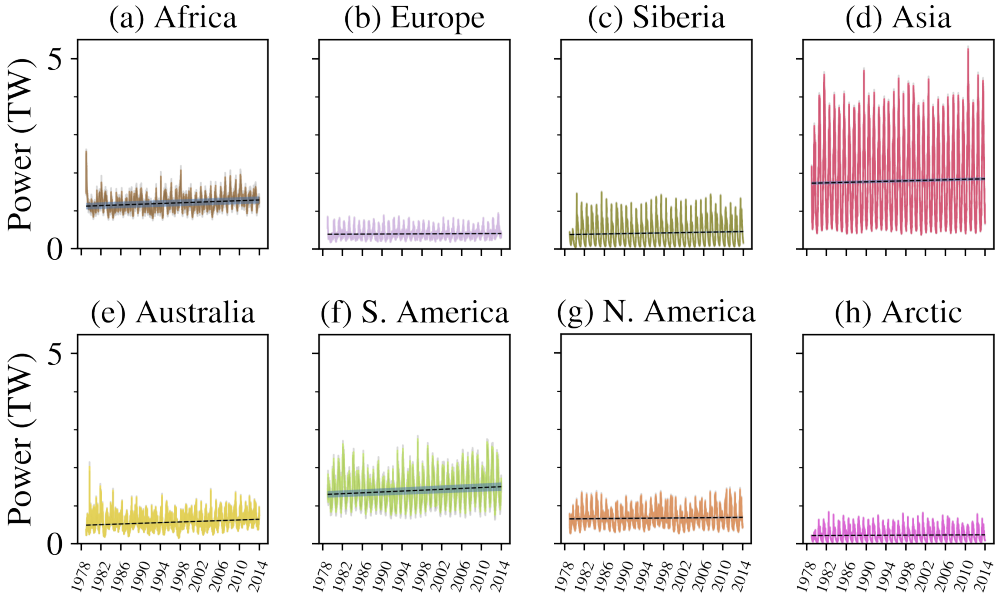

Figure 3.12: Total daily power for each continental-level basin (excluding Greenland and Antarctica), between 1979–2013.

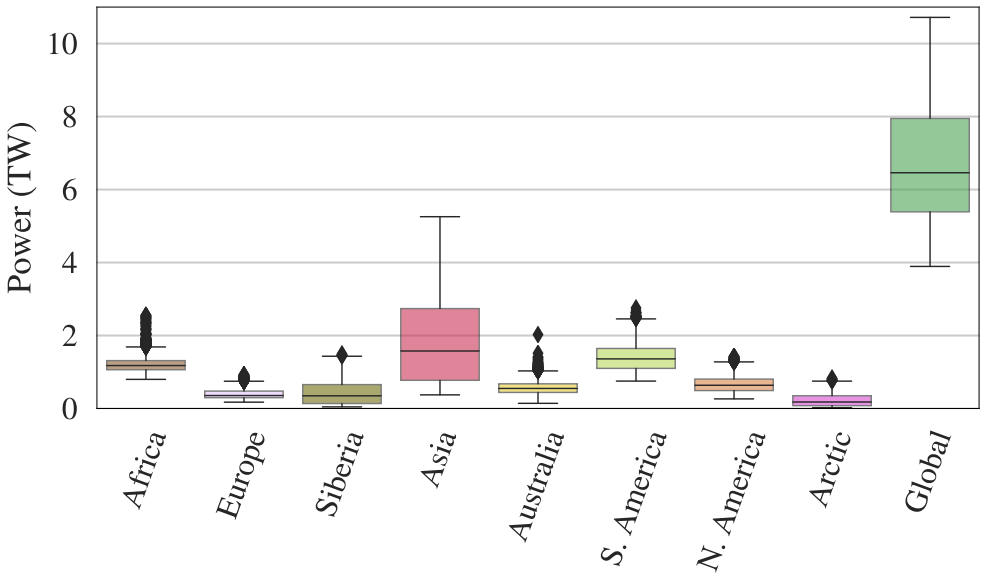

Figure 3.13: Box plots for the total daily power for each continental-level basin (excluding Greenland and Antarctica) and globally, between 1979–2013. Inside the boxes describes the range of values between the 25th percentile and the 75th percentile, with the horizontal line representing the median. The whiskers represent the 0th percentile and the 100th percentile.

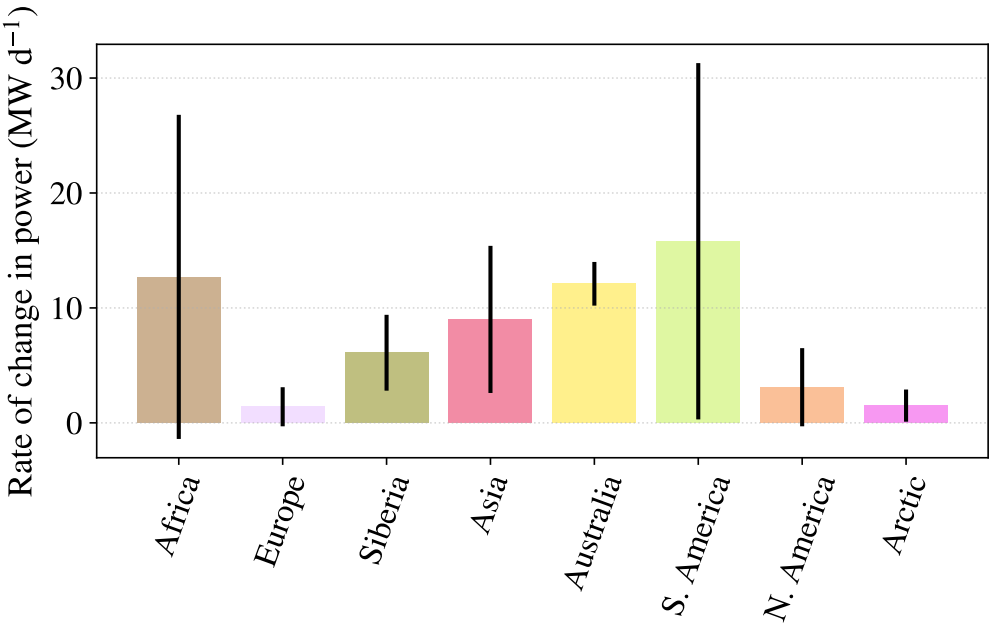

Figure 3.14: The rate of change of daily power, between 1979–2013, from measurement of the gradient of a least squares polynomial fit of daily values of power.

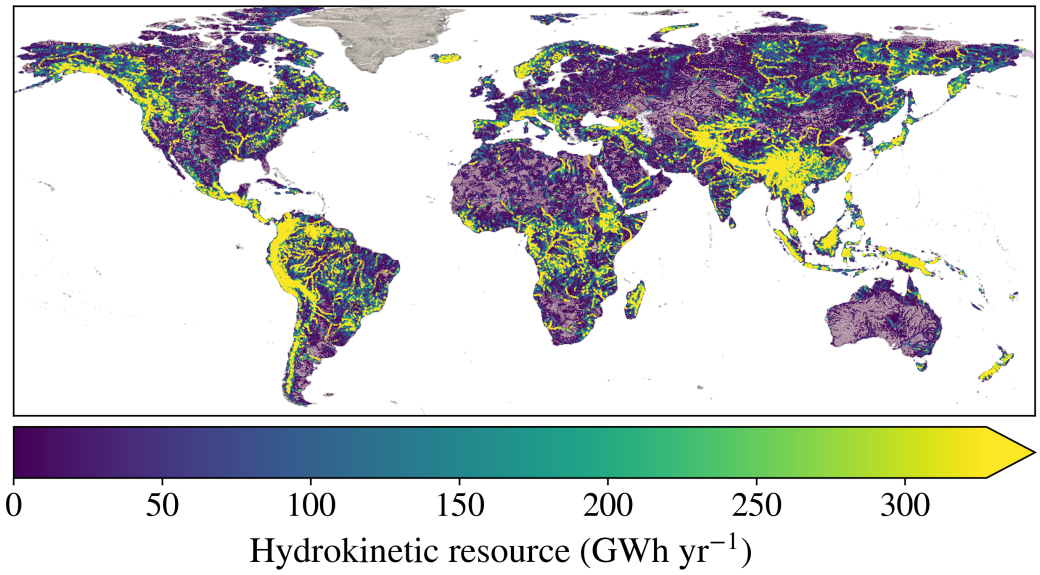

Figure 3.15: Global distribution of theoretical riverine hydrokinetic resource.

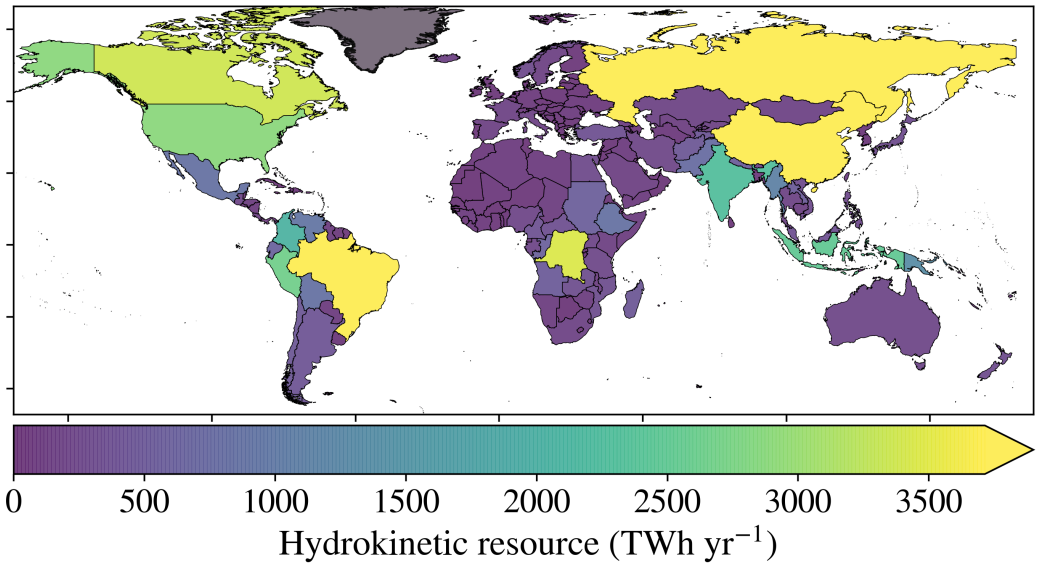

Figure 3.16: Mean hydrokinetic resource, by country, averaged over the period 1979–2013.

3.5 Concluding remarks

Though the uncertainty in the data for Q and H used within this study are significant, they may be deemed acceptable according to the stated aims. It is difficult to evaluate the accuracy of the estimates of power and hydrokinetic resource that are calculated with this data, for 2.94 million individual river reaches. For this reason, the results presented here might be best considered a first-order approximation, serving to provide an indication of where the most promise may lie and a first iteration of an assessment of the global resource. Laws and Epps [123] claim that previous large-scale HEC resource assessments of tidal sites have included a significant degree of error. For example, one such assessment that used a tidal model, predicted flow velocities that differed from onsite measurements by $\geq 30\,\%$, leading to an error of a factor of two or more [176]. They state that previous global tidal potential estimates range from 100 TW h yr^{-1} to 17,500 TW h yr^{-1}.

As discussed in Subsection 2.2.2, a previous riverine hydrokinetic resource assessment of the continental United States of America determined that there was a theoretical resource of 1,381 TWh yr^{-1} [187]. The study used different methods for the 48 contiguous states and for Alaska, due to the availability of the National Hydrograph Dataset Plus (NHDPlus) for the contiguous states only, at this time. This study used the same standard hydrological equation for determining theoretical hydraulic power (Eq. (3.31)) as has been used in the methodology described in this chapter. A difference is that only river reaches with a mean discharge $Q >$ 28 m^3 s^{-1}(1,000 cfs) were included in their assessment and river reaches containing dams or hydroelectric plants were excluded.

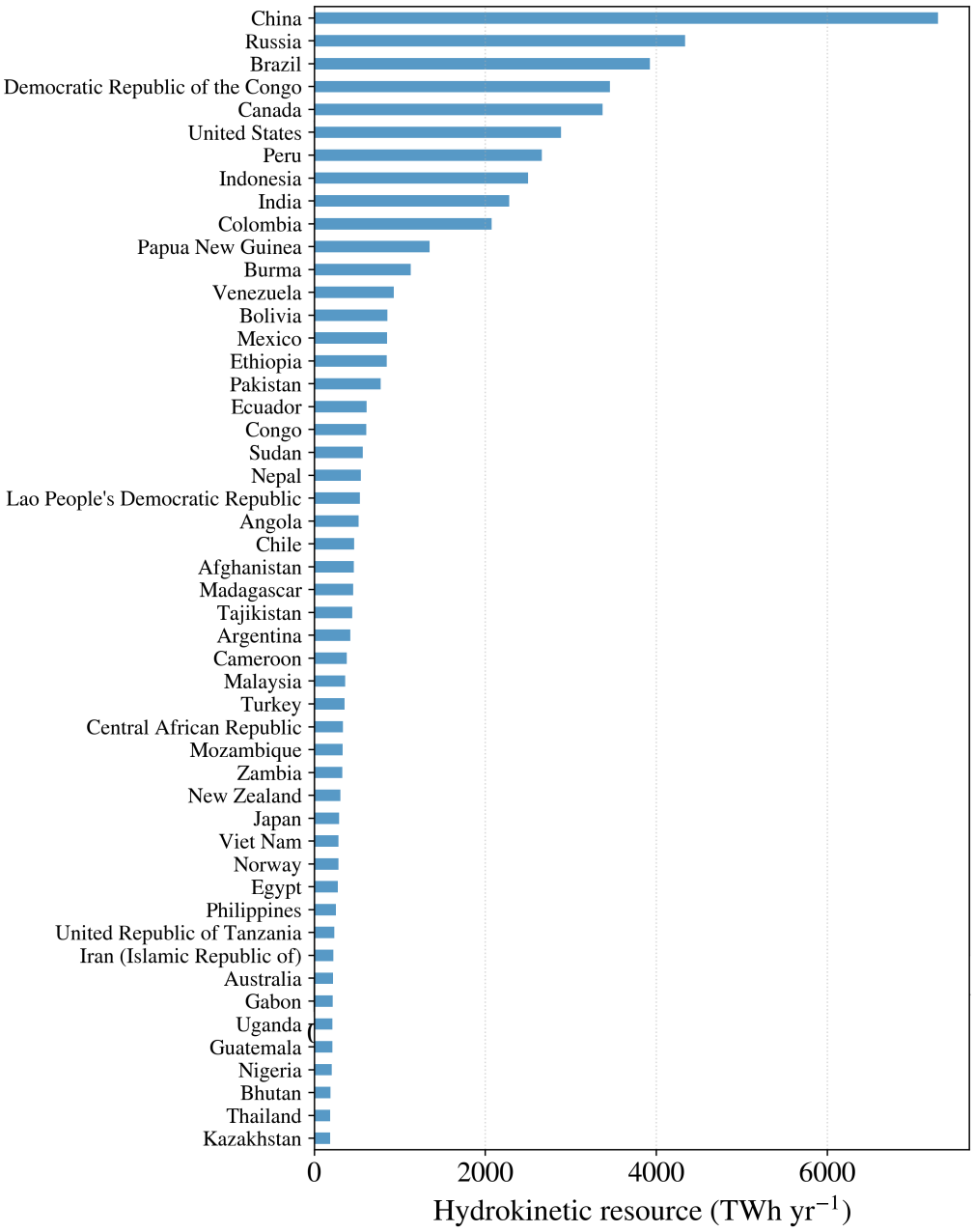

Figure 3.17: Mean hydrokinetic resource of the top 50 countries.

For comparison with this previous study, the method presented in this chapter was applied to a subset of data representing the contiguous states of the United States and Alaska, where only reaches with a mean discharge $Q > 28\,\mathrm{m^3\,s^{-1}}$ were included (Table 3.3). This calculation does not include a removal of reaches containing dams or hydroelectric plants.

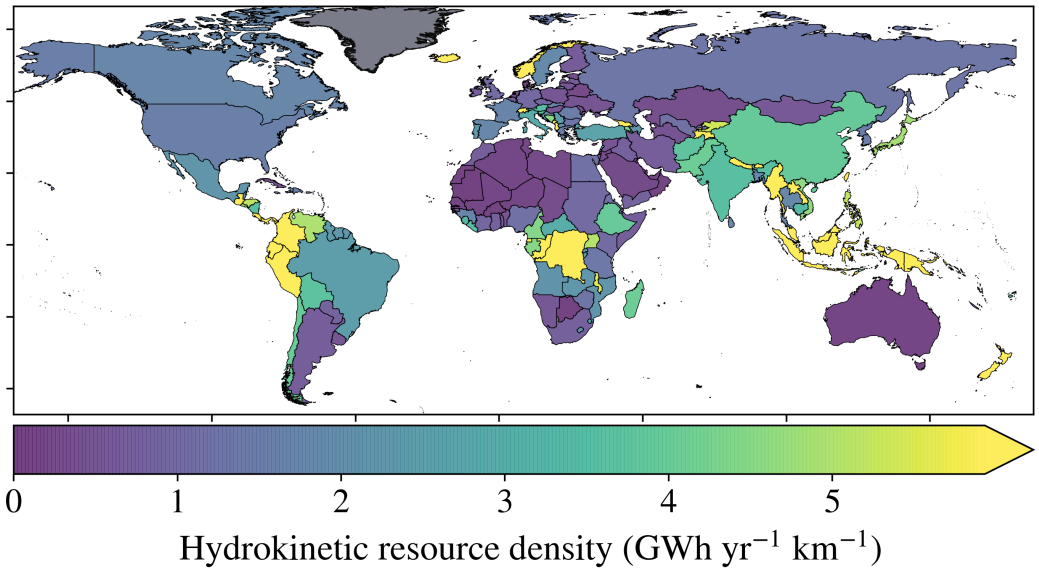

Figure 3.18: Mean hydrokinetic resource relative to total river length, by country, averaged over the period 1979–2013.

Jacobson et al. [187] state that validation of their hydrokinetic resource assessment was difficult, due to the lack of empirical data from existing HEC deployments. They further state that they know of no direct measurements of in-stream energy that could be used to validate their model and attribute this to both a lack of projects and also a reluctance to publish.

Miller et al. [188] carried out an earlier study to assess the technical riverine hydrokinetic resource of the United States. Accurately assessing a large-scale technical resource is challenging, requiring much more information and consideration of many more factors. Complications include determining the horizontal 2D distribution field for v and d; and for the deployment of an array of turbines, the backwater effect caused by energy extraction. Their study determined the river reaches with the most potential, in 12 of 16 hydraulic regions, chosen using a criteria for including the region if mean discharge $Q > 113\,\mathrm{m^3\,s^{-1}}$(4,000 cfs) and mean flow velocity $v > 1.3\,\mathrm{m\,s^{-1}}$(4.3 fps). An inconsistent criteria was used across these regions, but river reaches identified as having the greatest potential were assessed for recoverable power. An estimate was achieved by assuming turbine array deployment over 25 % of the width and 25 % of the length that met a minimum discharge criteria; with a turbine spacing of half a turbine diameter in each row and 5 turbine diameters spacing between the rows; where the turbine diameter is 80 % of the mean depth; and the power coefficient $C_p = 40\,\%$. This method resulted in an aggregate mean annual power of 12,500 MW, yielding 110 TWh yr^{-1}. This result is a technical resource assessment, not a theoretical resource assessment, so comparison is difficult. Still, a coarse estimate of the technical resource can be determined by multiplying the theoretical resource by a significant impact factor (SIF), which is intended to represent the percentage that can be extracted without significant economic, or environmental effect. It should be noted that this is a very rough, first-order estimate with high uncertainties, but still offers some means of comparison. Though this would be site specific, previous studies have used 20 %, with the assumption that this would yield an upper limit [186]. This current study determined that the United States has a theoretical resource of ~2,900 TWh yr^{-1}, without filtering out any reaches according to a criterion for Q. Applying an SIF of 20 % provides an estimate of the technical

resource to be 580 TWh yr^{-1}. An SIF of 4 % corresponds with an estimate of the technical resource of the United States being 110 TWh yr^{-1}, as calculated by Miller et al. [188], if assuming the theoretical resource to be 2,900 TWh yr^{-1}.

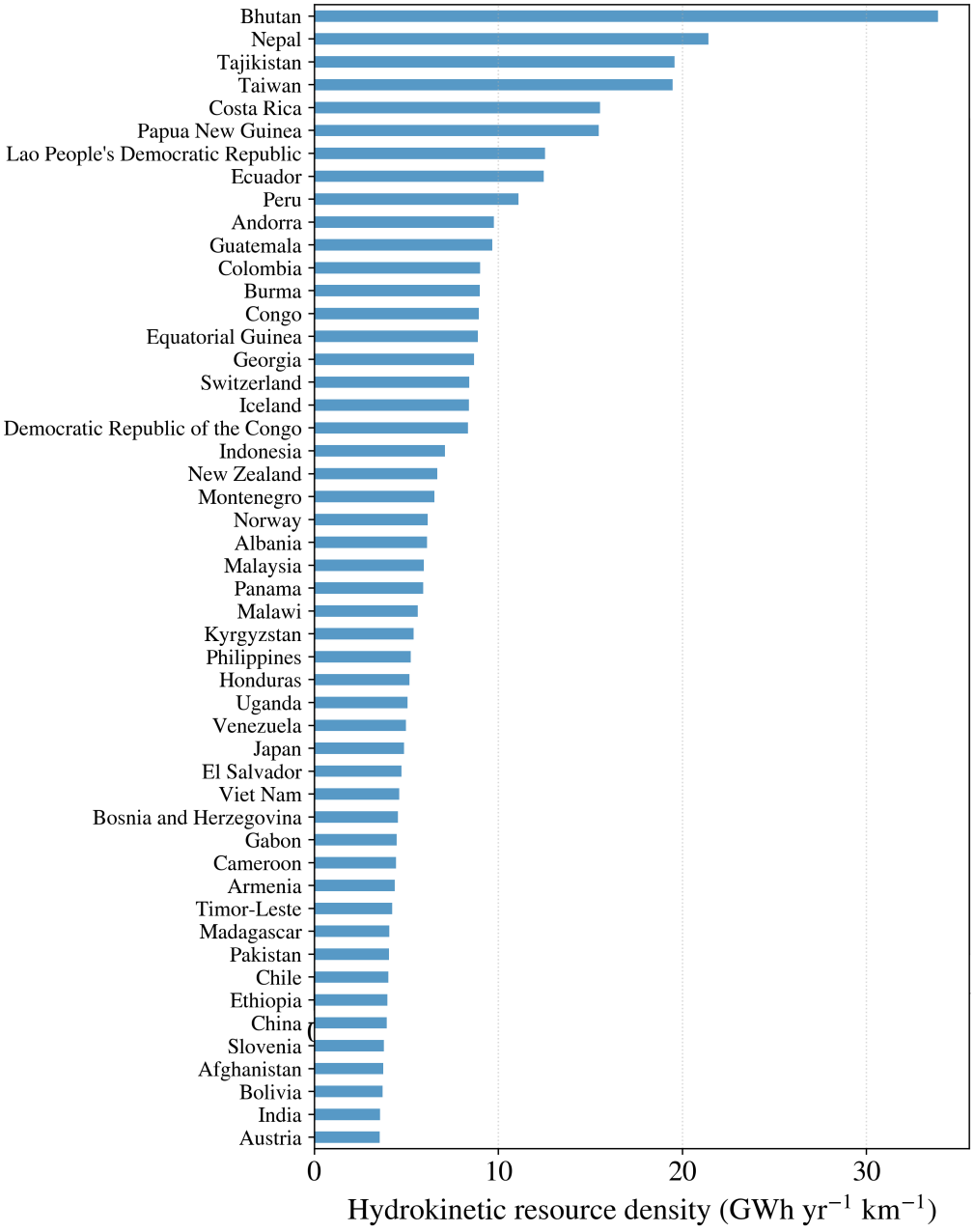

Figure 3.19: Mean hydrokinetic resource relative to total river length of the top 50 countries.

Close proximity of communities to rivers and streams is common, with over 50 % of the world's population living less than 3 km from a surface freshwater body and only 10 % living more than 10 km away [437]. A correlation has been identified between population, need for electrification, poverty and river distribution [122]. This correlation is more dominant in Asia, Central Africa and South America, which are regions which the results suggest offer promising

Table 3.3: Comparison of the results in this current study, for the continental states of America, to a previous resource assessment by Jacobson et al. [187].

	Estimated resource from Jacobson et al. [187] (TWh yr^{-1})	Estimated resource from this study with $Q > 28\,\mathrm{m^3\,s^{-1}}$ (TWh yr^{-1})
Contiguous states	1,146	1,350
Alaska	235	348
Total	1,381	1,698

potential for HEC.

Jacobson et al. [187] assessed the hydrokinetic resource of the contiguous United States, using a method similar to that outlined here. The results of their study are comparable to those we present for the same region (Table 3.3). Both their study and ours use the standard hydrological equation for determining theoretical hydraulic power (Eq. (3.31)). The derivation of this equation is from gravitational potential energy (see Section 4.1). For this reason, it could be argued that Eq. (3.31) is most applicable to a consideration of a resource assessment from a hydrostatic perspective, rather than a hydrokinetic perspective.

This sets thing up neatly for the next chapter, where these two perspectives are considered. In this chapter, a novel approach is proposed, intended to provide a truly hydrokinetic perspective.

Chapter 4

A hydrokinetic perspective

This chapter is based upon the article *Hydrokinetic energy conversion: A global riverine perspective* [138].

4.1 The conventional approach to hydrokinetic resource assessment

The energy within water is apparent in the propagation of gravity waves, density gradients, the gravitational potential energy attained through elevation change, or as kinetic energy due to its movement. The latter two examples are of most relevance to rivers, where the conversion of gravitational potential energy can be described as *hydrostatic*, and kinetic energy conversion as *hydrokinetic* [128]. The hydrostatic approach is commonly exploited by impounding a reservoir of gravitational potential energy, as a hydraulic head behind a dam, as in conventional hydropower plants. The hydrokinetic approach involves directly converting the 'free stream' kinetic energy of flowing water.

In previous hydrokinetic resource assessments [137, 187] and in the methodology of Chapter 3, theoretical hydraulic power P has been calculated using

$$P = \gamma Q H \tag{4.1}$$

where γ is the specific weight of water (9,800 $\mathrm{N\,m^{-3}}$), Q is discharge (volumetric flow rate) and H is the change in elevation of a given river section. The derivation of this equation, from the classical equation for calculating gravitational potential energy ($\mathrm{E_p}$ = MgH), is provided in Section 3.2. Considering this derivation, Eq. (4.1) is relevant from a hydrostatic, rather than a hydrokinetic, perspective. A methodology that focuses on flow velocity — to reflect a technology (hydrokinetic energy conversion) that uses the energy of free-flowing water directly, rather than a technology (conventional hydropower) that uses the impoundment of a hydraulic head — may be more appropriate. To support this argument, consider the quantification of power output by conventional hydropower, derived from a consideration of kinetic energy E_k, as defined by the classical equation

$$E_k = \frac{1}{2}Mv^2 \tag{4.2}$$

where v is velocity. Power is the rate of energy transfer

$$P = \frac{dE_k}{dt} \tag{4.3}$$

Using the product rule for derivatives gives

$$P = \frac{1}{2}\left(v^2\frac{dM}{dt} + M\frac{dv^2}{dt}\right) \tag{4.4}$$

When considering a flowing fluid, Bernoulli's equation [438] states that

$$E_p + E_k + U = \text{ constant} \tag{4.5}$$

where U is the internal energy. If considered per unit volume, this can be expressed as

$$\frac{1}{2}\rho v^2 + \rho g z + p = \text{constant} \tag{4.6}$$

where z is the elevation of the point above a reference plane and p is the pressure.

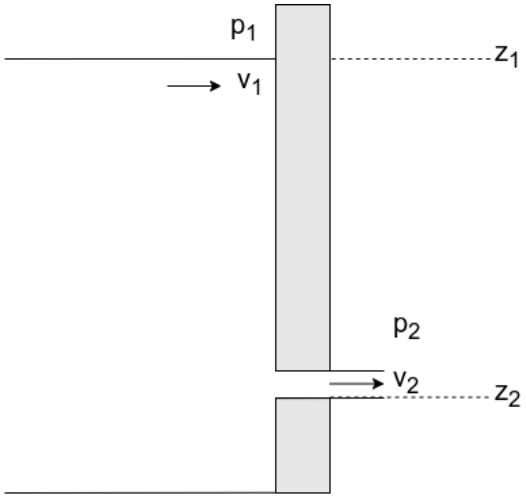

Figure 4.1: The pressure p, elevation z, and flow velocity v of a fluid at the surface behind a dam and flowing through a penstock at the base of the dam.

The conservation of energy means that there can be no loss of energy as the fluid flows between two points. Therefore, if considering fluid at the surface of a body of water constrained behind a dam and fluid flowing through a penstock at the base of the dam (Fig. 4.1), this can be described with

$$\frac{1}{2}\rho v_1^2 + \rho g z_1 + p_1 = \frac{1}{2}\rho v_2^2 + \rho g z_2 + p_2 \tag{4.7}$$

A fluid flowing through the penstock located at a height defined as $z_2 = 0$ will have a velocity

v_2. The surface is elevated above this at z_1, where the velocity of the fluid is $v_1 = 0$. Due to the surface and the outlet of the penstock being acted upon by atmospheric pressure, $p_1 = p_2$. Now,

$$\frac{1}{2}\rho v_2^2 = \rho g z_1 \tag{4.8}$$

which rearranges to give

$$v_2 = \sqrt{2gz_1} \tag{4.9}$$

More generally, the velocity of a fluid leaving a container, or a dam, is given by

$$v = \sqrt{2gH} \tag{4.10}$$

where, in this case, $H = z_1 - z_2$ represents the change in elevation from the penstock to the surface of the water impounded behind the dam, but is equivalent to the earlier definition of H. Since g and H remain constant, so does v, meaning

$$\frac{dv^2}{dt} = 0 \tag{4.11}$$

The rate of change of mass is

$$\frac{dM}{dt} = Q\rho \tag{4.12}$$

Substituting for Eqs. (4.11) and (4.12) into Eq. (4.4) gives

$$P = \frac{1}{2} \cdot 2gH \cdot Q\rho \tag{4.13}$$

Since $\gamma = \rho g$, this derivation from a consideration of kinetic energy agrees with the derivation of the equation for calculating power from a consideration of gravitational potential energy (Eq. (4.1)).

Implicit in Bernoulli's principle, is the idea that energy is conserved throughout a body of water. This means that the energy that a particle of water at the bottom of a column of water has is equal to the energy at the top of the water column. This is analogous to the conservation of energy that is exhibited by a body in free fall, as gravitational potential energy is converted into kinetic energy. Therefore, if ignoring all forms of friction, the velocity of the water released from below the surface of a body of water (Fig. 4.1), can be determined by consideration of the equation of motion, from classical physics,

$$v_f^2 = v_0^2 + 2a(r - r_0) \tag{4.14}$$

where v_f is a particle's final velocity, v_0 the initial velocity, a the acceleration, r the final position and r_0 the initial position. (This is also commonly stated as $v^2 = u^2 + 2as$.) With reference to Fig. 4.1, $v_f = v_2$, $v_0 = v_1 = 0$, $a = -g$ and $r - r_0 = z_2 - z_1$. Therefore, this becomes

$$v_2^2 = v_1^2 - 2g(z_2 - z_1) \tag{4.15}$$

If we assign a value for the height of water above the point of exit, such that $H = z_1 - z_2$, this gives

$$v^2 = 2gH \tag{4.16}$$

which can be rearranged to give Eq. (4.10). To illustrate what this means, an object released outside of the body of water and from the top of the container (at height z_1) will reach the same velocity in free fall (if excluding air resistance), when arriving at the bottom of the container, as the water released at the bottom of the container.

The power available from hydrokinetic energy conversion (HEC) is modest compared to that from conventional hydropower. To illustrate this, Eq. (4.10) can be used to show that a flow speed of $1\,\mathrm{m\,s^{-1}}$ (which is approximately the minimum flow speed necessary for HEC) would correspond to a static head height of only 50 mm. Therefore, even a modestly sized conventional impoundment hydropower plant can theoretically result in a considerable flow speed (Fig. 2.1).

The GRADES data set used in this study (see Subsection 3.1.3) includes river reaches with a median (mean) length of 6.8 km (9.2 km), but ranges from a minimum of 0.01 km to 424.67 km. The maximum change in elevation for a reach within this data set is $H = 3{,}734\,\mathrm{m}$. This corresponds to a flow velocity of $v = 271\,\mathrm{m\,s^{-1}}$, after applying Eq. (4.10). This is clearly unreasonably high, given that such a flow velocity is unrealistic.

Power is a measure of the rate of energy *conversion*, or the rate of energy *transfer*. Using the conventional equation (Eq. (4.1)) to calculate the theoretical hydrokinetic resource within a given reach, means considering the conversion from gravitational potential energy to kinetic energy that theoretically occurs within a reach. Of course, energy will be dissipated by friction against the bed and banks of this reach, in practice, but using this method of theoretical resource assessment means any friction is discounted. This point is confirmed by remembering the means of derivation of Eq. (4.1) and how Q is essentially a measure of the quantity of water, rather than a measure of volumetric flow rate, in this context. This method does not acknowledge a movement of water at all, in fact, only the change in energy that occurs, in a given mass of water, due to a change in elevation. Still, in practical terms, using the conventional equation implies unrealistic values for v as calculated by Eq. (4.10) and illustrated in Fig. 2.1. As will be discussed below, the dissipation of energy by friction is not equal throughout a river, from the upper to the lower courses. Therefore, this conventionally used equation, even if accounting for the fact that friction is omitted, may still be biased according to the position in a river network considered and provide an unrealistic perspective on the global distribution of HEC potential.

Furthermore, this approach implies that as the slope reduces, v will decrease. This is a common misconception and the opposite of what actually occurs. As we shall explain further below, Leopold and Maddock [297] predict an increase in v with an increase in Q (Eq. (4.25)). As you proceed downstream, Q will tend to increase because the drainage area progressively increases. Only in exceptional cases, particularly in arid areas, will rivers have Q decrease in a downstream direction.

The upper courses of a river flow down from high hills and mountains. They are often narrow, steep and marked by sharp valleys and abrupt changes of direction. The steepness means that there is much gravitational potential energy, often resulting in high turbulence, waterfalls and high levels of erosion. Upland streams can appear to have very fast flows, however this is usually very turbulent and in fact much of the water in the upper-course is almost stationary,

particularly close to the bed and banks where friction is highest. The transition from upper to middle courses is marked by a widening of channels and reduced steepness. The lower courses can be similar to the middle courses, but generally wider and less steep.

The Manning formula gives another means for determining v, using

$$v = \frac{R^{\frac{2}{3}} s^{\frac{1}{2}}}{n} \tag{4.17}$$

where R is the hydraulic radius, s is the slope, and n is the Manning roughness coefficient (see Subsection 4.2.1). The hydraulic radius is given by

$$R = \frac{A}{W} \tag{4.18}$$

where A is the cross-sectional area and W is the wetted perimeter. Both will increase in a downstream direction, but the rate of increase of A is greater than W, causing R to increase downstream. This can be confirmed by consideration of the Bradshaw model [439, 440]. This is an idealised model which describes the general change in river characteristics, from the upper courses, downstream to the lower courses. In this direction, the model describes an increase in Q, w, d, v and load quantity. Also in this direction, the model describes a decrease in n, s and load particle size. This suggests that both A and W will also increase in a downstream direction. It is fair to assume that w will increase at a far greater rate than d, along the length of a river. This is quite apparent, but if further explanation is required, the power law relationships of Leopold and Maddock [297] (Eqs. (2.35) and (2.36)) amply demonstrate this, when typical values for the coefficients and exponents of these power law relationships are considered (discussed in Subsection 4.2.3). This is also clearly illustrated in Fig. 4.4, when the downstream increase in Q is considered.

In Subsection 3.1.3, we considered R and a number of assumptions and approximations. In the lower course of a river, we can (for the most part) assume $w >> d$. Therefore, using the suggestion of Knighton [428], as before, we can assume that $W \approx w$. Since $A = wd$, this confirms that the rate of increase of A is greater than the increase in W, in a downstream direction. Though the relative change in magnitude of s and R in Eq. (4.17) cannot be quantified in general terms, apart from the likelihood that s will decrease and R will increase, it is important to notice that in Eq. (4.17) the exponent for R is greater than that for s. Therefore, moving downstream, the increase of R will have more affect than the decrease of s, implying a corresponding increase in v. This may be interpreted as meaning that the decrease in boundary-induced friction overcompensates for the decrease in slope. Acknowledging the counter-intuitive nature of v increasing in a downstream direction, Leopold [441] demonstrates that this is indeed the case, using empirical measurements in a number of different rivers.

A method of hydrokinetic resource assessment that focuses directly on the transfer of kinetic energy, rather than the conversion of gravitational potential energy to kinetic energy, potentially offers a more realistic and pragmatically useful approach. Perhaps this provides a meaningfully different, relevant and useful perspective, with sufficient evidence to support this being more accurate and representative of the riverine hydrokinetic resource. The remainder of this chapter will explore this idea further.

4.2 Hydraulic geometry

4.2.1 Hydraulics

Hydraulics is concerned with the conveyance of liquids through pipes, or channels. As a discipline, its origins can be traced to the digging of irrigation channels in prehistoric Mesopotamia, advancing slowly through the accumulation of empirical knowledge for many centuries. Roman viaducts stand as a testament to this process, which continued until the 18th century, when an acceleration in theoretical and experimental fluid dynamics can be observed. A marker for the beginning of modern hydraulics can arguably be provided by the identification of a relationship between v, s and R [442], as expressed by the Chézy equation

$$v = C\sqrt{Rs} \tag{4.19}$$

where C is the Chézy coefficient, determined by consideration of gravitational and frictional forces. Manning et al. [443] empirically determined a value for the Chézy coefficient as

$$C = \frac{1}{n}R^{\frac{1}{6}} \tag{4.20}$$

introducing n, known as the Manning roughness coefficient, as introduced in Eq. (4.17). This is an empirically determined value for given boundary conditions, which is intended to remain constant regardless of slope of channel, size of channel, or depth of flow [299]. Huggett [291] states that this value is often estimated from standard tables, or by comparison with photographs of channels with known roughness. The units of n are $\mathrm{s\,m^{-1/3}}$, though they are often omitted. A power law relationship between n and Q has been determined [298]:

$$n = NQ^p \tag{4.21}$$

where N and p are empirically determined parameters. In general, a power law relationship describes how a relative change in one quantity results in a proportional, relative change in another. It has the form

$$y = ax^k \tag{4.22}$$

where an independent variable y results from the affects of a coefficient a and exponent k upon an independent variable x. This principle represents an important corner-stone of what follows, allowing the estimate of a quantity, when little information on this variable is available, using a quantity where there is more. The coefficients and exponents, in this case, are either empirically determined, or described as mean values within a range of uncertainty, following statistical analysis.

Thus, the development of hydraulics continued and Manning et al. [443] introduced an alternative and more commonly used equation for estimating v (Eq. (4.17)).

Open-channel flow is distinct from flow in closed pipes, or free jets, due to this form of flow being supported from below and having an upper surface, which is exerted upon by atmospheric pressure. When an open channel is inclined, the flow will be caused to accelerate and continuity will cause its cross-section to thus decrease. Flow velocity depends on the flow

rate and the channel geometry related to the resistance and water surface slope. Huggett [291] lists the specific *geomorphological* factors that affect streamflow velocity: slope gradient, bed roughness and cross-sectional form of the channel.

4.2.2 Perspectives on hydraulic geometry

A detailed and high resolution explanation of river system geometry requires consideration of hydraulic geometry, in relation to variations in Q, in addition to the basin-scale geometry of drainage and channels. These later points are considered, in detail, in Section 5.1. Hydraulic geometry is a sub-field of fluvial geomorphology, which focuses on the evolution of river form and how the surrounding terrain and channel form influence this evolution. A stream must satisfy at least three physical relations in adjusting its geometry: continuity, flow resistance and sediment transport. Hydraulic geometry can be considered at a particular cross-section, or in terms of the influence upstream, or downstream. Characteristics responsive to analysis by hydraulic geometry include mean width w, mean depth d, v, s, suspended sediment and friction.

Past studies have attempted to interpret the spatial variation of channel geometry [301, 306, 444–447]. Moody and Troutman [448] recognised that this required consideration of the marginal probability of w and d. Prior to their own work, this has been considered in different contexts:

- at a few irregularly spaced cross-sections [297, 301, 449];
- at regularly spaced cross-sections on a few rivers [450–452]; and,
- at the plan-form scale (excluding an effective means for determining the characteristics of d), using aerial photography [445, 446, 453–455].

Moody and Troutman [448] state that the variability of w and d, in a given river reach, can be conceptualised as a wave spectrum in which deterministic processes are characterised by individual wavelengths [445, 450–453] and stochastic processes are characterised by bands of wavelengths [447, 455]. They suggest that these stochastic processes have a 'memory', since it has been found that there are autocorrelations[1] of w, s and thalweg[2], in the downstream direction, at the small-scale end of this spectrum [450–452, 456]. This 'memory' can also be viewed as a correlation distance, where the distance is defined as the integral length scale. This is analogous to the integral timescale used to characterise turbulence [457].

The importance of the work of Moody and Troutman [448] is that their study investigated the character of the spatial variability of channel morphology at the reach-scale, over a much wider range of Q than others: over 5 orders of magnitude, compared to earlier studies that typically had a range of ~1 order of magnitude. We will consider their work in more detail in Subsection 4.2.3.

Unfortunately, uncertainty in hydraulic geometry is often significant. Gonzalez and Pasternack [458] state that despite extensive use of hydraulic geometry, repeatability is not guaranteed, since few studies address assumptions, or explain procedural steps in sufficient detail. They highlight the complex array of considerations involved in generating hydraulic geometry

[1] An autocorrelation is the correlation of a signal with a delayed copy of itself as a function of delay. In other words, there is a similarity between observations as a function of the time lag between them.

[2] The line of lowest elevation within a valley, or watercourse, marking the natural direction of a watercourse.

relationships and claim that these decisions are seldom reported. For example, data can be obtained either empirically, from numerical modelling, from past studies, or from flow records. Obtaining empirical and numerical data involves a host of site-related factors and methodology decisions. All of these data types are subject to influence from methods chosen for data aggregation.

As stated above, hydraulic geometry considers the relationship between channel form and Q. In full, it refers to the width, depth, cross-section, meander length and sinuosity that describes a river channel form; the variables of mean slope, mean friction and mean velocity; in relation to the discharge, along a stream network in a hydrologically homogeneous basin. Assuming that Q is the dominant independent variable, Leopold and Maddock [297] proposed that the hydraulic geometry of a fluvial channel can be described, using power law relationships, as functions of Q:

$$w = aQ^b \tag{4.23}$$

$$d = cQ^f \tag{4.24}$$

$$v = kQ^m \tag{4.25}$$

where the parameters a, b, c, f, k, and m are empirically determined numerical constants that vary with location, climate, and discharge conditions.

A number of attempts have been made to explain the fundamental principles that drive hydraulic geometry [314, 336, 459–462]. Gleason [337] reviews a number of such efforts to provide evidence that the equations of Leopold and Maddock [297] (Eqs. (4.23), (4.24) and (4.25)) reasonably match empirical data and outlines attempts to derive its underlying physical principles. In this review, he points out that their equations are still widely used today, despite numerous verifications that there is no *theoretical* reason to do so.

These equations for describing hydraulic geometry can be applied at-a-station, or downstream [297], providing two approaches for empirically determining the parameters used in Eqs. (4.23), (4.24) and (4.25). Confusingly, Leopold and Maddock [297] used the same variables and naming conventions to describe at-a-station hydraulic geometry (AHG) and downstream hydraulic geometry (DHG). The AHG approach requires repeated field-measurements at a single cross-section. The DHG approach requires repeated field-measurements for some fixed frequency of discharge between cross-sections, either downstream, or on other rivers.

Repeated empirical measurements enabled Leopold and Maddock [297] to determine log-log trends when w, d and v were plotted against Q (Fig. 4.2), resulting in the establishment of the power law relationships (Eqs. (4.23), (4.24) and (4.25)). When applied to changes in Q over time at one cross-section, these equations address how channel geometry accommodates any fluctuations in Q. This understanding of a given river cross-section was termed AHG and is a function of cross-sectional geometry. Beginning with a triangular cross-section, and with reference to Eqs. (4.23) and (4.24), changes to the exponents b and f *bend* cross-sectional shape, while changes in the coefficients a and c *stretches* it [463]. Often referred to as the 'width exponent', b is widely used in fluvial geomorphology as a diagnostic measure of river behaviour and form. High values for b are characteristic of shallow, gravel beds and accommo-

date discharge increase through channel widening. Low values are characteristic of entrenched channels with cohesive banks.

Park [314] and Rhodes [459, 464, 465] compiled the results of a number of studies [301, 466–472] that aimed to empirically verify the AHG equations of Leopold and Maddock [297]. Both authors endeavoured to find a correlation between rivers, based upon the exponents of Eqs. (4.23), (4.24) and (4.25) (b, f and m). They both concluded that there existed little similarity across rivers, or physiographic settings. This caused Park to state that this 'cast doubt on the use of mean values of samples of exponents to characterise the hydraulic geometry of particular areas'. Gleason [337] notes that this work of Park and Rhodes, predominately in the late 1970s, marked a change in the perspective of researchers working in this area: rather than asking *if* AHG was occurring, they began to ask *why*.

Knighton [302] states that AHG changes over time, meaning that the parameters b, f, m, a, c, and k cannot be considered constant over a long period. Phillips and Harlin [473] demonstrated that AHG varied spatially, after observing a river that divided into two channels, of identical geology and climatology, before rejoining. The AHG parameters of both channels were found to be significantly different, demonstrating that these parameters are not transferable within the same physiography. Despite this, it has been common to consider a group of rivers within a physiographic or geographic area, rather than single rivers, when determining appropriate parameters for the use of hydraulic geometry relationships [428].

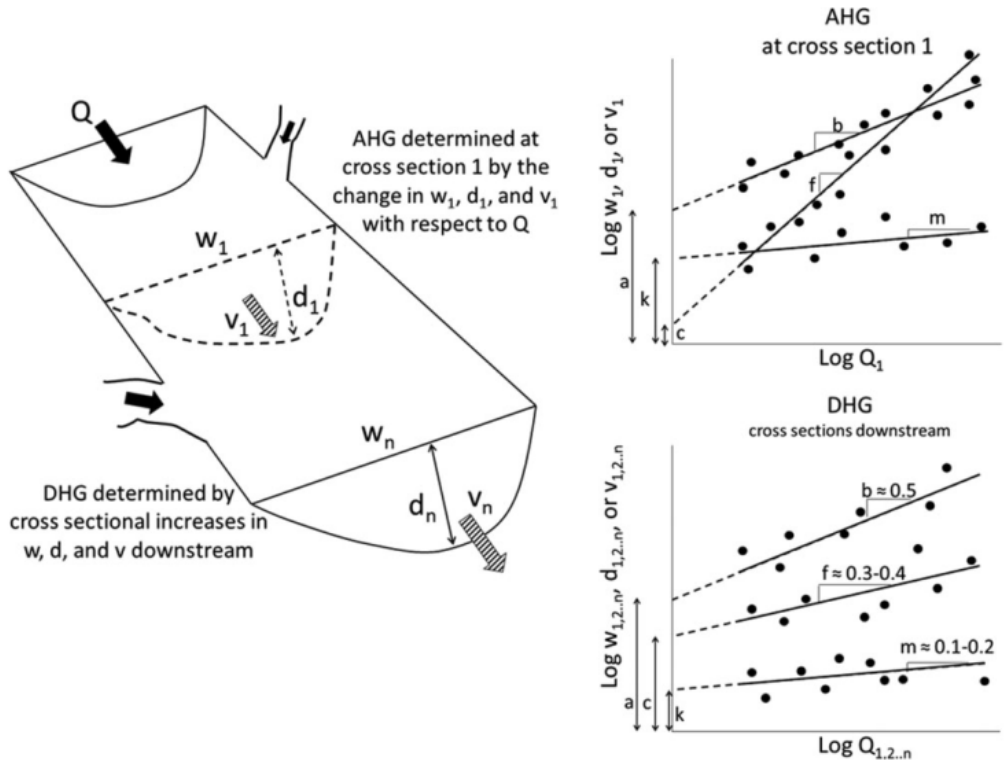

Figure 4.2: Representation of AHG and DHG relationships, illustrating how power laws can be determined to describe w, d and v as functions of Q [337].

Though rational deduction has been used to provide explanations for why AHG is observed [336], explicit formulations for the determination of the parameters used in Eqs. (4.23),

(4.24) and (4.25) have not been derived. Despite this, the application of AHG relationships is widespread: in estimating Q from satellites [217], stream classification [306, 474], river restoration [475, 476], geomorphic process assessment [444, 477, 478], waterfall systematics [463] and aquatic ecosystem evaluation [318, 479].

At a given cross-section, Eq. (4.24) has significant practical utility, since empirical determination of the parameters c and f permits the estimation of Q as a function of continuously recorded measurements of d. Measurement of a river's *stage* in this way is how many gauge stations operate, as was discussed in Subsection 2.3.2.

In addition to the log-log trends Leopold and Maddock [297] observed to explain AHG, similar log-log relationships were observed to describe DHG, when mean annual discharge Q_m was compared to w, d and v (Fig. 4.2). These relationships are also described by the power law relationships of Eqs. (4.23), (4.24) and (4.25).

Since the work of Leopold and Maddock [297], much empirical research has verified the validity of DHG [480–486]. Yet, in a review of hydraulic geometry, Gleason [337] states that no authoritative, universal, rational explanation for DHG has yet been determined. He also states that no study has yet defined explicit, universal formulations for the determination of the parameters in Eq. (4.23), (4.24) and (4.25).

A fundamental difference between these two definitions of hydraulic geometry is that AHG deals with temporal variations in flow variables as discharge fluctuates at a cross-section, for a range of discharges up until bankfull $Q < Q_b$, whereas DHG deals with spatial variations in channel properties with reference to a constant Q. AHG determination uses mean values of Q over a period, such as a week, a month, a season, or a year [298]. DHG determination of hydraulic geometry can be by two forms of analysis. The first uses Eqs. (4.23), (4.24) and (4.25), describing the regulation of flow adjustments by channel form in response to increases in Q downstream. The second type of analysis is a modification of the original hydraulic geometry concept and entails variation of channel geometry for a particular reference Q downstream with a given frequency. Implied in this analysis is an assumption of an appropriate value of Q that is the dominant flow controlling channel dimensions [481]. Initially, DHG used the mean annual flow Q_m as its independent variable. Since bankfull flows are more influential on channel morphology, Q_b became more commonly used and by the 2000s, was accepted as the norm [337]. A significant exception to this was the study of Moody and Troutman [448], which did not use a fixed value for Q. This study was very extensive and resulted in an estimation of parameters for Eqs. (4.23), (4.24) and (4.25) that have since been considered as globally applicable [206, 359, 363, 412, 487, 488]. The authors argue that since the overall range of Q investigated covered 5 orders of magnitude, at-a-station Q variability was small compared to overall Q variability and that regression relations they obtained would not have changed significantly had measurements of Q been fixed. We shall consider the globally applicable parameters they proposed further in Subsection 4.2.3

At-many-stations hydraulic geometry (AMHG) is a term defined by Gleason and Smith [217], after finding that the paired coefficients and exponents of AHG relationships along a river exhibit very strong semi-log relationships. They found that these relationships can exist over surprisingly long reaches (up to ~3,000 km). This finding indicates that AHG coefficient and exponent pairs (a and b; c and f; and, k and m) are functionally related and dependently predictable from one cross-section to the next. Thus, they demonstrate that AMHG effectively halves the number of parameters required by traditional hydraulic geometry, reducing the num-

ber of parameters from six to three.

AMHG is similar to DHG, in that it considers longitudinal trends, but differs due to the fact that all variations of Q are considered (not a single bankfull discharge Q_b), the correlations are log-linear (not log-log) and the trends do not follow a downstream direction [217].

Jowett [318] defined the term reach-averaged hydraulic geometry (RHG), which applies hydraulic geometry in an identical manner as AHG and DHG, but uses reach-averaged variables instead of single cross-sections. Following on from Jowett's original use of this definition, RHG remains closely associated with habitat assessment applications that seek to predict the suitability of river reach for a given species of interest, given RHG predicted hydraulics.

Gonzalez and Pasternack [458] proposed the concept of *hydraulic topography* as a more accurate representation of channel hydraulics than that provided by hydraulic geometry. They argue that sampling bias, differences in post-processing and a lack of recognition, or accounting, for the effects of channel variability and complexity, that is inherent in traditional hydraulic geometry-focused studies, results in the determination of parameters that are often inadequate. Instead, they claim that 'near-census', comprehensive, spatially explicit and process-based approaches to understanding channel hydraulics can be arrived at with the advent of advances that allow metre-scale topographic mapping [489–491] and multidimensional hydrodynamic modelling [492, 493]. They state that their use of the term 'near-census' leaves open the opportunity to move beyond metre-scale, towards decimetre-scale or beyond, with future technological developments. In fact they go further, claiming that moving beyond transect-based hydraulic geometry field methods is inevitable given the rate of such development.

4.2.3 Hydraulic geometry parameters

The hydraulic geometry parameters a, b, c, f, k and m of Eqs. (4.23), (4.24) and (4.25) result from a range of flows, acting over decadal or longer timescales, causing erosion and aggradation of the river geometry. From this perspective, river flow is a forcing condition for the long-term evolution of a channel. In contrary, the reverse is true from a short-term perspective, with channel geometry forcing the behaviour of the river flow. In such a way, we can observe a complex feedback loop in operation.

Moody and Troutman [448] used least-squares regression analysis, upon a number of studies of rivers, to determine values for the parameters in Eqs. (4.23) and (4.24). They drew upon existing data sets from around the world, exploring the possibility that there are universal scaling relations of w and d with respect to Q. They performed log-log regressions for a subset of world rivers, with values of Q ranging from 8×10^{-3} m^3 s^{-1} to 2×10^5 m^3 s^{-1}. The regression relations obtained were

$$w = 7.2Q^{0.50\pm0.02} \qquad (2.6 - 20.2) \tag{4.26}$$

$$d = 0.27Q^{0.30\pm0.01} \qquad (0.12 - 0.63) \tag{4.27}$$

with the numbers in parentheses corresponding to the 95 % confidence interval for the coefficients. These relationships and parameters have been assumed globally applicable by other studies [206, 359, 363, 412, 487, 488]. The regression standard error of estimate for Eqs. (4.26) and (4.27) are 0.22 and 0.18, respectively. The authors state that the estimate of the coefficients

and exponents would probably change little with more data, because the number of data pairs is 226 and include measurements for some of the largest rivers in the world and many of the smallest. As shown, the coefficients tend to vary more than the exponents, reflecting the multivariate character of the channel form control.

Frasson et al. [222] compared modelled annual flow, simulated by the water balance model WBMsed [494], with measurements of river width obtained from remote sensing (Fig. 4.3). It can be seen that the power law relationship between w and Q (Eq. (4.26)) agrees well with medians of the discharge box plots. They report that the disagreement at the lower end may be due to the increased uncertainty in the estimation of smaller river widths: a width of ~50 m approaches the 30 m resolution of the Landsat images used in the extraction of the river widths and may cause an overestimation [206].

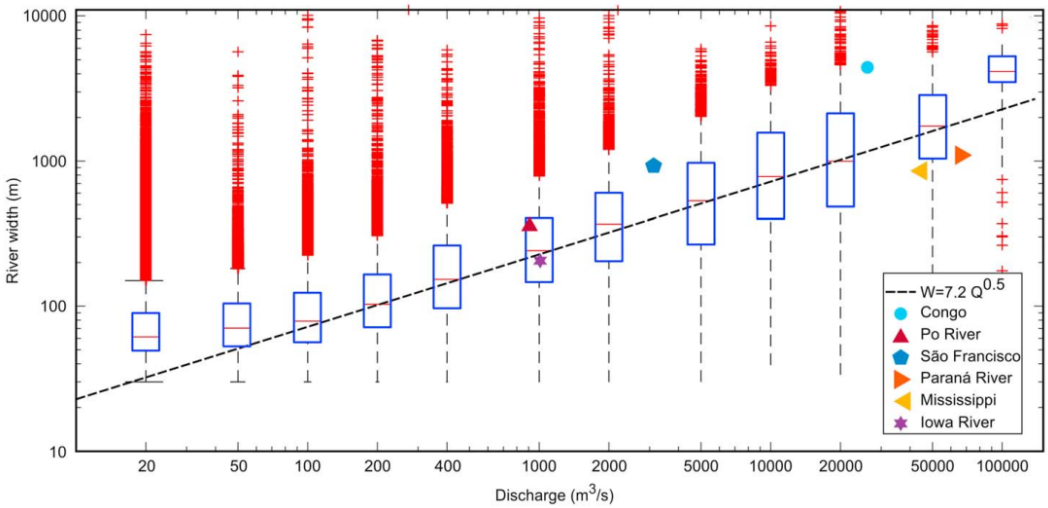

Figure 4.3: Relationship between river width and discharge, as determined by Frasson et al. [222]. A logarithmic scale is used on the y axis. The dashed line shows the power law relationship put forward by Moody and Troutman [448], illustrating close agreement between the application of this means of estimation, using a power law relationship, and empirical measurements.

Since $Q = wdv$ (Eq. (2.30)), and with reference to Eqs. (4.23), (4.24) and (4.25),

$$Q = aQ^b \times cQ^f \times kQ^m \tag{4.28}$$

or

$$Q = ackQ^{b+f+m} \tag{4.29}$$

These equations are thus unit sum constrained and it follows that

$$a \times c \times k = 1 \tag{4.30}$$

and

$$b + f + m = 1 \tag{4.31}$$

Now, with reference to Eq. (4.30)

$$k = \frac{1}{ac} \tag{4.32}$$

and with reference to Eq. (4.31)

$$m = 1 - (b + f) \tag{4.33}$$

Therefore, with consideration of Eq. (4.26) and (4.27), including the values for uncertainty, a means for estimating v can be derived:

$$v = 0.5Q^{0.20\pm0.03} \qquad (0.1 - 3.2) \tag{4.34}$$

Fig. 4.4 illustrates the range of uncertainty associated with the calculation of w, d and v using these equations, for a range of $Q = 0\,\mathrm{m^3\,s^{-1}}$ to $1{,}000\,\mathrm{m^3\,s^{-1}}$ and minimum, mean and maximum values of the associated parameters. This figure also provides a comparison of the equation derived here to estimate v (Eq. (4.34)), with an alternative equation (Eq. (4.38)), presented below in Subsection 4.2.4, based upon the study of Schulze et al. [495].

Clearly, Fig. 4.4 (c) shows that v is predicted to increase in a downstream direction, since Q would be assumed to increase in a downstream direction. It is worth recalling the argument made in Section 4.1 to support this potentially counter-intuitive idea and reiterate that empirical evidence [441] reinforces the legitimacy of this claim.

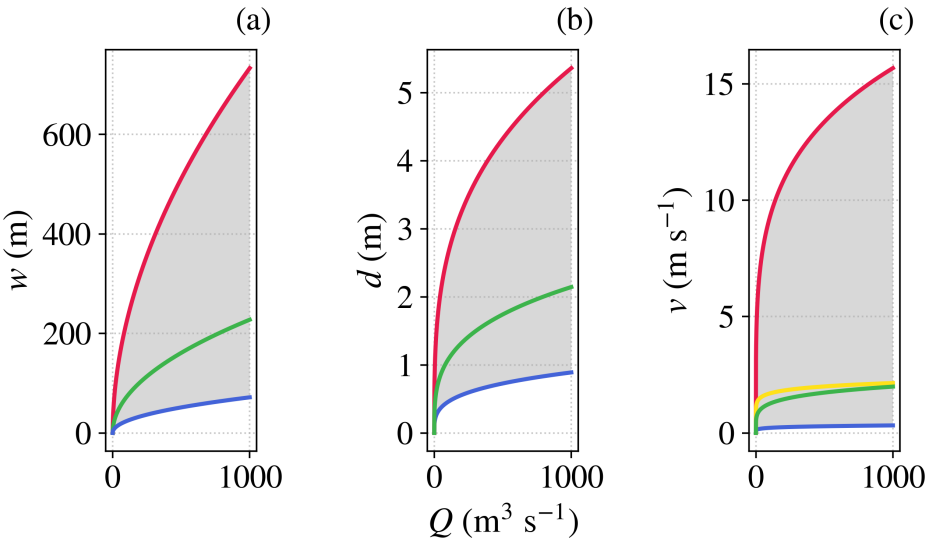

Figure 4.4: Power law relationships, as a function of discharge Q, for (a) width w, (b) depth d and (c) flow velocity v; with minimum (blue), mean (green) and maximum (red) values for power law parameters, according to uncertainty and 95 % confidence intervals (grey) as proposed by Moody and Troutman [448]. An alternation equation for esitimating v (Eq. (4.38)), derived in Subsection 4.2.4 is also plotted for comparison (yellow).

Table 4.1: Downstream hydraulic geometry parameters from previous studies [428].

Source	Discharge	a	c	b	f	Channel type
Kellerhals [309]	$\sim Q_3$	3.26	0.42	0.50	0.40	Threshold channel
Li et al. [496]	Q_b			0.46	0.46	Threshold channel
Nixon et al. [497]	Q_b	3.15		0.49		Gravel-bed
Brush [468]	$Q_{2.33}$	1.85	0.28	0.55	0.36	Gravel-bed
Simons and Albertson [498]	$\sim Q_b$	2.61	0.31	0.50	0.36	Gravel-bed
Emmett [499]	Q_b	2.77	0.27	0.56	0.34	Gravel-bed
Charlton et al. [500]	Q_b	3.74	0.31	0.45	0.40	Gravel-bed
Bray [501]	Q_2	4.79	0.26	0.53	0.33	Gravel-bed
Andrews [502]	Q_b	3.91	0.49	0.48	0.38	Gravel-bed, thick vegetation
Andrews [502]	Q_b	4.94	0.48	0.48	0.38	Gravel-bed, thin vegetation
Hey and Thorne [503]	Q_b	3.67	0.33	0.45	0.35	Gravel-bed
Parker [504]	Q_b	4.40	0.25	0.50	0.42	Gravel-bed
Chang [505]	Q_b			0.47	0.42	Gravel-bed
Lacey [506]	$\sim Q_b$	4.84	0.39	0.50	0.33	Sand-bed
Simons and Albertson [498]	$\sim Q_b$	5.23	0.69	0.50	0.36	Sand-bed, sandy banks
Simons and Albertson [498]	$\sim Q_b$	3.93	0.58	0.50	0.36	Sand-bed, small load
Simons and Albertson [498]	$\sim Q_b$	2.55	0.45	0.50	0.36	Sand-bed, large load
Mahmood et al. [507]	$\sim Q_b$	4.93	0.53	0.51	0.31	Sand-bed
Rundquist [508]	Q_b	4.39	0.38	0.52	0.32	Undifferentiated
Langbein [509]	$\sim Q_b$			0.50	0.38	Undifferentiated

Earlier studies have also determined values for hydraulic geometry parameters. Table 4.1 shows a range of values determined for the parameters used in calculating w and d in a DHG context, where the focus is upon spatial variations in channel properties for some reference Q. Tables 4.2 and 4.3 show a range of values for the exponents used in calculating w, d and v in an AHG context. In this case, the focus is upon temporal variations in Q. Regarding these tables, it can be seen that there are a variety of different contexts to consider, if attempting to determine the appropriate parameters. Furthermore, there can be seen great variation in values which, along with the large errors expressed in Eqs. (4.26) and (4.27), support the idea that universal values for the parameters are difficult to determine.

Table 4.2: Empirically determined at-a-station hydraulic geometry parameters from previous studies [428].

Source	b	f	m
Leopold and Maddock [297]	0.26	0.40	0.34
Wolman [301]	0.04	0.41	0.55
Leopold and Miller [466]	0.25	0.41	0.33
Lewis [510]	0.17	0.33	0.49
Wilcock [511]	0.09	0.36	0.53
Knighton [444]	0.12	0.40	0.48
Harvey [512]	0.14	0.42	0.43

Table 4.3: Theoretically determined at-a-station hydraulic geometry parameters from previous studies [428].

Source	Application	b	f	m
Li et al. [496]	Threshold theory	0.24	0.46	0.30
Langbein [509], Williams [513]	Minimum variance theory:			
	(i) vertical banks	0	0.57	0.43
	(ii) cohesive, but not vertical banks	0.10	0.53	0.37
	(iii) non-cohesive boundary	0.48	0.30	0.22

4.2.4 Using hydraulic geometry relationships in large-scale hydrology

Allen and Pavelsky [206] stated that, despite the widespread importance of rivers, relatively limited empirical information on river channel form was available at a continental-scale to constrain river system models, at that time. A study previous to this statement exemplifies this issue: Raymond et al. [514] aimed to estimate global river and stream surface area (RSSA) to determine CO_2 emissions from biogeochemical exchange at the river-atmosphere interface. Lack of empirical information on river channel form meant that it was necessary to apply a flow-routing algorithm to digital topography and assume globally constant hydraulic geometry relationships between w and Q, using Eq. (4.23). Static values for a and b were determined from an earlier study involving some of the same authors [515], that made use of 1,026 paired measurements of w and Q, in addition to an analysis of United States Geological Survey (USGS) gauging station rating curve data from 9,811 stations. This study lacked direct

observations of RSSA, quantification of statistical uncertainty and consideration of regional variability in hydraulic geometry. A later study by Allen and Pavelsky [220], the same authors who had earlier pointed out the problem of insufficient empirical information on river channel form, used satellite observations of rivers and a statistical approach. This allowed a more accurate determination of RSSA, removed the reliance upon hydraulic geometry relationships and demonstrated the importance of empirical information for river channel form.

Though hydraulic geometry relationships are intended to describe individual cross-sections, the idea that long river domains, of varying w and d, can be reasonably represented with limited cross-sectional data is prevalent [320, 509, 516]. Yet, others have observed high variability between cross-sections [444, 459], with context-specific differences: between braided and non-braided rivers [302, 459]; and, riffles and pools [428, 444]. Differences are also found due to variation in bank cohesion [302], bed substrate [513, 517] and bank vegetation [502].

With regards to their use of Eq. (4.26), Allen and Pavelsky [206] point out that this relationship was developed using measurements largely collected at gauging stations. Stream gauges are typically located at stable, single-channel sites, often near bridges or other fixed structures. They suggest that this could lead to bias that is unrepresentative of global values for w. Since multichannel rivers tend to be wider and because their widths are more sensitive to variations in discharge than single-channel rivers [518], average river widths away from gauging stations may be underestimated. This opinion is reiterated in other studies [243, 300].

In the field of large-scale river hydrology, there is predominately a focus on quantifying the volume of water in rivers and streams [220]. Therefore, it is noteworthy that Schulze et al. [495] attempted to model river flow velocity on a global scale using the Manning formula (Eq. (4.17)). To determine R, they assumed that the river cross-section can be considered as a rectangle, meaning R can be calculated as a function of d and w using

$$R = \frac{d \cdot w}{2d + w} \tag{4.35}$$

The hydraulic relationships of Leopold and Maddock [297] (Eqs. (4.23) and (4.24)) were used to determine w and d. Using the regression analysis of Allen et al. [482] to determine the parameters for these relationships, gives

$$w = 2.71Q^{0.557} \tag{4.36}$$

$$d = 0.349Q^{0.341} \tag{4.37}$$

Interestingly, they chose not to use these equations and continuity to derive parameters for v (Eq. (4.25)), preferring to use the Manning formula (Eq. (4.17)) instead. To explore the option that they ignored, substituting for w, d and v into $Q = wdv$ (Eq. (2.30)), using Eqs. (4.23), (4.24) and (4.25) and the method used above (Subsection 4.2.3) to derive Eq. (4.34), gives

$$v = 1.06Q^{0.102} \tag{4.38}$$

A comparison of this equation for estimating v with that derived earlier (Eq. (4.34)) is shown in Fig. 4.4.

The intention of Schulze et al. [495] was to use the results of their study to extend the Wa-

terGAP Global Hydrology Model (WGHM) [519]. This model already contains values for Q at a spatial resolution of 0.5°, allowing the determination of Eqs. (4.36), (4.37) and therefore Eq. (4.35). To calculate v, using the Manning Formula (Eq. (4.17)) requires s and n. Determination of s was achieved using an analysis of geographic information system (GIS) data. Unfortunately, a method to estimate n on a global scale was lacking and, as Kirby et al. [177] have commented upon, since the model was found to be very sensitive to this variable, this puts into question the suitability of this method for determining v for the purpose of hydrokinetic resource assessment.

The development of techniques for global-scale determination of w [205, 221, 228–239] reinforces the argument that reliance upon hydraulic geometry relationships is unnecessary, if considering this specific element of river channel form alone. When requiring knowledge of other elements, such as d or v, this is not the case and hydraulic geometry relationships may still be needed.

Given the improvement in global-scale, remote-sensed, empirical measurements of w, there would appear to be an opportunity to use regression to spatially map values for the parameters a and b. If improvements in remote sensing techniques allowed this for either d or v, the parameter relationships described above show how this would then provide a means for spatially mapping all of the hydraulic geometry parameters. Thus, knowledge of Q, spatially and temporally on a global-scale, would provide a means to determine river channel form, globally.

Knighton [428] states that although hydraulic geometry relationships are flexible and easily linearised, their application has not always been adequately justified. Further, the establishment of strong statistical relationships may provide the confidence to accept that a thorough explanation has been achieved and that the effects of the underlying processes can be described, when in fact this is not the case. Parker et al. [520] claim that the relationships established for hydraulic geometry can be considered quasi-universal, which suggests that while there is perhaps a use for them in a large-scale situation, consideration of their limitations must also be made. The use of hydraulic geometry relationships has been dominant in the field of fluvial geomorphology and provided the means for drawing valuable insights into the workings of the fluvial system. Knighton [428] suggested that a development of understanding would result from combining the predominately empirical approach of early work, but within a more theoretical structure. In fact, this process may be observed upon consideration of the many theories that have been proposed. Singh [298] has reviewed the many theories of hydraulic geometry relations and associated equations for determining the mean stream channel form from Q (Table 4.4). This review highlights the difficulty of applying these in all conditions and claims that little progress was made in the decades following the work of Leopold and Maddock [297]. For this reason, their equations are still considered useful, though imperfect, and have been used in a number of large-scale studies [412, 495, 521].

4.3 Measuring the hydrokinetic resource

4.3.1 Hydrokinetic power as the rate of energy transfer

As shown in Subsection 2.1.2 (Eq. (4.39)), the theoretical power passing the cross-sectional area A_D of the sweep of a turbine can be calculated. Similarly, if considering the cross-section of a river $A = wd$,

Table 4.4: Summary of theories of hydraulic geometry relationships.

Theory	Principle studies
Regime theory	Lindley [522]
Power function theory	Leopold and Maddock [297] and Wolman [301]
Tractive force theory	Lane [523, 524]
Threshold channel geometry theory	Li [525]
Channel stability theory	Schumm [526]
Similarity principle	Engelund and Hansen [527]
Hydrodynamic theory	Smith [528]
Theory of maximum sediment transport rate	White et al. [529]
Theory of maximum friction factor	Davies and Sutherland [530, 531]
Theory of maximum flow efficiency	Huang and Nanson [532]
Theory of least channel mobility	Dou [533]
Theory of least resistance	Ramette [534]
Theory of minimum Froude number	Jia [535]
Theory of minimum energy dissipation rate	Yang [536, 537], Yang and Song [538] and Barr et al. [539]
Theory of minimum stream power	Chang [540, 541]
Theory of minimum energy degradation rate	Brebner et al. [542]
Thermodynamic entropy theory	Yalin and Ferreira Da Silva [543]
Theory of minimum variance	Langbein [509], Kennedy et al. [544], Knighton [545], Williams [513], Dozier [546] and Riley [547]
Theory of maximum entropy	Deng and Zhang [548] and Cheema et al. [549]
Theory of maximum entropy-minimum energy	Singh et al. [550, 551]

$$P = \frac{1}{2}\rho A v^3 \tag{4.39}$$

This equation is derived from kinetic energy, as will be demonstrated below. For this reason, it is quantifying power as the rate of *transfer* of kinetic energy, as opposed to $P = \gamma QH$ (Eq. (3.31), or (4.1)), which was used in the methodology of Chapter 3. As was shown in Section 4.1, this equation was derived from gravitational potential energy ($E_p = MgH$) and, therefore, as a means for measuring hydrokinetic power, is quantifying power as the rate of *conversion* of gravitational potential energy to kinetic energy.

Applying Eq. (4.39) to rivers requires knowledge of w and d, in addition to knowing v. Large-scale resource assessments face the challenge of obtaining suitable data, with appropriate coverage and spatiotemporal resolution. Relatively limited empirical information on river channel form is available at a continental-scale [206] and v is highly variable in time and space [314]. With modelled data for reconstructed daily values of Q, GRADES provides near-global coverage and may be applicable in estimating appropriate values to determine river channel form and v.

As discussed above (see Subsection 4.2.2), the equations (Eqs. (4.23), (4.24) and (4.25)) for describing hydraulic geometry can be applied at-a-station, or downstream, providing two approaches for empirically determining hydraulic parameters. These relationships for estimating w, d, and v provide the possibility to derive an alternative methodology for hydrokinetic resource assessment.

Thus, with reference to Eq. (4.2), power is the rate of energy transfer

$$P = \frac{E_k}{t} = \frac{\frac{1}{2}Mv^2}{t} \tag{4.40}$$

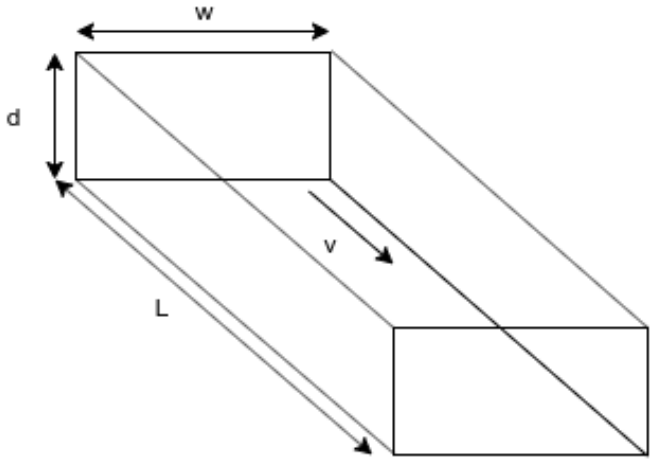

Figure 4.5: Approximate description of a river section of length L, using the hydraulic geometry parameters of width w, depth d, and flow velocity v.

The dimensions of a river reach can be approximately described as a rectangular shaped channel, which serves our purposes for now, using hydraulic geometry parameters w, d and the

length of the reach L (Fig. 4.5). The power of the water moving in this reach can be expressed in terms of these dimensions. Since M is the product of ρ and volume $V = wdL$, in relation to the water in a reach, this gives

$$M = \rho wdL \tag{4.41}$$

Substituting for M in Eq. (4.40), gives

$$P = \frac{\frac{1}{2}\rho wdLv^2}{t} \tag{4.42}$$

Since,

$$v = \frac{L}{t} \tag{4.43}$$

this simplifies to

$$P = \frac{1}{2}\rho wdv^3 \tag{4.44}$$

Since $A = wd$, this confirms the derivation of Eq. (4.39). Substituting for w, d and v using Eqs. (4.23), (4.24), and (4.25) gives

$$P = \frac{1}{2}\rho \cdot aQ^b \cdot cQ^f \cdot (kQ^m)^3 \tag{4.45}$$

Discharge is defined as the volume of water that passes through a cross-section. Therefore,

$$Q = wdv = aQ^b \cdot cQ^f \cdot kQ^m = ackQ^{b+f+m} \tag{4.46}$$

Using Eqs. (4.30) and (4.31), Eq. (4.45) can be simplified as

$$P = \frac{1}{2}\rho k^2 Q^{(2m+1)} \tag{4.47}$$

Threshold theory developed from a determination that the stability of irrigation canals, constructed with erodible materials, is optimum with cross-sections that cause material to be at the threshold of motion [552]. This was shown to apply to natural rivers as well [553]. With particles on the verge of movement at bankfull discharge, a resolution of the associated forces yields a cross-section that is roughly parabolic in shape [524]. The cross-sectional form of natural channels is irregular, but a parabolic shape is used here to generalise on a global-scale. The area of a parabolic cross-section is given by

$$A = \frac{2}{3}wd \tag{4.48}$$

Applying this to Eq. (4.47), and remembering that this was arrived at through a derivation that originally included w and d (Eq. (4.44)), we get an equation for determining the power of water flowing through a parabolic channel cross-section:

$$P = \frac{1}{3}\rho k^2 Q^{(2m+1)} \tag{4.49}$$

This equation is considered an alternative to the conventionally used equation (Eq. (4.1)) for determining theoretical hydraulic power and potentially more suitable for a hydrokinetic application. This can be modified to measure the energy E that flows through a river reach by multiplying through by t. With reference to Eq. (4.43), this gives

$$E = \frac{1}{3}\rho L k Q^{(m+1)} \tag{4.50}$$

In proposing Eqs. (4.49) and (4.50), here, it is important to clarify that only the kinetic energy of the flowing water is considered. Potential energy, due to elevation or slope, is not considered.

4.3.2 Globally applicable power law parameters

As demonstrated in Subsection 4.2.3, Moody and Troutman [448] used regression analysis upon a number of studies of rivers to determine values for the power law parameters in Eqs. (4.23) and (4.24). This analysis enabled the proposal of globally applicable formulas for the estimation of w and d, using Eqs. (4.26) and (4.27). Though these relationships and parameters have been assumed globally applicable by other studies [206, 359, 363, 412, 487, 488], they are not *strictly* traditional hydraulic geometry relationships and do not adhere to either the AHG, nor DHG, definitions. Moody and Troutman [448] justified their approach and argued that the range and quantity of data they used minimised the variability of the results.

As demonstrated in Subsection 4.2.3, knowledge of a, b, c, and f allows determination of k and m, such that a globally applicable formula for v can be derived (Eq. (4.34)). It should be noted that v is one of the most sensitive and variable properties of open-channel flow, due to its dependence upon so many other factors. It varies in four dimensions: with time, with distance from the bed, across stream, and downstream. In addition to the variations due to changes in Q, smaller timescale variations also occur because of the inherent variability caused by turbulence. Friction from the bed and banks may result in large velocity gradients. These provisos are clearly stated in offering these globally applicable values for the parameters $m = 0.5$ (with a 95 % confidence interval 0.1 to 3.2) and $k = 0.20 \pm 0.03$. A value of $m = 0.1$ has been proposed as appropriate previously [554].

Fig. 4.6 shows estimates of theoretical power as a function of Q using globally applicable power law parameters and assuming a rectangular cross-sectional profile. This illustrates that using Eq. (4.47) gives the same result as using Eq. (4.39), but with a reduced range of uncertainty. In the former case, only the parameters k and m are required. In the latter case power law equations are used to estimate w, d, and v. Therefore, the parameters a, b, c, f, k, and m are needed.

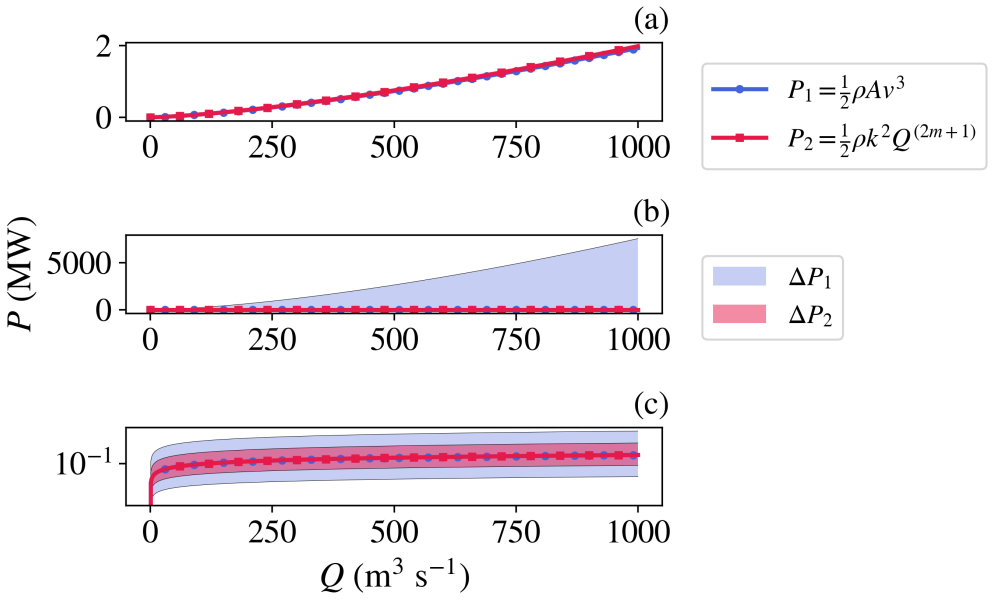

Figure 4.6: In (a), the calculation of power is seen to be the same if using power law relationships that are functions of Q to estimate w, d, and, v, to calculate $P_1 = \frac{1}{2}\rho A v^3$ (where $A = wd$); and, the derived equation $P_2 = \frac{1}{2}\rho k^2 Q^{2m+1}$. The range of uncertainty ΔP_1 is seen to be greater than that for ΔP_2. Shown with (b) a linear scale and (c) a logarithmic scale on the y axis.

As shown in Fig. 4.6, the 95 % confidence interval for the coefficients expressed in Eqs. (4.26), (4.27), and (4.34) cause an asymmetrical uncertainty in estimates of power using Eqs. (4.39), (4.47) and (4.49), when applying power law parameters that we are treating globally applicable, for the purpose of estimating hydraulic geometry parameters. Given the uncertainties associated with these parameters, their statistical distribution within the rivers of the world can be assumed (Fig. 4.7).

Though it may be reasonable to use the mean values for these globally applicable power law parameters in estimating P for an individual reach, when considered collectively, the asymmetrical statistical distribution would lead to an underestimate of the collective power of a number of reaches, as is illustrated by Fig. 4.6.

An analysis of estimated values for v that would be associated with the differing methodologies used for calculating the hydrokinetic resource — as proposed in this chapter and Ridgill et al. [138], compared to that proposed in Chapter 3 and Ridgill et al. [137] — is considered and presented as a density plot (Fig. 4.8). In the conventional, hydrostatic case (Fig. 4.8 (a)), an assumption is made that the resource is a measure of the conversion of gravitational potential energy to kinetic energy that occurs as the water travels the length of the reach, without any friction. As discussed previously (Section 4.1), this results in very high values for v (Fig. 2.1), as is shown to be the case here. The hydrokinetic case, proposed in Subsection 4.3.1 and summarised by Eq. (4.49), works in essentially the reverse of this, first estimating v and then calculating the hydrokinetic resource that would result from this. The global distribution of theoretical riverine hydrokinetic resource presented in this study (Fig. 4.15) uses mean values for globally applicable parameters of m and k, derived by hydraulic geometry continuity and

using globally applicable values for the parameters a, b, c and f (Fig. 4.7). The density plot that results from using these mean values for the parameters m and k, and mean values for Q provides a global distribution of values of v (Fig. 4.8 (b)) that appear more realistic. The uncertainties associated with estimating v in this way are large (Eq. (4.34)). Density plots for the estimated minimum values for v (Fig. 4.8 (c)) use both the lower-end of the values of m and k and the minimum values for Q that occur in each reach. Maximum values (Fig. 4.8 (d)) are similarly determined, using the upper-end estimates of these parameters and maximum values for Q. In these last two cases, estimates of v represent extremes, but it should be noted that unrealistic flow velocities can also result from the hydrokinetic methodology proposed in this chapter and which factor into the large range of uncertainty associated with this method. This is particularly true for calculation of the maximum values.

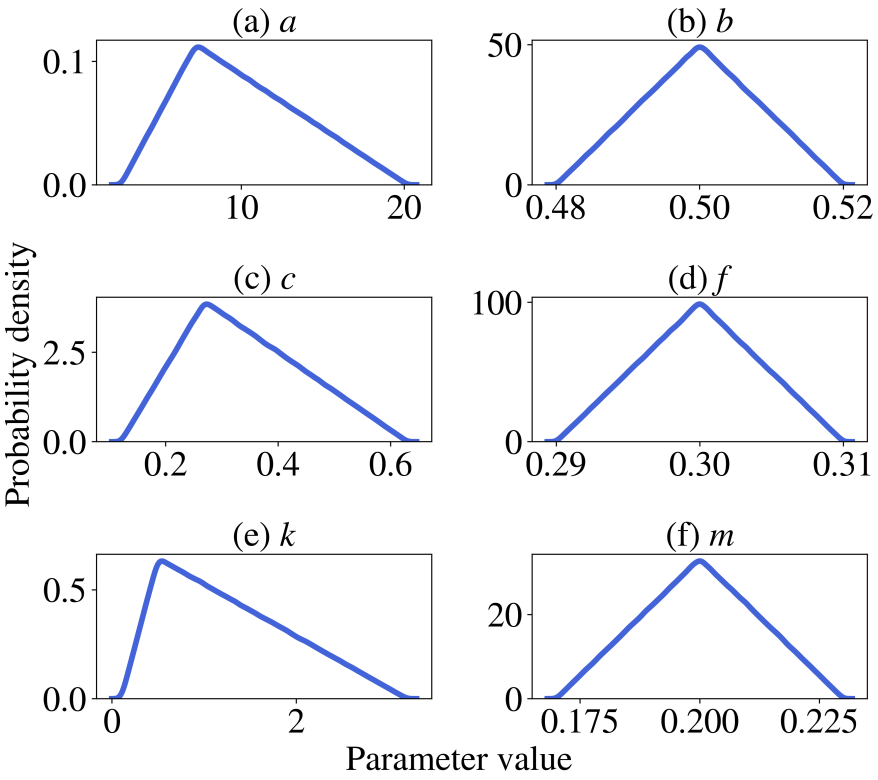

Figure 4.7: Here, we illustrate the statistical distribution of the power law parameters, according to the reported and derived uncertainty. Leopold and Maddock [297] proposed power law relationships to estimate hydraulic geometry parameters and Moody and Troutman [448] determined globally applicable coefficients and exponents for theses power laws for width w ((a) and (b)) and depth d ((c) and (d)), including the associated uncertainty. Hydraulic geometry continuity has been used to derive power law parameters and uncertainty for flow velocity v ((e) and (f)).

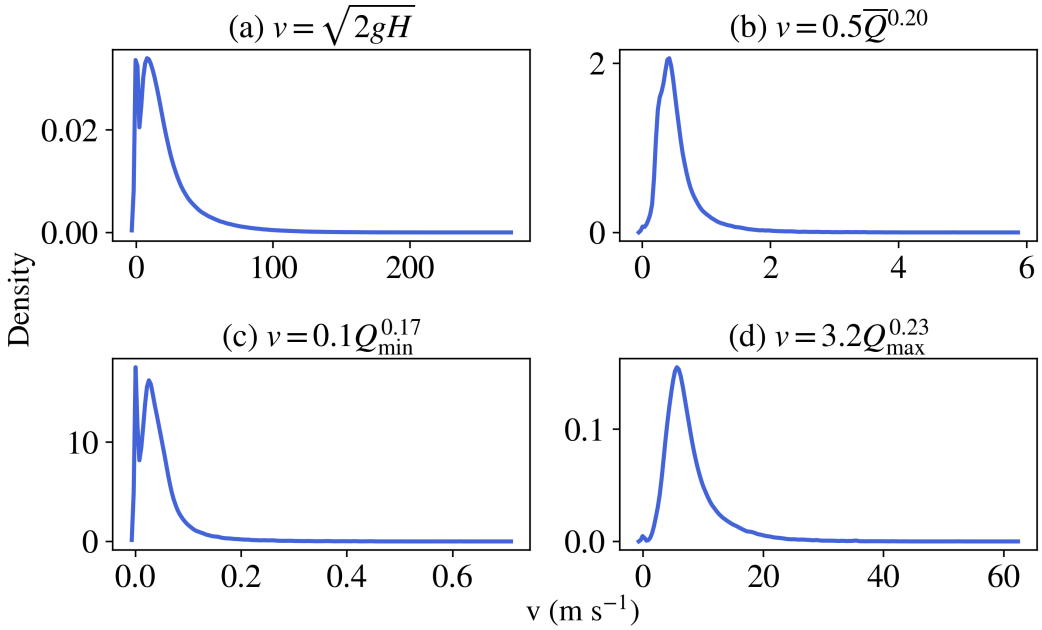

Figure 4.8: Density of values for flow velocity v, globally (excluding Greenland and Antarctica). In (a), v is calculated using the equation implied by using $P = \gamma QH$ to determine theoretical hydraulic power. An estimate of v from power law functions is given by (b) mean values for the parameters m and k that are consdiered globally applicable and reach-specific mean values for Q. The lower and upper limits of the 95 % confidence interval for these parameters and reach-specific minimum and maximum values for Q are used in (c) and (d), respectively.

4.3.3 Monte Carlo approach

The concept of repeated random sampling underlies the broad class of computational algorithms known as Monte Carlo methods. Though stochastic in nature, such methods can be used to solve problems that might be deterministic in principle. Here, repeated ($N = 1000$) and random application of power law parameters are applied to each river reach, such that the collective statistical distribution for each run aligns with that implied by their reported uncertainties (Fig. 4.7). The mean of these repeated runs permits an estimate of the global theoretical riverine hydrokinetic resource, that reduces the effects of the asymmetric uncertainties and arguably results in a more accurate representation. The accuracy of the Monte Carlo method is proportional to $\sqrt{N}$, meaning computation cost quadruples when accuracy is doubled [555]. In most cases, $N \geq 100$ is considered 'best practice' [556]. Convergence tests provide a means to determine if the number of runs were sufficient and to quantify the reliability, or 'stability', of a result. Here $N = 1000$ and a measurement of the root mean square error (RMSE) after each run is found to converge to almost zero (Fig. 4.9). In this case, over the 35 year record ($\alpha = 12{,}784$ days), a running mean vector $\overline{\vec{E}}_{\text{MC}}$ (Eq. (4.60)) gathered from a growing matrix of increasing numbers of completed runs $\mathbf{E}_{\text{MC}} \in \mathbb{R}^{\alpha \times N}$ for $N = 1, 2, 3, \ldots, 1000$ is calculated after each run and compared with the eventual mean vector for $N = 1000$. This is achieved by running the Monte Carlo method twice.

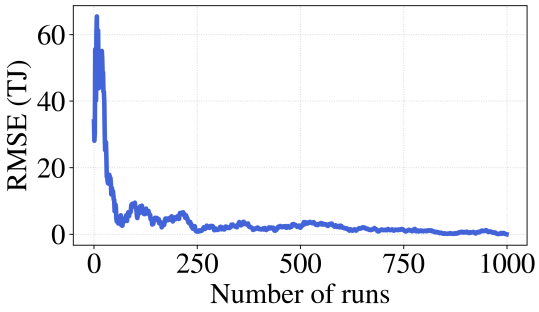

Figure 4.9: Root mean square error (RMSE) of the Monte Carlo method after each run.

The equation derived to estimate the power within a given river reach (Eq. (4.49)) can be modified to measure the energy E that flows through a river reach by multiplying through by time (Eq. (4.50)). This can be applied to all reaches simultaneously, meaning that we discretise each reach, such that they can be considered individually and summed to quantify the energy in all reaches collectively. All water within the global network of rivers can be thought of as flowing through one of these reaches and only one, when considered as a whole. The sum of these individual reaches is therefore the total energy of all reaches.

A matrix $\mathbf{E}_{\text{MP}} \in \mathbb{R}^{\alpha\times\beta}$ can be used to represent the energy in each of all β = 2,898,501 river reaches, over the α days of the record, where mean power law parameters are applied for all reaches of length L, to give an estimate of energy $E_{\text{MP},y,x}$ on day y in reach x. This gives

$$\mathbf{E}_{\text{MP}} = \begin{bmatrix} E_{\text{MP},1,1} & E_{\text{MP},1,2} & \cdots & E_{\text{MP},1,x} & \cdots & E_{\text{MP},1,\beta} \\ E_{\text{MP},2,1} & E_{\text{MP},2,2} & \cdots & E_{\text{MP},2,x} & \cdots & E_{\text{MP},2,\beta} \\ \vdots & \vdots & \ddots & \vdots & & \vdots \\ E_{\text{MP},y,1} & E_{\text{MP},y,2} & \cdots & E_{\text{MP},y,x} & \cdots & E_{\text{MP},y,\beta} \\ \vdots & \vdots & & \vdots & \ddots & \vdots \\ E_{\text{MP},\alpha,1} & E_{\text{MP},\alpha,2} & \cdots & E_{\text{MP},\alpha,x} & \cdots & E_{\text{MP},\alpha,\beta} \end{bmatrix} \tag{4.51}$$

We can produce a vector $\vec{E}_{\text{MP}}$, in this case, representing the daily total energy of all river reaches,

$$\vec{E}_{\text{MP}} = \begin{bmatrix} \sum E_{\text{MP},1} \\ \sum E_{\text{MP},2} \\ \vdots \\ \sum E_{\text{MP},y} \\ \vdots \\ \sum E_{\text{MP},\alpha} \end{bmatrix} \tag{4.52}$$

This is given by

$$\vec{E}_{\text{MP},y} = \sum_{x=1}^{\beta} \frac{1}{3}\rho L_x k Q_{xy}^{(m+1)} \qquad \text{where } \vec{E}_{\text{MP}} \in \mathbb{R}^{\alpha} \tag{4.53}$$

Here the mean globally applicable power law parameters are k = 0.5 and m = 0.20. The value $\overline{E}_{\text{MP}}$ represents the mean energy of all river reaches over the time period, given by

$$\overline{E}_{\mathrm{MP}} = \frac{1}{\alpha} \sum_{y=1}^{\alpha} \sum_{x=1}^{\beta} \frac{1}{3} \rho L_x k Q_{xy}^{(m+1)} \qquad \text{where } \overline{E}_{\mathrm{MP}} \in \mathbb{R} \tag{4.54}$$

A vector $\vec{E}_{\mathrm{MC}}$ representing daily total energy of all reaches

$$\vec{E}_{\mathrm{MC}} = \begin{bmatrix} \sum E_{\mathrm{MC},1} \\ \sum E_{\mathrm{MC},2} \\ \vdots \\ \sum E_{\mathrm{MC},y} \\ \vdots \\ \sum E_{\mathrm{MC},\alpha} \end{bmatrix} \tag{4.55}$$

can be produced using random power law parameters, with

$$\vec{E}_{\mathrm{MC},y} = \sum_{x=1}^{\beta} \frac{1}{3} \rho L_x k_x Q_{xy}^{(m_x+1)} \qquad \text{where } \vec{E}_{\mathrm{MC}} \in \mathbb{R}^{\alpha} \tag{4.56}$$

In this case, the statistical distribution of the randomly assigned parameters k_x and m_x, when considered collectively, align to an interpretation of the global statistical distribution (Fig. 4.7). In other words, for each element of $\vec{E}_{\mathrm{MC}}$, there exists corresponding, randomly created vectors

$$\vec{k} = \begin{bmatrix} k_1 \\ k_2 \\ \vdots \\ k_x \\ \vdots \\ k_\beta \end{bmatrix} \tag{4.57}$$

and

$$\vec{m} = \begin{bmatrix} m_1 \\ m_2 \\ \vdots \\ m_x \\ \vdots \\ m_\beta \end{bmatrix} \tag{4.58}$$

such that a statistical analysis of each — as randomly recreated and applied for every element of $\vec{E}_{\mathrm{MC}}$ — would result in the described distributions of Figs. 4.7(e) and 4.7(f), respectively.

Applying the Monte Carlo method, N multiples of this vector can be produced and appended together (Fig. 4.10) to form a matrix $\mathbf{E}_{\mathrm{MC}} \in \mathbb{R}^{\alpha \times N}$,

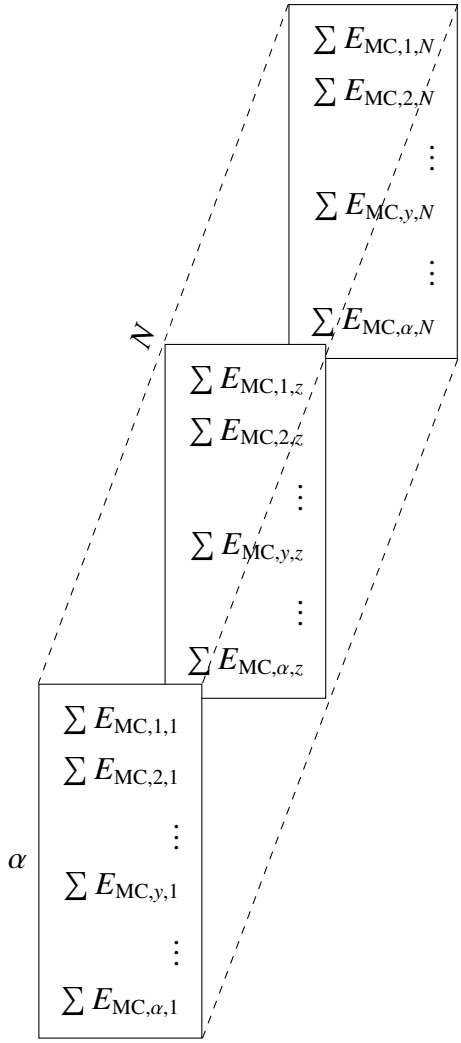

Figure 4.10: A graphical description of how the matrix $\mathbf{E}_{\mathrm{MC}}$ (Eq. (4.59)) is created, by appending N Monte Carlo runs using Eq. (4.56). Here, the dimensions are displayed such that $\mathbf{E}_{\mathrm{MC}} \in \mathbb{R}^{\alpha \times 1 \times N}$, to demonstrate how this matrix is related to the representation of $\mathbf{E}_{\mathrm{MC}}$ shown in Fig. 4.11. The representation expressed by Eq. (4.59) therefore necessitates a reshaping operation, such that $\mathbf{E}_{\mathrm{MC}} \in \mathbb{R}^{\alpha \times N}$.

$$\mathbf{E}_{\mathrm{MC}} = \begin{bmatrix} \sum E_{\mathrm{MC},1,1} & \sum E_{\mathrm{MC},1,2} & \cdots & \sum E_{\mathrm{MC},1,z} & \cdots & \sum E_{\mathrm{MC},1,N} \\ \sum E_{\mathrm{MC},2,1} & \sum E_{\mathrm{MC},2,2} & \cdots & \sum E_{\mathrm{MC},2,z} & \cdots & \sum E_{\mathrm{MC},2,N} \\ \vdots & \vdots & \ddots & \vdots & & \vdots \\ \sum E_{\mathrm{MC},y,1} & \sum E_{\mathrm{MC},y,2} & \cdots & \sum E_{\mathrm{MC},y,z} & \cdots & \sum E_{\mathrm{MC},y,N} \\ \vdots & \vdots & & \vdots & \ddots & \vdots \\ \sum E_{\mathrm{MC},\alpha,1} & \sum E_{\mathrm{MC},\alpha,2} & \cdots & \sum E_{\mathrm{MC},\alpha,z} & \cdots & \sum E_{\mathrm{MC},\alpha,N} \end{bmatrix} \tag{4.59}$$

A vector $\overline{\vec{E}}_{\mathrm{MC}}$ representing the mean of these runs is given by

$$\overline{\vec{E}}_{\mathrm{MC,y}} = \frac{1}{N} \sum_{z=1}^{N} E_{\mathrm{MC,y,z}} \qquad \text{where } \overline{\vec{E}}_{\mathrm{MC}} \in \mathbb{R}^{\alpha} \tag{4.60}$$

The mean of this vector $\overline{\overline{E}}_{\mathrm{MC}}$ represents the mean energy of all river reaches over this period, achieved with the Monte Carlo method, which can be summarised by

$$\overline{\overline{E}}_{\mathrm{MC}} = \frac{1}{N} \sum_{z=1}^{N} \frac{1}{\alpha} \sum_{y=1}^{\alpha} \sum_{x=1}^{\beta} \frac{1}{3} \rho L_x k_{xz} Q_{xy}^{(m_{xz}+1)} \qquad \text{where } \overline{\overline{E}}_{\mathrm{MC}} \in \mathbb{R} \tag{4.61}$$

This process, as described above, lends itself to an interpretation which appears to involve many iterations and liberal use of inefficient computational 'for loops'. In practical terms, these operations can be reinterpreted to allow their calculation in a more computationally efficient manner. Using linear algebra and matrix operations permits vectorisation, such that computations can be carried out in parallel, providing large savings in computation time, assuming sufficient memory is available [557].

The matrix $\mathbf{E}_{\mathrm{MC}}$ (Eq. (4.59)) can be alternatively expressed as a 3D matrix (Fig. 4.11. With the creation of this 3D matrix, a time series of the change of global hydrokinetic energy $\overline{\vec{E}}_{\mathrm{MC}}$ (Eq. (4.60)) and an estimate of the mean global hydrokinetic energy $\overline{\overline{E}}_{\mathrm{MC}}$ (Eq. (4.61)) can easily be determined. For the former, sum $\mathbf{E}_{\mathrm{MC}}$ along the β axis (rows) and calculate the mean along the N axis (corridors). In the latter case, make an extra step and calculate the mean along the α axis (columns). So, how to most efficiently construct $\mathbf{E}_{\mathrm{MC}}$?

Essentially, and more obviously, the same principles are true for determining $\vec{E}_{\mathrm{MP},y}$ (Eq. (4.53)) and $\overline{E}_{\mathrm{MP}}$ (Eq. (4.54)), using the matrix $\mathbf{E}_{\mathrm{MP}}$ (Eq. (4.51)), where mean parameters are used for k and m. In this case, though, k and m are scalars and the matrix is 2D. Therefore, its construction is more easily considered. Let us begin with this more straightforward case.

Informed by Eq. (4.50),

$$\mathbf{E}_{\mathrm{MP}} = \frac{\rho k}{3} \cdot \left(\vec{L} \cdot \vec{1}_{\alpha}^{T} \right)^{T} \circ \mathbf{Q}^{\circ(m+1)} \tag{4.62}$$

where $\vec{L} \in \mathbb{R}^{\beta}$ represents the river length of all β river reaches and $\vec{1}_{\alpha} \in \mathbb{R}^{\alpha}$ is a vector of ones. With the operation $(\vec{L} \cdot \vec{1}_{\alpha}^{T})^{T}$ a matrix $\mathbf{L} \in \mathbb{R}^{\alpha \times \beta}$ is created. The matrix $\mathbf{Q} \in \mathbb{R}^{\alpha \times \beta}$ represents the discharge in all reaches, on all days of the record. The operations $\circ$ and $^{\circ}$ describes the Hadamard (element-wise) product and power, respectively.

With the 2D version defined, the 3D version is given by

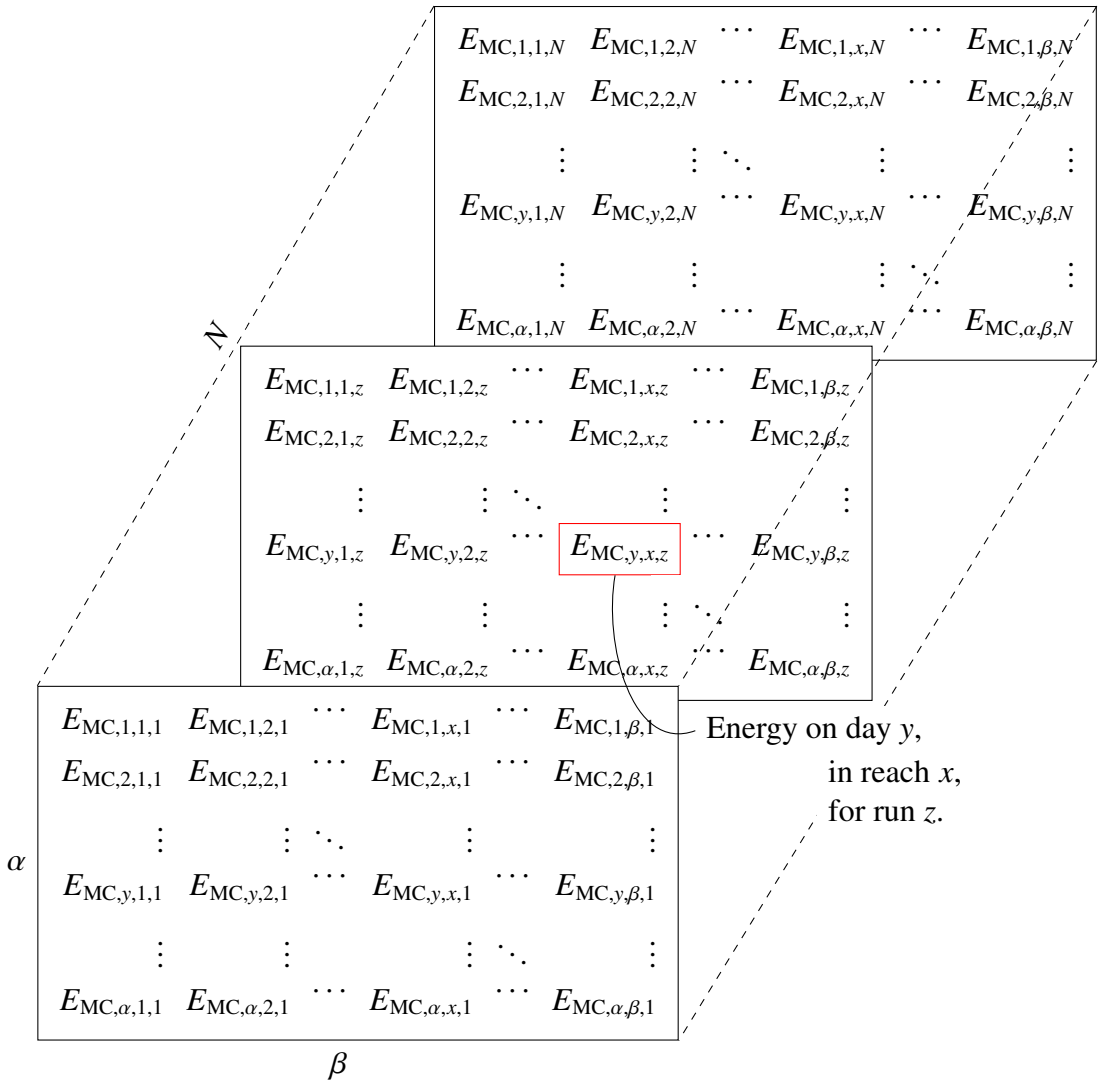

Figure 4.11: An alternative, 3D representation of matrix $\mathbf{E}_{\mathrm{MC}}$ (Eq. (4.59)). Each element $E_{\mathrm{MC},y,x,z}$ describes an estimate of the hydrokinetic energy on day y, in reach x, for a Monte Carlo run z, where hydraulic parameters m and k are applied according to the statistical distributions described by Figs. 4.7(e) and 4.7(f), respectively.

$$\mathbf{E}_{\mathrm{MC}} = \frac{\rho}{3} \cdot \mathbf{k}_{3\mathrm{D}} \circ \mathbf{L}_{3\mathrm{D}} \circ \mathbf{Q}_{3\mathrm{D}}^{\circ(\mathbf{m}_{3\mathrm{D}}+1)} \tag{4.63}$$

In this case, $\mathbf{k}_{3\mathrm{D}}$, $\mathbf{L}_{3\mathrm{D}}$, $\mathbf{Q}_{3\mathrm{D}}$ and $\mathbf{m}_{3\mathrm{D}}$ are 3D matrices, each $\in \mathbb{R}^{\alpha\times\beta\times N}$. With $\mathbf{L}$ and $\mathbf{Q}$ defined above,

$$\mathbf{L}_{3\mathrm{D}} = \begin{bmatrix} \mathbf{L}_1 & \mathbf{L}_2 & \cdots & \mathbf{L}_z & \cdots & \mathbf{L}_N \end{bmatrix} \tag{4.64}$$

and

$$\mathbf{Q}_{3\mathrm{D}} = \begin{bmatrix} \mathbf{Q}_1 & \mathbf{Q}_2 & \cdots & \mathbf{Q}_z & \cdots & \mathbf{Q}_N \end{bmatrix} \tag{4.65}$$

describing the replication, or 'stacking', of $\mathbf{L}$ and $\mathbf{Q}$ in the N direction.

With $\mathbf{k}_{3\mathrm{D}}$ and $\mathbf{m}_{3\mathrm{D}}$, a similar operation is needed. In this case, though, the 'stacking' of $\vec{k}$ (Eq. (4.57)) and $\vec{m}$ (Eq. (4.58)) must occur in both the β and N directions. Also, there should be no replication, in this case, with the vectors randomly created anew for every 'stack'.

4.4 Global theoretical riverine hydrokinetic resource

An estimate of the global theoretical riverine hydrokinetic resource is achieved by calculating the total kinetic energy in the rivers of the world, excluding Greenland and Antarctica, over a 35 year period. Time series (Fig. 4.12) representing daily estimates of hydrokinetic energy in all river reaches, during the years 1979–2013, are created in two ways (Eqs. (4.52) and (4.55)). The first approach ($\vec{E}_{\mathrm{MP}}$) uses the mean values for power law parameters, as proposed by Moody and Troutman [448], that are considered globally applicable (Fig. 4.7) to estimate the relevant hydraulic parameters required to quantify the kinetic energy flowing through a given river reach. The second approach ($\overrightarrow{E}_{\mathrm{MC}}$) uses a Monte Carlo method that randomly assigns power law parameters across all river reaches according to an inference of their statistical distribution. The former approach results in an estimate of $\overline{E}_{\mathrm{MP}} = 2.315 \pm 0.004$ PJ (Eq. (4.54)) and the latter, the mean of the averages of $N = 1000$ runs, gives $\overline{\overline{E}}_{\mathrm{MC}} = 5.911 \pm 0.009$ PJ (Eq. (4.61)). Alternatively, these could be expressed as $\overline{E}_{\mathrm{MP}} = 0.643 \pm 0.001$ TWh and $\overline{\overline{E}}_{\mathrm{MC}} = 1.642 \pm 0.003$ TWh. In each case, the uncertainty of these estimates is a calculation of the standard error of the mean (SEM) (Eq. (3.38)), applied to each time series. The Monte Carlo method has been applied to address the asymmetrical statistical distribution of these parameters. The argument being that this asymmetry leads to a marked underestimate, as illustrated in Fig. 4.12 and represented by the first approach ($\vec{E}_{\mathrm{MP}}$), where global mean values for the power law parameters k and m were applied. For this reason, the second approach ($\overrightarrow{E}_{\mathrm{MC}}$) is considered a more accurate representation of the global resource. In plotting the time series from both approaches, in addition to the mean values presented above, an illustration is provided of the magnitude of the underestimate if uncertainties associated with the power law parameters are disregarded.

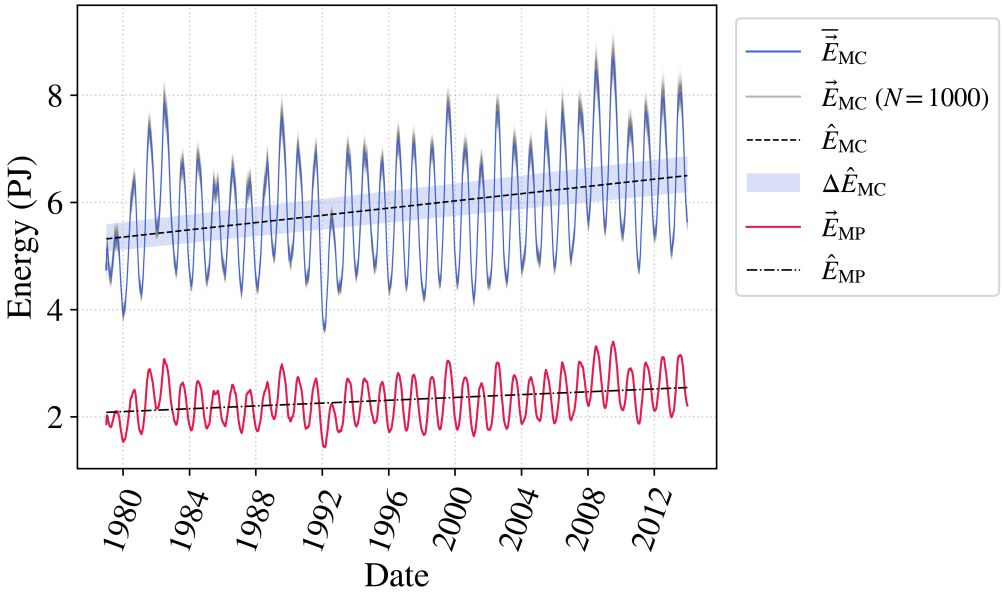

Figure 4.12: Total daily energy of global rivers (excluding Greenland and Antarctica) between 1979–2013, with $\vec{E}_{MP}$ calculated using mean values for power law parameters and $\overline{\vec{E}}_{MC}$ representing the mean of $N = 1000$ Monte Carlo simulations, where in each case $\vec{E}_{MC}$ is calculated with randomised power law parameters, applied to all reaches such that the statistical distribution aligns with the assumed global statistical distribution. $\hat{E}_{MP}$ and $\hat{E}_{MC}$ provide a least squares fit in each case and $\Delta\hat{E}_{MC}$ indicates the uncertainty as described by the range of values calculated by the Monte Carlo method.

It is typical to express an energy resource with units of TWh yr^{-1}, or similar, describing the average annual energy yield. Since this is a measure of energy conversion over a given time, it is a measure of power and actually an expression of the mean annual power. A global theoretical riverine hydrokinetic resource assessment considers the resource provided by the continuous movement of water through a global network of rivers. This could be regarded as analogous to a flywheel, which is often used to store energy, for example in an automobile engine. Though the energy transfer through any cross-section of this flywheel can be determined, providing a measure of power from a Eulerian perspective, the power of the flywheel as a whole is not possible to quantify. The flywheel has rotational energy and any measure of power would depend upon the rate of extraction.

A clear rising trend (92 ± 46 GJ d^{-1}) in inter-annual energy ($\hat{E}_{MC}$) is estimated (Fig. 4.12). The method applied in calculating energy is a function of Q and therefore any trends or fluctuations are due to changes in this variable. Reasons for this may be attributed to changes in factors such as precipitation, or the rate of snow- and ice-melt. Though and snow- and ice-melt do not appear to be directly input to the VIC model, used within GRADES, the later calibration steps include the use of a large number of empirical gauge measurements, which would certainly include the signal of any increase in Q due to these factors. Adler et al. [558] have considered global precipitation over a period (1979–2014), which coincides almost exactly with GRADES. Though they report an increase in atmospheric water vapour, coinciding with increased surface temperature, they find no overall significant trend for global precipitation. However, they do

recognise regional patterns of positive and negative trends across the planet, with increases over tropical oceans and decreases over some middle latitude regions. Reiterating what was stated in Chapter 3, an inter-annual trend may be attributed to longer-term changes in these factors, implying a change in the global climate. The rate of snow- and ice-melt would be expected to correlate with a rise in global temperature [559]. Rising global temperature has been linked to an increase in the intensity of the hydrological cycle [432], but Held and Soden [433] advise against a simple assumption that global systems become more energetic as they warm, concluding that the complexity of such systems should guard against over-confidence in simple arguments.

An intra-annual oscillation ($\overline{\vec{E}}_{\mathrm{MC}}$) is also seen in the time series, representing daily estimates of hydrokinetic energy (Fig. 4.12). This can be explained by natural seasonal variations in precipitation and the rates of snow- and ice-melt. A representation of an average year is achieved by calculating the mean energy on each calendar day (omitting leap days) throughout the 35 years considered (Fig. 4.13(a)). Globally, a minimum of 4.8 ± 0.2 PJ occurs on 30 January and a maximum of 7.1 ± 0.4 PJ occurs on 23 July, corresponding with the Northern Hemisphere (NH) winters and summers, respectively (Table 4.5 summarises all values associated with Fig. 4.13). The stated uncertainty of these estimates result from the extremes of the Monte Carlo simulations. The Monte Carlo method ($N = 1000$) is also applied to subsets of the data to determine the relative contributions from the NH and Southern Hemisphere (SH). Total river length (and percentage of global rivers, excluding Greenland and Antarctica) for the NH is 2.05×10^7 km (74.2 %) and for the SH is 6.9×10^6 km (25.8 %). Given this large difference in total river length between the two hemispheres, it is notable that the SH contributes a greater proportion to the global total. It is useful to also compare how hydrokinetic energy varies through the respective seasons of the two hemispheres (Fig. 4.13(b)). Here, the numbering of the calendar days begins on the first day of spring, for each hemisphere, according to the meteorological definition (1 March and 1 September). The minimum and maximum in the NH are seen to occur at the beginning of spring and beginning of autumn. For the SH, these occur at the end of spring and end of autumn, illustrating a phase difference of approximately a season.

With regards to this observed phase difference, Dettinger and Diaz [560] describe dominant modes of streamflow seasonality, that can be used to explain the maximum observed for the NH:

- a late spring stream flow maximum across the Timansky and Ural mountain ranges of Russia, along the southern edge of the Siberia, and in parts of the mountainous south-western North America;
- the effects of a mid- to late-summer monsoon in the Indian subcontinent, eastern Africa and Sahelian western Africa; and,
- a slightly later (September) monsoon affecting tropical West Africa, Central America and the subtropics of western North America.

The SH signal is dominated by South America, which we shall discuss below, when comparing and contrasting individual continental basins.

Weather can be described as a manifestation of solar energy, which varies through the seasons due to the periodic oscillations of variables related to the earth's orbit of the sun and relative tilt of its axis. Precipitation and the rate of snow- and ice-melt are thus influenced by

the effects of this process, dictating the observed seasonal variation of hydrokinetic energy. Beyond this, macroscopic weather events which would be most relevant in understanding seasonal variation in these factors, are the occurrence of monsoons and the freezing and thawing of water at high elevation and high latitude [561]. The NH has substantially more landmass located at high latitude (Fig. 3.3) and is where many of the world's largest mountain ranges are found, although South America contains the Andes. Therefore, this would imply a greater effect from freezing and thawing in the NH, providing a plausible reason for the especially low minimum for the NH. Further, it offers a valid hypothesis for the disproportionately greater hydrokinetic energy of the SH, overall, despite having markedly less total river length relative to the NH.

Verdin and Verdin [407] developed the Pfafstetter system to delineate and code hierarchically nested catchments (see Subsection 3.1.2). The GRADES data set is divided into 9 continental-level divisions, which are defined as Level 1 basins (Fig. 3.3). These 9 continental-level divisions do not align to the conventional definition of the 7 continents, with the exception of Africa and South America. This division allows investigation of the contribution to the global hydrokinetic resource by these regions (Fig. 4.14(a)). South America is notable, with a mean of 2.870 ± 0.007 PJ (797 ± 2 GWh) accounting for 48.6 % of the global mean (Table 4.5 summarises all values associated with Fig. 4.14). Further, a minimum and maximum occurring on 28 December and 21 June, both approximately a month prior to the global values, confirms the dominant signal of this continental-level basin.

The continental-level basins of Africa and Asia, with mean values of 1.103 ± 0.002 PJ (306.4 ± 0.6 GWh) and 0.771 ± 0.004 PJ (214 ± 1 GWh), are the next greatest. Though the continental-level basins of South America and Africa align with the contemporary definitions of these continents, that is not the case for Asia. For a thorough quantification of the Asian continent, a consideration of portions of the continental-level basins of Siberia and Australia would be needed and surely result in the energy attributed to this continent increasing. Therefore, the results of this resource assessment would suggest that the continents of South America, Africa and Asia are those that offer the most potential, in terms of HEC.

The Siberia and Arctic continental-level basins, though containing major rivers (e.g. Mackenzie, Yukon, Kolyma, Lena, Khatanga, Yenisey and Ob), contribute modestly to the global total, with mean values of 0.460 ± 0.001 PJ (127.8 ± 0.3 GWh) and 103.1 ± 0.3 TJ (28.64 ± 0.08 GWh), respectively. The low values for these regions of higher latitudes would suggest that the contributions from Greenland and Antarctica, which are not part of this study, would also be low. Both regions are similarly affected by the colder temperatures found at high latitude, causing much water to be held as ice and snow, and neither region contains any notably large rivers. Further, high latitudes are associated with reduced precipitation [562, 563]. These factors reinforce the assertion that higher latitude, less hydrokinetic energy abundant, areas of the NH result in the disproportionately high estimation for the hydrokinetic energy for the SH, with respect to the latter having less total river length.

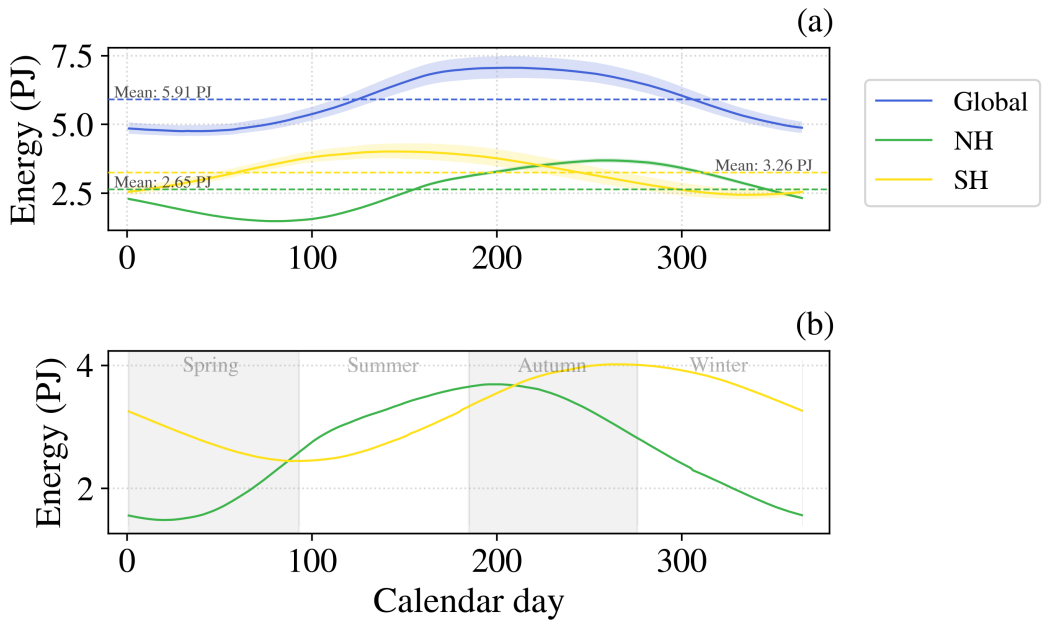

Figure 4.13: Average year of daily energy for rivers, globally, in the Northern Hemisphere (NH) and Southern Hemisphere (NH). The uncertainty of $N = 1000$ Monte Carlo simulations is indicated by the shaded area in (a) with calendar days from 1 January and in (b) from the beginning of spring (1 March for the NH and 1 September for the SH).

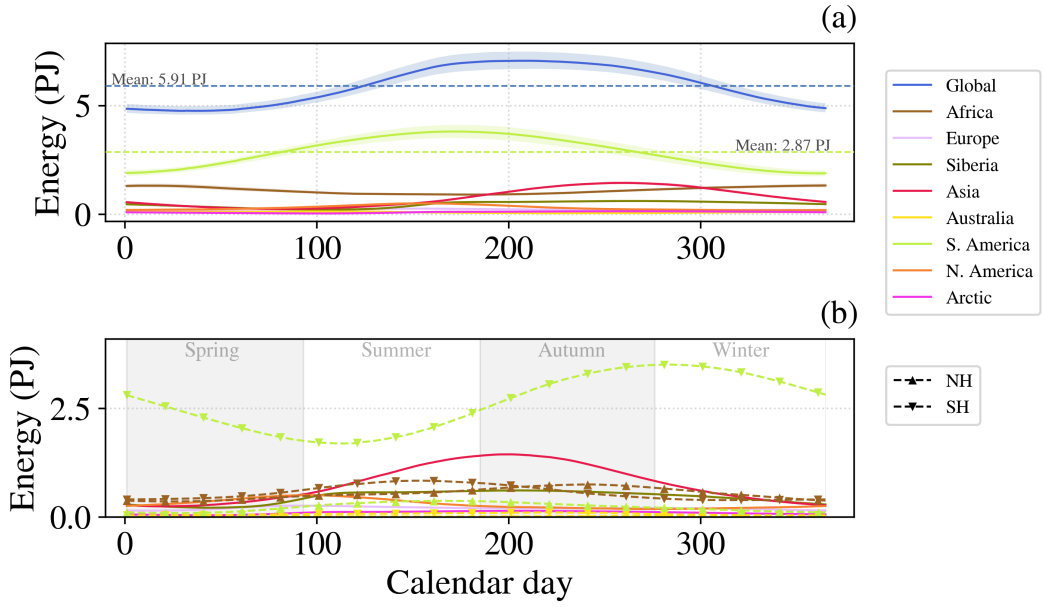

Figure 4.14: Average year of daily energy for rivers globally and by continental-level division. The uncertainty of $N = 1000$ Monte Carlo simulations is indicated by the shaded area in (a) with calendar days from 1 January and in (b) are from the beginning of spring (1 March for the NH and 1 September for the SH). Continental-level divisions represented in the NH and SH are appropriately divided.

Table 4.5: . Complimentary data, corresponding with Figs. 4.13 and 4.14, stating mean, minimum, and maximum values: globally, by hemisphere, by continental-level basin, and hemisphere subdivisions of basins that straddle the equator. Calendar day and date of when minimums and maximums occur are also given. The uncertainty stated with mean values is a calculation of the standard error of the mean, applied to the time series. Other uncertainties result from the extremes of the Monte Carlo simulations.

Basin	Hydrokinetic energy (TJ)				Day		Date	
	Mean	Min	Max	Range	Min	Max	Min	Max
Global	5,911 ± 9	4,800 ± 200	7,100 ± 400	2,300 ± 600	30	204	30 Jan	23 Jul
NH	2,645 ± 7	1,490 ± 60	3,690 ± 80	2,200 ± 140	80	260	21 Mar	17 Sep
SH	3,266 ± 7	2,500 ± 300	4,000 ± 300	1,500 ± 600	334	145	30 Nov	25 May
Africa	1,103 ± 2	910 ± 60	1,330 ± 100	420 ± 160	181	365	30 Jun	31 Dec
Europe	207.0 ± 0.4	150 ± 10	270 ± 10	120 ± 20	75	152	16 Mar	1 Jun
Siberia	460 ± 1	220 ± 20	620 ± 30	400 ± 50	103	265	13 Apr	22 Sep
Asia	771 ± 4	250 ± 10	1,450 ± 70	1,200 ± 80	80	261	21 Mar	18 Sep
Australia	96.3 ± 0.3	57 ± 4	135 ± 9	78 ± 13	230	98	18 Aug	8 Apr
S. America	2,873 ± 7	1,900 ± 100	3,800 ± 300	1,900 ± 400	362	172	28 Dec	21 Jun
N. America	302 ± 1	190 ± 20	510 ± 60	320 ± 80	331	154	27 Nov	3 Jun
Arctic	103.1 ± 0.3	44 ± 5	143 ± 10	99 ± 15	103	267	13 Apr	24 Sep
Africa (NH)	543 ± 1	360 ± 30	750 ± 40	390 ± 70	84	303	25 Mar	30 Oct
Africa (SH)	562 ± 2	390 ± 50	830 ± 100	440 ± 150	199	34	18 Jul	3 Feb
Australia (NH)	24.52 ± 0.09	15 ± 2	33 ± 3	18 ± 5	229	15	17 Aug	15 Jan
Australia (SH)	71.9 ± 0.3	42 ± 3	110 ± 7	68 ± 10	234	98	22 Aug	8 Apr
S. America (NH)	231.8 ± 0.9	97 ± 8	376 ± 32	279 ± 40	89	225	30 Mar	13 Aug
S. America (SH)	2,634 ± 7	1,700 ± 200	3,500 ± 300	1,800 ± 500	357	162	23 Dec	11 Jun

The continental-level basins of Africa, Australia, and South America straddle the equator, with each having 30 %, 92 %, and 83 % of their total river length located in the SH and the remainder in the NH. Therefore, consideration of the the average annual years for these basins, plotted with calendar days beginning from a hemisphere-specific start of spring (1 March and 1 September), required dividing the data into further subsets (Fig. 4.14(b)). The strongest signals for the NH and SH, respectively, are the continental-level basins of Asia and the SH subset of South America (Table 4.5). The continental-level basin of Asia has a minimum occurring on the same day as for the overall NH subset and a maximum that occurs a day later. This basin contains a number of major rivers which transport water from the Himalayas and is governed by strong precipitation seasonality, with up to 80 % of the annual rainfall occurring during the Indian summer monsoon season [564]. Though the Indian summer monsoon exhibits a wide spectrum of variability, the season is generally from June to September [564, 565], describing the meteorological definition of the NH summer. This monsoon and the East Asian monsoon are the major components of the larger Asian monsoon system [565]. The East Asian summer monsoon also contributes significant precipitation during the NH summer, with two peaks from late June to mid-July and from mid-August to early September [566]. These high precipitation events occur during a corresponding rise in the estimated hydrokinetic energy for this basin, following the initiation of the rise from probable ice- and snow-melt at the beginning of the spring, marked by the minimum on 21 March and maximum on 18 September (40 and 201 days after the beginning of spring).

The SH subset of the South America continental-level basin is seen to lead Asia (and the NH as a whole, as discussed above) by approximately a season, with a rise beginning from a minimum on 23 December and maximum on 11 June (113 and 283 days after the beginning of spring). Zhou and Lau [567] first confirmed that a monsoon climate exists over South America and describe the South American summer monsoon as a complex and multi-phase process, involving much regional variation. This can be summarised, more generally, as involving increased precipitation on the continent from late spring to late summer. This period correlates with the maximum gradient of increased hydrokinetic energy, before a gradual reduction, reaching a maximum at the end of the autumn. Since the effects of monsoons occur in approximately the same seasons, for the Asia basin and SH subset of the South America basin, the lag of a season between the former and the latter must be due to another factor. Transmission time, which describes how long it takes for rainfall to flow through a catchment, is inevitably important here and provides some explanation for the observed lag of maximum hydrokinetic energy behind expected maximum rainfall. Yet, this would be the case for both the Asia and the SH subset of the South America continental-level basins and does therefore not explain the difference in the length of the lag between them. Given the heavy influence of the Himalayas on the rivers of the Asia basin, and the fact that it is the most significant and highest mountain range on Earth, it might be the case that the freezing and thawing process, which affects the volume of water available to contribute to the overall discharge, is relevant. Indeed, Bookhagen and Burbank [564] provide a detailed description of the spatiotemporal variability of the Indian summer monsoon in the Himalayas and highlight the importance of ice- and snow-melt in the hydrological budget of Himalayan rivers. The authors state that this is particularly significant in the pre- and early monsoon months from March to June, accounting for >40 % of river discharge.

4.5 Global distribution of riverine hydrokinetic resource

The spatial distribution of the riverine hydrokinetic resource is determined by river reach (Fig. 4.15), using an equation derived from a consideration of the rate of transfer of kinetic energy (Eq. (4.49)). It is increasingly common for hydrological studies to use a reach-scale frame of reference [358–360]. A reach is a length of a river, between points of confluence, bifurcation, or channel initiation. It usually suggests a level, uninterrupted stretch. This definition allows hydrological characteristics to be considered at an intermediate scale, between catchment- and field-scale. The growth of 'big data' in geosciences allows higher fidelity data than can be achieved at the catchment-scale. Yet, a better understanding can be achieved at the reach-scale than for field-scale, as the numerous assumptions and approaches used in hydrological modelling still work reasonably well at this scale.

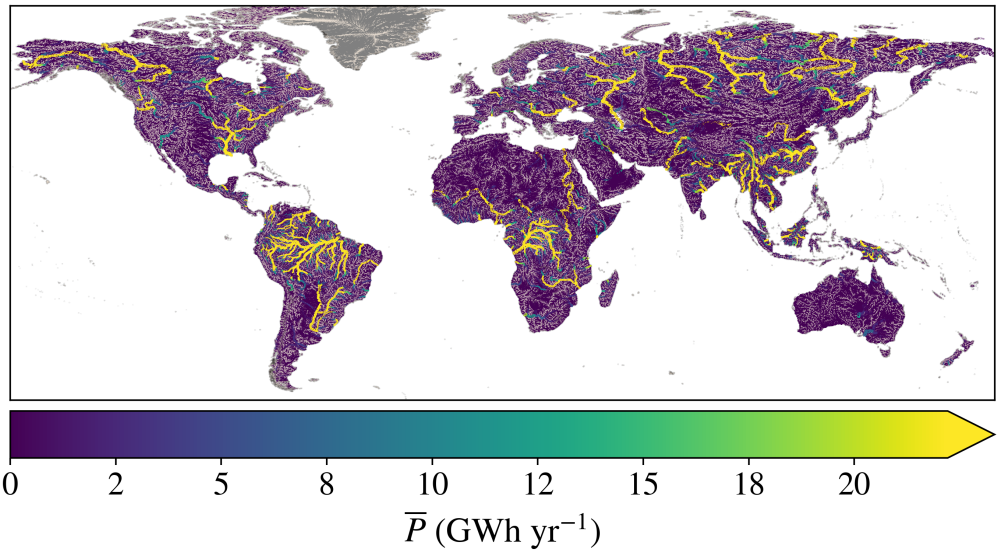

Figure 4.15: Global (excluding Greenland and Antarctica) spatial distribution of theoretical riverine hydrokinetic mean annual power $\overline{P}$. Lines representing rivers have a width that is proportional to stream order. The colourbar maximum is determined by the 99th percentile.

Leopold and Maddock [297] established a method for estimating hydraulic parameters as a function of Q (Eqs. (4.23), (4.24) and (4.25)). Estimated global mean values for the power law parameters k and m in Eq. (4.25) were used to calculate mean hydrokinetic power. Although consideration of a single reach is best represented, statistically, by these mean values, when considered collectively this results in a marked underestimation. In publishing globally applicable numerical constants for the coefficients and exponents of power law relationships to estimate the hydraulic parameters w and d, Moody and Troutman [448] provided an indication of the 95 % confidence intervals associated with the coefficients of these relationships. These confidence intervals are asymmetric about the mean values (Fig. 4.7), being notably larger in the positive direction. These published values have been used to derive corresponding values for k, m and their associated uncertainty (Eq. (4.34)). Therefore, this asymmetry also exists

for the 95 % confidence interval for the coefficient k. Given that confidence intervals would reflect the statistical distribution of these parameters, this asymmetry implies empirical values of annual mean power that, though they can be calculated using power law coefficients falling within this confidence interval, are of a magnitude that greatly exceeds that predicted by an estimation using an application of the mean values. Conversely, empirical values of annual mean power, that can also be calculated using power law coefficients that fall within the confidence interval, but of a magnitude that is below that estimated using an application of mean values, would tend to have a lesser magnitude of variance, overall.

4.6 Comparison with existing studies

The results presented in Chapter 3 and published by Ridgill et al. [137], using the same GRADES data applied here, provides a global perspective for comparison (Fig. 4.16(b)). Both this earlier methodology and what is presented here use a similar approach, with the earlier study applying the conventional equation $P = \gamma QH$ (Eq. (4.1)), providing a measurement of the theoretical rate of *conversion* of gravitational potential energy to kinetic energy. In contrast, the equation $P = \frac{1}{3}\rho k^2 Q^{(2m+1)}$ (Eq. (4.49)) as applied in this chapter, provides a measurement of the theoretical rate of *transfer* of kinetic energy through river systems.

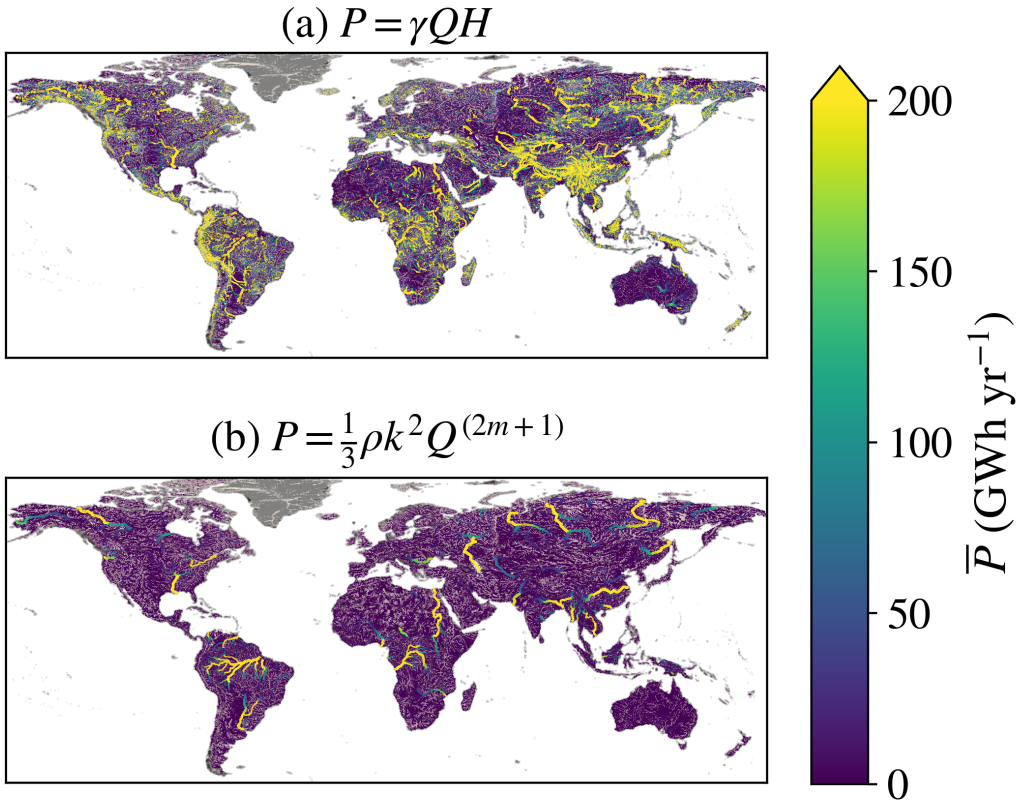

Figure 4.16: Global (excluding Greenland and Antarctica) spatial distribution of theoretical riverine hydrokinetic annual mean power $\overline{P}$, using an equation derived from a perspective of (a) the transfer of kinetic energy and (b) the conversion from gravitational potential energy. The colourbar maximum is set 'by eye', to best compare and contrast the plots.

Comparison of these two sets of results reveals distinct differences. A qualitative description of regions that are prominent, from the perspective of Chapter 3, would include: the Himalayas, Tibetan Plateau and surrounding areas; the large, mountainous islands of Borneo, Indonesia and New Guinea; New Zealand; the Andes; the Pacific Northwest; Scandinavia; the Congo Basin and Equatorial Africa; Madagascar; and, many of the major rivers of the world (Fig. 4.16(b)). Or, more succinctly: regions with large changes in elevation and many major rivers. This contrasts with the revised methodology applied in this chapter, which highlights that the resource resides predominately in the major rivers of the world, with the resource increasing in the downstream direction (Fig. 4.16(a)). In addition to the qualitative differences described, overall estimates of the annual mean power also tends to be notably lower in the hydrokinetic approach applied in this chapter.

A relative assessment of this difference (Fig. 4.17) is considered by subtracting the normalised hydrostatic annual mean power from the normalised hydrokinetic annual mean power. The calculation of this normalised difference in power $\overline{P}_{\text{diff}}$, for each reach, can be summarised as

$$\overline{P}_{\text{diff}} = \frac{\overline{P}_{\text{GPE}}}{\overline{P}_{\text{GPE,99}}} - \frac{\overline{P}_{\text{KE}}}{\overline{P}_{\text{KE,99}}} \tag{4.66}$$

where $\overline{P}_{\text{GPE}}$ is the mean annual power of a reach from a gravitational potential energy derived (hydrostatic) perspective (Eq. (4.1)), $\overline{P}_{\text{KE}}$ is the mean annual power of a reach from a kinetic energy derived (hydrokinetic) perspective (Eq. (4.49)), and the associated global 99th percentile values are $\overline{P}_{\text{GPE,99}}$ and $\overline{P}_{\text{KE,99}}$, respectively. The hydrostatic resource assessment is seen to favour areas with large elevation change, whereas the hydrokinetic resource assessment favours major rivers, thus confirming the interpretation of Fig. 4.16 stated above. In the former, the conventional equation for determining theoretical hydraulic power ($P = \gamma QH$) is used, which is derived from considering the rate of conversion of gravitational potential energy to kinetic energy that occurs as water travels along the length of a river reach (see Section 4.1). In the latter, an equation is proposed ($P = \frac{1}{3}\rho k^2 Q^{(2m+1)}$) that considers the rate of transfer of energy that propagates through any cross-section within a given river reach and is derived by a process that involves (or implies) estimating w, d and v for this reach, as a function of Q (see Subsection 4.3.1). Power, conceptually, is defined as either the rate of energy conversion, or the rate of energy transfer. The two perspectives (hydrostatic and hydrokinetic) align with these two definitions, respectively. In stating this, we more precisely understand what is being measured by these two approaches and make clear what might be expected to result from assessing the global hydrokinetic resource through these two lenses. Thus, these two methods provide different results and disagree on a qualitative and quantitative description of the regions of the world that have the most potential for HEC.

The two approaches differ in their frame of reference and therefore offer slightly different ways of viewing the resource. The hydrostatic perspective uses a Lagrangian frame of reference, giving an estimate of the kinetic energy of the water flowing through only the final cross-section of a river reach. In contrast, the hydrokinetic perspective is Eulerian and considers the rate of transfer of energy that is transferred through a given cross-section. Since hydraulic geometry parameters are considered constant along reaches, in this study, the hydrokinetic energy approach is applicable to any cross-section within a reach, including the final cross-section. This point, concerning the final cross-sections, is the reason why the two meth-

ods can be compared and contrasted. In describing a Lagrangian frame of reference, we are considering a discrete body of water moving through space and time. This can be extended to a global view, where the river network comprises many individual discrete bodies of water and is defined by the sum of these individual reaches. In this way, a global resource assessment is achieved by considering a 'snapshot', where the flow of each of these discrete bodies is considered flowing through each of these reaches. Though the period in which this occurs for each reach will differ, this is not important, since the sum of these discrete bodies of water equals the sum of all water in the global network. In the derivation of the equation used for the hydrokinetic approach, a body of water was described travelling a given length in a given time (see Subsection 4.3.1). This leads to a complication when considering all global reaches concurrently, since the time will vary for each reach, if considering a discretised body of water travelling through these reaches. To put this another way, if two reaches with the same value for discharge but different length are considered, they will have the same calculation of power, but will transfer a different quantity of energy when considered over the same time period. Alternatively, a different period of time will elapse if considering the transfer of these discrete quantities of water. This inconsistency is another reason that a value for the global theoretical riverine resource as an expression of annual energy yield, using the usual units of TWh yr^{-1} or similar, is not offered in this chapter. The means for achieving an estimate of the mean total energy of all rivers as 5.911 ± 0.009 PJ (1.642 ± 0.003 TWh) (as presented in Section 4.4) involved discretising the water contained within each reach and is therefore now Lagrangian in nature, in contrast to the Eulerian method of measuring power transferred through the reach. Though operating within different frames of reference, both still offer a hydrokinetic perspective.

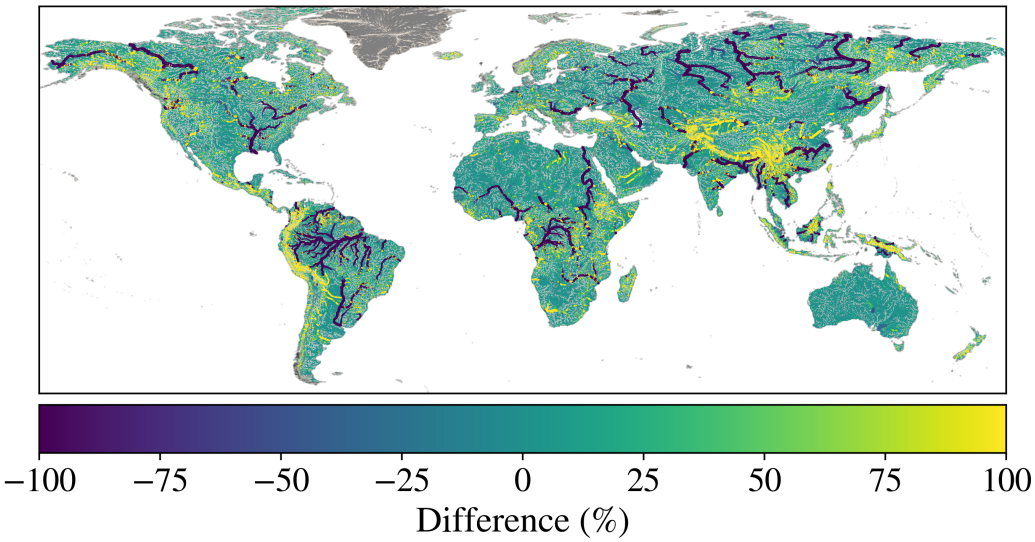

Figure 4.17: The difference between resource assessment from a hydrokinetic and hydrostatic approach, where 0 % implies no difference between the normalised values from each, 100 % a maximum difference biased towards the hydrostatic calculation and −100 % a maximum difference towards the hydrokinetic calculation. Line width is proportional to stream order.

Studies providing accurate measurements of the theoretical hydrokinetic resource in rivers are few. Punys et al. [128] used the one-dimensional hydraulic model HEC RAS 4.1 to determine the theoretical hydrokinetic power passing through cross-sections at three locations in

Lithuania. Determination of the coordinates of these locations (P. Punys and E. Kasiulis [128]; Pers. Comm.) allowed identification of the corresponding river reaches, such that a comparison could be made between the two methods considered here (Table 4.6).

The values for annual mean power calculated using the hydrostatic approach ($\overline{P}_{\mathrm{GPE}}$) for the locations Jonava, Vilnius, and Buivydziai differ from the hydraulic model calculations ($\overline{P}_{\mathrm{mod}}$) by 840 %, 27,413 % and 27,450 %, respectively. The hydrokinetic approach ($\overline{P}_{\mathrm{KE}}$), using mean values $m = 0.5$ and $k = 0.20$, yielded values that differed by 23 %, 60 %, and 117 %, respectively. Percentage bias (PBIAS) measures the average tendency of simulated values to be larger or smaller than observed values, using

$$\mathrm{PBIAS} = \frac{\sum_{i=1}^{N}(S_i - O_i)}{\sum_{i=1}^{N} O_i} \times 100\% \tag{4.67}$$

with an optimal value of PBIAS = 0 % and low-magnitude values indicating accurate model simulation. Positive and negative values signify over- and under-estimation bias, respectively. If we treat the calculations from these two studies as simulated values and the data from Punys et al. [128] as observed values, the PBIAS for the hydrostatic and hydrokinetic approach are $+11{,}000 \pm 5{,}435$ % and $+40^{+7{,}994}_{-139}$%, respectively. The uncertainty in the former case is a measure of the mean absolute error (MAE). In the latter case, addressing the most prominent source of uncertainty, this is determined by using the upper and lower limits for the 95 % confidence interval and uncertainty of the power law parameters m and k, respectively, giving an uncertainty that is asymmetric with respect to the mean values (Eq. (4.34)). While this is a small sample size to provide a complete validation and there are large uncertainties associated with the parameters m and k used to calculate the mean power from the hydrokinetic perspective ($\overline{P}_{\mathrm{KE}}$), this comparison would suggest that the hydrokinetic method for estimating hydrokinetic resource provides a result that agrees more closely to the results from the hydraulic model applied by Punys et al. [128]. To reiterate, the sample size is small, but one can clearly observe that considerable differences are seen between these two approaches, sufficient perhaps to conclude that this is a meaningful difference.

Table 4.6: Comparison of annual mean power ($\overline{P}_{\mathrm{mod}}$), as calculated by Punys et al. [128], with that calculated using a hydrostatic method ($P_{\mathrm{GPE}} = \gamma QH$) and a hydrokinetic method ($P_{\mathrm{KE}} = \frac{1}{3}\rho k^2 Q^{(2m+1)}$).

Location	$\overline{P}_{\mathrm{mod}}$ (kW)	$\overline{P}_{\mathrm{GPE}}$ (kW)	$\overline{P}_{\mathrm{KE}}$ (kW)
Jonava	124	1,165	153
Vilnius	52	14,307	83
Buivydziai	24	6,612	52

4.7 Idealised model

An idealised model can be used to further investigate the difference between the hydrostatic ($P = \gamma QH$) and hydrokinetic ($P = \frac{1}{3}\rho k^2 Q^{(2m+1)}$) perspectives. Here, a river network is constructed (Fig. 4.18) such that, from the mouth of the river, a reach of stream order 9 splits into

two reaches of stream order 8 and so on upstream, such that in each case there is a doubling of the number of reaches, from stream order 9 to 1. Global mean values, within the GRADES data set, are assigned in this model (Table 4.7). Starting from any reach of stream order 1 within this idealised river network and following a route to the mouth, the route is the same (Fig. 4.19).

In accordance with the methodology of Chapter 3, the total energy conversion from gravitational potential energy to kinetic energy of the river network can be calculated by summing the energy conversion for all reaches (Fig. 4.18 (b)). In this case, an estimate of 17.3 TWh yr^{-1} is given. For the reasons discussed in Section 4.6, the hydrokinetic method of Chapter 4 is inappropriate for determining this same measure and instead can be used to estimate the total kinetic energy of the river network by summing the results of applying Eq. (4.50) to each reach. Here, values of $k = 0.5$ and $m = 0.02$ were applied, representing globally applicable mean values (see Subsection 4.2.3). In this case, an estimate of 61.9 MWh is given. Providing a useful, if unrealistic, representation of a globally 'average' river network, this idealised model also reiterates the points made in the previous section.

Table 4.7: Global mean values from the GRADES data set, for H, L and Q, grouped by stream order, are used to construct an idealised model. For reaches of each stream order, these values are used to calculate the rate of energy conversion from gravitational potential energy to kinetic energy by the hydrostatic method ($P = \gamma QH$) and the rate of kinetic energy transfer by the hydrokinetic method ($P = \frac{1}{3}\rho k^2 Q^{(2m+1)}$).

Stream order	H (m)	L (km)	Q ($m^3\ s^{-1}$)	P_{GPE} (GWh yr^{-1})	P_{KE} (GWh yr^{-1})
1	64.5	9.0	0.7	3.7	4.7×10^{-4}
2	38.2	9.8	2.9	9.4	2.2×10^{-3}
3	19.6	9.4	13.3	22.4	1.1×10^{-2}
4	10.3	8.9	57.7	51.0	5.0×10^{-2}
5	5.5	8.4	257.5	122.3	0.2
6	3.0	8.0	943.1	245.6	0.9
7	1.6	8.0	3,632.6	491.7	3.7
8	0.6	7.9	10,568.0	550.7	11.2
9	0.8	9.0	76,296.2	5,141.7	87.4

4.8 Concluding remarks

Since hydrokinetic power is proportional to flow velocity cubed (Eq. (4.39)), it follows that flow velocity is of fundamental importance to a meaningful resource assessment. Leopold and Maddock [297] have demonstrated that flow velocity is proportional to discharge (Eq. (4.25)). Major rivers have high values for discharge and this would tend to increase in a downstream direction, reinforcing the finding that downstream regions contain the greatest potential for HEC. An increase in flow velocity in a downstream direction also accords with the Bradshaw model of upper to lower river course trends [439, 440].

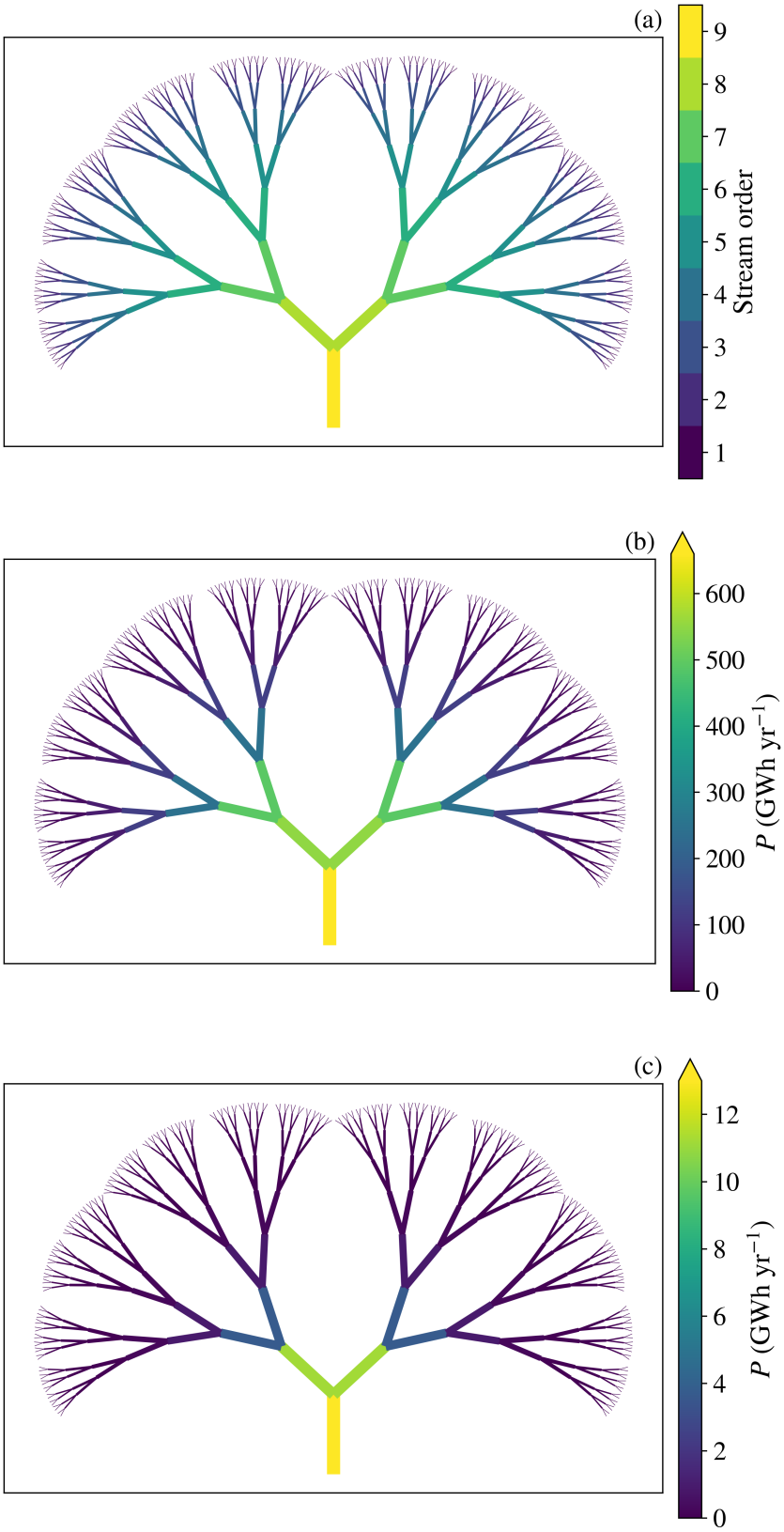

Figure 4.18: An idealised river network, showing in (a) the doubling of number of reaches for each stream order 9 to 1; in (b), the rate of energy conversion from gravitational potential energy to kinetic energy ($P = \gamma QH$) through each reach; and, in (c), the rate of kinetic energy transfer ($P = \frac{1}{3}\rho k^2 Q^{(2m+1)}$) for any cross-section within each reach. To enable visualising the river network, reach lengths have been modified from that used in any calculations and line widths are proportional to stream order.

A dynamic equilibrium between tectonic uplift, tectonic deformation, and geomorphic processes of erosion, modulated by geology, substrate erodability, and climate, drives the evolution of a river network. The resulting geometry is that which serves the role of draining a terrestrial landscape of water and sediment most efficiently. Constructal theory describes a law of design and evolution in nature and states that finite-size flow systems must evolve to provide increasing access to the currents that flow through them [568]. Examples are seen in the evolution of lungs, animal locomotion, vegetation, turbulent flow structure, self-lubrication, natural multi-scale porous media and also river basins [569]. This law has been suggested not only for temporal evolution, but also in a downstream direction [570] and implies an increase in efficiency and therefore increase in energy. Such a perspective would align with a view that the lower-courses of major rivers would potentially offer river flow with the greatest kinetic energy, corresponding to the hydrokinetic focused methodology and associated results presented here.

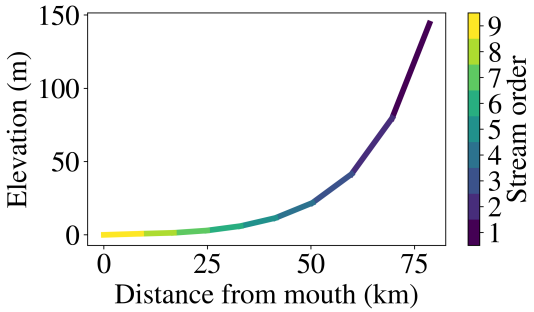

Figure 4.19: Route through the idealised river network, starting from any reach of stream order 1.

The argument put forward here, therefore, is that a methodology that focuses on flow velocity and the rate of transfer of kinetic energy, in considering the global theoretical riverine hydrokinetic resource, rather than an unrealistic measurement of the rate of conversion of gravitational potential energy to kinetic energy, better supports the development of HEC technology, in an immature industry where such information has been identified as one of the main barriers to progress [122, 123]. A hydrostatic perspective of this resource is still relevant and permits an estimation of the overall annual mean energy yield which can be compared with other renewable energy technologies. Yet, it must be realised that this hydrostatic approach is theoretical and discounts energy loss due to boundary-induced friction. This issue is compounded by the fact that friction from the bed and banks of a channel is not constant throughout a river network, from upper to lower courses, resulting in a bias when used as a means for determining global distribution (see Section 4.1).

Large uncertainties are associated with the power law parameters used in the hydrokinetic approach proposed. This could be summarised as giving a method that is less *precise*, relative to the conventional hydrostatic perspective, but arguably more *accurate*. Future studies could look to improve this precision. Development of techniques for estimating continental- and global-scale river widths have shown steady improvement [205, 221, 238]. Since $Q = wdv$ (Eq. (2.30)), a corresponding improvement of techniques to determine d, in combination with data sets for Q, such as used in this study, would lead to a better estimate of v, which is probably the most challenging of these variables to determine remotely.

Given the focus upon v in the methodology and results presented, it is necessary to acknowledge and highlight the limitations of this approach, due to this fact, in addition to the benefits laid out thus far. Attempting a global-scale resource assessment necessitates an acceptance of decreased resolution. With decreasing resolution comes ever-decreasing representation of the variability of flow velocity. At the reach-scale, the natural variability of channel form results

in corresponding effects for v and an accompanying impact upon hydrokinetic energy. This reach-scale variability is not captured in this study. In their review of riverine hydrokinetic resource assessments, Kirby et al. [177] found that the methodology applied to site-specific assessments were not entirely consistent. Further, they state that these issues are amplified for regional-scale, or larger-scale, resource assessments. Though the standards published by the International Electrotechnical Commission [173] propose a standardised approach to site-specific resource assessment (see Subsection 2.2.3), they provide no advice on how this site is first identified. This study looks to offer something in the way of a first-order approximation that can bridge this gap. Overall, a general perspective is offered, to describe where hydrokinetic energy is to be found and make explicit the difference between conventional hydropower and HEC, and the need for different approaches to resource assessment for each.

Chapter 5

Prominent rivers and the basin-scale

5.1 Describing rivers at the basin-scale

In Chapter 4, when considering the global hydrokinetic resource, the great significance of major rivers was proposed. Therefore, we will now consider individual prominent rivers and the basin-scale with which we can describe them.

Building upon the definition given earlier in Subsection 2.3.1, Mark and Smith [571] define geomorphology as a science of topography and list 26 broad land form types with which to categorise the surface of the planet. Those relevant for fluvial geomorphology are: floodplain, basin and catchment.

Bankfull discharge Q_b occurs when river flow fills the entire channel (the different conventions for defining river discharge are described in Subsection 2.3.2). A further increase in discharge Q will result in flooding. An occurrence of Q_b typically has a return period of between 1 and 2 years [572], but can be subject to great regional variation [573]. A floodplain is the land that borders a stream, which is inundated when $Q > Q_b$.

A drainage basin is an area that is drained by a river and its tributaries, acting as the source for water and sediment that moves from higher elevation through the river system to lower elevations, as they reshape channel forms. Generally, river systems trace a network that moves water eventually to the ocean, but endorheic basins are a class of basin that do not drain to the ocean. Drainage basins are the principal hydrologic unit considered in fluvial geomorphology and many socioeconomic activities depend on water resources in drainage basins.

The area of a drainage basin A_B is the variable most directly correlated to peak discharge Q_p [574]. This has prompted several studies to estimate the bankfull discharge Q_b (considered more useful) from A_B [412, 499, 572, 575–580], using

$$Q_b = qA_B^r \tag{5.1}$$

where q and r are empirically determined constants which are specific to a basin. Power law relationships like this are common in fluvial geomorpholgy and hydraulic geometry (as discussed in Section 4.2). Another example of such a power law relationship is seen when considering the relationship between A_B and channel slope s, often referred to as Flint's law [466, 581–585].

This relationship is given by

$$s = k_s A_B^{-\theta} \tag{5.2}$$

where k_s is referred to as channel steepness and θ is the channel concavity. Yet another example of a power law relationship is used to describe the relationship between the total channel length within the basin area L_B and A_B, as

$$L_B = s_L A_B^{t_L} \tag{5.3}$$

where the parameters s_L and t_L provide constants that vary by region.

Table 5.1: Influence of river charateristics on drainage density D_d.

Characterisitic	High drainage denity ($D_d > 2\,\text{km}$)	Low drainage density ($D_d < 2\,\text{km}$)
Precipitation rate	High	Low
Permeability of surface materials	Low	High
Resistance to erosion of surface materials	High	Low
Degree of protection by vegetation	Low	High
Channel frequency (tributaries)	High	Low
Bank steepness	High	Low

Drainage density D_d, which provides a measure of how well a basin area is drained by stream channels, is described by

$$D_d = \frac{L_B}{A_B} \tag{5.4}$$

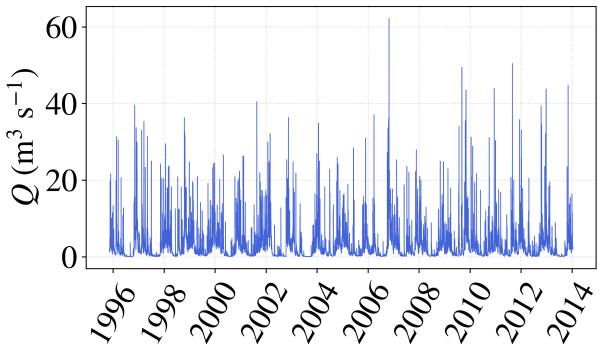

Figure 5.1: Hydrograph for the Tarroul station on the River Wick (Nov 1995–Jan 2014). Data from the National River Flow Archive [586].

Generally, the higher the drainage density, the more quickly water drains to a river, according to the influence of certain characteristics (Table 5.1). Drainage density varies by region. For example, it is high in semi-arid regions, because of temporally concentrated precipitation and lack of vegetation. The vegetation cover found in humid temperate areas causes drainage density to be low. Regional variations in the characteristics can be linked to the predominate climate of that region, but are also sensitive to the perspective of time chosen. For example, on a seasonal and inter-annual scale, flow variability in the UK is relatively low, due to its maritime climate. On a daily and sub-daily scale, in contrast, flow variability can be large and sensitive to precipitation, due to the predominance of catchment areas which are relatively small and often steep [587–589].

A hydrograph shows a time series of Q at a specific location (Fig. 5.1). High discharge density means increased potential for a rising limb, followed by a recession limb, in a hydrograph and is indicative of a greater risk of flooding. A rising limb describes a prolonged increase in Q, typically in response to a rainfall event. A recession limb describes the withdrawal of water from the storage built up in the basin during the earlier phases of the hydrograph. A subset of this data illustrates a peak discharge event (Fig. 5.2).

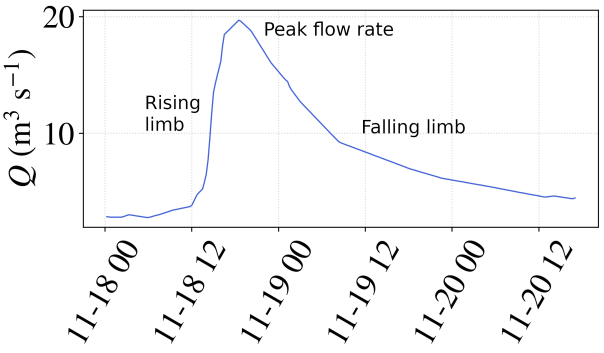

Figure 5.2: Hydrograph for a peak discharge event at the Tarrould station on the River Wick (18–20 November 1995). Data from the National River Flow Archive [586].

The third and final of the land form types listed above is a catchment area, which is very similar to a basin. The difference being that a catchment area defines an area from which water drains into a particular lake, river, etc., whereas a drainage basin means a topographic region in which all water drains to a common outlet. Thus, as with a basin, a catchment area also describes a region which collects precipitation and weathered material. This is transferred through a system of hillslopes and a network of channels, contributing runoff to a stream system and concluding in a single output at the mouth of the catchment [1]. In terms of hydrology, it provides a clearly defined physical unit and acts as an open system, with inputs, throughputs and outputs of energy and matter. Attributes that influence how a catchment stores and transfers water, include: climate, hydrology, land cover, soil geology, topography and river network. These attributes provide the means for characterisation [590–593]. Investigation of how these attributes interact can help to describe the events that occurs within catchments. For example, the combined affect of climate and topography in vegetation productivity [594].

The flashiness of a catchment indicates the speed of response to a large influx of water to the system. A flashy catchment will show a fast response and is characterised by a small area, steep slopes and impermeable geology. The gamma distribution can be used for examining hydrograph models and is defined as

$$f(t;k,\theta) = t^{k-1}\frac{e^{-\frac{t}{\theta}}}{\theta^k\Gamma(k)} \qquad [\text{for } t>0 \text{ and } k,\theta>0] \tag{5.5}$$

where k is a shape parameter and θ is a scale parameter of the hydrograph curve. The gamma function $\Gamma(k)$ is evaluated at k. The flashiness of a catchment can be determined by considering the standard deviation σ of the gamma distribution

$$\sigma = \sqrt{k\theta^2} \tag{5.6}$$

where a higher value of σ indicates more flashiness of the catchment being considered.

The geometry of a river system evolves due to a dynamic equilibrium between tectonic uplift, tectonic deformation and geomorphic processes of erosion, modulated by geology, sub-

[1] Outputs through evapotranspiration and groundwater seepage also occur.

strate erodability and climate. What results is the geometry which most efficiently serves the role of draining a terrestrial landscape of water and sediment. Thus, the plan-form geometry of river networks plays an important role in the evolution of continental landmasses, ecosystems and human geography.

The basin-scale geometry of a river system (Fig. 5.3) is comprised of some, or all, of the following elements:

- a drainage basin, which is the area that contributes water and sediment to the river system;
- a drainage divide;
- a mountain belt;
- an alluvial fan;
- broad alluvial valleys, with flood plains and alluvial channels; and,
- a delta.

The river network is described by channels and tributaries. Methods have been developed for measuring the shape of a river, providing knowledge of its morphometry, as we shall consider below.

Rivers are open channels resulting from streamflow, as water flows from higher to lower elevation. Driven by gravity, rivers always flow downhill. In this downhill direction, rivers can be described by division into three distinct stages: the upper, middle and lower river courses (the differences between these stages was described in Section 4.1). They may be further classified as either bedrock, or alluvial channels. Wohl [595] suggests that they can also be a combination of both and are then known as semi-controlled channels.

The headwaters of a river system are found at the most upstream points of the system, furthest from its meeting with the sea, or the confluence with another river. Headwaters, or first-order catchments, are very influential on drainage basins, as a whole. They contribute ~70 % of the mean annual water volume in second-order streams and ~55 % in fourth- and higher-order streams rivers [596]. Here we are categorising according to *stream order*, which provides a means for describing a river system as a network, with nodes and links. Channel links are defined to be channel reaches between two adjacent junctions, or nodes, in a river network [597]. Interestingly, Moody and Troutman [448] point out that although the length and change in elevation of channel links have been much investigated [581, 598–601], the statistical characteristics of channel width and depth have been less so.

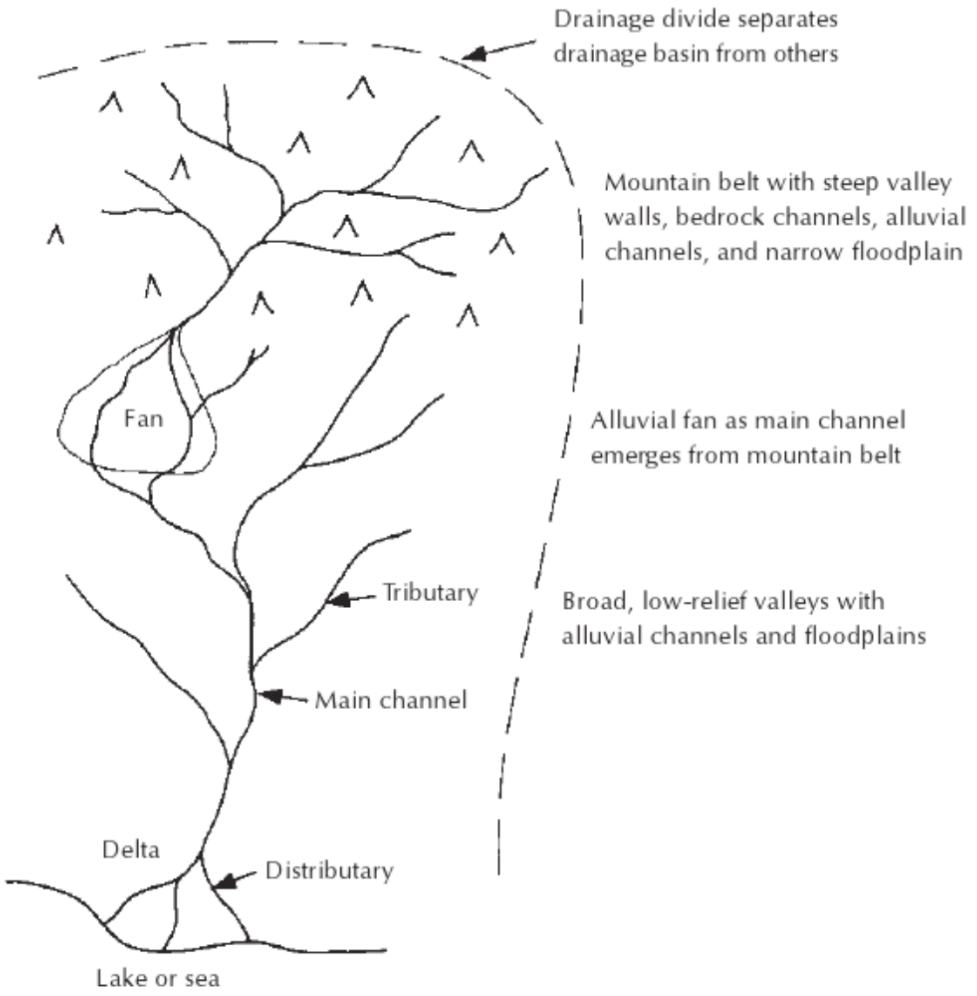

Figure 5.3: River system geometry [357].

The method of applying stream order as a way of describing river networks grew initially from the work of Horton [581] and then Strahler [602]. Eventually, Strahler [583] proposed stream order as a method for quantitative analysis of fluvial geomorphology, denoting a hierarchy to classify individual stream segments and drainage basins and a method for assigning values. Consider the river network of the Amazon (Fig. 5.4). It can be seen that stream order gives some indication of the distribution of reaches that are contained in larger river networks and their relative positions within these river networks. The river is shown developing in a downstream direction and illustrates that the lower-courses of large river system are assigned a high value for stream order, with the final reaches having the maximum values. In contrast, smaller river networks reach the sea at lower stream orders. Thus, stream order, considered at global-scale, gives an overall description of both river network size and distance downstream.

Stream order numbers are assigned to each node, in bottom-up order, according to the following criteria:

- if the node is a leaf (has no children), its number is 1;
- if the node has one child with number i, and all other children have numbers less than i,

then the number of the node is i again; and,

- if the node has two or more children with number i, and no children with greater number, then the number of the node is $i + 1$.

The upper river courses flow down from high hills and mountains. They are usually narrow, steep and marked by sharp valleys and abrupt changes of direction. The steepness means that there is much gravitational potential energy, often resulting in high turbulence, waterfalls and high levels of erosion.

The transition from upper to middle river sources is marked by a widening of channels and reduced steepness. River channel sinuosity increases and lakes feature more frequently. Sinuosity S is a measurement made of an oscillating curve. For a river channel, it is defined as

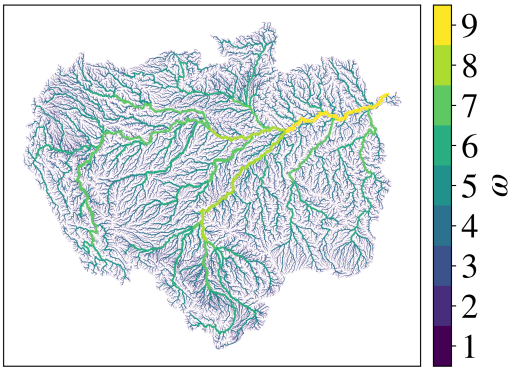

Figure 5.4: Distribution of stream order ω in the Amazon river network.

$$S = \frac{\text{channel length}}{\text{shortest path length}} \tag{5.7}$$

For example, Fig. 5.5 illustrates a channel length between two points of 7.42 km and the shortest path length between these two points being 1.05 km. In this case, the sinuosity would be a dimensionless value of $S = 7.07$.

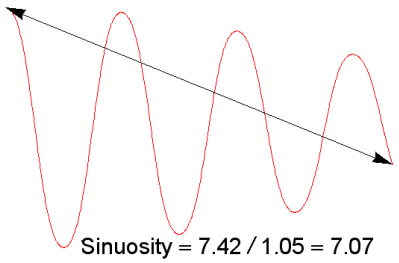

Figure 5.5: Calculation of sinuosity for an oscillating curve [603].

Sinuosity was found to have a global median of $S = 1.11$ and shown to decrease with increasing channel width [222]. Alternatively, Schulze et al. [495] estimated a global average for this factor to be $S = 1.3$.

Continuing the description of rivers downstream, sediment carried from further upstream is now deposited at the edges of river channels, forming levees which cause the water level to be higher that the surrounding landscape. During periods of high discharge, water level can overflow river banks, depositing sediment beyond the river channel and creating marshy floodplains.

The lower river courses can be similar to the middle river courses, but generally wider and less steep. The journey of a river concludes at estuaries and deltas. The hydrodynamic processes of an estuary are influenced by both tidal forcing and river flow. Estuary dynamics involve the interaction of a river current and a tidal current. The biogeochemical, hydrological and hydrodynamic

process involved in the transition from river to estuary are often limited in both observations and in model predictions [296]. The river influence can be estimated as a ratio of the hydrograph volume to the estuarine volume [604]. Daily-averaged values for river discharge have been shown to be inadequate for understanding the influence of river input upon estuarine hydrodynamics, for catchments which are particularly flashy, and it is unknown how sensitive estuarine models are to the boundary forcing from river flows [296].

In developing the means for a more detailed description, and using the elements discussed thus far, Horton [581] proposed laws to quantify a stream system in terms of stream order ω, drainage density D_d (Eq. (5.4)), bifurcation ratio R_b and stream-length ratio R_l. Regarding these last two terms, R_b is the ratio of a number of the stream segments of specified order and a number of streams in the next higher order and R_l is the ratio of the total stream length of the one order to the next lower order of stream segment.

The *law of stream numbers* states that there exists a geometric relationship between the number of streams of a given order N_ω and the corresponding value of ω

$$N_\omega = R_b^{\Omega-\omega} \tag{5.8}$$

where Ω is the highest stream order of the basin.

The *law of mean stream length* states that there exists a geometric relationship between the mean length of streams of a given order $\overline{L}_\omega$ and the corresponding value of ω

$$\overline{L}_\omega = \overline{L}_1 R_l^{\omega-1} \tag{5.9}$$

where $\overline{L}_1$ is the mean length of the 1st order streams of the basin. These two equations (Eq. (5.8) and (5.9)) are the two fundamental laws that connect the numbers and lengths of streams of different orders in a basin. Two additional laws proposed by Horton relate to these properties. The *law of total stream lengths* states that there is a relationship between the total length of streams of a given order L_ω and the corresponding value of ω

$$\sum L_\omega = \overline{L}_1 R_b^{\Omega-\omega} R_l^{\omega-1} \tag{5.10}$$

The *law of basin areas* states that there is a relationship between the mean area of a basin of a given order $\overline{A}_\omega$ and and the corresponding value of ω

$$\overline{A}_\omega = \overline{A}_1 R_a^{\omega-1} \tag{5.11}$$

where $\overline{A}_1$ is the mean area of the 1st order basins and R_a is the basin area ratio.

A further of Horton's laws relates to stream gradient. The *law of stream gradients* states that there is a relationship between the mean gradients of a given order $\overline{s}_\omega$ and the corresponding value of ω

$$\overline{s}_\omega = \overline{s}_1 R_s^{\Omega-\omega} \tag{5.12}$$

where R_s is the stream gradient ratio, describing the ratio of the stream gradient of a stream channel of one order to the stream gradient of the next higher order.

Thus, in this section we have defined the basin-scale representation of rivers and explored the different ways in which a description of rivers at this scale can be determined.

5.2 The importance of major rivers

In Chapter 4 and Ridgill et al. [138], it is proposed that hydrokinetic power predominately resides in major rivers, increasing in a downstream direction. Since larger rivers will tend to contain reaches with higher values for ω, and all rivers see an increase in ω in the downstream direction, an increase in the mean power $\overline{P}$, calculated for each reach, should correspond with an increase in ω. Fig. 5.6 confirms that this is indeed the case.

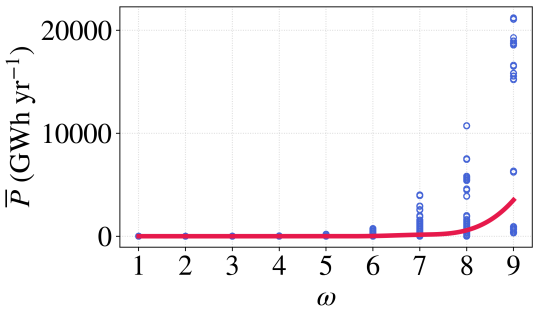

Figure 5.6: Hydrokinetic annual mean power $\overline{P}$ of all reaches, globally, plotted against stream order.

Having been identified as containing the highest estimated hydrokinetic resource (Fig. 4.14), it is instructive to isolate the South America continental-level basin (Fig. 5.7). Here, a number of major rivers can be identified, including the Amazon, Orinoco, Río de la Plata, Tocantins, Magdalena, São Francisco, and their tributaries. This identification is achieved as a result of the colours in this choropleth plot, which in addition to tracing out these rivers, also demonstrates their considerable hydrokinetic power. Further, because the width of the line used for each reach is proportional to ω, the thicker lines that are discernible in these larger river networks illustrates the distribution of ω and confirms the increase in $\overline{P}$ in a downstream direction. Individual plots for each of the other continental-level basins are shown in Appendix 6.1.

A consideration of the relative global distribution of $\overline{P}$ was made, according to corresponding ω (Fig. 5.8). Also included was an identification of the value of ω at which global rivers terminate, i.e. the stream order of the final reaches that meet the sea. It can be seen that the majority of these reaches are represented by low values for ω. This general trend is confirmed by Tagestad et al. [605], who found that 66 % of tidally-influenced stream length in the contiguous United States is contributed from reaches of $\omega < 4$. The maximum number of final reaches in the global river network that terminate at the sea corresponds to $\omega = 1$, with the number of reaches that terminate at the sea and $\omega = 2$ being approximately half this number.

In terms of hydrokinetic power, this figure illustrates the mean value for $\overline{P}$, calculated using daily values for P provided by the hydrostatic method (using $P = \gamma QH$) of Chapter 3 and Ridgill et al. [137] and the hydrokinetic method (using $P = \frac{1}{3}\rho k^2 Q^{(2m+1)}$) of Chapter 4 and Ridgill et al. [138], for each value of ω. In each case, to normalise the data, the bar is made relative to the maximum value calculated using each method. This maximum value is plotted as 100 % and other bars as a corresponding percentage of this maximum value. So, the maximum value for $\overline{P}$, corresponding to the mean value for all reaches of this stream order, occurs in reaches of $\omega = 9$. This is true for both the hydrostatic and hydrokinetic approach. The mean value of $\overline{P}$ for reaches of $\omega = 8$ is ~10 % and ~18 % of this maximum value for the hydrostatic and hydrokinetic cases, respectively.

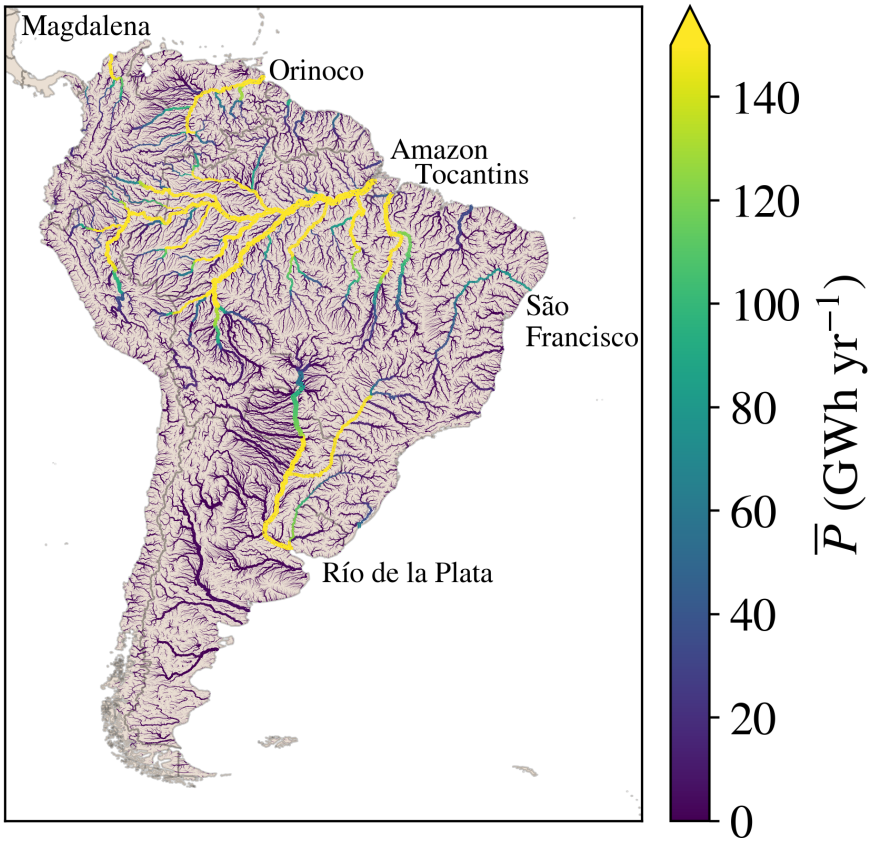

Figure 5.7: Spatial distribution of hydrokinetic annual mean power $\overline{P}$ within the South America continental-level basin. Prominent rivers of the region are labelled.

It is apparent that calculations of $\overline{P}$ are more skewed towards the higher values for ω. This is more pronounced for the hydrokinetic method than the hydrostatic method. The majority of rivers terminate at lower values for ω and it is sensible to presume that the smaller number of rivers that terminate at higher values are larger-sized rivers. The number of smaller river networks is greater than the number of larger river networks. Therefore, it may be assumed that the river reaches with greatest potential for HEC are to be found at the lower ends of large rivers.

A consideration of the relative global distribution of $\overline{P}$ was also made according to the elevation of reaches above sea level (Fig. 5.9). Reaches were grouped according to elevation and the mean value for $\overline{P}$ for each group was calculated, using daily values for P provided by the hydrostatic method and the hydrokinetic method. These values were then expressed relative to the maximum value calculated, as before.

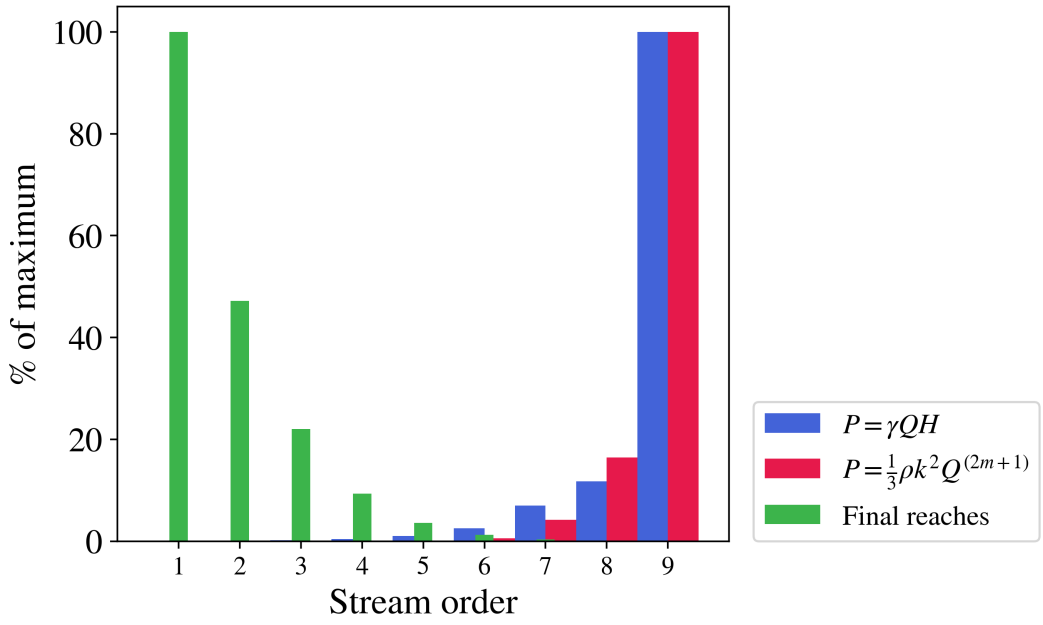

Figure 5.8: Relative global (excluding Greenland and Antarctica) distribution of mean annual power $\overline{P}$, by stream order ω, with daily values of P provided by a hydrostatic approach ($P = \gamma QH$) and a hydrokinetic approach ($P = \frac{1}{3}\rho k^2 Q^{(2m+1)}$). Also, an indication of the number of rivers that terminate (reach the sea) at which value of ω.

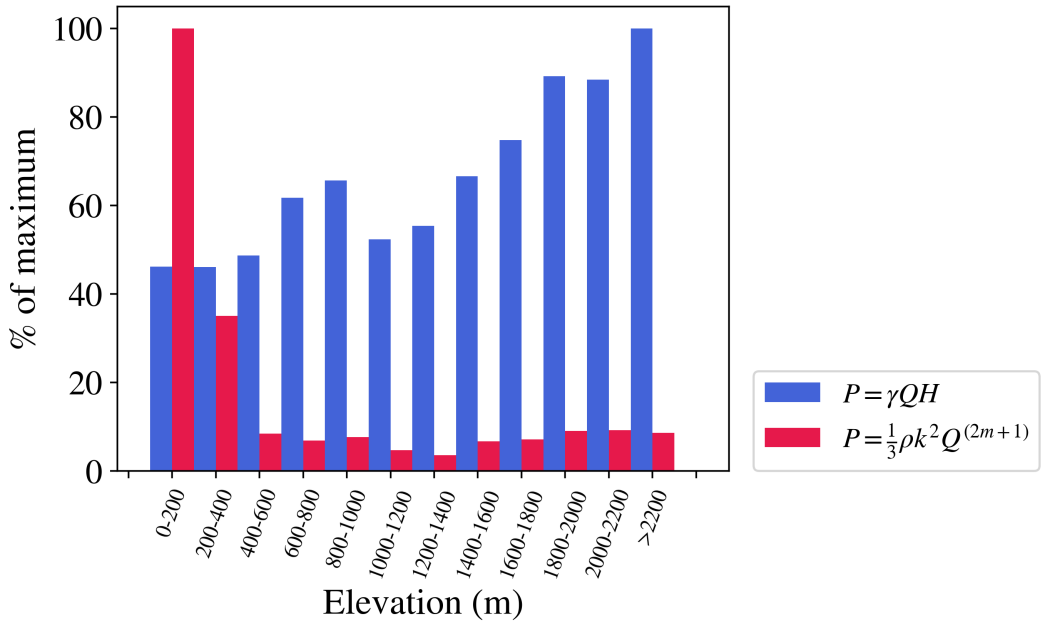

Figure 5.9: Relative global (excluding Greenland and Antarctica) distribution of mean annual power $\overline{P}$, by elevation, with daily values of P provided by a hydrostatic approach ($P = \gamma QH$) and a hydrokinetic approach ($P = \frac{1}{3}\rho k^2 Q^{(2m+1)}$)

In this case, it is apparent that the hydrostatic ($P = \gamma QH$) and hydrokinetic ($P = \frac{1}{3}\rho k^2 Q^{(2m+1)}$) approaches give two distinctly different results. The hydrostatic perspective shows some change according to elevation, with a bias towards higher elevations. In contrast, the hydrokinetic perspective shows a pronounced bias towards lower elevation, suggesting that the potential for HEC is mainly located in the lower-courses of river networks.

5.3 Basin-scale resource assessment of prominent rivers

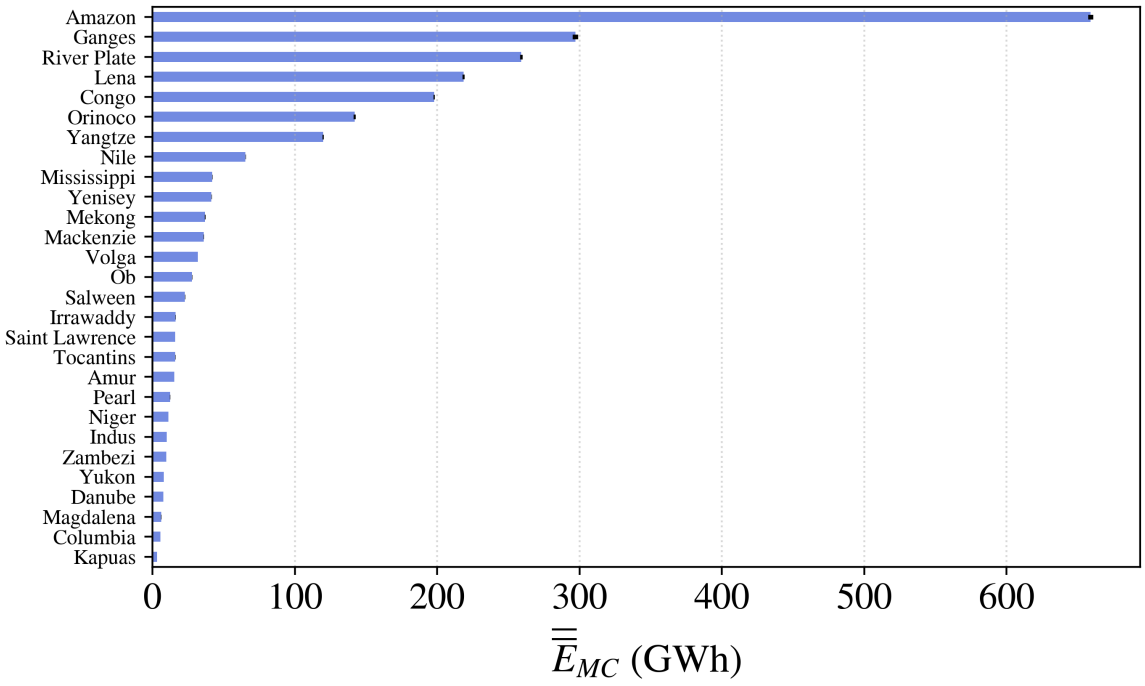

Figure 5.10: Mean hydrokinetic energy $\overline{\overline{E}}_{\mathrm{MC}}$ in globally prominent rivers.

The most prominent rivers, from the results presented in Chapter 4 and published in Ridgill et al. [138], were identified, such that individual basin-scale resource assessments could be made. Fig. 5.10 illustrates the estimates of total energy for each and ranks them accordingly. The total energy $\overline{\overline{E}}_{MC}$ represents the sum of energy in all reaches within the river basin. This is calculated using the Monte Carlo method and statistical distribution of parameters across all reaches, as proposed in Section 4.3. The distribution of $\overline{P}$ within the reaches of the top three rivers (Amazon, Ganges and River Plate) is shown in Figs. 5.11, 5.12 and 5.13. Figures for each of the remaining rivers can be found in Appendix 6.2.

The major rivers identified in these basin-scale resource assessments often also include other notable rivers as tributaries. In some cases, the definition of a river and the basin within which it is contained is complicated by alternative naming, according to the country it is running through or language used. For example, the river which is described here as the Ganges, is also known as the Padma and includes the significant rivers of the Brahmaputra, Ghaghara, Yamuna, Koshi, Gandaki and Meghna. The Amazon includes many tributaries which are important in

their own right. Table 5.2 describes the contributions from other rivers to those identified as prominent, demonstrating the definition of each that is used.

In Section 4.4, the Arctic and Siberia continental-level basins are shown to provide a modest contribution to the global hydrokinetic resource. Their being at high-latitude, and the climatic conditions that this implies, is given as the most likely reason for this. Yet, despite this, a number of rivers within these continental-level basins are shown to populate the prominent rivers listed in Fig. 5.10. These rivers are: Lena, Yenisey, Mackenzie, Ob and Yukon.

The continental-level basin of Australia provides the lowest contribution to the global resource and has only one river basin listed. The river basin of Kapuas is also seen to represent the lowest contribution of all those listed.

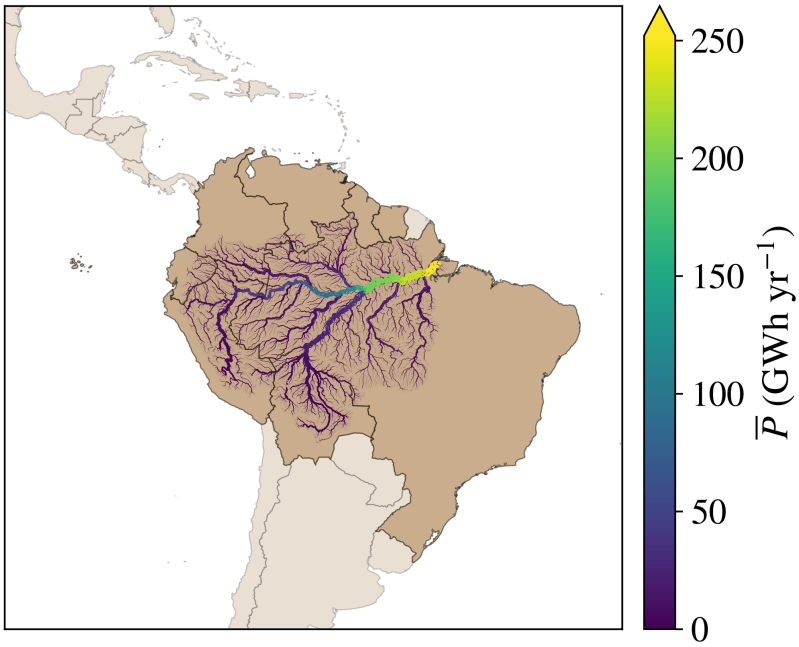

Figure 5.11: The distribution of mean hydrokinetic power $\overline{P}$ within the Amazon. The mean hydrokinetic energy is estimated to be $\overline{\overline{E}}_{\mathrm{MC}} = 659.01 \pm 1.79$ GWh, contained within a river network with a combined total length of 1,134,483 km, that flows within the countries of Brazil, Guyana, Venezuela, Colombia, Suriname, Ecuador, Peru and Bolivia.

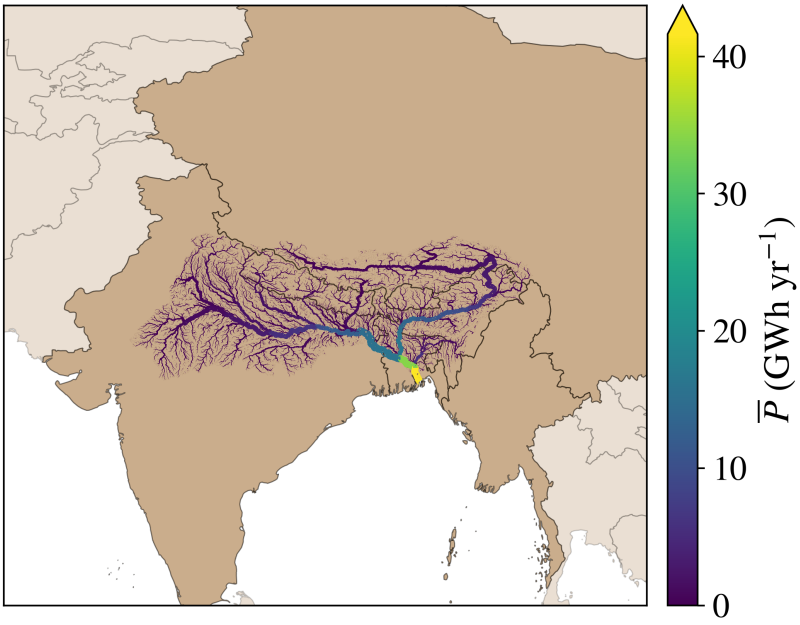

Figure 5.12: The distribution of mean hydrokinetic power $\overline{P}$ within the Ganges. The mean hydrokinetic energy is estimated to be $\overline{\overline{E}}_{\mathrm{MC}} = 297.04 \pm 1.85$ GWh, contained within a river network with a combined total length of 2,544,613 km, that flows within the countries of India, China, Nepal, Bhutan, Bangladesh and Burma.

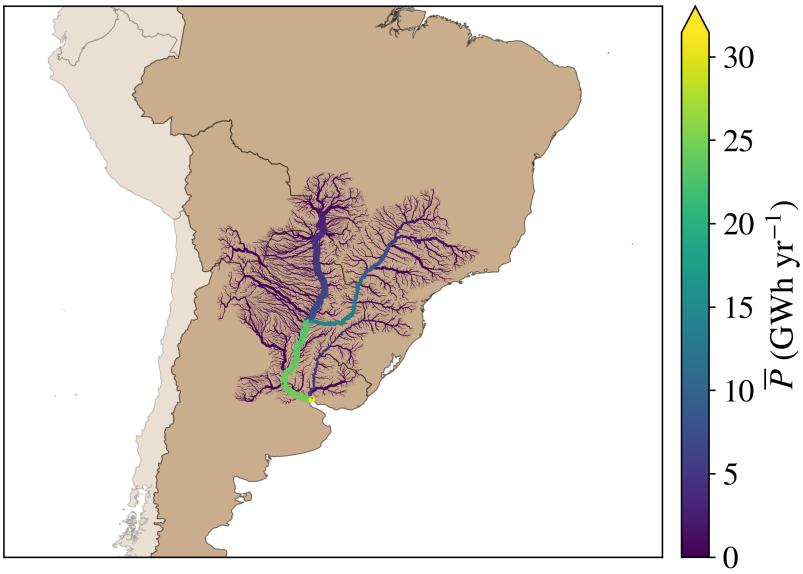

Figure 5.13: The distribution of mean hydrokinetic power $\overline{P}$ within the River Plate. The mean hydrokinetic energy is estimated to be $\overline{\overline{E}}_{\mathrm{MC}} = 258.98 \pm 0.94$ GWh, contained within a river network with a combined total length of 3,219,417 km, that flows within the countries of Brazil, Bolivia, Paraguay, Argentina and Uruguay.

Table 5.2: Rivers associated with identified prominent rivers.

Prominent river	Associated rivers
Amazon	Madeira, Guainía, Negro, Caquetá, Japurá, Marañón, Tapajos, Ucayali, Xingu-Culuene, Putumayo, Içá, Juruá, Purus, Napo, Jutai, Trombetas, Javari
Ganges	Padma, Brahmaputra, Ghaghara, Yamuna, Koshi, Gandaki, Meghna
River Plate	Paraná, Uruguay
Lena	Aldan, Vitim
Congo	Kasai, Ubangi, Ruki, Sangha, Aruwimi
Orinoco	Guaviare, Meta, Caroní, Caura, Apure, Ventuari, Vichada
Yangtze	Gan, Xiang, Jialing
Nile	N/A
Mississippi	Ohio, Missouri
Yenisey	Angara, Nizhnyaya Tunguska
Mekong	N/A
Mackenzie	Liard
Volga	Kama
Ob	Irtysh
Salween	N/A
Irrawaddy	Chindwin
Saint Lawrence	N/A
Tocantins	Araguaia
Amur	Songhua
Pearl	Xi
Niger	Benue
Indus	N/A
Zambesi	N/A
Yukon	N/A
Danube	N/A
Magdalena	Cauca
Columbia	N/A
Kapuas	N/A

5.4 Concluding remarks

An intention has been made in this thesis to make prominent the global and consequential problem of energy poverty. An argument for the role hydrokinetic energy conversion (HEC) can play in alleviating this problem has also been put forward. Any flowing water, in any of the rivers and streams of the world, potentially offers an opportunity to convert hydrokinetic energy into electricity, to produce and store hydrogen (see Subsection 1.1.4), or be used in any other way deemed useful (e.g. mechanically pumping water for irrigation, milling, etc.). In an effort to also highlight the opportunities for HEC at the other end of the spectrum, the results presented here describe locations of particularly notable quantities and densities of hydrokinetic energy.

Given the arguments made and conclusions drawn, in Chapter 4 and Ridgill et al. [138], the basin-scale resource assessments presented here represent the locations in the world with the greatest potential for HEC.

Chapter 6

Conclusions

- Providing a means for generating useful energy from free-flowing water, hydrokinetic energy conversion (HEC) is a renewable energy technology which offers benefits that complement other renewable energy technologies; having characteristics that make it appropriate to support isolated communities and those living in energy poverty.

- When compared with conventional hydropower, in a riverine context, HEC offers the advantages of modularity and scalability; less environmental and social impact; and, ease of construction due to being lower cost, quicker to construct and requiring less planning consent.

- A methodology for determining the global riverine hydrokinetic resource, which measures the conversion of gravitational potential energy to kinetic energy, as rivers flow downhill, provides an estimate of 58,400 ± 109 TWh yr^{-1} (6.660 ± 0.012 TW).

- From this *hydrostatic* perspective, areas with significant elevation change and major rivers are identified as foremost. Qualitatively, regions that are prominent would include: the Himalayas, Tibetan Plateau and surrounding areas; the large, mountainous islands of Borneo, Indonesia and New Guinea; New Zealand; the Andes; the Pacific Northwest; Scandinavia; the Congo Basin and Equatorial Africa; Madagascar; and, many of the major rivers of the world. China, Russia and Brazil are found to be the countries with the greatest potential. After normalisation by total river length, Bhutan, Nepal and Tajikistan also show great potential.

- A methodology for determining the global riverine hydrokinetic resource, which directly measures the kinetic energy of free-flowing rivers, provides an estimate of 1.642 ± 0.003 TWh (5.911 ± 0.009 PJ). Given the large uncertainties in the hydraulic geometry parameters used, application at large-scale and a Monte Carlo approach is more appropriate than for an individual river reach.

- From this *hydrokinetic* perspective, major rivers, and particularly the lower-courses of major-rivers, are found to offer the most potential for hydrokinetic energy conversion.

South Africa, Asia and Africa are the continents recognised as those with the most hydrokinetic energy. At the basin-scale, the Amazon, Ganges and River Plate are highlighted as areas with the highest concentration of hydrokinetic energy.

- Benefits and limitations can be identified for both the approaches presented, but the hydrokinetic perspective provided by a method that focuses directly on the transfer of kinetic energy, rather than the conversion of gravitational potential energy to kinetic energy, potentially offers a more realistic and pragmatically useful approach.

Appendices

6.1 Appendix 1

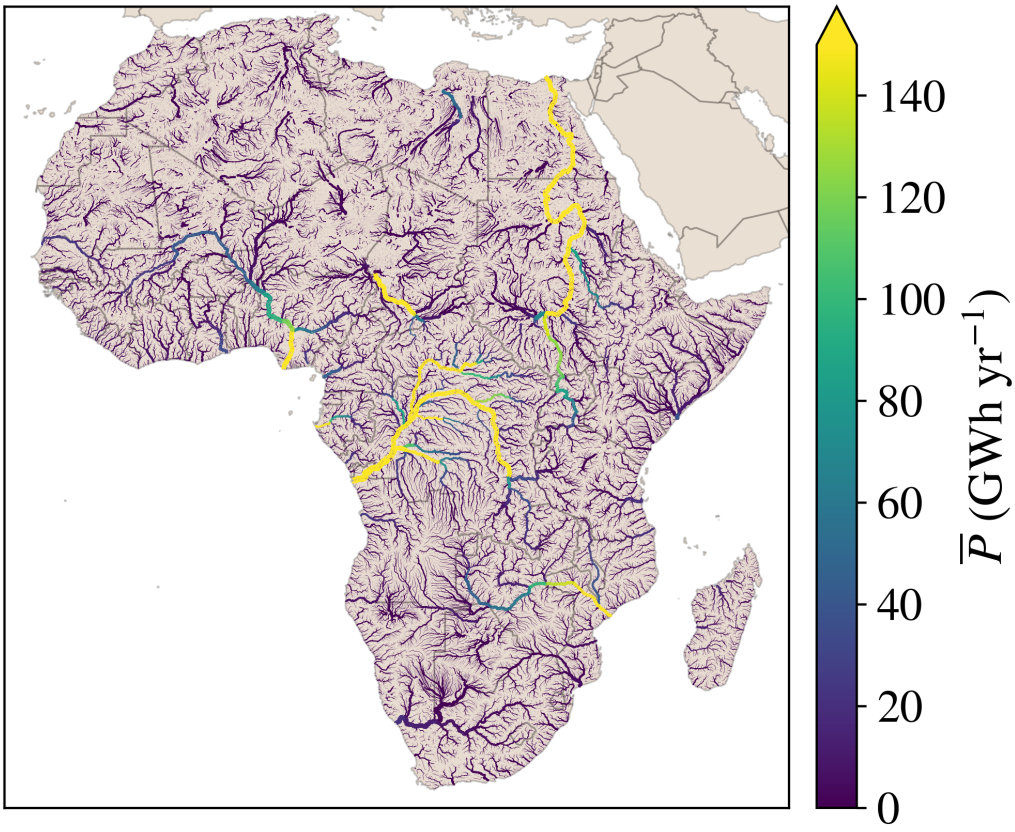

Figure 6.1: Distribution of mean hydrokinetic power $\overline{P}$ within the Africa continental-level basin.

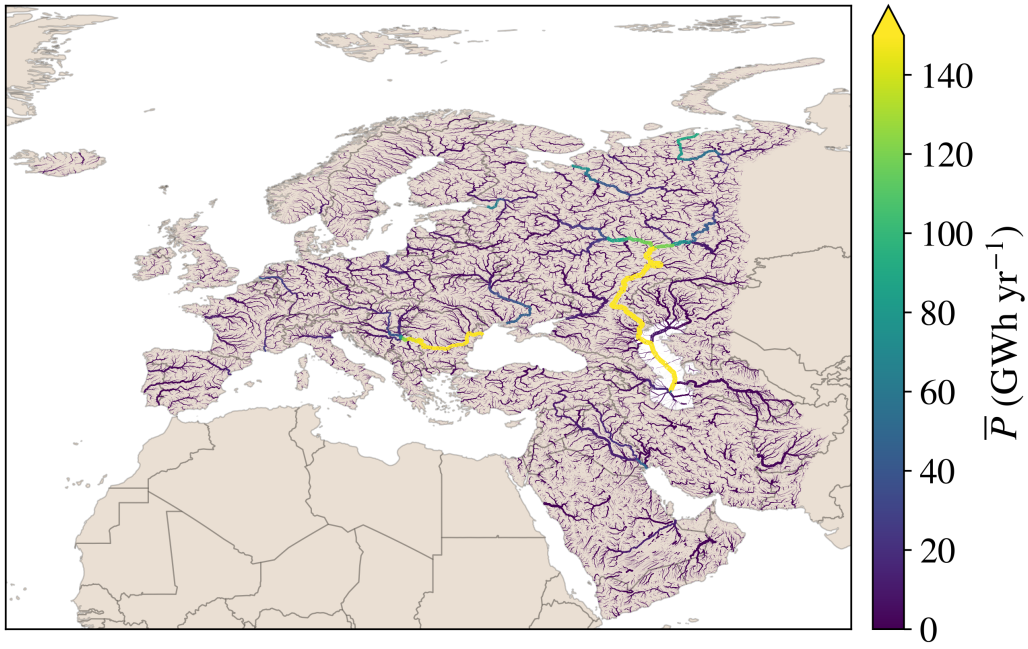

Figure 6.2: Distribution of mean hydrokinetic power $\overline{P}$ within the Europe continental-level basin.

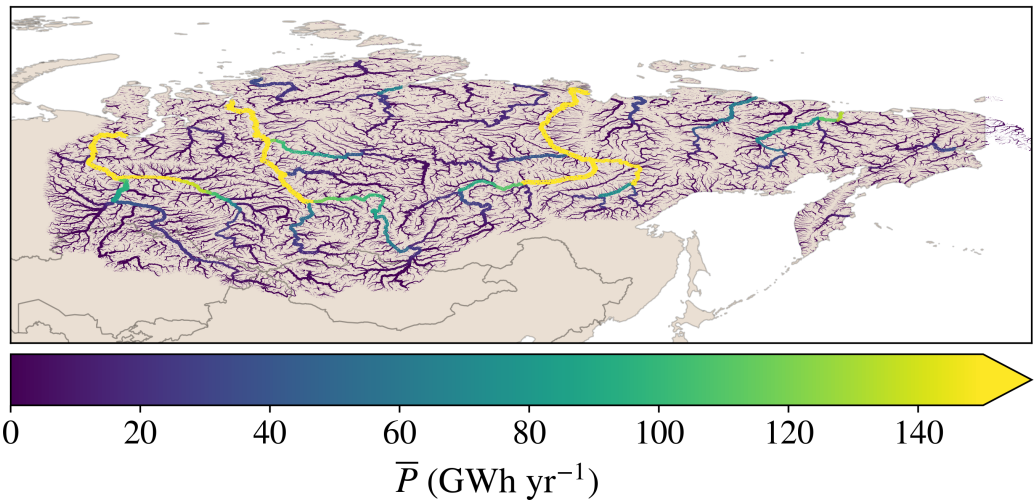

Figure 6.3: Distribution of mean hydrokinetic power $\overline{P}$ within the Siberia continental-level basin.

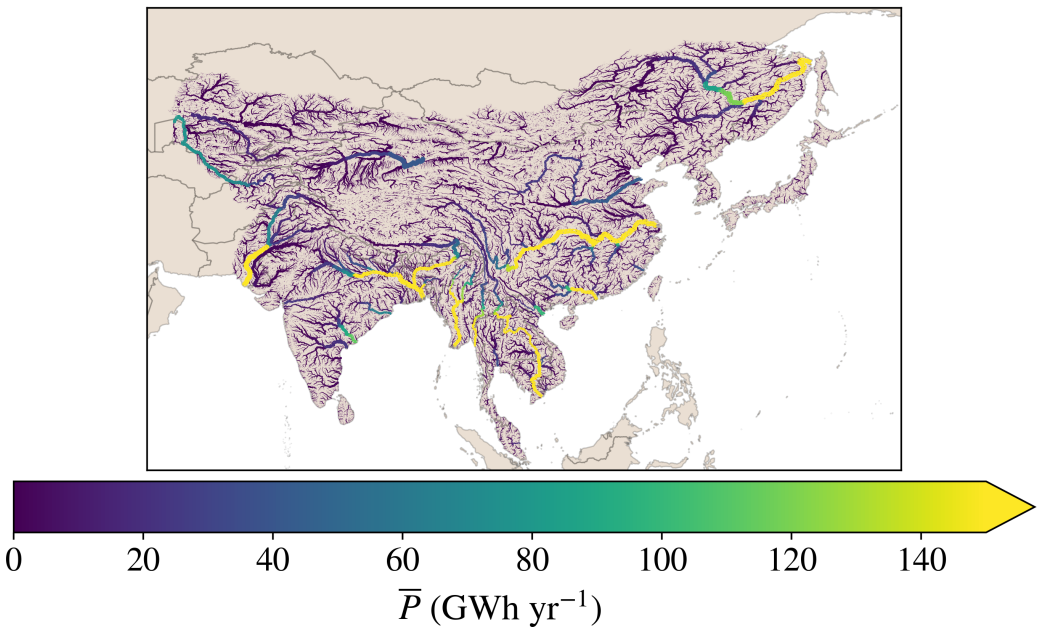

Figure 6.4: Distribution of mean hydrokinetic power $\overline{P}$ within the Asia continental-level basin.

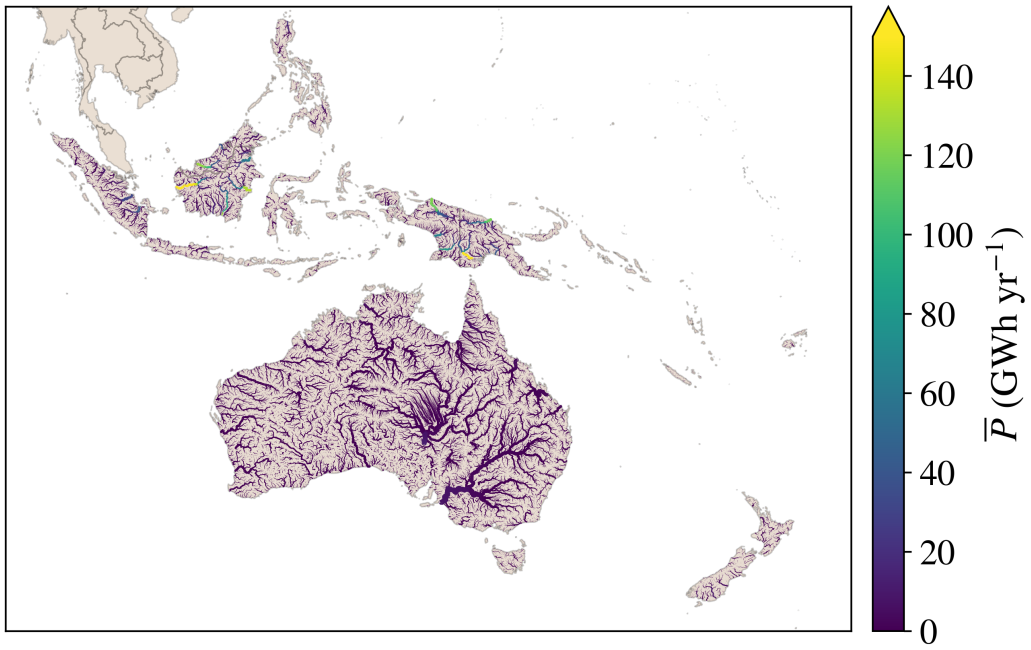

Figure 6.5: Distribution of mean hydrokinetic power $\overline{P}$ within the Australia continental-level basin.

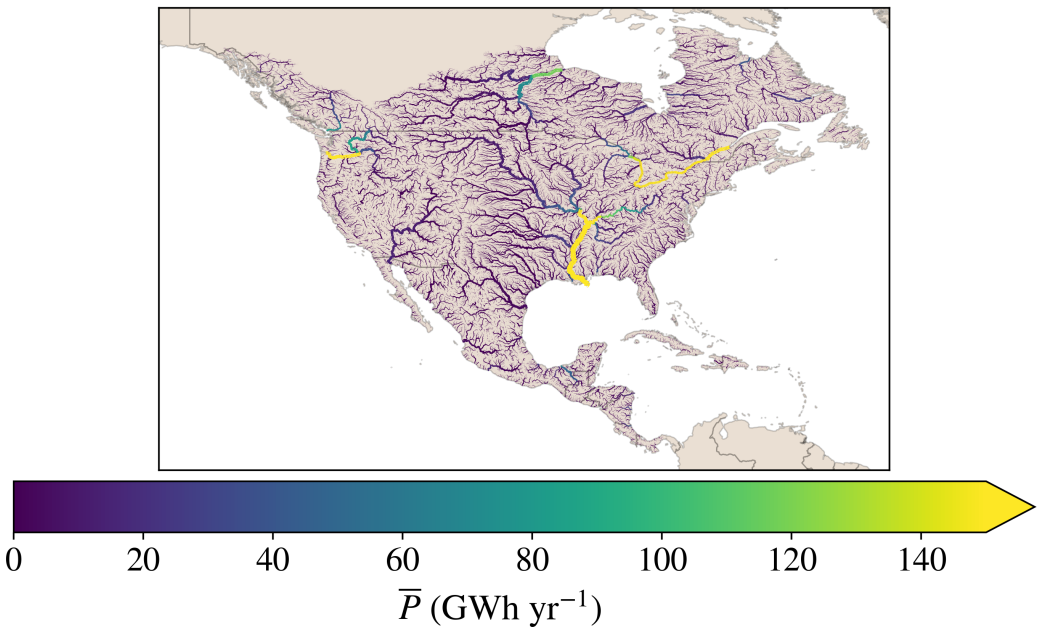

Figure 6.6: Distribution of mean hydrokinetic power $\overline{P}$ within the North America continental-level basin.

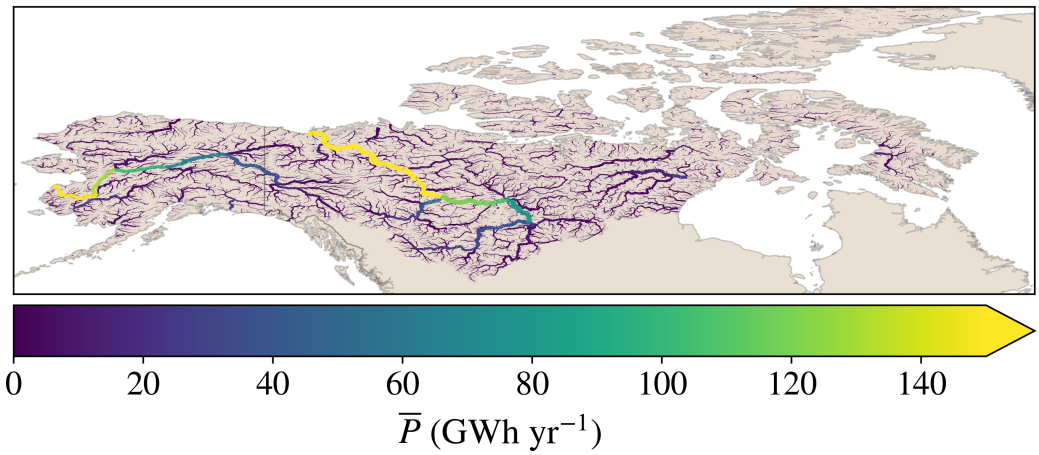

Figure 6.7: Distribution of mean hydrokinetic power $\overline{P}$ within the Arctic continental-level basin.

6.2 Appendix 2

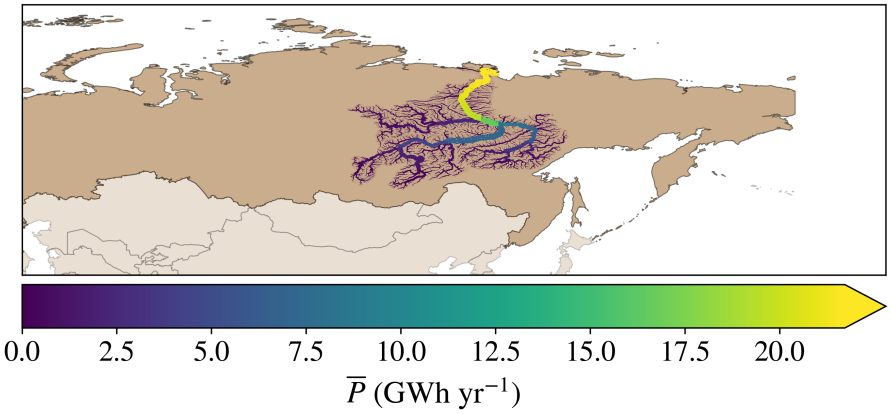

Figure 6.8: The distribution of mean hydrokinetic power $\overline{P}$ within the Lena. The mean hydrokinetic energy is estimated to be $\overline{\overline{E}}_{\mathrm{MC}} = 218.45 \pm 0.65$ GWh, contained within a river network with a combined total length of 2,280,563 km, that flows within the country of Russia.

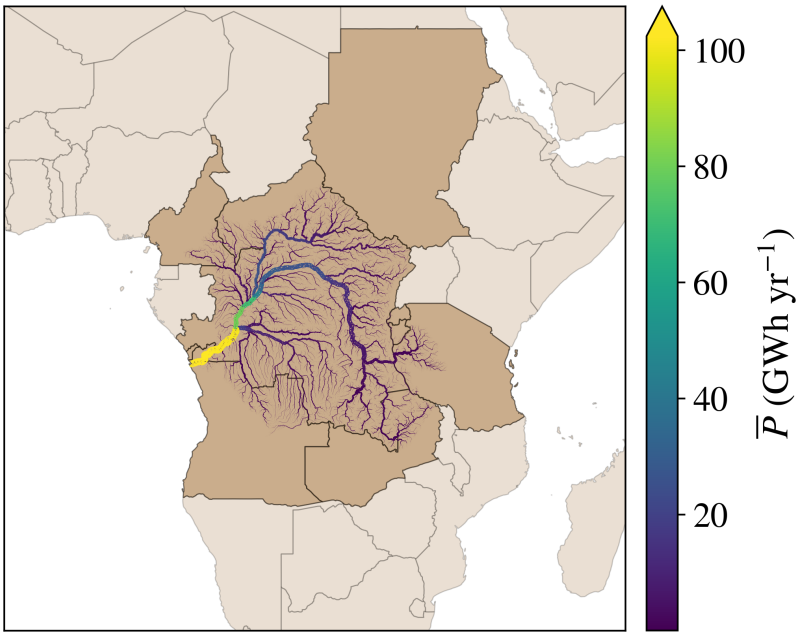

Figure 6.9: The distribution of mean hydrokinetic power $\overline{P}$ within the Congo. The mean hydrokinetic energy is estimated to be $\overline{\overline{E}}_{\mathrm{MC}} = 197.80 \pm 0.49$ GWh, contained within a river network with a combined total length of 660,785 km, that flows within the countries of Central African Republic, Sudan, Cameroon, Democratic Republic of the Congo, Congo, Rwanda, Burundi, United Republic of Tanzania, Angola and Zambia.

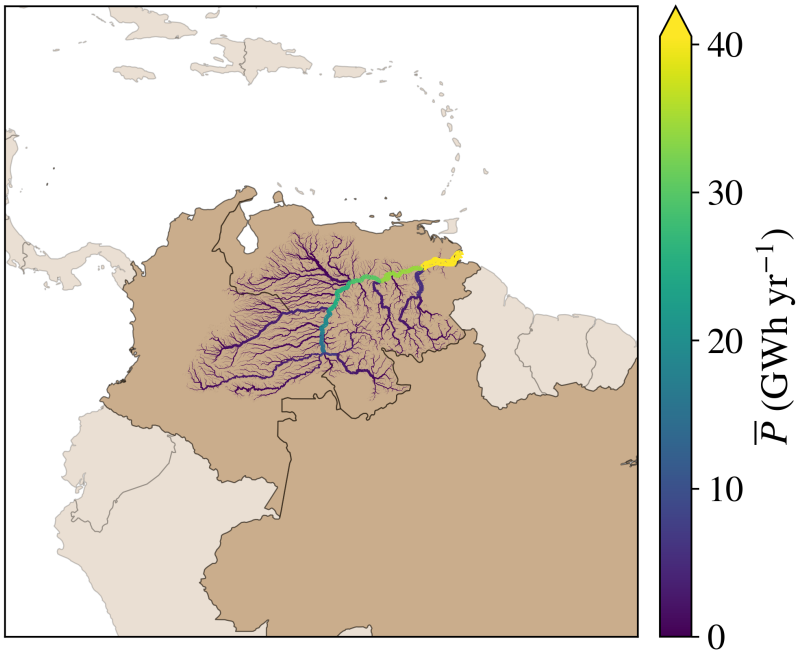

Figure 6.10: The distribution of mean hydrokinetic power $\overline{P}$ within the Orinoco. The mean hydrokinetic energy is estimated to be $\overline{\overline{E}}_{\mathrm{MC}} = 141.97 \pm 0.68$ GWh, contained within a river network with a combined total length of 596,478 km, that flows within the countries of Venezuela, Colombia and Brazil.

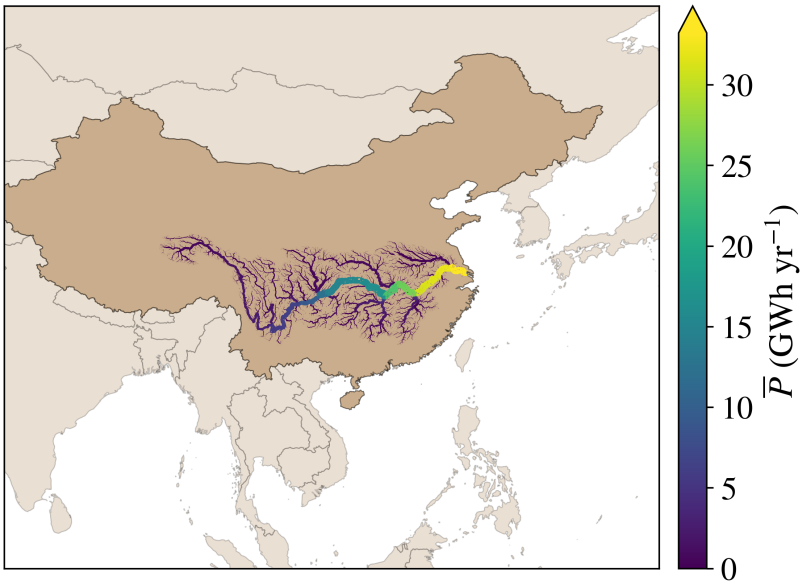

Figure 6.11: The distribution of mean hydrokinetic power $\overline{P}$ within the Yangtze. The mean hydrokinetic energy is estimated to be $\overline{\overline{E}}_{\mathrm{MC}} = 119.79 \pm 0.53$ GWh, contained within a river network with a combined total length of 698,503 km, that flows within the country of China.

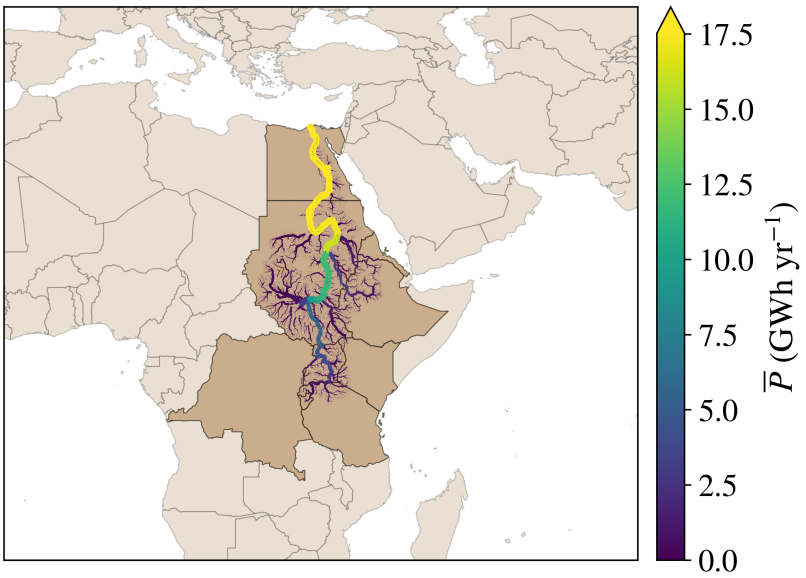

Figure 6.12: The distribution of mean hydrokinetic power $\overline{P}$ within the Nile. The mean hydrokinetic energy is estimated to be $\overline{\overline{E}}_{\mathrm{MC}} = 65.41 \pm 0.06$ GWh, contained within a river network with a combined total length of 632,357 km, that flows within the countries of Egypt, Sudan, Eritrea, Ethiopia, Kenya, Uganda, Democratic Republic of the Congo, United Republic of Tanzania, Rwanda and Burundi.

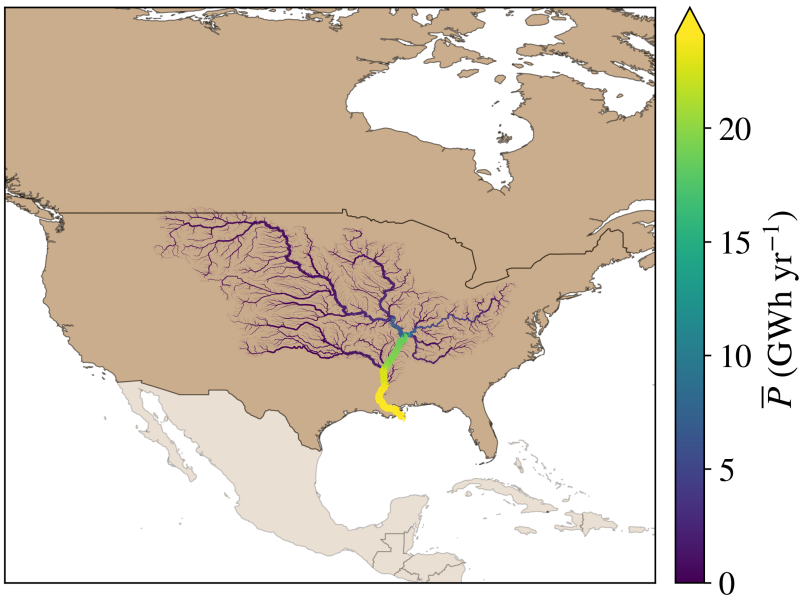

Figure 6.13: The distribution of mean hydrokinetic power $\overline{P}$ within the Mississippi. The mean hydrokinetic energy is estimated to be $\overline{\overline{E}}_{\mathrm{MC}} = 42.05 \pm 0.21$ GWh, contained within a river network with a combined total length of 596,032 km, that flows within the countries of the United States and Canada.

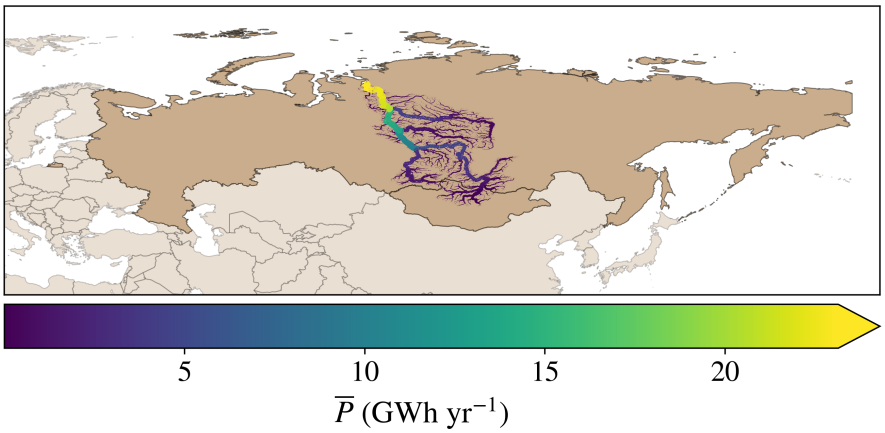

Figure 6.14: The distribution of mean hydrokinetic power $\overline{P}$ within the Yenisey. The mean hydrokinetic energy is estimated to be $\overline{\overline{E}}_{\mathrm{MC}} = 41.37 \pm 0.16$ GWh, contained within a river network with a combined total length of 463,086 km, that flows within the countries of Russia and Mongolia.

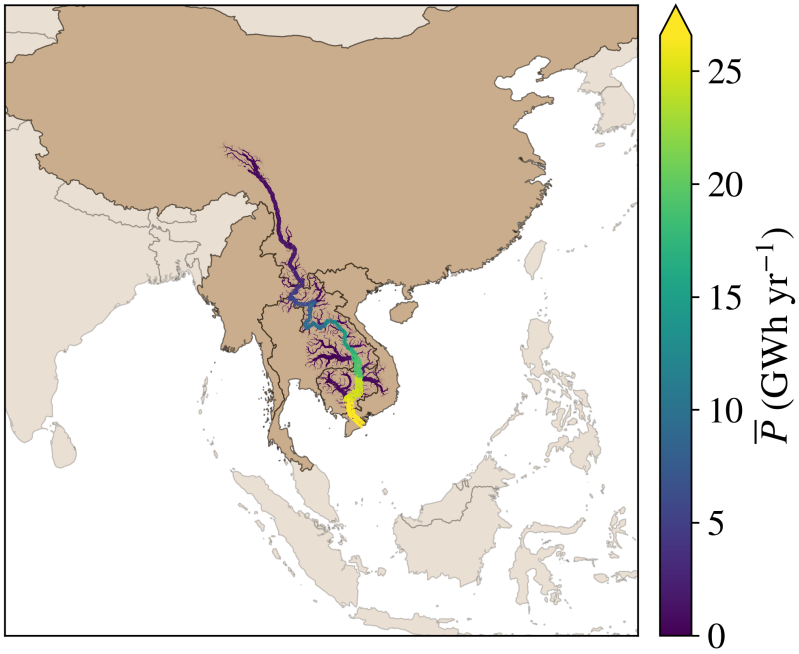

Figure 6.15: The distribution of mean hydrokinetic power $\overline{P}$ within the Mekong. The mean hydrokinetic energy is estimated to be $\overline{\overline{E}}_{\mathrm{MC}} = 36.85 \pm 0.26$ GWh, contained within a river network with a combined total length of 148,912 km, that flows within the countries of China, Lao People's Democratic Republic, Burma, Vietnam, Thailand and Cambodia.

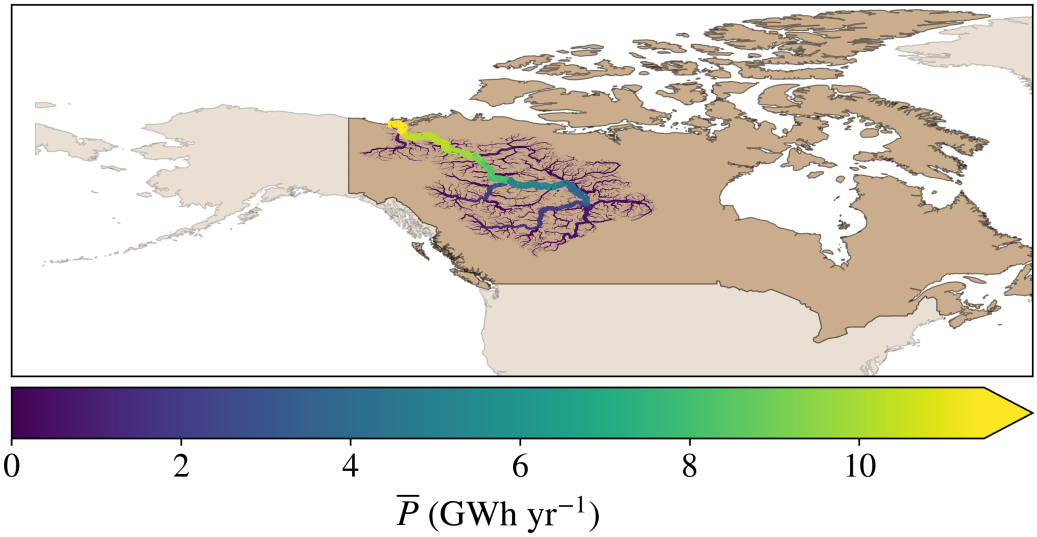

Figure 6.16: The distribution of mean hydrokinetic power $\overline{P}$ within the Mackenzie. The mean hydrokinetic energy is estimated to be $\overline{\overline{E}}_{\mathrm{MC}} = 35.98 \pm 0.11$ GWh, contained within a river network with a combined total length of 723,874 km, that flows within the country of Canada.

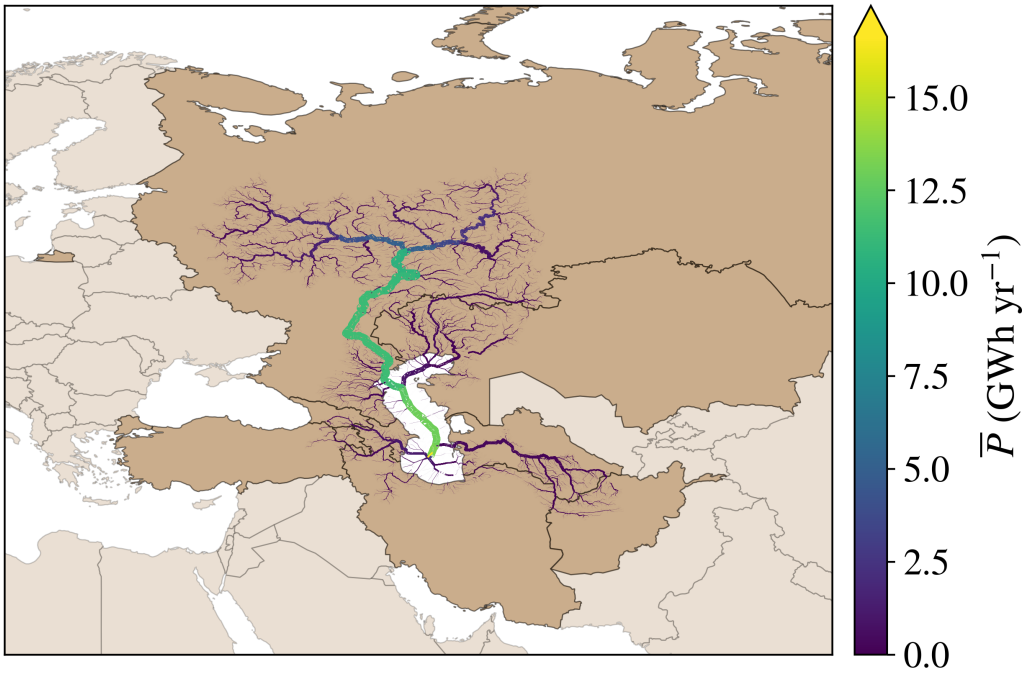

Figure 6.17: The distribution of mean hydrokinetic power $\overline{P}$ within the Volga. The mean hydrokinetic energy is estimated to be $\overline{\overline{E}}_{\mathrm{MC}} = 31.95 \pm 0.09$ GWh, contained within a river network with a combined total length of 620,220 km, that flows within the countries of Russia, Kazakhstan, Georgia, Azerbaijan, Turkmenistan, Armenia, Turkey, Iran and Afghanistan.

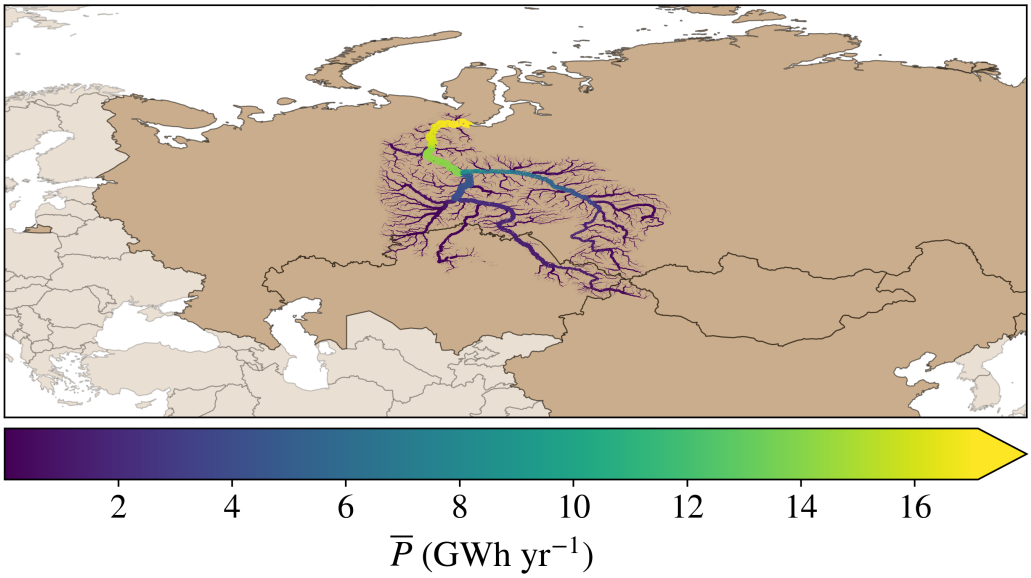

Figure 6.18: The distribution of mean hydrokinetic power $\overline{P}$ within the Ob. The mean hydrokinetic energy is estimated to be $\overline{\overline{E}}_{\mathrm{MC}} = 27.90 \pm 0.08$ GWh, contained within a river network with a combined total length of 535,664 km, that flows within the countries of Russia, Kazakhstan, China and Mongolia.

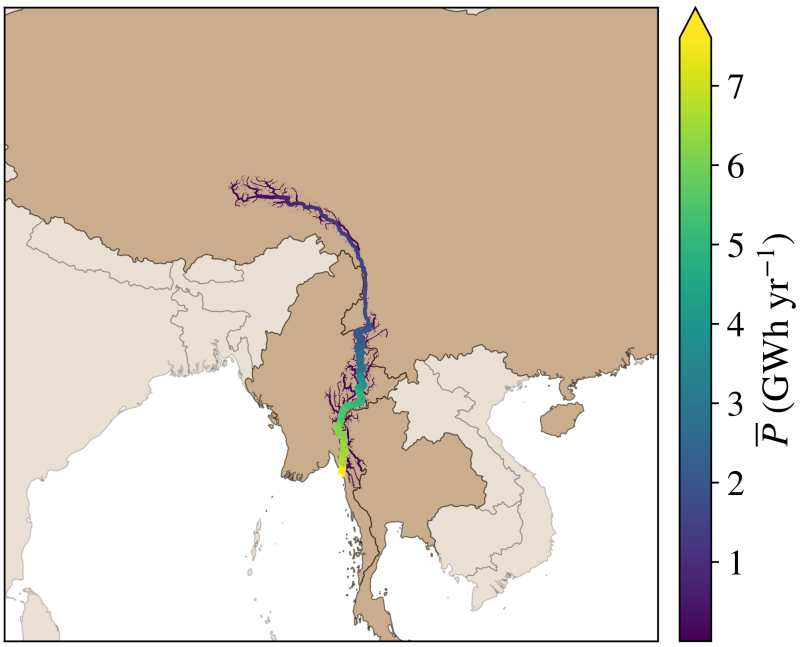

Figure 6.19: The distribution of mean hydrokinetic power $\overline{P}$ within the Salween. The mean hydrokinetic energy is estimated to be $\overline{\overline{E}}_{\mathrm{MC}} = 22.88 \pm 0.18$ GWh, contained within a river network with a combined total length of 187,856 km, that flows within the countries of China, Burma and Thailand.

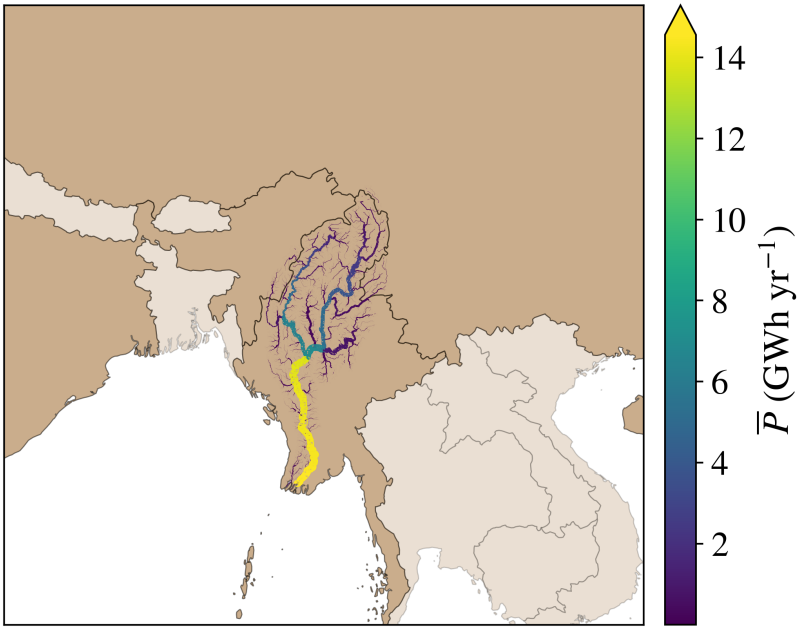

Figure 6.20: The distribution of mean hydrokinetic power $\overline{P}$ within the Irrawaddy. The mean hydrokinetic energy is estimated to be $\overline{\overline{E}}_{\mathrm{MC}} = 16.15 \pm 0.11$ GWh, contained within a river network with a combined total length of 74,389 km, that flows within the countries of China, Burma and India.

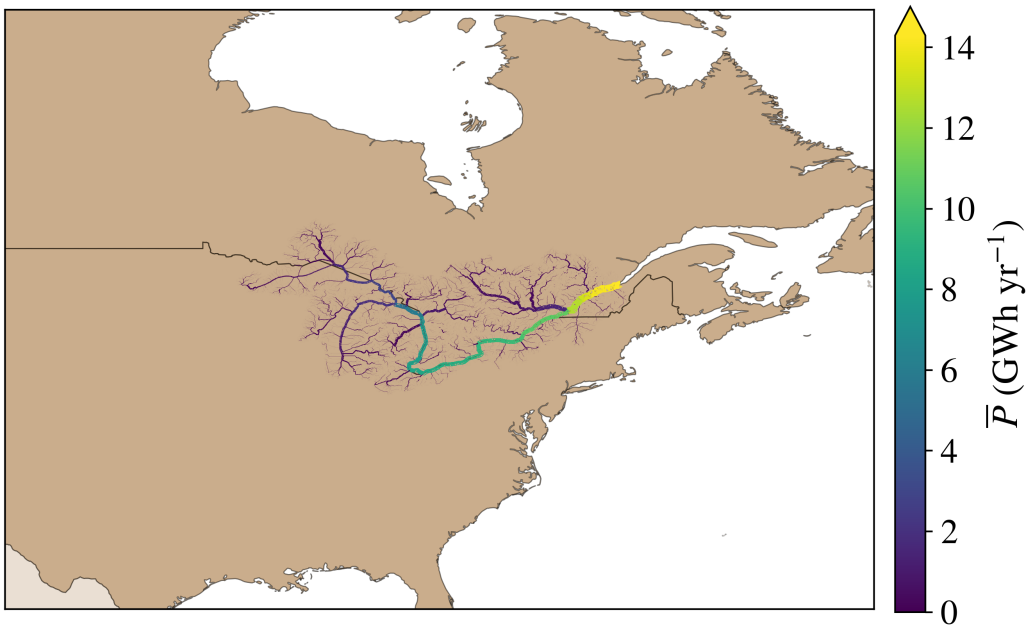

Figure 6.21: The distribution of mean hydrokinetic power $\overline{P}$ within the Saint Lawrence. The mean hydrokinetic energy is estimated to be $\overline{\overline{E}}_{\mathrm{MC}} = 15.99 \pm 0.07$ GWh, contained within a river network with a combined total length of 190,063 km, that flows within the countries of Canada and the United States.

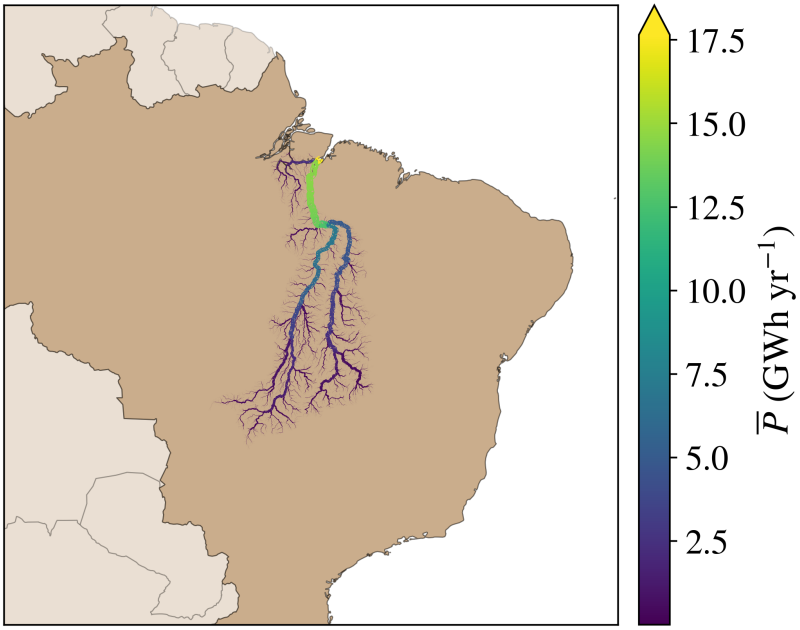

Figure 6.22: The distribution of mean hydrokinetic power $\overline{P}$ within the Tocantins. The mean hydrokinetic energy is estimated to be $\overline{\overline{E}}_{\mathrm{MC}} = 15.99 \pm 0.11$ GWh, contained within a river network with a combined total length of 162,517 km, that flows within the country of Brazil.

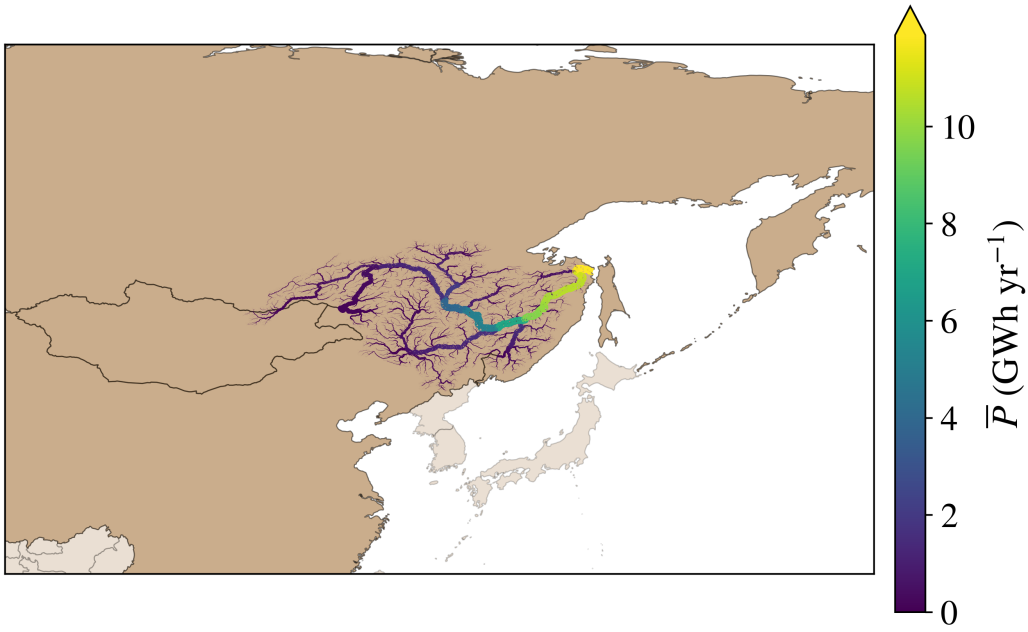

Figure 6.23: The distribution of mean hydrokinetic power $\overline{P}$ within the Amur. The mean hydrokinetic energy is estimated to be $\overline{\overline{E}}_{\mathrm{MC}} = 15.39 \pm 0.06$ GWh, contained within a river network with a combined total length of 360,666 km, that flows within the countries of Russia, China and Mongolia.

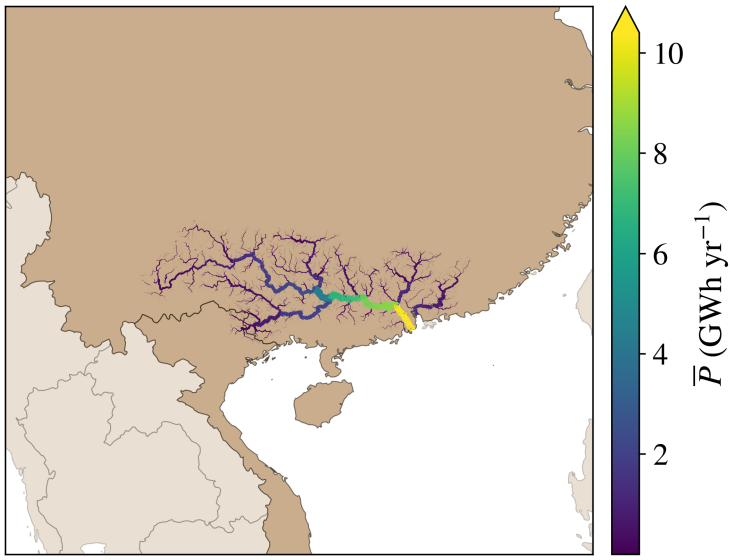

Figure 6.24: The distribution of mean hydrokinetic power $\overline{P}$ within the Pearl. The mean hydrokinetic energy is estimated to be $\overline{\overline{E}}_{\mathrm{MC}} = 12.31 \pm 0.10$ GWh, contained within a river network with a combined total length of 714,990 km, that flows within the countries of China and Vietnam.

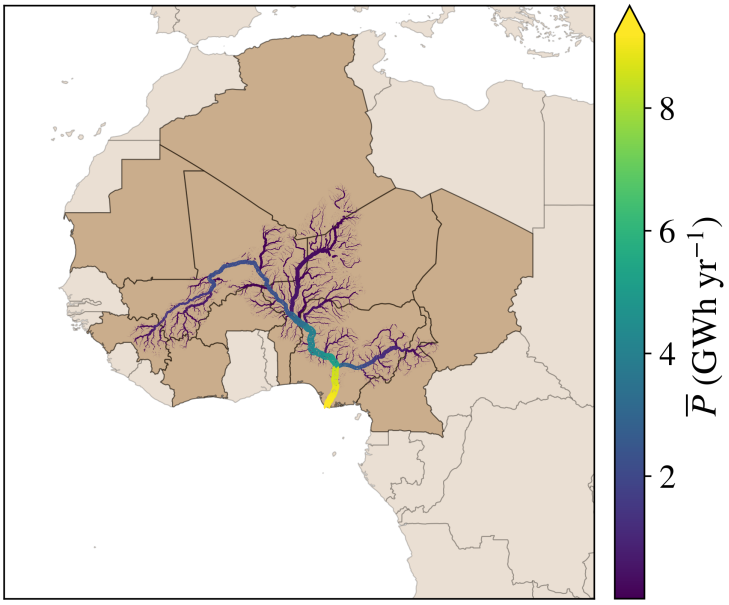

Figure 6.25: The distribution of mean hydrokinetic power $\overline{P}$ within the Niger. The mean hydrokinetic energy is estimated to be $\overline{\overline{E}}_{\mathrm{MC}} = 11.15 \pm 0.06$ GWh, contained within a river network with a combined total length of 386,372 km, that flows within the countries of Algeria, Niger, Mali, Mauritania, Burkina Faso, Nigeria, Benin, Guinea, Cote d'Ivoire, Cameroon and Chad.

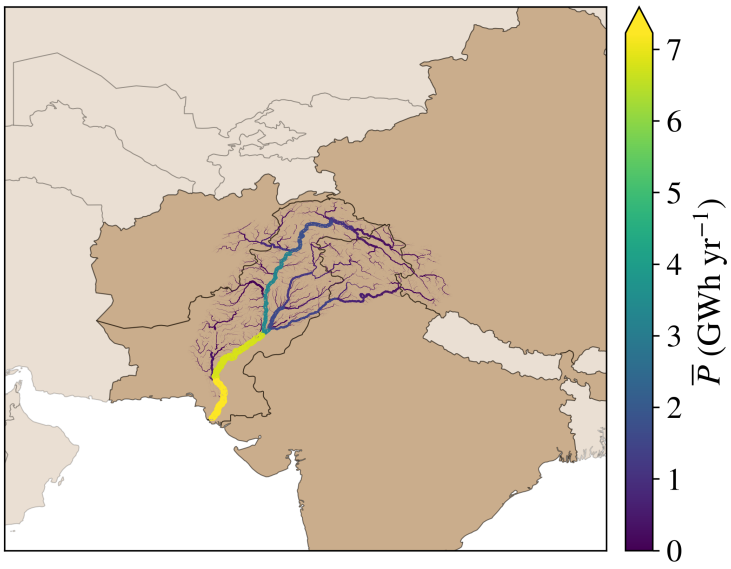

Figure 6.26: The distribution of mean hydrokinetic power $\overline{P}$ within the Indus. The mean hydrokinetic energy is estimated to be $\overline{\overline{E}}_{\mathrm{MC}} = 9.97 \pm 0.03$ GWh, contained within a river network with a combined total length of 161,816 km, that flows within the countries of Pakistan, Afghanistan, India and China.

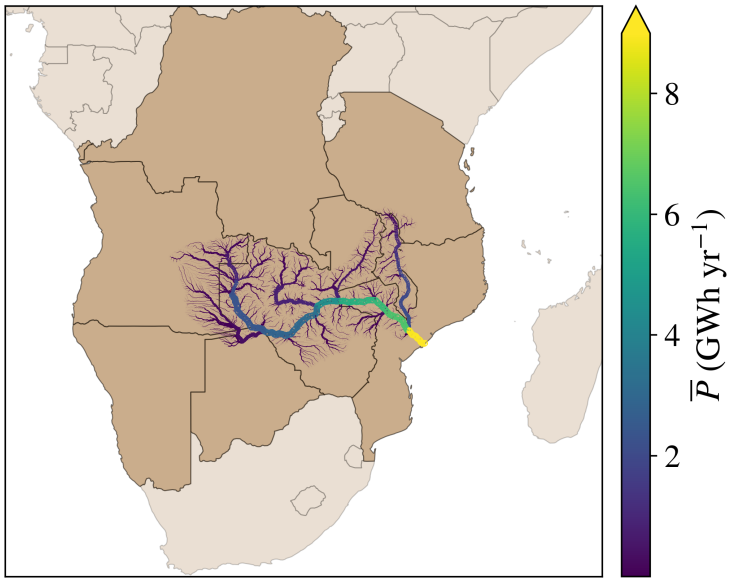

Figure 6.27: The distribution of mean hydrokinetic power $\overline{P}$ within the Zambezi. The mean hydrokinetic energy is estimated to be $\overline{\overline{E}}_{\mathrm{MC}} = 9.69 \pm 0.05$ GWh, contained within a river network with a combined total length of 263,003 km, that flows within the countries of United Republic of Tanzania, Malawi, Zambia, Angola, Democratic Republic of the Congo, Mozambique, Zimbabwe, Namibia and Botswana.

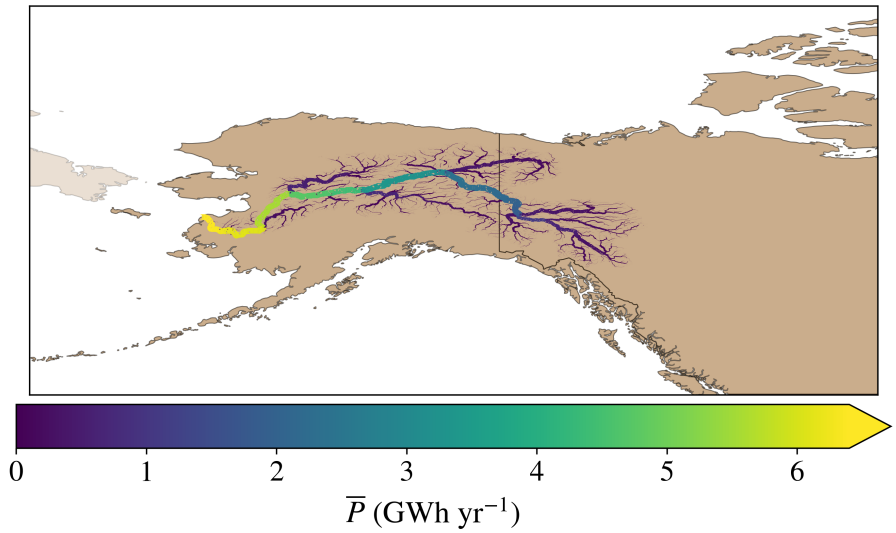

Figure 6.28: The distribution of mean hydrokinetic power $\overline{P}$ within the Yukon. The mean hydrokinetic energy is estimated to be $\overline{\overline{E}}_{\mathrm{MC}} = 8.08 \pm 0.03$ GWh, contained within a river network with a combined total length of 168,158 km, that flows within the countries of the United States and Canada.

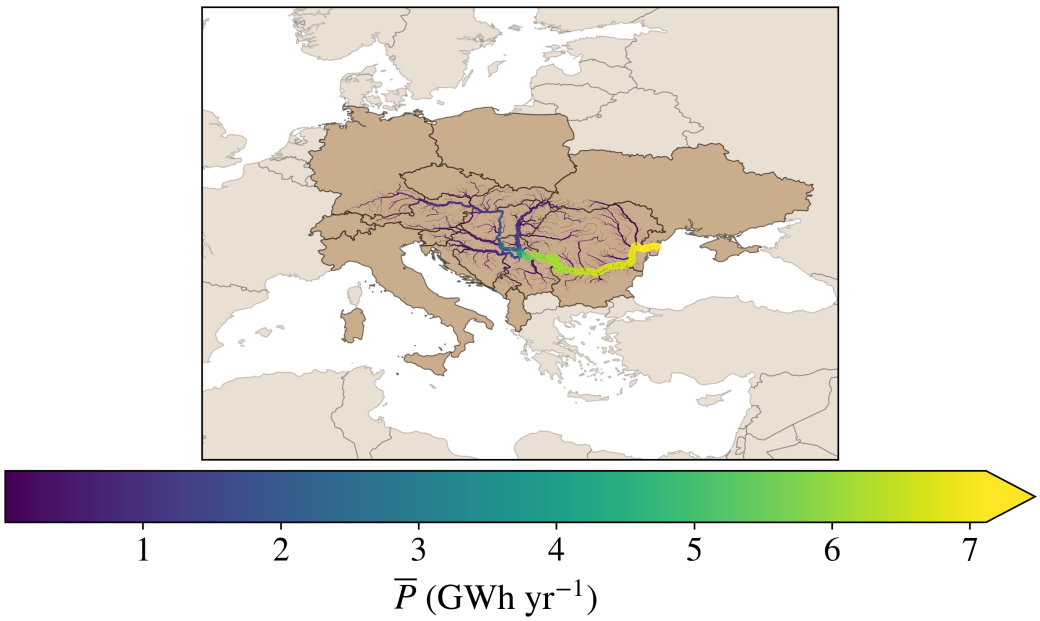

Figure 6.29: The distribution of mean hydrokinetic power $\overline{P}$ within the Danube. The mean hydrokinetic energy is estimated to be $\overline{\overline{E}}_{\mathrm{MC}} = 7.67 \pm 0.03$ GWh, contained within a river network with a combined total length of 156,809 km, that flows within the countries of Czech Republic, Germany, Slovakia, Poland, Austria, Ukraine, Hungary, Romania, Republic of Moldova, Slovenia, Switzerland, Italy, Croatia, Serbia, Bosnia and Herzegovina, Bulgaria, Montenegro and Albania.

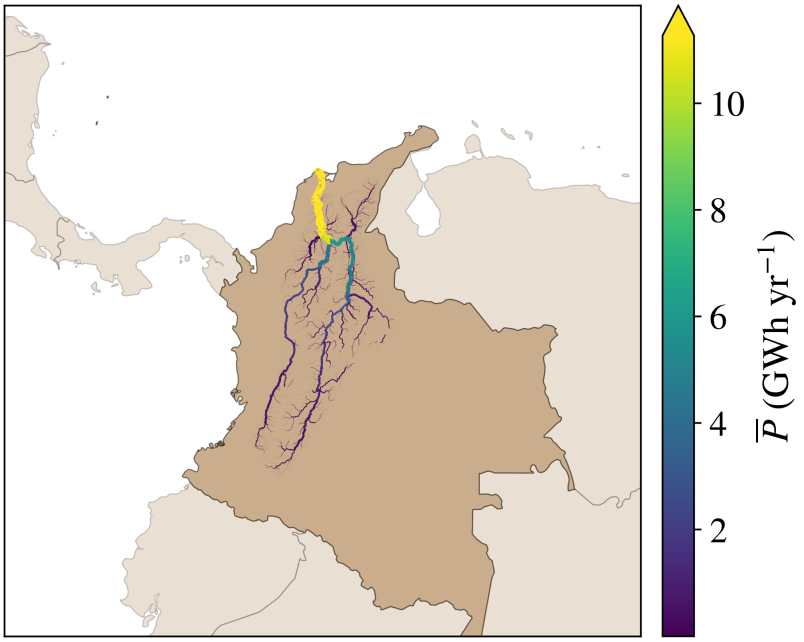

Figure 6.30: The distribution of mean hydrokinetic power $\overline{P}$ within the Magdalena. The mean hydrokinetic energy is estimated to be $\overline{\overline{E}}_{\mathrm{MC}} = 6.06 \pm 0.02$ GWh, contained within a river network with a combined total length of 51,443 km, that flows within the country of Colombia.

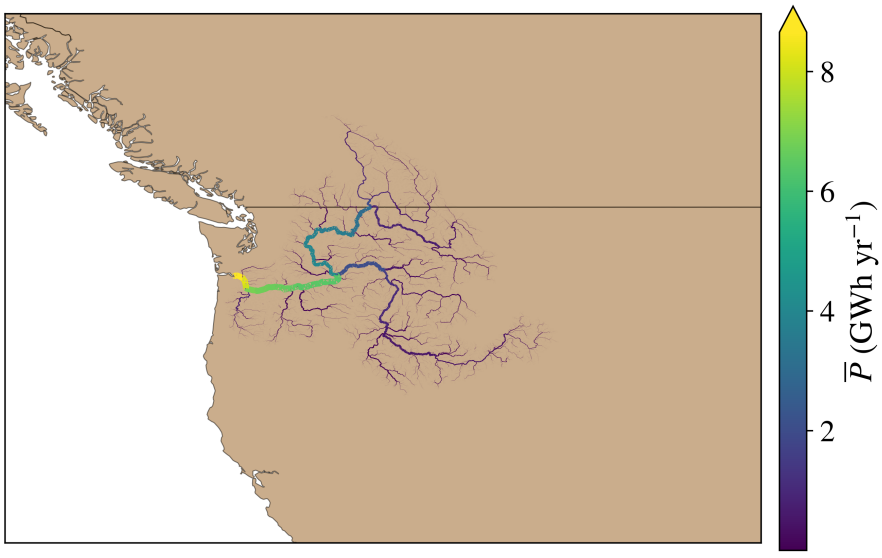

Figure 6.31: The distribution of mean hydrokinetic power $\overline{P}$ within the Columbia. The mean hydrokinetic energy is estimated to be $\overline{\overline{E}}_{\mathrm{MC}} = 5.55 \pm 0.03$ GWh, contained within a river network with a combined total length of 113,227 km, that flows within the countries of the United States and Canada.

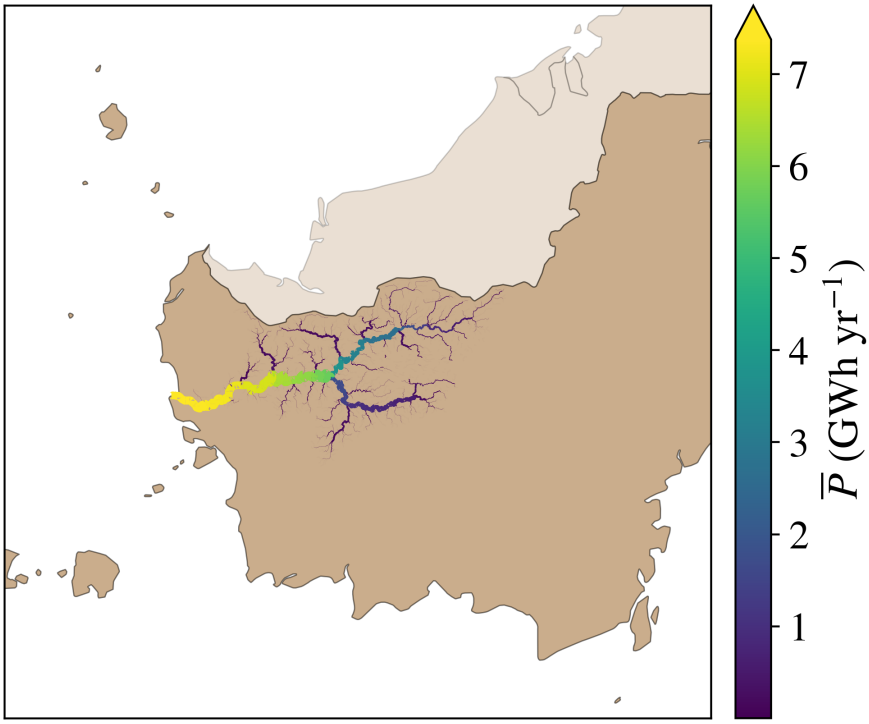

Figure 6.32: The distribution of mean hydrokinetic power $\overline{P}$ within the Kapuas. The mean hydrokinetic energy is estimated to be $\overline{\overline{E}}_{\mathrm{MC}} = 3.36 \pm 0.02$ GWh, contained within a river network with a combined total length of 16,673 km, that flows within the country of Indonesia.

Bibliography

[1] David Attenborough. The blue planet: Seas of life. Nature documentary, 2001.

[2] Brian Skinner. *The blue planet : an introduction to earth system science*. Wiley, Hoboken, NJ, 2011. ISBN 9780471236436.

[3] Carl Sagan. *Pale blue dot : a vision of the human future in space*. Random House, New York, 1994. ISBN 0679438416.

[4] U.S. Geological Survey. How much water is there on, in, and above the earth?, 2016. URL `http://water.usgs.gov/edu/earthhowmuch.html`. [Online. Accessed: 2018-10-23].

[5] E. T. Engman and R. J. Gurney. *Remote sensing in hydrology*. Remote sensing applications. Chapman and Hall, 1991. ISBN 0412244500.

[6] DE Walling. Rainfall runoff and erosion of the land: A global view. *Energetics of physical environment*, pages 87–117, 1987.

[7] World Nuclear Asscociation. Plans for new reactors worldwide, 1 2022. URL `http://www.world-nuclear.org/information-library/current-and-future-generation/plans-for-new-reactors-worldwide.aspx`. Accessed: 2022-01-19. Archive: https://archive.ph/tWYeA.

[8] IEA. Renewables information: overview. Technical report, Paris: Internaltional Energy Agency(IEA)/Organisation for Economic Co-operation and Development (OECD), 2020.

[9] Huayang Cai, Sebastiano Piccolroaz, Jingzheng Huang, Zhiyong Liu, Feng Liu, and Marco Toffolon. Quantifying the impact of the Three Gorges Dam on the thermal dynamics of the Yangtze River. *Environmental Research Letters*, 13(5):054016, 2018. doi: 10.1088/1748-9326/aab9e0.

[10] IRENA. Renewable capacity statistics 2019. Technical report, International Renewable Energy Agency (IRENA), 2019.

[11] Vaclav Smil. *Energy and civilization: a history*. MIT Press, 2018.

[12] Richard P Feynman, Robert B Leighton, and Matthew Sands. The feynman lectures on physics; vol. i. *American Journal of Physics*, 33(9):750–752, 1965.

[13] Andrew P Allen, James F Gillooly, James H Brown, et al. Recasting the species-energy hypothesis: the different roles of kinetic and potential energy in regulating biodiversity. *Scaling biodiversity*, 1, 2007.

[14] Robert H Fraser and David J Currie. The species richness-energy hypothesis in a system where historical factors are thought to prevail: coral reefs. *The American Naturalist*, 148 (1):138–159, 1996. doi: 10.1086/285915.

[15] KL Evans and KJ Gaston. Can the evolutionary-rates hypothesis explain species-energy relationships? *Functional Ecology*, 19(6):899–915, 2005. doi: 10.1111/j.1365-2435.2005.01046.x.

[16] Wen-Chi Liu. The relationship between primary energy consumption and real gross domestic product: evidence from major asian countries. *Sustainability*, 12(6):2568, 2020. doi: 10.3390/su12062568.

[17] Our World in Data. Gdp per capita vs. energy use, 2015, 1 2022. URL `https://ourworldindata.org/grapher/energy-use-per-capita-vs-gdp-per-capita`. Accessed: 2022-01-17. Archive: https://archive.ph/GkwsJ.

[18] David I Stern. Energy and economic growth. In *Routledge Handbook of Energy Economics*, pages 28–46. Routledge, 2019. ISBN 9781315459653.

[19] Bimal K Bose. Energy, environment, and advances in power electronics. In *ISIE'2000. Proceedings of the 2000 IEEE International Symposium on Industrial Electronics (Cat. No. 00TH8543)*, volume 1, pages TU1–T14. IEEE, 2000. doi: 10.1109/ISIE.2000.930467.

[20] Leslie A White. *The evolution of culture: the development of civilization to the fall of Rome*. Routledge, 2016.

[21] Leslie A White. Energy and the evolution of culture. *American Anthropologist*, 45(3): 335–356, 1943.

[22] Leslie A White. The concept of culture. *American anthropologist*, 61(2):227–251, 1959.

[23] Edward Anthony Wrigley. Energy and the english industrial revolution. *Philosophical Transactions of the Royal Society A: Mathematical, Physical and Engineering Sciences*, 371(1986):20110568, 2013. doi: 10.1098/rsta.2011.0568.

[24] Joel Mokyr and Robert H Strotz. The second industrial revolution, 1870-1914. *Storia dell'economia Mondiale*, 21945:1, 1998.

[25] Nikola Tesla. Experiments with alternate currents of very high frequency and their application to methods of artificial illumination. *Transactions of the American Institute of Electrical Engineers*, 8(1):266–319, 1891.

[26] Jeremy Greenwood. *The third industrial revolution: Technology, productivity, and income inequality*. Number 435. American Enterprise Institute, 1997.

[27] Tim Berners-Lee. Information management: a proposal. 1989. URL `https://www.w3.org/History/1989/proposal.html`. Accessed: 2020-10-11. Archive: https://archive.vn/YwbR.

[28] Joseph Finkelstein and David Newman. The third industrial revolution: a special challenge to managers. *Organizational Dynamics*, 13(1):53–65, 1984. doi: 10.1016/0090-2616(84)90031-7.

[29] Klaus Schwab. *The fourth industrial revolution*. Currency, 2017.

[30] Peter Goodman. *Davos man : how the billionaires devoured the world*. Custom House, New York, NY, 2022. ISBN 9780063078307.

[31] Chi-Wei Su, Meng Qin, Ran Tao, and Muhammad Umar. Financial implications of fourth industrial revolution: Can bitcoin improve prospects of energy investment? *Technological Forecasting and Social Change*, 158:120178, 2020. doi: 10.1016/j.techfore.2020.120178.

[32] Isaac Newton. *Principes mathématiques de la philosophie naturelle*, volume 1. Desaint & Saillant, 1756.

[33] IEA. World energy balances, 2019. URL `https://www.iea.org/statistics/balances/`. Accessed: 2019-08-12.

[34] IEA. World energy outlook. Technical report, Paris: IEA/OECD, 2017.

[35] Keywan Riahi, Arnulf Grübler, and Nebojsa Nakicenovic. Scenarios of long-term socio-economic and environmental development under climate stabilization. *Technological Forecasting and Social Change*, 74(7):887–935, 2007. doi: 10.1016/j.techfore.2006.05.026.

[36] Hans-Wilhelm Schiffer. Wec energy policy scenarios to 2050. *Energy policy*, 36(7):2464–2470, 2008. doi: 10.1016/j.enpol.2008.02.045.

[37] Paul D Raskin, Christi Electris, and Richard A Rosen. The century ahead: searching for sustainability. *Sustainability*, 2(8):2626–2651, 2010. doi: 10.3390/su2082626.

[38] Patrick Moriarty and Damon Honnery. Renewable energy in a warming world. *International Journal of Energy, Environment and Economics*, 16(4):343–69, 2009.

[39] Patrick Moriarty and Damon Honnery. What is the global potential for renewable energy? *Renewable and Sustainable Energy Reviews*, 16(1):244–252, 2012. doi: 10.1016/j.rser.2011.07.151.

[40] Dilip Ahuja and Marika Tatsutani. Sustainable energy for developing countries. *SAPI EN. S. Surveys and Perspectives Integrating Environment and Society*, (2.1), 2009.

[41] Paul G Munro and Anne Schiffer. Ethnographies of electricity scarcity: Mobile phone charging spaces and the recrafting of energy poverty in africa. *Energy and Buildings*, 188:175–183, 2019. doi: 10.1016/j.enbuild.2019.01.038.

[42] Patrick Nussbaumer, Morgan Bazilian, and Vijay Modi. Measuring energy poverty: Focusing on what matters. *Renewable and Sustainable Energy Reviews*, 16(1):231–243, 2012. doi: 10.1016/j.rser.2011.07.150.

[43] IEA. *World Energy Outlook 2002*. International Energy Agency (IEA) Paris, France, 2002.

[44] Benjamin K Sovacool. The political economy of energy poverty: a review of key challenges. *Energy for Sustainable Development*, 16(3):272–282, 2012. doi: 10.1016/j.esd.2012.05.006.

[45] WHO. *Fuel for life: household energy and health*. World Health Organization, 2006.

[46] Jamil Masud, Diwesh Sharan, and Bindu N Lohani. Energy for all: addressing the energy, environment, and poverty nexus in asia, 2007.

[47] Bianca Van der Kroon, Roy Brouwer, and Pieter Jh Van Beukering. The energy ladder: Theoretical myth or empirical truth? results from a meta-analysis. *Renewable and Sustainable Energy Reviews*, 20:504–513, 2013. doi: 10.1016/j.rser.2012.11.045.

[48] John P Holdren, Kirk R Smith, Tord Kjellstrom, David Streets, Xiaodong Wang, and S Fischer. Energy, the environment and health. *New York: United Nations Development Programme*, 2000.

[49] Douglas F Barnes and Willem M Floor. Rural energy in developing countries: a challenge for economic development. *Annual review of energy and the environment*, 21, 1996. doi: 10.1146/annurev.energy.21.1.497.

[50] Greg Hiemstra-Van der Horst and Alice J Hovorka. Reassessing the "energy ladder": household energy use in Maun, Botswana. *Energy Policy*, 36(9):3333–3344, 2008. doi: 10.1016/j.enpol.2008.05.006.

[51] F Barnes Douglas, Krutilla Kerry, and Hyde William. The urban household energy transition: energy, poverty, and the environment in the developing world. *Washington, DC: Resources for the Future*, 2004.

[52] Shoibal Chakravarty and Massimo Tavoni. Energy poverty alleviation and climate change mitigation: Is there a trade off? *Energy economics*, 40:S67–S73, 2013. doi: 10.1016/j.eneco.2013.09.022.

[53] Paul Lewis. *Fuel poverty can be stopped*. National Right to Fuel Campaign, 1982.

[54] DEFRA and DTI. The uk fuel poverty strategy. Technical report, Department of the Environment, Food and Rural Affairs and the Department of Trade and Industry, 2001.

[55] John Hills. Fuel poverty: The problem and its measurement. Interim report of the Fuel Poverty Review. Technical report, Centre for Analysis of Social Exclusion, LSE, 2011.

[56] DECC. Annual report on fuel poverty statistics. Technical report, Department for Energy and Climate Change, London UK, 2013.

[57] Catherine Waddams Price, Karl Brazier, and Wenjia Wang. Objective and subjective measures of fuel poverty. *Energy Policy*, 49:33–39, 2012. doi: 10.1016/j.enpol.2011.11.095.

[58] Kang Li, Bob Lloyd, Xiao-Jie Liang, and Yi-Ming Wei. Energy poor or fuel poor: What are the differences? *Energy Policy*, 68:476–481, 2014. doi: 10.1016/j.enpol.2013.11.012.

[59] Akanksha Chaurey, Malini Ranganathan, and Parimita Mohanty. Electricity access for geographically disadvantaged rural communities—technology and policy insights. *Energy Policy*, 32(15):1693–1705, 2004. doi: 10.1016/j.enpol.2008.01.041.

[60] Makoto Kanagawa and Toshihiko Nakata. Assessment of access to electricity and the socio-economic impacts in rural areas of developing countries. *Energy Policy*, 36(6): 2016–2029, 2008. doi: 10.1016/j.enpol.2008.01.041.

[61] S Joffe and S Jones. Stimulating private investment and market development for agriculture: new approaches and experience. *London: Oxford Policy Management*, 2004.

[62] Morgan Bazilian, Ambuj Sagar, Reid Detchon, and Kandeh Yumkella. More heat and light. *Energy Policy*, 38(10):5409–5412, 2010. doi: 10.1016/j.enpol.2010.06.007.

[63] Manfred Lenzen and Jesper Munksgaard. Energy and CO2 life-cycle analyses of wind turbines—review and applications. *Renewable energy*, 26(3):339–362, 2002. doi: 10.1016/S0960-1481(01)00145-8.

[64] Damon Honnery and Patrick Moriarty. Estimating global hydrogen production from wind. *International journal of hydrogen energy*, 34(2):727–736, 2009. doi: 10.1016/j.ijhydene.2008.11.001.

[65] Monique Hoogwijk, Bert de Vries, and Wim Turkenburg. Assessment of the global and regional geographical, technical and economic potential of onshore wind energy. *Energy Economics*, 26(5):889–919, 2004. doi: 10.1016/j.eneco.2004.04.016.

[66] John Twidell and Tony Weir. *Renewable Energy Resources*. Routledge, 2015.

[67] Bent Sørensen. *Renewable Energy, Second Edition*. Academic Press, 2000. ISBN 0126561524.

[68] John Theodore Houghton, Geoffrey J Jenkins, and Jim J Ephraums. Climate change. 1990.

[69] Donald J Wuebbles and Atul K Jain. Concerns about climate change and the role of fossil fuel use. *Fuel processing technology*, 71(1-3):99–119, 2001. doi: 10.1016/S0378-3820(01)00139-4.

[70] Ross Garnaut. The garnaut climate change review. *Cambridge, Cambridge*, 2008.

[71] Mikael Höök and Xu Tang. Depletion of fossil fuels and anthropogenic climate change—a review. *Energy policy*, 52:797–809, 2013. doi: 10.1016/j.enpol.2012.10.046.

[72] Shahriar Shafiee and Erkan Topal. When will fossil fuel reserves be diminished? *Energy policy*, 37(1):181–189, 2009. doi: 10.1016/j.enpol.2008.08.016.

[73] Iñigo Capellán-Pérez, Margarita Mediavilla, Carlos de Castro, Óscar Carpintero, and Luis Javier Miguel. Fossil fuel depletion and socio-economic scenarios: An integrated approach. *Energy*, 77:641–666, 2014. doi: 10.1016/j.energy.2014.09.063.

[74] Fred Sissine. Energy independence and security act of 2007: a summary of major provisions. Library of Congress Washington DC Congressional Research Service, 2007.

[75] Dan Chiras. *The Homeowner's Guide to Renewable Energy: Achieving Energy Independence Through Solar, Wind, Biomass, and Hydropower*. New Society Publishers, 2011.

[76] Stan Mark Kaplan. *Smart Grid: Modernizing electric power transmission and distribution; Energy independence, Storage and security; Energy independence and security act of 2007 (EISA); Improving electrical grid efficiency, communication, reliability, and resiliency; integrating new and renewable energy sources*. The Capitol Net Inc, 2009.

[77] Ioannis Vardopoulos. Multi-criteria analysis for energy independence from renewable energy sources case study zakynthos island, greece. *International Journal of Environmental Science and Development*, 8(6):460–465, 2017.

[78] Simon P. Neill and M. Reza Hashemi. *Fundamentals of Ocean Renewable Energy*. Elsevier, 2018. doi: 10.1016/c2016-0-00230-9.

[79] Shikha Lakhanpal. Contesting renewable energy in the global south: A case-study of local opposition to a wind power project in the western ghats of india. *Environmental Development*, 30:51–60, 2019. doi: 10.1016/j.envdev.2019.02.002.

[80] Noel Cass and Gordon Walker. Emotion and rationality: The characterisation and evaluation of opposition to renewable energy projects. *Emotion, Space and Society*, 2(1): 62–69, 2009. doi: 10.1016/j.emospa.2009.05.006.

[81] Martin J Pasqualetti. Social barriers to renewable energy landscapes. *Geographical review*, 101(2):201–223, 2011. doi: 10.1111/j.1931-0846.2011.00087.x.

[82] John P Barton and David G Infield. Energy storage and its use with intermittent renewable energy. *IEEE transactions on energy conversion*, 19(2):441–448, 2004. doi: 10.1109/TEC.2003.822305.

[83] Michael Joos and Iain Staffell. Short-term integration costs of variable renewable energy: Wind curtailment and balancing in Britain and Germany. *Renewable and Sustainable Energy Reviews*, 86:45–65, 2018. doi: 10.1016/j.rser.2018.01.009.

[84] Daniel R Drew, Phil J Coker, Hannah C Bloomfield, David J Brayshaw, Janet F Barlow, and Andrew Richards. Sunny windy sundays. *Renewable Energy*, 138:870–875, 2019. doi: 10.1016/j.renene.2019.02.029.

[85] Juan Manuel Carrasco, Leopoldo Garcia Franquelo, Jan T Bialasiewicz, Eduardo Galván, Ramón Carlos PortilloGuisado, MA Martin Prats, José Ignacio León, and Narciso Moreno-Alfonso. Power-electronic systems for the grid integration of renewable energy sources: A survey. *IEEE Transactions on industrial electronics*, 53(4):1002–1016, 2006. doi: 10.1109/TIE.2006.878356.

[86] Marco Liserre, Thilo Sauter, and John Y Hung. Future energy systems: Integrating renewable energy sources into the smart power grid through industrial electronics. *IEEE industrial electronics magazine*, 4(1):18–37, 2010. doi: 10.1109/MIE.2010.935861.

[87] Patrick Milan, Matthias Wächter, and Joachim Peinke. Stochastic modeling and performance monitoring of wind farm power production. *Journal of Renewable and Sustainable Energy*, 6(3):033119, 2014. doi: 10.1063/1.4880235.

[88] Anya Castillo and Dennice F Gayme. Grid-scale energy storage applications in renewable energy integration: A survey. *Energy Conversion and Management*, 87:885–894, 2014. doi: 10.1016/j.enconman.2014.07.063.

[89] Shafiqur Rehman, Luai M Al-Hadhrami, and Md Mahbub Alam. Pumped hydro energy storage system: A technological review. *Renewable and Sustainable Energy Reviews*, 44:586–598, 2015. doi: 10.1016/j.rser.2014.12.040.

[90] K Agbossou, R Chahine, J Hamelin, F Laurencelle, A Anouar, J-M St-Arnaud, and TK Bose. Renewable energy systems based on hydrogen for remote applications. *Journal of power sources*, 96(1):168–172, 2001. doi: 10.1016/S0378-7753(01)00495-5.

[91] Tanay Sıdkı Uyar and Doğancan Beşikci. Integration of hydrogen energy systems into renewable energy systems for better design of 100% renewable energy communities. *International Journal of Hydrogen Energy*, 42(4):2453–2456, 2017. doi: 10.1016/j.ijhydene.2016.09.086.

[92] Henrik Lund and Georges Salgi. The role of compressed air energy storage (CAES) in future sustainable energy systems. *Energy conversion and management*, 50(5):1172–1179, 2009. doi: 10.1016/j.enconman.2009.01.032.

[93] Marcus Budt, Daniel Wolf, Roland Span, and Jinyue Yan. A review on compressed air energy storage: Basic principles, past milestones and recent developments. *Applied energy*, 170:250–268, 2016. doi: 10.1016/j.apenergy.2016.02.108.

[94] Rodrigo F Abdo, Hugo TC Pedro, Ricardo NN Koury, Luiz Machado, Carlos FM Coimbra, and Matheus P Porto. Performance evaluation of various cryogenic energy storage systems. *Energy*, 90:1024–1032, 2015. doi: 10.1016/j.energy.2015.08.008.

[95] Tugberk Hakan Cetin, Mehmet Kanoglu, and Neslihan Yanikomer. Cryogenic energy storage powered by geothermal energy. *Geothermics*, 77:34–40, 2019. doi: 10.1016/j.geothermics.2018.08.005.

[96] Matthew T Lawder, Bharatkumar Suthar, Paul WC Northrop, Sumitava De, C Michael Hoff, Olivia Leitermann, Mariesa L Crow, Shriram Santhanagopalan, and Venkat R

Subramanian. Battery energy storage system (BESS) and battery management system (BMS) for grid-scale applications. *Proceedings of the IEEE*, 102(6):1014–1030, 2014. doi: 10.1109/JPROC.2014.2317451.

[97] Xuan Phuong Nguyen and Anh Tuan Hoang. The flywheel energy storage system: An effective solution to accumulate renewable energy. In *2020 6th International Conference on Advanced Computing and Communication Systems (ICACCS)*, pages 1322–1328. IEEE, 2020. doi: 10.1109/ICACCS48705.2020.9074469.

[98] Warren Buckles and William V Hassenzahl. Superconducting magnetic energy storage. *IEEE Power Engineering Review*, 20(5):16–20, 2000. doi: 10.1109/39.841345.

[99] Atul Sharma, V Veer Tyagi, CR Chen, and Dharam Buddhi. Review on thermal energy storage with phase change materials and applications. *Renewable and Sustainable energy reviews*, 13(2):318–345, 2009. doi: 10.1016/j.rser.2007.10.005.

[100] CD Botha and MJ Kamper. Capability study of dry gravity energy storage. *Journal of Energy Storage*, 23:159–174, 2019. doi: 10.1016/j.est.2019.03.015.

[101] M Puchta, J Bard, C Dick, D Hau, B Krautkremer, F Thalemann, and H Hahn. Development and testing of a novel offshore pumped storage concept for storing energy at seastensea. *Journal of Energy Storage*, 14:271–275, 2017. doi: 10.1016/j.est.2017.06.004.

[102] IEA/NEA. Projected costs of generating electricity — 2015 edition. Technical report, Organisation for Economic Co-operation and Development, Paris, France, 2015.

[103] Patrick Moriarty and Damon Honnery. *Rise and Fall of the Carbon Civilisation: Resolving Global Environmental and Resource Problems*. Springer Science & Business Media, 2010.

[104] Ralph EH Sims, Robert N Schock, Anthony Adegbululgbe, Jørgen Fenhann, Inga Konstantinaviciute, William Moomaw, Hassan B Nimir, Bernhard Schlamadinger, Julio Torres-Martinez, Clive Turner, et al. Energy supply. In *Climate Change 2007: Mitigation. Contribution of Working Group III to the Fourth Assessment Report of the Intergovernmental Panel on Climate Change. Metz, B.; Davidson, OR; Bosch, PR; Dave, R.; Meyer, LA (eds)*, pages 252–322. Cambridge University Press, 2007. ISBN 9780521705981.

[105] SA Abbasi and Naseema Abbasi. The likely adverse environmental impacts of renewable energy sources. *Applied Energy*, 65(1-4):121–144, 2000. doi: 10.1016/S0306-2619(99)00077-X.

[106] Matthew McCartney. Living with dams: managing the environmental impacts. *Water Policy*, 11(S1):121–139, 2009. doi: 10.2166/wp.2009.108.

[107] David Pimentel, Megan Herz, Michele Glickstein, Mathew Zimmerman, Richard Allen, Katrina Becker, Jeff Evans, Benita Hussain, Ryan Sarsfeld, Anat Grosfeld, et al. Renewable energy: current and potential issues: renewable energy technologies could, if developed and implemented, provide nearly 50% of US energy needs; this would

require about 17% of US land resources. *Bioscience*, 52(12):1111–1120, 2002. doi: 10.1641/0006-3568(2002)052[1111:RECAPI]2.0.CO;2.

[108] Adrian Cho. Energy's tricky tradeoffs. *Science*, 329(5993):786–787, 2010. doi: 10.1126/science.329.5993.786.

[109] Justin G Boyles, Paul M Cryan, Gary F McCracken, and Thomas H Kunz. Economic importance of bats in agriculture. *Science*, 332(6025):41–42, 2011. doi: 10.1126/science.1201366.

[110] William P Kuvlesky Jr, Leonard A Brennan, Michael L Morrison, Kathy K Boydston, Bart M Ballard, and Fred C Bryant. Wind energy development and wildlife conservation: challenges and opportunities. *The Journal of Wildlife Management*, 71(8):2487–2498, 2007. doi: 10.2193/2007-248.

[111] Christopher A Simon. Cultural constraints on wind and solar energy in the US context. *Comparative Technology Transfer and Society*, 7(3):251–269, 2009. doi: 10.1353/ctt.0.0046.

[112] W Dixie Dean. Wind turbine mechanical vibrations: potential environmental threat. *Energy & environment*, 19(2):303–307, 2008. doi: 10.1260/095830508783900771.

[113] R Saidur, NA Rahim, MR Islam, and KH Solangi. Environmental impact of wind energy. *Renewable and sustainable energy reviews*, 15(5):2423–2430, 2011. doi: 10.1016/j.rser.2011.02.024.

[114] Maarten Wolsink. Wind power implementation: The nature of public attitudes: Equity and fairness instead of 'backyard motives'. *Renewable and sustainable energy reviews*, 11(6):1188–1207, 2007. doi: 10.1016/j.rser.2005.10.005.

[115] Thomas H Kunz, Edward B Arnett, Wallace P Erickson, Alexander R Hoar, Gregory D Johnson, Ronald P Larkin, M Dale Strickland, Robert W Thresher, and Merlin D Tuttle. Ecological impacts of wind energy development on bats: questions, research needs, and hypotheses. *Frontiers in Ecology and the Environment*, 5(6):315–324, 2007. doi: 10.1890/1540-9295(2007)5[315:EIOWED]2.0.CO;2.

[116] Eli Kintisch. Out of site, 2010.

[117] Theocharis Tsoutsos, Niki Frantzeskaki, and Vassilis Gekas. Environmental impacts from the solar energy technologies. *Energy Policy*, 33(3):289–296, 2005. doi: 10.1016/S0301-4215(03)00241-6.

[118] Damon Honnery and Patrick Moriarty. Liquid fuels from woody biomass. *International journal of global energy issues*, 27(2):103–114, 2007.

[119] Anastassia M Makarieva, Victor G Gorshkov, and Bai-Lian Li. Energy budget of the biosphere and civilization: Rethinking environmental security of global renewable and non-renewable resources. *Ecological complexity*, 5(4):281–288, 2008. doi: 10.1016/j.ecocom.2008.05.005.

[120] George W Boehlert and Andrew B Gill. Environmental and ecological effects of ocean renewable energy development: a current synthesis. *Oceanography*, 23(2):68–81, 2010.

[121] Milan Meszaros. Lethal kickback of largescale renewable energy exploitation. *Mészáros Milán, A megújuló energiák kitermelésének káros hatásairól*, 2009.

[122] MJ Khan, MT Iqbal, and JE Quaicoe. River current energy conversion systems: Progress, prospects and challenges. *Renewable and Sustainable Energy Reviews*, 12 (8):2177–2193, 2008. doi: 10.1016/j.rser.2007.04.016.

[123] Nicholas D Laws and Brenden P Epps. Hydrokinetic energy conversion: Technology, research, and outlook. *Renewable and Sustainable Energy Reviews*, 57:1245–1259, 2016. doi: 10.1016/j.rser.2015.12.189.

[124] Hisham Khatib. *Economic Evaluation of Projects in the Electricity Supply Industry*. Number 44. The Institution of Engineering and Technology, 2014.

[125] Hisham Khatib. A review of the iea/nea projected costs of electricity–2015 edition. *Energy Policy*, 88:229–233, 2016. doi: 10.1016/j.enpol.2015.10.030.

[126] IK Bhat, Ravi Prakash, et al. LCA of renewable energy for electricity generation systems—a review. *Renewable and sustainable energy reviews*, 13(5):1067–1073, 2009. doi: 10.1016/j.rser.2008.08.004.

[127] Atif Ansar, Bent Flyvbjerg, Alexander Budzier, and Daniel Lunn. Should we build more large dams? The actual costs of hydropower megaproject development. *Energy Policy*, 69:43–56, 2014. doi: 10.1016/j.enpol.2013.10.069.

[128] Petras Punys, I Adamonyte, Algis Kvaraciejus, Erikas Martinaitis, G Vyciene, and Egidijus Kasiulis. Riverine hydrokinetic resource assessment. A case study of a lowland river in Lithuania. *Renewable and Sustainable Energy Reviews*, 50:643–652, 2015. doi: 10.1016/j.rser.2015.04.155.

[129] Subhes C Bhattacharyya and Sanusi Ohiare. The Chinese electricity access model for rural electrification: approach, experience and lessons for others. *Energy Policy*, 49: 676–687, 2012. doi: 10.1016/j.enpol.2012.07.003.

[130] Bikash Pandey and Ajoy Karki. *Hydroelectric Energy: Renewable Energy and the Environment*. CRC Press, 2017. ISBN 9781439811672.

[131] David Archer and Stefan Rahmstorf. *The climate crisis: An introductory guide to climate change*. Cambridge University Press, 2010.

[132] Raymond Pierrehumbert. There is no plan b for dealing with the climate crisis. *Bulletin of the Atomic Scientists*, 75(5):215–221, 2019. doi: 10.1080/00963402.2019.1654255.

[133] Eric Klinenberg, Malcolm Araos, and Liz Koslov. Sociology and the climate crisis. *Annual Review of Sociology*, 46:649–669, 2020. doi: 10.1146/annurev-soc-121919-054750.

[134] REN21. Renewables 2018 global status report. Technical report, Paris: REN21 Secretariat, 2018.

[135] National Research Council. *Assessment of Marine and Hydrokinetic Energy Technology*. National Academies Press, 2011. doi: 10.17226/13202.

[136] Simon P. Neill, Athanasios Angeloudis, Peter E. Robins, Ian Walkington, Sophie L. Ward, Ian Masters, Matt J. Lewis, Marco Piano, Alexandros Avdis, Matthew D. Piggott, George Aggidis, Paul Evans, Thomas A.A. Adcock, Audrius Židonis, Reza Ahmadian, and Roger Falconer. Tidal range energy resource and optimization - past perspectives and future challenges. *Renewable Energy*, 127(nil):763–778, 2018. doi: 10.1016/j.renene.2018.05.007.

[137] Michael Ridgill, Simon P Neill, Matt J Lewis, Peter E Robins, and Sopan D Patil. Global riverine theoretical hydrokinetic resource assessment. *Renewable Energy*, 174:654–665, 2021. doi: 10.1016/j.renene.2021.04.109.

[138] Michael Ridgill, Matt J Lewis, Peter E Robins, Sopan D Patil, and Simon Neill. Hydrokinetic energy conversion: A global riverine perspective. *Journal of Renewable and Sustainable Energy*, 2022.

[139] DM Fouz, Rodrigo Carballo, V Ramos, and Gregorio Iglesias. Hydrokinetic energy exploitation under combined river and tidal flow. *Renewable Energy*, 143:558–568, 2019. doi: 10.1016/j.renene.2019.05.035.

[140] Carmen Zarzuelo, Alejandro López-Ruiz, Manuel Díez-Minguito, and Miguel Ortega-Sánchez. Tidal and subtidal hydrodynamics and energetics in a constricted estuary. *Estuarine, Coastal and Shelf Science*, 185:55–68, 2017. doi: 10.1016/j.ecss.2016.11.020.

[141] M Ishak Yuce and Abdullah Muratoglu. Hydrokinetic energy conversion systems: a technology status review. *Renewable and Sustainable Energy Reviews*, 43:72–82, 2015. doi: 10.1016/j.rser.2014.10.037.

[142] Ivan Felipe Silva dos Santos, Ramiro Gustavo Ramirez Camacho, Geraldo Lúcio Tiago Filho, Antonio Carlos Barkett Botan, and Barbara Amoeiro Vinent. Energy potential and economic analysis of hydrokinetic turbines implementation in rivers: An approach using numerical predictions (cfd) and experimental data. *Renewable Energy*, 143:648–662, 2019. doi: 10.1016/j.renene.2019.05.018.

[143] Intergovernmental Panel on Climate Change. *Global warming of 1.5° C: An IPCC special report on the impacts of global warming of 1.5° C above pre-industrial levels and related global greenhouse gas emission pathways, in the context of strengthening the global response to the threat of climate change, sustainable development, and efforts to eradicate poverty*. Intergovernmental Panel on Climate Change, 2018.

[144] Steven J Davis, Nathan S Lewis, Matthew Shaner, Sonia Aggarwal, Doug Arent, Inês L Azevedo, Sally M Benson, Thomas Bradley, Jack Brouwer, Yet-Ming Chiang, et al. Net-zero emissions energy systems. *Science*, 360(6396):eaas9793, 2018. doi: 10.1126/science.aas9793.

[145] Holly Jean Buck. *Ending Fossil Fuels: Why Net Zero is Not Enough*. Verso Books, 2021.

[146] Sam Fankhauser, Stephen M Smith, Myles Allen, Kaya Axelsson, Thomas Hale, Cameron Hepburn, J Michael Kendall, Radhika Khosla, Javier Lezaun, Eli Mitchell-Larson, et al. The meaning of net zero and how to get it right. *Nature Climate Change*, 12(1):15–21, 2022. doi: 10.1038/s41558-021-01245-w.

[147] PL Fraenkel. Marine current turbines: pioneering the development of marine kinetic energy converters. *Proceedings of the Institution of Mechanical Engineers, Part A: Journal of Power and Energy*, 221(2):159–169, 2007. doi: 10.1243/09576509JPE307.

[148] Patrícia da Silva Holanda, Claudio José Cavalcante Blanco, André Luiz Amarante Mesquita, Antônio César Pinho Brasil Junior, Nelio Moura de Figueiredo, Emanuel Negrão Macêdo, and Yves Secretan. Assessment of hydrokinetic energy resources downstream of hydropower plants. *Renewable Energy*, 101:1203–1214, 2017. doi: 10.1016/j.renene.2016.10.011.

[149] Yue Liu and Daniel J Packey. Combined-cycle hydropower systems–the potential of applying hydrokinetic turbines in the tailwaters of existing conventional hydropower stations. *Renewable energy*, 66:228–231, 2014. doi: 10.1016/j.renene.2013.12.007.

[150] Jerome B Johnson and Dominique J Pride. River, tidal, and ocean current hydrokinetic energy technologies: status and future opportunities in alaska. *Prepared for Alaska Center for Energy and Power*, 2010.

[151] Ryan N Tyler. River debris: Causes, impacts, and mitigation techniques. *Alaska Center for Energy and Power*, pages p1–33, 2011.

[152] Mohammadmehdi Armandei, Antonio Carlos Fernandes, and A Bakhshandeh Rostami. Hydroelastic buffeting assessment over a vertically hinged flat plate. *Experimental Techniques*, 40(2):833–839, 2016. doi: 10.1007/s40799-016-0084-y.

[153] George W Taylor, Joseph R Burns, SA Kammann, William B Powers, and Thomas R Welsh. The energy harvesting eel: a small subsurface ocean/river power generator. *IEEE journal of oceanic engineering*, 26(4):539–547, 2001. doi: 10.1109/48.972090.

[154] Michael M Bernitsas, Kamaldev Raghavan, Y Ben-Simon, and EMH Garcia. VIVACE (Vortex Induced Vibration Aquatic Clean Energy): A new concept in generation of clean and renewable energy from fluid flow. *J. Offshore Mech. Arct. Eng.*, 130(4), 2008. doi: 10.1115/1.2957913.

[155] Penglei Ma, Zhihong Yang, Yong Wang, Haibin Liu, and Yudong Xie. Energy extraction and hydrodynamic behavior analysis by an oscillating hydrofoil device. *Renewable Energy*, 113:648–659, 2017. doi: 10.1016/j.renene.2017.06.036.

[156] Tidal Sails AS. Tidal sails, 1 2022. URL `https://tidalsails.com/`. Accessed: 2022-01-29. Archive: https://archive.ph/zs6lA.

[157] MJ Khan, G Bhuyan, MT Iqbal, and JE Quaicoe. Hydrokinetic energy conversion systems and assessment of horizontal and vertical axis turbines for river and tidal applications: A technology status review. *Applied energy*, 86(10):1823–1835, 2009. doi: 10.1016/j.apenergy.2009.02.017.

[158] Richard Fraser, Claire Deschênes, Claude O'Neil, and Marc Leclerc. Vlh: Development of a new turbine for very low head sites. *Proceeding of the 15th Waterpower*, 10(157): 23–26, 2007. doi: 10.1.1.557.8586.

[159] Philippe Lautier, Claude O'Neil, Claire Deschenes, Herve Joel Nanga Ndjana, and R Eraser. Variable speed operation of a new very low head hydro turbine with low environmental impact. In *Electrical Power Conference, 2007. EPC 2007. IEEE Canada*, pages 85–90. IEEE, 2007. doi: 10.1109/EPC.2007.4520311.

[160] Brian Kirke. Hydrokinetic and ultra-low head turbines in rivers: A reality check. *Energy for Sustainable Development*, 52:1–10, 2019. doi: 10.1016/j.esd.2019.06.002.

[161] Herman Jacobus Vermaak, Kanzumba Kusakana, and Sandile Philip Koko. Status of micro-hydrokinetic river technology in rural applications: a review of literature. *Renewable and Sustainable Energy Reviews*, 29:625–633, 2014. doi: 10.1016/j.rser.2013.08.066.

[162] Paul Duvoy and Horacio Toniolo. Hydrokal: a module for in-stream hydrokinetic resource assessment. *Computers & geosciences*, 39:171–181, 2012. doi: 10.1016/j.cageo.2011.06.016.

[163] Ogunjuyigbe Ayodeji Samson Olatunji, Ayodele Temitope Raphael, and Ibitoye Tahir Yomi. Hydrokinetic energy opportunity for rural electrification in nigeria. *International Journal of Renewable Energy Development*, 7(2):183, 2018. doi: 10.14710/ijred.7.2.183-190.

[164] Albert Betz. *Introduction to the theory of flow machines*. Elsevier, 2014.

[165] Robert L Radkey and B Hibbs. Definition of cost-effective river-turbine designs. *NASA STI/Recon Technical Report N*, 83, 1981.

[166] Emilia Lalander and Mats Leijon. Numerical modeling of a river site for in-stream energy converters. In *Proceedings of the 8th European Wave and Tidal Energy Conference, EWTEC09, Uppsala, Sweden*, volume 710, page 826832, 2009.

[167] Scott J Couch and Ian G Bryden. The impact of energy extraction on tidal flow development. In *3rd International Conference on Marine Renewable Energy, Blyth*, 2004.

[168] Peter Fraenkel. Too much torque and not enough action, 2014. URL `https://www.waterpowermagazine.com/opinion/opiniontoo-much-torque-and-not-enough-action-4190252/`. [Online. Accessed: 2018-11-21].

[169] George Hagerman, Brian Polagye, Roger Bedard, and Mirko Previsic. Methodology for estimating tidal current energy resources and power production by tidal in-stream energy conversion (tisec) devices. *EPRI North American tidal in stream power feasibility demonstration project*, 1, 2006.

[170] Ross Vennell, Simon W Funke, Scott Draper, Craig Stevens, and Tim Divett. Designing large arrays of tidal turbines: A synthesis and review. *Renewable and Sustainable Energy Reviews*, 41:454–472, 2015. doi: 10.1016/j.rser.2014.08.022.

[171] Ross Vennell. Exceeding the betz limit with tidal turbines. *Renewable Energy*, 55: 277–285, 2013. doi: 10.1016/j.renene.2012.12.016.

[172] Simon P Neill, Emmer J Litt, Scott J Couch, and Alan G Davies. The impact of tidal stream turbines on large-scale sediment dynamics. *Renewable Energy*, 34(12):2803–2812, 2009. doi: 10.1016/j.renene.2009.06.015.

[173] IEC. IEC TC 114: Marine energy — wave, tidal and other water current converters. Technical report, International Electrotechnical Commission, 2018.

[174] Chris Garrett and Patrick Cummins. The efficiency of a turbine in a tidal channel. *Journal of fluid mechanics*, 588:243–251, 2007. doi: 10.1017/S0022112007007781.

[175] Chris Garrett and Patrick Cummins. Limits to tidal current power. *Renewable Energy*, 33(11):2485–2490, 2008. doi: 10.1016/j.renene.2008.02.009.

[176] National Research Council, Ocean Studies Board, Marine, Hydrokinetic Energy Technology Assessment Committee, et al. *An Evaluation of the US Department of Energy's Marine and Hydrokinetic Resource Assessments*. National Academies Press, 2013.

[177] Katelyn Kirby, Sean Ferguson, Colin Rennie, Ioan NISTOR, and Julien Cousineau. Assessments of available riverine hydrokinetic energy: A review. *Canadian Journal of Civil Engineering*, (ja), 2021. doi: 10.1139/cjce-2021-0178.

[178] Andrea Copping, Hoyt Battey, Jocelyn Brown-Saracino, Meghan Massaua, and Courtney Smith. An international assessment of the environmental effects of marine energy development. *Ocean & coastal management*, 99:3–13, 2014. doi: 10.1016/j.ocecoaman.2014.04.002.

[179] Gemma Keenan, Carol Sparling, Hannah Williams, and Frank Fortune. Seagen environmental monitoring programme final report. *Royal Haskoning: Edinburgh, UK, January*, 2011.

[180] Chris Tomichek, Jonathan Colby, Mary Ann Adonizio, Michael Firsk, Keith Dunton, Dewayne Fox, Adrian Jordaan, et al. Tagged species detection: approach to monitoring marine species at marine hydrokinetic projects. 2014.

[181] Paul T Jacobson, Stephen V Amaral, Theodore Castro-Santos, Dan Giza, Alexander J Haro, George Hecker, Brian McMahon, Norman Perkins, and Nick Pioppi. Environmental effects of hydrokinetic turbines on fish: desktop and laboratory flume studies. Technical report, Electric Power Research Institute, 2012.

[182] Theodore Castro-Santos and Alex Haro. Survival and behavioral effects of exposure to a hydrokinetic turbine on juvenile atlantic salmon and adult american shad. *Estuaries and Coasts*, 38(1):203–214, 2015. doi: 10.1007/s12237-013-9680-6.

[183] Vincent S Neary and Budi Gunawan. Field measurements at river and tidal current sites for hydrokinetic energy development: best practices manual. Technical report, Oak Ridge National Lab.(ORNL), Oak Ridge, TN (United States), 2011.

[184] Luna B Leopold and Thomas Dunne. Water in environmental planning. *New York, 818p*, 1978.

[185] National River Flow Archive, . URL `https://nrfa.ceh.ac.uk/data`. Accessed: 2017-08-01.

[186] Emilia Lalander. *Hydrokinetic resource assessment: measurements and models*. PhD thesis, Acta Universitatis Upsaliensis, 2013.

[187] Paul T Jacobson, Thomas M Ravens, Keith W Cunningham, and George Scott. Assessment and mapping of the riverine hydrokinetic resource in the continental United States. Technical report, Electric Power Research Institute, 2012.

[188] G Miller, J Franceschi, W Lese, and J Rico. The allocation of kinetic hydro energy conversion systems (KHECS) in USA drainage basins: regional resource and potential power. *Final Report, NYUDAS*, pages 86–151, 1986.

[189] Budi Gunawan, Vincent S Neary, and Jonathan Colby. Tidal energy site resource assessment in the east river tidal strait, near roosevelt island, new york, new york. *Renewable Energy*, 71(SAND-2013-9197J), 2014. doi: 10.1016/j.renene.2014.06.002.

[190] UMA Group. An evaluation of the kinetic energy of Canadian rivers & estuaries. Technical report, Technical report, Canadian National Research Council-Canadian Hydraulics Centre, 1980.

[191] Ron Monk, S Joyce, and Mike Homenuke. Rapid hydropower assessment model: Identify hydroelectric sites using geographic information systems. In *Proceedings of the Small Hydro Conference 2009*, pages 28–29, 2009.

[192] RW Jenkinson and J Bomhof. Assessment of Canada's hydrokinetic power potential: Phase III report, resource estimation. Technical report, National Research Council of Canada, 2014.

[193] Gary W Brunner. Hec-ras river analysis system. hydraulic reference manual. version 1.0. Technical report, Hydrologic Engineering Center Davis CA, 1995.

[194] US Army Corps of Engineers. Hydrologic engineering centers river analysis system (HEC-RAS). 2014.

[195] Maria Kartezhnikova and Thomas M Ravens. Hydraulic impacts of hydrokinetic devices. *Renewable energy*, 66:425–432, 2014. doi: 10.1016/j.renene.2013.12.034.

[196] Thierry Faure. Methodology for the assessment of hydraulic kinetic energy in rivers. 2008.

[197] Environment Canada. National Water Data Archive: HYDAT, 2018. URL https://www.canada.ca/en/environment-climate-change/services/water-overview/quantity/monitoring/survey/data-products-services/national-archive-hydat.html. [Online. Accessed: 2019-12-10].

[198] Paolo Tarolli. High-resolution topography for understanding earth surface processes: Opportunities and challenges. *Geomorphology*, 216:295–312, 2014. doi: 10.1016/j.geomorph.2014.03.008.

[199] Ling Liu and M Tamer Özsu. *Encyclopedia of database systems*, volume 6. Springer New York, NY, USA:, 2009.

[200] Juan Remondo and Takashi Oguchi. GIS and SDA applications in geomorphology. *Geomorphology*, 111(1-2):1–3, 2009. doi: 10.1016/j.geomorph.2009.04.015. URL https://doi.org/10.1016/j.geomorph.2009.04.015.

[201] Zafer Defne, Kevin A Haas, Hermann M Fritz, Lide Jiang, Steven P French, Xuan Shi, Brennan T Smith, Vincent S Neary, and Kevin M Stewart. National geodatabase of tidal stream power resource in USA. *Renewable and Sustainable Energy Reviews*, 16(5): 3326–3338, 2012. doi: 10.1016/j.rser.2012.02.061.

[202] Kevin A Haas, Hermann M Fritz, Steven P French, Brennan T Smith, and Vincent Neary. Assessment of energy production potential from tidal streams in the united states. Technical report, Georgia Tech Research Corporation, Atlanta, GA (United States), 2011.

[203] Bernhard Lehner, Kristine Verdin, and Andy Jarvis. New global hydrography derived from spaceborne elevation data. *Eos, Transactions American Geophysical Union*, 89 (10):93, 2008. doi: 10.1029/2008eo100001.

[204] Bernhard Lehner and Günther Grill. Global river hydrography and network routing: baseline data and new approaches to study the world's large river systems. *Hydrological Processes*, 27(15):2171–2186, 2013. doi: 10.1002/hyp.9740.

[205] Dai Yamazaki, Fiachra O'Loughlin, Mark A Trigg, Zachary F Miller, Tamlin M Pavelsky, and Paul D Bates. Development of the global width database for large rivers. *Water Resources Research*, 50(4):3467–3480, 2014. doi: 10.1002/2013WR014664.

[206] George H Allen and Tamlin M Pavelsky. Patterns of river width and surface area revealed by the satellite-derived North American river width data set. *Geophysical Research Letters*, 42(2):395–402, 2015. doi: 10.1002/2014GL062764.

[207] Dai Yamazaki, Daiki Ikeshima, Jeison Sosa, Paul D Bates, George Allen, and Tamlin Pavelsky. MERIT Hydro: A high-resolution global hydrography map based on latest topography datasets. *Water Resources Research*, 55(6):5053–5073, 2019. doi: 10.1029/2019WR024873.

[208] Xinyi Shen, Emmanouil N Anagnostou, Yiwen Mei, and Yang Hong. A global distributed basin morphometric dataset. *Scientific Data*, 4:160124, 2017. doi: 10.1038/sdata.2016.124.

[209] F Nardi, A Annis, Giuliano Di Baldassarre, ER Vivoni, and S Grimaldi. GFPLAIN250m, a global high-resolution dataset of Earth's floodplains. *Scientific Data*, 6:180309, 2019. doi: 10.1038/sdata.2018.309.

[210] G Robert Brakenridge. Flood risk mapping from orbital remote sensing. *Global Flood Hazard: Applications in Modeling, Mapping, and Forecasting*, pages 43–54, 2018. doi: 10.1002/9781119217886.ch3.

[211] Albert IJM Van Dijk, G Robert Brakenridge, Albert J Kettner, Hylke E Beck, Tom De Groeve, and Jaap Schellekens. River gauging at global scale using optical and passive microwave remote sensing. *Water Resources Research*, 52(8):6404–6418, 2016. doi: 10.1002/2015WR018545.

[212] Konstantinos M Andreadis, Guy J-P Schumann, Dimitrios Stampoulis, Paul D Bates, G Robert Brakenridge, and Albert J Kettner. Can atmospheric reanalysis data sets be used to reproduce flooding over large scales? *Geophysical Research Letters*, 44(20): 10–369, 2017. doi: 10.1002/2017GL075502.

[213] G Robert Brakenridge, Son V Nghiem, Elaine Anderson, and Rodica Mic. Orbital microwave measurement of river discharge and ice status. *Water Resources Research*, 43 (4), 2007. doi: 10.1029/2006WR005238.

[214] Angelica Tarpanelli, Silvia Barbetta, Luca Brocca, and Tommaso Moramarco. River discharge estimation by using altimetry data and simplified flood routing modeling. *Remote Sensing*, 5(9):4145–4162, 2013. doi: 10.3390/rs5094145.

[215] MJ Tourian, N Sneeuw, and A Bárdossy. A quantile function approach to discharge estimation from satellite altimetry (ENVISAT). *Water Resources Research*, 49(7):4174–4186, 2013. doi: 10.1002/wrcr.20348.

[216] Colin J Gleason, Laurence C Smith, and Jinny Lee. Retrieval of river discharge solely from satellite imagery and at-many-stations hydraulic geometry: sensitivity to river form and optimization parameters. *Water Resources Research*, 50(12):9604–9619, 2014. doi: 10.1002/2014WR016109.

[217] Colin J Gleason and Laurence C Smith. Toward global mapping of river discharge using satellite images and at-many-stations hydraulic geometry. *Proceedings of the National Academy of Sciences*, 111(13):4788–4791, 2014. doi: 10.1073/pnas.1317606111.

[218] Colin J Gleason and Jida Wang. Theoretical basis for at-many-stations hydraulic geometry. *Geophysical Research Letters*, 42(17):7107–7114, 2015. doi: 10.1002/2015GL064935.

[219] MJ Tourian, C Schwatke, and N Sneeuw. River discharge estimation at daily resolution from satellite altimetry over an entire river basin. *Journal of Hydrology*, 546:230–247, 2017. doi: 10.1016/j.jhydrol.2017.01.009.

[220] George H Allen and Tamlin M Pavelsky. Global extent of rivers and streams. *Science*, 361(6402):585–588, 2018. doi: 10.1126/science.aat0636.

[221] Xiao Yang, Tamlin M Pavelsky, George H Allen, and Gennadii Donchyts. RivWidthCloud: An automated Google Earth Engine algorithm for river width extraction from remotely sensed imagery. *IEEE Geoscience and Remote Sensing Letters*, 17(2):217–221, 2019. doi: 10.1109/LGRS.2019.2920225.

[222] Renato Prata de Moraes Frasson, Tamlin M Pavelsky, Mark A Fonstad, Michael T Durand, George H Allen, Guy Schumann, Christine Lion, R Edward Beighley, and Xiao Yang. Global relationships between river width, slope, catchment area, meander wavelength, sinuosity, and discharge. *Geophysical Research Letters*, 46(6):3252–3262, 2019. doi: 10.1029/2019GL082027.

[223] Jet Propulsion Laboratory. Swot: Surface qater and ocean topography, 2019. URL `https://swot.jpl.nasa.gov`. [Online. Accessed: 2019-03-07].

[224] Cedric H. David, Konstantinos M. Andreadis, Edward Beighley, James S. Famiglietti, Aaron A. Boone, Vincent Fortin, Hyungjun Kim, Ernesto Rodriguez, and Dai Yamazaki. Integrating SWOT measurements into global hydrologic and hydraulic models, 2019. URL `https://swot.odyseallc.net/project-david.htm`. [Online. Accessed: 2020-08-18].

[225] Sylvain Biancamaria, Dennis P Lettenmaier, and Tamlin M Pavelsky. The swot mission and its capabilities for land hydrology. In *Remote Sensing and Water Resources*, pages 117–147. Springer, 2016. doi: 10.1007/978-3-319-32449-4_6.

[226] A Domeneghetti, GJ-P Schumann, RPM Frasson, R Wei, TM Pavelsky, A Castellarin, A Brath, and MT Durand. Characterizing water surface elevation under different flow conditions for the upcoming swot mission. *Journal of hydrology*, 561:848–861, 2018. doi: 10.1016/j.jhydrol.2018.04.046.

[227] Renato Prata de Moraes Frasson, Rui Wei, Michael Durand, J Toby Minear, Alessio Domeneghetti, Guy Schumann, Brent A Williams, Ernesto Rodriguez, Christophe Picamilh, Christine Lion, et al. Automated river reach definition strategies: Applications for the surface water and ocean topography mission. *Water Resources Research*, 53(10): 8164–8186, 2017. doi: 10.1002/2017WR020887.

[228] Tamlin M Pavelsky and Laurence C Smith. Rivwidth: A software tool for the calculation of river widths from remotely sensed imagery. *IEEE Geoscience and Remote Sensing Letters*, 5(1):70–73, 2008. doi: 10.1109/LGRS.2007.908305.

[229] George H Allen, Jason B Barnes, Tamlin M Pavelsky, and Eric Kirby. Lithologic and tectonic controls on bedrock channel form at the northwest Himalayan front. *Journal of Geophysical Research: Earth Surface*, 118(3):1806–1825, 2013. doi: 10.1002/jgrf.20113.

[230] F O'loughlin, MA Trigg, GJ-P Schumann, and PD Bates. Hydraulic characterization of the middle reach of the Congo River. *Water Resources Research*, 49(8):5059–5070, 2013. doi: 10.1002/wrcr.20398.

[231] Tamlin M Pavelsky, George H Allen, and Zachary F Miller. Spatial patterns of river width in the yukon river basin. In *Remote Sensing of the Terrestrial Water Cycle*, volume 206, page 131. American Geophysical Union (AGU), 2014.

[232] Zachary F Miller, TM Pavelsky, and GH Allen. Quantifying river form variations in the mississippi basin using remotely sensed imagery. *Hydrology and Earth System Sciences*, 18(12):4883–4895, 2014. doi: 10.5194/hess-18-4883-2014.

[233] G. Sofia, P. Tarolli, F. Cazorzi, and G. Dalla Fontana. Downstream hydraulic geometry relationships: Gathering reference reach-scale width values from lidar. *Geomorphology*, 250(nil):236–248, 2015. doi: 10.1016/j.geomorph.2015.09.002. URL `https://doi.org/10.1016/j.geomorph.2015.09.002`.

[234] Kang Yang, Manchun Li, Yongxue Liu, Liang Cheng, Qiuhao Huang, and Yangming Chen. River detection in remotely sensed imagery using gabor filtering and path opening. *Remote Sensing*, 7(7):8779–8802, 2015. doi: 10.3390/rs70708779.

[235] Joel C Rowland, Eitan Shelef, Paul A Pope, Jordan Muss, Chandana Gangodagamage, Steven P Brumby, and Cathy J Wilson. A morphology independent methodology for quantifying planview river change and characteristics from remotely sensed imagery. *Remote Sensing of Environment*, 184:212–228, 2016. doi: 10.1016/j.rse.2016.07.005.

[236] Jon Schwenk, Ankush Khandelwal, Mulu Fratkin, Vipin Kumar, and Efi Foufoula-Georgiou. High spatiotemporal resolution of river planform dynamics from Landsat: The RivMAP toolbox and results from the Ucayali River. *Earth and Space Science*, 4 (2):46–75, 2017. doi: 10.1002/2016EA000196.

[237] Antonius Golly and Jens M Turowski. Deriving principal channel metrics from bank and long-profile geometry with the R package cmgo. *Earth Surface Dynamics*, 5(3): 557, 2017. doi: 10.5194/esurf-5-557-2017.

[238] Furkan Isikdogan, Alan Bovik, and Paola Passalacqua. RivaMap: An automated river analysis and mapping engine. *Remote Sensing of Environment*, 202:88–97, 2017. doi: 10.1016/j.rse.2017.03.044.

[239] Federico Monegaglia, Guido Zolezzi, Inci Güneralp, Alexander J Henshaw, and Marco Tubino. Automated extraction of meandering river morphodynamics from multitemporal remotely sensed data. *Environmental Modelling & Software*, 105:171–186, 2018. doi: 10.1016/j.envsoft.2018.03.028.

[240] Michael D King, Steven Platnick, W Paul Menzel, Steven A Ackerman, and Paul A Hubanks. Spatial and temporal distribution of clouds observed by modis onboard the terra and aqua satellites. *IEEE Transactions on Geoscience and remote sensing*, 51(7): 3826–3852, 2013. doi: 10.1109/TGRS.2012.2227333.

[241] Christopher C Sampson, Andrew M Smith, Paul D Bates, Jeffrey C Neal, Lorenzo Alfieri, and Jim E Freer. A high-resolution global flood hazard model. *Water resources research*, 51(9):7358–7381, 2015. doi: 10.1002/2015WR016954.

[242] G Farina, S Alvisi, M Franchini, G Corato, and T Moramarco. Estimation of bathymetry (and discharge) in natural river cross-sections by using an entropy approach. *Journal of Hydrology*, 527:20–29, 2015. doi: 10.1016/j.jhydrol.2015.04.037.

[243] Laurence C Smith and Tamlin M Pavelsky. Estimation of river discharge, propagation speed, and hydraulic geometry from space: Lena River, Siberia. *Water Resources Research*, 44(3), 2008. doi: 10.1029/2007WR006133.

[244] Arthur P Cracknell. *Introduction to remote sensing*. CRC press, 2007.

[245] Jamie Carter, Keil Schmid, Kirk Waters, Lindy Betzhold, Brian Hadley, Rebecca Mataosky, and Jennifer Halleran. Lidar 101: An introduction to lidar technology, data, and applications. *National Oceanic and Atmospheric Administration (NOAA) Coastal Services Center, Charleston, South Carolina, coast. noaa. gov/digitalcoast/_/pdf/lidar101. pdf. Last accessed December*, 30:2015, 2012.

[246] Christian Venzin. Analyzing the impact of high resolution DEM uncertainty on hydrological models using a parallel computing approach. Master's thesis, University of Zurich, 2013.

[247] U.S. Geological Survey. Digital surface model of the west fork mine in missouri, 2020. URL `https://www.usgs.gov/media/images/digital-surface-model-west-fork-mine-missouri`. [Online. Accessed: 2020-02-05].

[248] I Molloy and Tomasz F Stepinski. Automatic mapping of valley networks on mars. *Computers & Geosciences*, 33(6):728–738, 2007. doi: 10.1016/j.cageo.2006.09.009.

[249] Nathalie Thommeret, Jean-Stéphane Bailly, and C Puech. Extraction of thalweg networks from DTMs: application to badlands. *Hydrology and Earth System Sciences*, 14 (8):1527–1536, 2010. doi: 10.5194/hess-14-1527-2010.

[250] Paola Passalacqua, Patrick Belmont, and Efi Foufoula-Georgiou. Automatic geomorphic feature extraction from lidar in flat and engineered landscapes. *Water Resources Research*, 48(3), 2012. doi: 10.1029/2011WR010958.

[251] Jon D Pelletier. A robust, two-parameter method for the extraction of drainage networks from high-resolution digital elevation models (DEMs): Evaluation using synthetic and real-world DEMs. *Water Resources Research*, 49(1):75–89, 2013. doi: 10.1029/2012WR012452.

[252] Fiona J Clubb, Simon M Mudd, David T Milodowski, Martin D Hurst, and Louise J Slater. Objective extraction of channel heads from high-resolution topographic data. *Water Resources Research*, 50(5):4283–4304, 2014. doi: 10.1002/2013WR015167.

[253] Giulia Sofia, Francesco Marinello, and Paolo Tarolli. A new landscape metric for the identification of terraced sites: the Slope Local Length of Auto-Correlation (SLLAC). *ISPRS Journal of Photogrammetry and Remote Sensing*, 96:123–133, 2014. doi: 10.1016/j.isprsjprs.2014.06.018.

[254] Jianping Chen, Ke Li, Kuo-Jen Chang, Giulia Sofia, and Paolo Tarolli. Open-pit mining geomorphic feature characterisation. *International Journal of Applied Earth Observation and Geoinformation*, 42:76–86, 2015. doi: 10.1016/j.jag.2015.05.001.

[255] Paolo Tarolli, Giulia Sofia, Simone Calligaro, Massimo Prosdocimi, Federico Preti, and Giancarlo Dalla Fontana. Vineyards in terraced landscapes: new opportunities from lidar data. *Land Degradation & Development*, 26(1):92–102, 2015. doi: 10.1002/ldr.2311.

[256] Massimo Prosdocimi, Simone Calligaro, Giulia Sofia, Giancarlo Dalla Fontana, and Paolo Tarolli. Bank erosion in agricultural drainage networks: new challenges from structure-from-motion photogrammetry for post-event analysis. *Earth Surface Processes and Landforms*, 40(14):1891–1906, 2015. doi: 10.1002/esp.3767.

[257] Giulia Sofia, Francesco Marinello, and Paolo Tarolli. Metrics for quantifying anthropogenic impacts on geomorphology: road networks. *Earth Surface Processes and Landforms*, 41(2):240–255, 2016. doi: 10.1002/esp.3842.

[258] R Weibel and M Heller. *Digital terrain modelling*. London: Longman, 1991.

[259] A Nelson, HI Reuter, and P Gessler. DEM production methods and sources. *Developments in soil science*, 33:65–85, 2009. doi: 10.1016/S0166-2481(08)00003-2.

[260] Laurence Hawker, Paul Bates, Jeffrey Neal, and Jonathan Rougier. Perspectives on digital elevation model (DEM) simulation for flood modeling in the absence of a high-accuracy open access global DEM. *Frontiers in Earth Science*, 6:233, 2018. doi: 10.3389/feart.2018.00233.

[261] Land Info Worldwide Mapping. Land Info Satellite Imagery Solutions & Digital Map Data, 2018. URL `http://www.landinfo.com`. [Online. Accessed: 2020-02-05].

[262] Matthias Ulmer. *Unsicherheitsanalyse und Validierung eines Modells der Hangstabilität*. PhD thesis, Geographisches Institut der Universität Zürich, 2007.

[263] Ernesto Rodriguez, Charles S Morris, and J Eric Belz. A global assessment of the srtm performance. *Photogrammetric Engineering & Remote Sensing*, 72(3):249–260, 2006. doi: 10.14358/PERS.72.3.249.

[264] Tesfaye H Tarekegn and Takahiro Sayama. Correction of srtm dem artefacts by fourier transform for flood inundation modeling. *Journal of Japan Society of Civil Engineers, Ser. B1 (Hydraulic Engineering)*, 69(4):I_193–I_198, 2013. doi: 10.2208/jscejhe.69.I_193.

[265] JC Gallant and A Read. Enhancing the SRTM data for Australia. *Proceedings of Geomorphometry*, 31:149–154, 2009.

[266] R Crippen, S Buckley, E Belz, E Gurrola, S Hensley, M Kobrick, M Lavalle, J Martin, M Neumann, Q Nguyen, et al. Nasadem global elevation model: methods and progress. 2016.

[267] Junichi Takaku, Akira Iwasaki, and Takeo Tadono. Adaptive filter for improving quality of ALOS PRISM DSM. In *2016 IEEE International Geoscience and Remote Sensing Symposium (IGARSS)*, pages 5370–5373. IEEE, 2016. doi: 10.1109/IGARSS.2016.7730399.

[268] FE O'Loughlin, RCD Paiva, M Durand, DE Alsdorf, and PD Bates. A multi-sensor approach towards a global vegetation corrected SRTM DEM product. *Remote Sensing of Environment*, 182:49–59, 2016. doi: 10.1016/j.rse.2016.04.018.

[269] Stephen Wise. Assessing the quality for hydrological applications of digital elevation models derived from contours. *Hydrological processes*, 14(11-12):1909–1929, 2000. doi: 10.1002/1099-1085(20000815/30)14:11/12%3C1909::AID-HYP45%3E3.0.CO;2-6.

[270] HI Reuter, T Hengl, P Gessler, and Pierre Soille. Preparation of DEMs for geomorphometric analysis. *Developments in soil science*, 33:87–120, 2009. doi: 10.1016/S0166-2481(08)00004-4.

[271] Felix Hebeler and Ross S Purves. The influence of elevation uncertainty on derivation of topographic indices. *Geomorphology*, 111(1-2):4–16, 2009. doi: 10.1016/j.geomorph.2007.06.026.

[272] Jet Propulsion Laboratory. U.S. releases enhanced shuttle land elevation data, 2018. URL `https://www2.jpl.nasa.gov/srtm/`. [Online. Accessed: 2018-11-29].

[273] Tom G Farr and Mike Kobrick. Shuttle radar topography mission produces a wealth of data. *Eos, Transactions American Geophysical Union*, 81(48):583–585, 2000. doi: 10.1029/EO081i048p00583.

[274] Richard Bamler et al. The SRTM mission: A world-wide 30 m resolution DEM from SAR interferometry in 11 days. In *Photogrammetric week*, volume 99, pages 145–154. Berlin, Germany: Wichmann Verlag, 1999.

[275] Peter G Chirico, Katherine C Malpeli, and Sarah M Trimble. Accuracy evaluation of an ASTER-derived global digital elevation model (GDEM) version 1 and version 2 for two sites in western Africa. *GIScience & remote sensing*, 49(6):775–801, 2012. doi: 10.2747/1548-1603.49.6.775.

[276] Djamel Athmania and Hammadi Achour. External validation of the ASTER GDEM2, GMTED2010 and CGIAR-CSI-SRTM v4. 1 free access digital elevation models (DEMs) in Tunisia and Algeria. *Remote Sensing*, 6(5):4600–4620, 2014. doi: 10.3390/rs6054600.

[277] Moritz Rexer and Christian Hirt. Comparison of free high resolution digital elevation data sets (ASTER GDEM2, SRTM v2. 1/v4. 1) and validation against accurate heights from the Australian National Gravity Database. *Australian Journal of Earth Sciences*, 61(2):213–226, 2014. doi: 10.1080/08120099.2014.884983.

[278] Jet Propulsion Laboratory. Pia04965: Srtm data release for africa, colored height, 2004. URL `https://photojournal.jpl.nasa.gov/catalog/PIA04965`. [Online. Accessed: 2018-11-29].

[279] Dai Yamazaki, Daiki Ikeshima, Ryunosuke Tawatari, Tomohiro Yamaguchi, Fiachra O'Loughlin, Jeffery C Neal, Christopher C Sampson, Shinjiro Kanae, and Paul D Bates. A high-accuracy map of global terrain elevations. *Geophysical Research Letters*, 44(11): 5844–5853, 2017. doi: 10.1002/2017GL072874.

[280] Huili Chen, Qiuhua Liang, Yong Liu, and Shuguang Xie. Hydraulic correction method (HCM) to enhance the efficiency of SRTM DEM in flood modeling. *Journal of Hydrology*, 559:56–70, 2018. doi: 10.1016/j.jhydrol.2018.01.056.

[281] Laurence Hawker, Jonathan Rougier, Jeffrey Neal, Paul Bates, Leanne Archer, and Dai Yamazaki. Implications of simulating global digital elevation models for flood inundation studies. *Water resources research*, 54(10):7910–7928, 2018. doi: 10.1029/2018WR023279.

[282] Laurence Hawker, Jeffrey Neal, and Paul Bates. Accuracy assessment of the TanDEM-X 90 digital elevation model for selected floodplain sites. *Remote Sensing of Environment*, 232:111319, 2019. doi: 10.1016/j.rse.2019.111319.

[283] Tom G Farr, Paul A Rosen, Edward Caro, Robert Crippen, Riley Duren, Scott Hensley, Michael Kobrick, Mimi Paller, Ernesto Rodriguez, Ladislav Roth, et al. The shuttle radar topography mission. *Reviews of geophysics*, 45(2), 2007. doi: 10.1029/2005RG000183.

[284] Jet Propulsion Laboratory. Aster global digital elevation map announcement, 2012. URL `https://asterweb.jpl.nasa.gov/gdem.asp`. [Online. Accessed: 2019-03-07].

[285] Gerhard Krieger, Alberto Moreira, Hauke Fiedler, Irena Hajnsek, Marian Werner, Marwan Younis, and Manfred Zink. TanDEM-X: A satellite formation for high-resolution SAR interferometry. *IEEE Transactions on Geoscience and Remote Sensing*, 45(11): 3317–3341, 2007. doi: 10.1109/TGRS.2007.900693.

[286] Manfred Zink, Markus Bachmann, Benjamin Brautigam, Thomas Fritz, Irena Hajnsek, Alberto Moreira, Birgit Wessel, and Gerhard Krieger. TanDEM-X: The new global DEM takes shape. *IEEE Geoscience and Remote Sensing Magazine*, 2(2):8–23, 2014. doi: 10.1109/MGRS.2014.2318895.

[287] Paola Rizzoli, Michele Martone, Carolina Gonzalez, Christopher Wecklich, Daniela Borla Tridon, Benjamin Bräutigam, Markus Bachmann, Daniel Schulze, Thomas Fritz, Martin Huber, et al. Generation and performance assessment of the global TanDEM-X digital elevation model. *ISPRS Journal of Photogrammetry and Remote Sensing*, 132:119–139, 2017. doi: 10.1016/j.isprsjprs.2017.08.008.

[288] B Wessel. TanDEM-X Ground Segment–DEM Products Specification Document, EOC, DLR, Oberpfaffenhofen, Germany, Public Document TD-GS-PS-0021, Issue 3.1, 2016.

[289] Birgit Wessel, Martin Huber, Christian Wohlfart, Ursula Marschalk, Detlev Kosmann, and Achim Roth. Accuracy assessment of the global TanDEM-X digital elevation model with GPS data. *ISPRS Journal of Photogrammetry and Remote Sensing*, 139:171–182, 2018. doi: 10.1016/j.isprsjprs.2018.02.017.

[290] Carolina Gonzalez and Paola Rizzoli. Landcover-dependent assessment of the relative height accuracy in TanDEM-X DEM products. *IEEE Geoscience and Remote Sensing Letters*, 15(12):1892–1896, 2018. doi: 10.1109/LGRS.2018.2864774.

[291] Richard John Huggett. *Fundamentals of Geomorphology*. Routledge, 2017. ISBN 1138940658.

[292] Ross D Arnold and Jon P Wade. A definition of systems thinking: A systems approach. *Procedia computer science*, 44:669–678, 2015. doi: 10.1016/j.procs.2015.03.050.

[293] Richard J Chorley and Barbara A Kennedy. *Physical geography: a systems approach*. Prentice Hall, 1971.

[294] Alan H Strahler. The use of prior probabilities in maximum likelihood classification of remotely sensed data. *Remote sensing of Environment*, 10(2):135–163, 1980. doi: 10.1016/0034-4257(80)90011-5.

[295] Günther Grill. Free-flow river assessment documentation, 2017. URL `http://hydrolab.io/docs/`. [Online. Accessed: 2019-05-03].

[296] Peter E. Robins, Matt J. Lewis, Jim Freer, David M. Cooper, Christopher J. Skinner, and Tom J. Coulthard. Improving estuary models by reducing uncertainties associated with river flows. *Estuarine, Coastal and Shelf Science*, 207(nil):63–73, 2018. doi: 10.1016/j.ecss.2018.02.015. URL `https://doi.org/10.1016/j.ecss.2018.02.015`.

[297] Luna B. Leopold and Thomas Maddock. The hydraulic geometry of stream channels and some physiographic implications. *U.S. Geological Survey Professional Paper*, 252: 481–492, 1953.

[298] Vijay P Singh. On the theories of hydraulic geometry. *International journal of sediment research*, 18(3):196–218, 2003.

[299] R.J. Chorley. *Introduction to Physical Hydrology*. University Paperbacks. Methuen, 1973.

[300] David M Bjerklie, S Lawrence Dingman, Charles J Vorosmarty, Carl H Bolster, and Russell G Congalton. Evaluating the potential for measuring river discharge from space. *Journal of Hydrology*, 278(1-4):17–38, 2003. doi: 10.1016/S0022-1694(03)00129-X.

[301] Markley Gordon Wolman. *The natural channel of Brandywine creek, Pennsylvania*, volume 271. US Government Printing Office, 1955.

[302] A David Knighton. Variation in width-discharge relation and some implications for hydraulic geometry. *Geological Society of America Bulletin*, 85(7):1069–1076, 1974. doi: 10.1130/0016-7606(1974)85%3C1069:VIWRAS%3E2.0.CO;2.

[303] Ronald L Shreve. The probabilistic-topologic approach to drainage-basin geomorphology. *Geology*, 3(9):527–529, 1975. doi: 10.1130/0091-7613(1975)3%3C527:TPATDG%3E2.0.CO;2.

[304] Arthur N Strahler. Dynamic basis of geomorphology. *Geological Society of America Bulletin*, 63(9):923–938, 1952. doi: 10.1130/0016-7606(1952)63[923:DBOG]2.0.CO;2.

[305] GH Dury. Bed-width and wave-length in meandering valleys. *Nature*, 176(4470):31, 1955. doi: 10.1038/176031a0.

[306] Luna Bergere Leopold and Markley Gordon Wolman. *River channel patterns: braided, meandering, and straight*. US Government Printing Office, 1957.

[307] Stanley Alfred Schumm. The shape of alluvial channels in relation to sediment type. *US Geol. Survey Prof Paper., B*, 352:17–30, 1960.

[308] Charles W Carlston. The relation of free meander geometry to stream discharge and its geomorphic implications. *American Journal of Science*, 263(10):864–885, 1965. doi: 10.2475/ajs.263.10.864.

[309] Rolf Kellerhals. Stable channels with gravel-paved beds. *Journal of the Waterways and Harbors Division*, 93(1):63–84, 1967. doi: 10.1061/JWHEAU.0000482.

[310] Luna B Leopold and M Gordon Wolman. River meanders. *Geological Society of America Bulletin*, 71(6):769–793, 1960.

[311] Stuart N. Lane and Keith S. Richards. Linking river channel form and process: Time, space and causality revisited. *Earth Surface Processes and Landforms*, 22(3):249–260, 1997. doi: 10.1002/(sici)1096-9837(199703)22:3$<$249::aid-esp752>3.0.co;2-7.

[312] JH Mackin. Methods of investigation in geology: in the fabric of geology, ed. cc albritton, jr, 1963.

[313] LB Leopold and WB Langbein. Association and indeterminacy in geomorphology, the fabric of geology, 184–192, 1963.

[314] Chris C Park. World-wide variations in hydraulic geometry exponents of stream channels: an analysis and some observations. *Journal of Hydrology*, 33(1-2):133–146, 1977. doi: 10.1016/0022-1694(77)90103-2.

[315] Bofu Yu and M Gordon Wolman. Some dynamic aspects of river geometry. *Water Resources Research*, 23(3):501–509, 1987. doi: 10.1029/WR023i003p00501.

[316] KS Richards. Complex width-discharge relations in natural river sections. *Geological Society of America Bulletin*, 87(2):199–206, 1976. doi: 10.1130/0016-7606(1976)87%3C199:CWRINR%3E2.0.CO;2.

[317] Jonathan D Phillips. The instability of hydraulic geometry. *Water Resources Research*, 26(4):739–744, 1990. doi: 10.1029/WR026i004p00739.

[318] IG Jowett. Hydraulic geometry of new zealand rivers and its use as a preliminary method of habitat assessment. *Regulated Rivers: Research & Management: An International Journal Devoted to River Research and Management*, 14(5):451–466, 1998. doi: 10.1002/(SICI)1099-1646(1998090)14:5%3C451::AID-RRR512%3E3.0.CO;2-1.

[319] Boyko Dodov and Efi Foufoula-Georgiou. Generalized hydraulic geometry: Derivation based on a multiscaling formalism. *Water resources research*, 40(6), 2004. doi: 10.1029/2003WR002082.

[320] Michael Stewardson. Hydraulic geometry of stream reaches. *Journal of hydrology*, 306 (1-4):97–111, 2005. doi: 10.1016/j.jhydrol.2004.09.004.

[321] MA Carson and MF Lapointe. The inherent asymmetry of river meander planform. *The Journal of Geology*, 91(1):41–55, 1983. doi: 10.1086/628743.

[322] William E Dietrich and J Dungan Smith. Influence of the point bar on flow through curved channels. *Water Resources Research*, 19(5):1173–1192, 1983. doi: 10.1029/WR019i005p01173.

[323] William E Dietrich and J Dungan Smith. Bed load transport in a river meander. *Water Resources Research*, 20(10):1355–1380, 1984. doi: 10.1029/WR020i010p01355.

[324] PJ Ashworth and RI Ferguson. Interrelationships of channel processes, changes and sediments in a proglacial braided river. *Geografiska Annaler: Series A, Physical Geography*, 68(4):361–371, 1986. doi: 10.1080/04353676.1986.11880186.

[325] James L Best. The morphology of river channel confluences. *Progress in Physical Geography*, 10(2):157–174, 1986. doi: 10.1177/030913338601000201.

[326] WE Dietrich. Mechanics of flow and sediment transport in river bends, river channels, environment and process ks richards, 179–227, 1987.

[327] AndréG Roy and Normand Bergeron. Flow and particle paths at a natural river confluence with coarse bed material. *Geomorphology*, 3(2):99–112, 1990. doi: 10.1016/0169-555X(90)90039-S.

[328] PE Ashmore, RI Ferguson, KL Prestegaard, PJ Ashworth, and Chris Paola. Secondary flow in anabranch confluences of a braided, gravel-bed stream. *Earth Surface Processes and Landforms*, 17(3):299–311, 1992. doi: 10.1002/esp.3290170308.

[329] NJ Clifford and KS Richards. The reversal hypothesis and the maintenance of riffle-pool sequences: A review and field appraisal. *Lowland floodplain rivers: Geomorphological perspectives*, pages 43–70, 1992.

[330] JB Laronne and MJ Duncan. Bedload transport paths and gravel bar formation. *Dynamics of gravel-bed rivers*, pages 177–202, 1992.

[331] Jeff Warburton. Observations of bed load transport and channel bed changes in a proglacial mountain stream. *Arctic and Alpine Research*, 24(3):195–203, 1992. doi: 10.1080/00040851.1992.12002946.

[332] P Biron, B De Serres, AG Roy, and JL Best. Shear layer turbulence at an unequal depth channel confluence. *Turbulence: Perspectives on flow and sediment transport*, pages 197–213, 1993.

[333] James R Goff and Peter Ashmore. Gravel transport and morphological change in braided sunwapta river, alberta, canada. *Earth Surface Processes and Landforms*, 19(3):195–212, 1994. doi: 10.1002/esp.3290190302.

[334] SN Lane, KS Richards, and JH Chandler. Morphological estimation of the time-integrated bed load transport rate. *Water Resources Research*, 31(3):761–772, 1995. doi: 10.1029/94WR01726.

[335] Bruce L Rhoads and Stephen T Kenworthy. Flow structure at an asymmetrical stream confluence. *Geomorphology*, 11(4):273–293, 1995. doi: 10.1016/0169-555X(94)00069-4.

[336] Robert I Ferguson. Hydraulics and hydraulic geometry. *Progress in Physical Geography*, 10(1):1–31, 1986. doi: 10.1177/030913338601000101.

[337] Colin J. Gleason. Hydraulic geometry of natural rivers. *Progress in Physical Geography*, 39(3):337–360, 2015. doi: 10.1177/0309133314567584. URL `https://doi.org/10.1177/0309133314567584`.

[338] Theodore K Miller. An assessment of the equable change principle in at-a-station hydraulic geometry. *Water resources research*, 27(10):2751–2758, 1991. doi: 10.1029/91WR01716.

[339] Gregory S Ridenour and John R Giardino. The statistical study of hydraulic geometry: a new direction for compositional data analysis. *Mathematical Geology*, 23(3):349–366, 1991. doi: 10.1007/BF02065787.

[340] Gregory S Ridenour and John R Giardino. Logratio linear modelling of hydraulic geometry using indices of flow resistance as covariates. *Geomorphology*, 14(1):65–72, 1995. doi: 10.1016/0169-555X(95)00018-Z.

[341] Stephen E Darby. Refined hydraulic geometry data for british gravel-bed rivers. *Journal of Hydraulic Engineering*, 131(1):60–64, 2005. doi: 10.1061/(ASCE)0733-9429(2005)131:1(60).

[342] Nicholas Pinter and Reuben A Heine. Hydrodynamic and morphodynamic response to river engineering documented by fixed-discharge analysis, lower missouri river, usa. *Journal of Hydrology*, 302(1-4):70–91, 2005. doi: 10.1016/j.jhydrol.2004.06.039.

[343] S Lawrence Dingman. Analytical derivation of at-a-station hydraulic–geometry relations. *Journal of Hydrology*, 334(1-2):17–27, 2007. doi: 10.1016/j.jhydrol.2006.09.021.

[344] Rachel A Nanson, Gerald C Nanson, and He Qing Huang. The hydraulic geometry of narrow and deep channels; evidence for flow optimisation and controlled peatland growth. *Geomorphology*, 117(1-2):143–154, 2010. doi: 10.1016/j.geomorph.2009.11.021.

[345] Donald E Reid, Edward J Hickin, and Scott C Babakaiff. Low-flow hydraulic geometry of small, steep mountain streams in southwest british columbia. *Geomorphology*, 122 (1-2):39–55, 2010. doi: 10.1016/j.geomorph.2010.05.012.

[346] Jim McKean, Dave Nagel, Daniele Tonina, Philip Bailey, Charles Wayne Wright, Carolyn Bohn, and Amar Nayegandhi. Remote sensing of channels and riparian zones with a narrow-beam aquatic-terrestrial LIDAR. *Remote Sensing*, 1(4):1065–1096, 2009. doi: 10.3390/rs1041065.

[347] Kasper Johansen, Dirk Tiede, Thomas Blaschke, Lara A Arroyo, and Stuart Phinn. Automatic geographic object based mapping of streambed and riparian zone extent from LiDAR data in a temperate rural urban environment, Australia. *Remote Sensing*, 3(6): 1139–1156, 2011. doi: 10.3390/rs3061139.

[348] Pascale M Biron, Guénolé Choné, Thomas Buffin-Bélanger, Sylvio Demers, and Taylor Olsen. Improvement of streams hydro-geomorphological assessment using LiDAR DEMs. *Earth Surface Processes and Landforms*, 38(15):1808–1821, 2013. doi: 10.1002/esp.3425.

[349] G Burch Fisher, Bodo Bookhagen, and Colin B Amos. Channel planform geometry and slopes from freely available high-spatial resolution imagery and DEM fusion: Implications for channel width scalings, erosion proxies, and fluvial signatures in tectonically active landscapes. *Geomorphology*, 194:46–56, 2013. doi: 10.1016/j.geomorph.2013.04.011.

[350] İnci Güneralp, Anthony M Filippi, and Billy Hales. Influence of river channel morphology and bank characteristics on water surface boundary delineation using high-resolution passive remote sensing and template matching. *Earth Surface Processes and Landforms*, 39(7):977–986, 2014. doi: 10.1002/esp.3560.

[351] Sara G Bangen, Joseph M Wheaton, Nicolaas Bouwes, Boyd Bouwes, and Chris Jordan. A methodological intercomparison of topographic survey techniques for characterizing wadeable streams and rivers. *Geomorphology*, 206. doi: 10.1016/j.geomorph.2013.10.010.

[352] George L Heritage, David J Milan, Andrew RG Large, and Ian C Fuller. Influence of survey strategy and interpolation model on DEM quality. *Geomorphology*, 112(3-4): 334–344. doi: 10.1016/j.geomorph.2009.06.024.

[353] David J Milan, George L Heritage, Andrew RG Large, and Ian C Fuller. Filtering spatial error from DEMs: Implications for morphological change estimation. *Geomorphology*, 125(1):160–171. doi: 10.1016/j.geomorph.2010.09.012.

[354] W Andrew Marcus. Remote sensing of the hydraulic environment in gravel-bed rivers. *Gravel-bed rivers: Processes, tools, environments*, pages 259–285, 2012. doi: 10.1002/9781119952497.ch21.

[355] Giulia Sofia, Giancarlo Dalla Fontana, and Paolo Tarolli. High-resolution topography and anthropogenic feature extraction: testing geomorphometric parameters in floodplains. *Hydrological Processes*, 28(4):2046–2061, 2014. doi: 10.1002/hyp.9727.

[356] Giulia Sofia, Massimo Prosdocimi, Giancarlo Dalla Fontana, and Paolo Tarolli. Modification of artificial drainage networks during the past half-century: Evidence and effects in a reclamation area in the veneto floodplain (italy). *Anthropocene*, 6:48–62, 2014. doi: 10.1016/j.ancene.2014.06.005.

[357] J. S Bridge. *Rivers and floodplains : forms, processes, and sedimentary record*. Blackwell Pub., Malden, MA, 2003. ISBN 0632064897.

[358] JN Callow and GS Boggs. Studying reach-scale spatial hydrology in ungauged catchments. *Journal of Hydrology*, 496:31–46, 2013. doi: 10.1016/j.jhydrol.2013.05.030.

[359] Peirong Lin, Ming Pan, Hylke E Beck, Yuan Yang, Dai Yamazaki, Renato Frasson, Cédric H David, Michael Durand, Tamlin M Pavelsky, George H Allen, et al. Global reconstruction of naturalized river flows at 2.94 million reaches. *Water Resources Research*, 55(8):6499–6516, 2019. doi: 10.1029/2019WR025287.

[360] Colin F Byrne, Gregory B Pasternack, Hervé Guillon, Belize A Lane, and Samuel Sandoval-Solis. Reach-scale bankfull channel types can exist independently of catchment hydrology. *Earth Surface Processes and Landforms*, 45(9):2179–2200, 2020. doi: 10.1002/esp.4874.

[361] Ben R Hodges, Frank Liu, et al. *Rivers and Electric Networks: Crossing Disciplines in Modeling and Simulation*. Now Publishers, 2014.

[362] David M Hannah, Siegfried Demuth, Henny AJ van Lanen, Ulrich Looser, Christel Prudhomme, Gwyn Rees, Kerstin Stahl, and Lena M Tallaksen. Large-scale river flow archives: importance, current status and future needs. *Hydrological Processes*, 25(7): 1191–1200, 2011. doi: 10.1002/hyp.7794.

[363] Tamlin M Pavelsky, Michael T Durand, Konstantinos M Andreadis, R Edward Beighley, Rodrigo CD Paiva, George H Allen, and Zachary F Miller. Assessing the potential global extent of SWOT river discharge observations. *Journal of Hydrology*, 519:1516–1525, 2014. doi: 10.1016/j.jhydrol.2014.08.044.

[364] Gemma Coxon, Jim Freer, Rosanna Lane, Toby Dunne, Wouter JM Knoben, Nicholas JK Howden, Niall Quinn, Thorsten Wagener, and Ross Woods. Decipher v1: Dynamic fluxes and connectivity for predictions of hydrology. *Geoscientific Model Development*, 12(6):2285–2306, 2019. doi: 10.5194/gmd-12-2285-2019.

[365] Vijay P Singh and Donald K Frevert. *Mathematical models of large watershed hydrology*. Water Resources Publication, 2002.

[366] Gerald Augusto Corzo Perez. *Hybrid models for hydrological forecasting: Integration of data-driven and conceptual modelling techniques*. IHE Delft Institute for Water Education, 2009.

[367] AD PJ De Roo, Ben Gouweleeuw, Jutta Thielen, Jens Bartholmes, Paolina Bongioannini-Cerlini, Ezio Todini, Paul D Bates, Matt Horritt, Neil Hunter, Keith Beven, et al. Development of a European flood forecasting system. *International Journal of River Basin Management*, 1(1):49–59, 2003. doi: 10.1080/15715124.2003.9635192.

[368] Florence Habets, Pierre Etchevers, Catherine Golaz, Etienne Leblois, Emmanuel Ledoux, Eric Martin, Joël Noilhan, and Catherine Ottlé. Simulation of the water budget and the river flows of the Rhone basin. *Journal of Geophysical Research: Atmospheres*, 104(D24):31145–31172, 1999. doi: 10.1029/1999JD901008.

[369] F Habets, J Noilhan, C Golaz, JP Goutorbe, P Lacarrere, E Leblois, E Ledoux, E Martin, C Ottlé, and D Vidal-Madjar. The ISBA surface scheme in a macroscale hydrological model applied to the Hapex-Mobilhy area: Part i: Model and database. *Journal of Hydrology*, 217(1-2):75–96, 1999. doi: 10.1016/S0022-1694(99)00019-0.

[370] F Habets, J Noilhan, C Golaz, JP Goutorbe, P Lacarrere, E Leblois, E Ledoux, E Martin, C Ottlé, and D Vidal-Madjar. The ISBA surface scheme in a macroscale hydrological model applied to the Hapex-Mobilhy area: Part ii: Simulation of streamflows and annual water budget. *Journal of Hydrology*, 217(1-2):97–118, 1999. doi: 10.1016/S0022-1694(99)00020-7.

[371] Florence Habets, Aaron Boone, Jean-Louis Champeaux, Pierre Etchevers, Laurent Franchisteguy, Etienne Leblois, Emmanuel Ledoux, P Le Moigne, Eric Martin, Sophie Morel, et al. The SAFRAN-ISBA-MODCOU hydrometeorological model applied over France. *Journal of Geophysical Research: Atmospheres*, 113(D6), 2008. doi: 10.1029/2007JD008548.

[372] Dag Lohmann, Ehrhard Raschke, Bart Nijssen, and DP Lettenmaier. Regional scale hydrology: I. Formulation of the VIC-2L model coupled to a routing model. *Hydrological sciences journal*, 43(1):131–141, 1998. doi: 10.1080/02626669809492107.

[373] Dag Lohmann, Ehrhard Raschke, Bart Nijssen, and DP Lettenmaier. Regional scale hydrology: II. Application of the VIC-2L model to the Weser River, Germany. *Hydrological sciences journal*, 43(1):143–158, 1998. doi: 10.1080/02626669809492108.

[374] Dag Lohmann, Kenneth E Mitchell, Paul R Houser, Eric F Wood, John C Schaake, Alan Robock, Brian A Cosgrove, Justin Sheffield, Qingyun Duan, Lifeng Luo, et al. Streamflow and water balance intercomparisons of four land surface models in the North American Land Data Assimilation System project. *Journal of Geophysical Research: Atmospheres*, 109(D7), 2004. doi: 10.1029/2003JD003517.

[375] Edwin P Maurer, Greg M O'Donnell, Dennis P Lettenmaier, and John O Roads. Evaluation of the land surface water budget in NCEP/NCAR and NCEP/DOE reanalyses using an off-line hydrologic model. *Journal of Geophysical Research: Atmospheres*, 106(D16):17841–17862, 2001. doi: 10.1029/2000JD900828.

[376] Taikan Oki, Yasushi Agata, Shinjiro Kanae, Takao Saruhashi, Dawen Yang, and Katumi Musiake. Global assessment of current water resources using total runoff integrating pathways. *Hydrological Sciences Journal*, 46(6):983–995, 2001. doi: 10.1080/02626660109492890.

[377] Francisco Olivera, James Famiglietti, and Kwabena Asante. Global-scale flow routing using a source-to-sink algorithm. *Water Resources Research*, 36(8):2197–2207, 2000. doi: 10.1029/2000WR900113.

[378] Bernhard Lehner, Kris Verdin, and Andy Jarvis. HydroSHEDS technical documentation, version 1.0. *World Wildlife Fund US, Washington, DC*, 2006.

[379] Cédric H David, David R Maidment, Guo-Yue Niu, Zong-Liang Yang, Florence Habets, and Victor Eijkhout. River network routing on the NHDPlus dataset. *Journal of Hydrometeorology*, 12(5):913–934, 2011. doi: 10.1175/2011JHM1345.1.

[380] Cédric H. David. Rapid v1.7.0.

[381] Hylke E Beck, Eric F Wood, Ming Pan, Colby K Fisher, Diego G Miralles, Albert IJM Van Dijk, Tim R McVicar, and Robert F Adler. MSWEP V2 global 3-hourly 0.1° precipitation: methodology and quantitative assessment. *Bulletin of the American Meteorological Society*, 100(3):473–500, 2019.

[382] Hui Zheng, Zong-Liang Yang, Peirong Lin, Jiangfeng Wei, Wen-Ying Wu, Lingcheng Li, Long Zhao, and Shu Wang. On the sensitivity of the precipitation partitioning into evapotranspiration and runoff in land surface parameterizations. *Water Resources Research*, 55(1):95–111, 2019. doi: 10.1029/2017WR022236.

[383] Luis Samaniego, Rohini Kumar, and Sabine Attinger. Multiscale parameter regionalization of a grid-based hydrologic model at the mesoscale. *Water Resources Research*, 46 (5), 2010. doi: 10.1029/2008WR007327.

[384] Marc FP Bierkens, Victoria A Bell, Peter Burek, Nathaniel Chaney, Laura E Condon, Cédric H David, Ad de Roo, Petra Döll, Niels Drost, James S Famiglietti, et al. Hyperresolution global hydrological modelling: what is next? "Everywhere and locally relevant". *Hydrological processes*, 29(2):310–320, 2015. doi: 10.1002/hyp.10391.

[385] Fayez A Abdulla and Dennis P Lettenmaier. Development of regional parameter estimation equations for a macroscale hydrologic model. *Journal of hydrology*, 197(1-4): 230–257, 1997. doi: 10.1016/S0022-1694(96)03262-3.

[386] Jan Seibert. Regionalisation of parameters for a conceptual rainfall-runoff model. *Agricultural and forest meteorology*, 98:279–293, 1999. doi: 10.1016/S0168-1923(99)00105-7.

[387] Yeshewatesfa Hundecha, Taha BMJ Ouarda, and András Bárdossy. Regional estimation of parameters of a rainfall-runoff model at ungauged watersheds using the "spatial" structures of the parameters within a canonical physiographic-climatic space. *Water Resources Research*, 44(1), 2008. doi: 10.1029/2006WR005439.

[388] Markus Hrachowitz, HHG Savenije, G Blöschl, JJ McDonnell, M Sivapalan, JW Pomeroy, Berit Arheimer, Theresa Blume, MP Clark, U Ehret, et al. A decade of predictions in ungauged basins (PUB)—a review. *Hydrological sciences journal*, 58 (6):1198–1255, 2013. doi: 10.1080/02626667.2013.803183.

[389] Hilary K McMillan, Martyn P Clark, William B Bowden, Maurice Duncan, and Ross A Woods. Hydrological field data from a modeller's perspective: Part 1. Diagnostic tests for model structure. *Hydrological Processes*, 25(4):511–522, 2011. doi: 10.1002/hyp.7841.

[390] Martyn P Clark, Hilary K McMillan, Daniel BG Collins, Dmitri Kavetski, and Ross A Woods. Hydrological field data from a modeller's perspective: Part 2: process-based evaluation of model hypotheses. *Hydrological Processes*, 25(4):523–543, 2011. doi: 10.1002/hyp.7902.

[391] Fabrizio Fenicia, Dmitri Kavetski, Hubert HG Savenije, Martyn P Clark, Gerrit Schoups, Laurent Pfister, and Jim Freer. Catchment properties, function, and conceptual model representation: is there a correspondence? *Hydrological Processes*, 28(4):2451–2467, 2014. doi: 10.1002/hyp.9726.

[392] Jeffrey J McDonnell and Keith Beven. Debates—The future of hydrological sciences: A (common) path forward? A call to action aimed at understanding velocities, celerities and residence time distributions of the headwater hydrograph. *Water Resources Research*, 50(6):5342–5350, 2014. doi: 10.1002/2013WR015141.

[393] Upmanu Lall. Debates—The future of hydrological sciences: A (common) path forward? One water. One world. Many climes. Many souls. *Water resources research*, 50 (6):5335–5341, 2014. doi: 10.1002/2014WR015402.

[394] Hoshin V Gupta and Grey S Nearing. Debates—The future of hydrological sciences: A (common) path forward? Using models and data to learn: A systems theoretic perspective on the future of hydrological science. *Water Resources Research*, 50(6):5351–5359, 2014. doi: 10.1002/2013WR015096.

[395] Rocko A Brown and Gregory B Pasternack. Engineered channel controls limiting spawning habitat rehabilitation success on regulated gravel-bed rivers. *Geomorphology*, 97 (3-4):631–654, 2008. doi: 10.1016/j.geomorph.2007.09.012.

[396] Oldrich Navratil and M-B Albert. Non-linearity of reach hydraulic geometry relations. *Journal of Hydrology*, 388(3-4):280–290, 2010. doi: 10.1016/j.jhydrol.2010.05.007.

[397] Xu Liang, Dennis P Lettenmaier, Eric F Wood, and Stephen J Burges. A simple hydrologically based model of land surface water and energy fluxes for general circulation models. *Journal of Geophysical Research: Atmospheres*, 99(D7):14415–14428, 1994. doi: 10.1029/94JD00483.

[398] Joseph J Hamman, Bart Nijssen, Theodore J Bohn, Diana R Gergel, and Yixin Mao. The Variable Infiltration Capacity model version 5 (VIC-5): infrastructure improvements for new applications and reproducibility. *Geoscientific Model Development (Online)*, 11(8), 2018. doi: 10.5194/gmd-11-3481-2018.

[399] Keith Beven and Jim Freer. A dynamic TOPMODEL. *Hydrological processes*, 15(10): 1993–2011, 2001. doi: 10.1002/hyp.252.

[400] Jim E Freer, H McMillan, JJ McDonnell, and KJ Beven. Constraining dynamic TOPMODEL responses for imprecise water table information using fuzzy rule based performance measures. *Journal of Hydrology*, 291(3-4):254–277, 2004. doi: 10.1016/j.jhydrol.2003.12.037.

[401] Yanli Liu, Jim Freer, Keith Beven, and Patrick Matgen. Towards a limits of acceptability approach to the calibration of hydrological models: Extending observation error. *Journal of Hydrology*, 367(1-2):93–103, 2009. doi: 10.1016/j.jhydrol.2009.01.016.

[402] Peter Metcalfe, Keith Beven, Barry Hankin, and Rob Lamb. A modelling framework for evaluation of the hydrological impacts of nature-based approaches to flood risk management, with application to in-channel interventions across a 29-km^2 scale catchment in the United Kingdom. *Hydrological Processes*, 31(9):1734–1748, 2017. doi: 10.1002/hyp.11140.

[403] Trevor Page, Keith J Beven, Jim Freer, and Colin Neal. Modelling the chloride signal at Plynlimon, Wales, using a modified dynamic TOPMODEL incorporating conservative chemical mixing (with uncertainty). *Hydrological Processes: An International Journal*, 21(3):292–307, 2007. doi: 10.1002/hyp.6186.

[404] Phil M Younger, AM Gadian, C-G Wang, JE Freer, and Keith J Beven. The usability of 250 m resolution data from the UK Meteorological Office Unified Model as input data for a hydrological model. *Meteorological Applications: A journal of forecasting, practical applications, training techniques and modelling*, 15(2):207–217, 2008. doi: 10.1002/met.46.

[405] AJ Newman, MP Clark, Kevin Sampson, Andrew Wood, LE Hay, A Bock, RJ Viger, D Blodgett, L Brekke, JR Arnold, et al. Development of a large-sample watershed-scale hydrometeorological data set for the contiguous USA: data set characteristics and assessment of regional variability in hydrologic model performance. *Hydrology and Earth System Sciences*, 19(1):209, 2015. doi: 10.5194/hess-19-209-2015.

[406] WWF. HydroSHEDS, 2018. URL `https://www.worldwildlife.org/pages/hydrosheds`. [Online. Accessed: 2018-12-11].

[407] Kristine L Verdin and James P Verdin. A topological system for delineation and codification of the Earth's river basins. *Journal of Hydrology*, 218(1–2):1–12, 1999. doi: 10.1016/S0022-1694(99)00011-6.

[408] GRDC. Global Runoff Data Centre, 2018. URL `https://www.bafg.de/GRDC/EN/Home/homepage_node.html`. [Online. Accessed: 2018-12-02].

[409] JL Stein. An enhanced Pfafstetter catchment reference system. *Water Resources Research*, 54(12):9951–9963, 2018. doi: 10.1029/2018WR023218.

[410] L Zhang, GQ Wang, BX Dai, and TJ Li. Classification and codification methods of stream network in a river basin, a review. *Environmental Informatics Archives*, 5:364–372, 2007.

[411] B Lehner. Hydrobasins: Global watershed boundaries and sub-basin delineations derived from hydrosheds data at 15 second resolution—technical documentation version 1. c, 2014. URL `http://hydrosheds.org/images/inpages/HydroBASINS_TechDoc_v1c.pdf`. [Online. Accessed: 2020-09-11].

[412] Konstantinos M. Andreadis, Guy J.-P. Schumann, and Tamlin Pavelsky. A simple global river bankfull width and depth database. *Water Resources Research*, 49(10):7164–7168, 2013. doi: 10.1002/wrcr.20440.

[413] Huan Wu, John S Kimball, Hongyi Li, Maoyi Huang, L Ruby Leung, and Robert F Adler. A new global river network database for macroscale hydrologic modeling. *Water Resources Research*, 48(9), 2012. doi: 10.1029/2012WR012313.

[414] Hylke E Beck, Ad De Roo, and Albert IJM van Dijk. Global maps of streamflow characteristics based on observations from several thousand catchments. *Journal of Hydrometeorology*, 16(4):1478–1501, 2015.

[415] Yongqiang Zhang, Francis HS Chiew, Ming Li, and David Post. Predicting runoff signatures using regression and hydrological modeling approaches. *Water Resources Research*, 54(10):7859–7878, 2018.

[416] Gerald T McCarthy. The unit hydrograph and flood routing. In *proceedings of Conference of North Atlantic Division, US Army Corps of Engineers, 1938*, pages 608–609, 1938.

[417] J A Cunge. On the subject of a flood propagation computation method. *Journal of Hydraulic Research*, 7(2):205–230, 1969.

[418] Cédric H David, Zong-Liang Yang, and Seungbum Hong. Regional-scale river flow modeling using off-the-shelf runoff products, thousands of mapped rivers and hundreds of stream flow gauges. *Environmental Modelling & Software*, 42:116–132, 2013.

[419] Peirong Lin, Larry J Hopper Jr, Zong-Liang Yang, Mark Lenz, and Jon W Zeitler. Insights into hydrometeorological factors constraining flood prediction skill during the May and October 2015 Texas Hill Country flood events. *Journal of Hydrometeorology*, 19(8):1339–1361, 2018.

[420] Peirong Lin, Mohammad Adnan Rajib, Zong-Liang Yang, Marcelo Somos-Valenzuela, Venkatesh Merwade, David R Maidment, Yan Wang, and Li Chen. Spatiotemporal evaluation of simulated evapotranspiration and streamflow over Texas using the WRF-Hydro-RAPID modeling framework. *JAWRA Journal of the American Water Resources Association*, 54(1):40–54, 2018.

[421] Ahmad A Tavakoly, Alan D Snow, Cédric H David, Michael L Follum, David R Maidment, and Zong-Liang Yang. Continental-scale river flow modeling of the Mississippi River basin using high-resolution NHDPlus dataset. *JAWRA Journal of the American Water Resources Association*, 53(2):258–279, 2017. doi: 10.1111/1752-1688.12456.

[422] Dai Yamazaki, Gustavo AM de Almeida, and Paul D Bates. Improving computational efficiency in global river models by implementing the local inertial flow equation and a vector-based river network map. *Water Resources Research*, 49(11):7221–7235, 2013.

[423] Robin E Bell, Alison F Banwell, Luke D Trusel, and Jonathan Kingslake. Antarctic surface hydrology and impacts on ice-sheet mass balance. *Nature Climate Change*, 8 (12):1044–1052, 2018. doi: 10.1038/s41558-018-0326-3.

[424] DL Fread. Flow routing. *Handbook of hydrology*, pages 101–1036, 1993.

[425] Antonis D Koussis. Theoretical estimation of flood routing parameters. *Journal of the Hydraulics Division*, 104(1):109–115, 1978.

[426] M Kleitz. Note sur la théorie du mouvement non permanent des liquids et sur son application à la propagation des crues des rivières. *Ann. Ponts Chaussées*, 14(5):133–196, 1877.

[427] James A Seddon. River hydraulics. In *Proceedings of the American Society of Civil Engineers*, volume 25, pages 619–669. ASCE, 1900.

[428] David Knighton. *Fluvial Forms and Processes: A New Perspective*. Routledge, 2014.

[429] Harald Kling, Martin Fuchs, and Maria Paulin. Runoff conditions in the upper Danube basin under an ensemble of climate change scenarios. *Journal of Hydrology*, 424:264–277, 2012. doi: 10.1016/j.jhydrol.2012.01.011.

[430] Hoshin V Gupta, Harald Kling, Koray K Yilmaz, and Guillermo F Martinez. Decomposition of the mean squared error and NSE performance criteria: Implications for improving hydrological modelling. *Journal of hydrology*, 377(1-2):80–91, 2009. doi: 10.1016/j.jhydrol.2009.08.003.

[431] Hylke E Beck, Albert IJM van Dijk, Ad de Roo, Emanuel Dutra, Gabriel Fink, Rene Orth, and Jaap Schellekens. Global evaluation of runoff from ten state-of-the-art hydrological models. *Hydrology and Earth System Sciences*, 21(6):2881–2903, 2017. doi: 10.5194/hess-21-2881-2017.

[432] Ed Houghton. *Climate Change 1995: The Science of Climate Change: Contribution of Working Group I to the Second Assessment Report of the Intergovernmental Panel on Climate Change*, volume 2. Cambridge University Press, 1996.

[433] Isaac M Held and Brian J Soden. Robust responses of the hydrological cycle to global warming. *Journal of Climate*, 19(21):5686–5699, 2006. doi: 10.1175/JCLI3990.1.

[434] David WJ Thompson, John M Wallace, and Gabriele C Hegerl. Annular modes in the extratropical circulation. part ii: Trends. *Journal of climate*, 13(5):1018–1036, 2000. doi: 10.1175/1520-0442(2000)013<1018:AMITEC>2.0.CO;2.

[435] David W. J. Thompson and Susan Solomon. Interpretation of recent southern hemisphere climate change. *Science*, 296(5569):895–899, 2002. doi: 10.1126/science.1069270.

[436] Benjamin S. Giese, S. Cristina Urizar, and Neven S. Fučkar. Southern hemisphere origins of the 1976 climate shift. *Geophysical Research Letters*, 29(2):1–1–1–4, 2002. doi: https://doi.org/10.1029/2001GL013268.

[437] Matti Kummu, Hans De Moel, Philip J Ward, and Olli Varis. How close do we live to water? A global analysis of population distance to freshwater bodies. *PLOS ONE*, 6(6): e20578, 2011. doi: 10.1371/journal.pone.0020578.

[438] Daniel Bernoulli. *Hydrodynamica: Sive de Viribus et Motibus Fluidorum Commentarii*. Johannis Reinholdi Dulseckeri, 1738.

[439] Michael John Bradshaw, Arthur J Abbott, and AP Gelsthorpe. *The Earth's Changing Surface*. John Wiley & Sons, 1978.

[440] Stanley Alfred Schumm. *The Fluvial System*. New York, NY (USA) Wiley-Interscience Pub., 1977.

[441] Luna Bergere Leopold. Downstream change of velocity in rivers. *American Journal of Science*, 251(8):606–624, 1953.

[442] A Chézy. Memoire sur la vitesse de l'eau conduit dans une rigole donne. *Dossier*, 847: 363–368, 1775.

[443] Robert Manning, John Purser Griffith, TF Pigot, and Leveson Francis Vernon-Harcourt. *On the flow of water in open channels and pipes*. 1890.

[444] A David Knighton. Variations in at-a-station hydraulic geometry. *American Journal of Science*, 275(2):186–218, 1975. doi: 10.2475/ajs.275.2.186.

[445] JG Speight. Meander spectra of the angabunga river. *Journal of Hydrology*, 3(1):1–15, 1965. doi: 10.1016/0022-1694(65)90063-6.

[446] Robert I Ferguson. Meander irregularity and wavelength estimation. *Journal of Hydrology*, 26(3-4):315–333, 1975. doi: 10.1016/0022-1694(75)90012-8.

[447] RI Ferguson. Disturbed periodic model for river meanders. *Earth Surface Processes*, 1 (4):337–347, 1976. doi: 10.1002/esp.3290010403.

[448] John A. Moody and Brent M. Troutman. Characterization of the spatial variability of channel morphology. *Earth Surface Processes and Landforms*, 27(12):1251–1266, 2002. doi: 10.1002/esp.403.

[449] Edmund D Andrews. *Scour and fill in a stream channel, East Fork River, western Wyoming*, volume 1117. Department of the Interior, Geological Survey, 1979.

[450] Michael Church. Baffin Island sandurs: a study of Arctic fluvial processes. *Survey Canada Bull*, 216:208, 1972.

[451] John B Thornes. *Semi-arid erosional systems: case studies from Spain*. Number 7. Geography Department, London School of Economics and Political Science, 1976.

[452] JB Thornes. Autogeometry of semi-arid channel systems. In *Symposium on Inland Waterways for Navigation, Flood Control and Water Diversions*, volume 2, pages 10–12, 1976.

[453] TP Chang and GH Toebes. A statistical comparison of meander planforms in the Wabash Basin. *Water Resources Research*, 6(2):557–578, 1970. doi: 10.1029/WR006i002p00557.

[454] GH Dury. Abrupt variation in channel width along part of the River Severn, near Shrewsbury, Shropshire, England. *Earth surface processes and landforms*, 9(5):485–492, 1984. doi: 10.1002/esp.3290090509.

[455] Alan D Howard and Allen T Hemberger. Multivariate characterization of meandering. *Geomorphology*, 4(3-4):161–186, 1991. doi: 10.1016/0169-555X(91)90002-R.

[456] Mary Ann Madej. Temporal and spatial variability in thalweg profiles of a gravel-bed river. *Earth Surface Processes and Landforms: The Journal of the British Geomorphological Research Group*, 24(12):1153–1169, 1999. doi: 10.1002/(SICI)1096-9837(199911)24:12%3C1153::AID-ESP41%3E3.0.CO;2-8.

[457] George Keith Batchelor. *The theory of homogeneous turbulence*. Cambridge university press, 1953.

[458] R.L. Gonzalez and G.B. Pasternack. Reenvisioning cross-sectional at-a-station hydraulic geometry as spatially explicit hydraulic topography. *Geomorphology*, 246(nil):394–406, 2015. doi: 10.1016/j.geomorph.2015.06.024. URL `https://doi.org/10.1016/j.geomorph.2015.06.024`.

[459] Dallas D Rhodes. The bfm diagram; graphical representation and interpretation of at-a-station hydraulic geometry. *American Journal of Science*, 277(1):73–96, 1977. doi: 10.2475/ajs.277.1.73.

[460] Nicholas J Clifford. Classics in physical geography revisited: Leopold, LB and Maddock, TM jr 1953: The hydraulic geometry of stream channels and some physiographic implications. USGS Professional Paper 252. *Progress in physical geography*, 20(1):81–87, 1996. doi: 10.1177/030913339602000105.

[461] CR Thorne, Carlos Alonso, Deva Borah, Stephen Darby, Panos Diplas, Pierre Julien, Donald Knight, Jim Pizzuto, Michael Quick, and Andrew Simon. River width adjustment. I: Processes and mechanisms. *Journal of Hydraulic Engineering, ASCE*, 124, 1998.

[462] BC Eaton. Hydraulic geometry: Empirical investigations and theoretical approaches. *Treatise on geomorphology*, 9:313–329, 2013.

[463] Joshua R Wyrick and Gregory B Pasternack. Modeling energy dissipation and hydraulic jump regime responses to channel nonuniformity at river steps. *Journal of Geophysical Research: Earth Surface*, 113(F3), 2008. doi: 10.1029/2007JF000873.

[464] Dallas D Rhodes. World-wide variations in hydraulic geometry exponents of stram channels: An analysis and some observations—Comments. *Journal of Hydrology*, 39(1-2):193–197, 1978. doi: 10.1016/0022-1694(78)90123-3.

[465] Dallas D Rhodes. The bfm diagram for downstream hydraulic geometry. *Geografiska Annaler: Series A, Physical Geography*, 69(1):147–161, 1987. doi: 10.1080/04353676.1987.11880203.

[466] Luna Bergere Leopold and John Preston Miller. *Ephemeral streams: Hydraulic factors and their relation to the drainage net*, volume 282. US Government Printing Office, 1956.

[467] John P Miller. High mountain streams: effects of geology on channel characteristics and bed material. 1958.

[468] Lucien M Brush. *Drainage basins, channels, and flow characteristics of selected streams in central Pennsylvania*, volume 282. US Government Printing Office, 1961.

[469] Robert K Fahnestock. *Morphology and hydrology of a glacial stream—White River, Mount Rainier, Washington*, volume 422. US Government Printing Office, 1963.

[470] Peter Ackers. Experiments on small streams in alluvium. *Journal of the Hydraulics Division*, 90(4):1–37, 1964. doi: 10.1061/JYCEAJ.0001060.

[471] Laurence A Lewis. The adjustment of some hydraulic variables at discharges less than one cfs. *The professional geographer*, 18(4):230–234, 1966. doi: 10.1111/j.0033-0124.1966.00230.x.

[472] John B Stall, Yu-Si Fok, et al. Hydraulic geometry of Illinois streams. 1968.

[473] Patrick J Phillips and John M Harlin. Spatial dependency of hydraulic geometry exponents in a subalpine stream. *Journal of Hydrology*, 71(3-4):277–283, 1984. doi: 10.1016/0022-1694(84)90101-X.

[474] David L Rosgen. A classification of natural rivers. *Catena*, 22(3):169–199, 1994. doi: 10.1016/0341-8162(94)90001-9.

[475] Ronald R Copeland, Dinah N McComas, Colin R Thorne, Philip J Soar, and Meg M Jonas. Hydraulic design of stream restoration projects. Technical report, Engineer Research and Development Center Vicksburg MS Coastal and Hydraulicslab, 2001.

[476] F Douglas Shields Jr, Ronald R Copeland, Peter C Klingeman, Martin W Doyle, and Andrew Simon. Design for stream restoration. *Journal of Hydraulic Engineering*, 129 (8):575–584, 2003. doi: 10.1061/(ASCE)0733-9429(2003)129:8(575).

[477] Michael F Merigliano. Hydraulic geometry and stream channel behavior: A uncertain link 1. *JAWRA Journal of the American Water Resources Association*, 33(6):1327–1336, 1997. doi: 10.1111/j.1752-1688.1997.tb03556.x.

[478] Gregory Brian Pasternack. *2D modeling and ecohydraulic analysis*. University of California at Davis, 2011.

[479] Daniel L Hogan and Michael Church. Hydraulic geometry in small, coastal streams: progress toward quantification of salmonid habitat. *Canadian Journal of Fisheries and Aquatic Sciences*, 46(5):844–852, 1989. doi: 10.1139/f89-106.

[480] John B Thornes. The hydraulic geometry of stream channels in the Xingu-Araguaia headwaters. *The Geographical Journal*, 136(3):376–382, 1970. doi: 10.2307/1795188.

[481] Bruce L. Rhoads. A continuously varying parameter model of downstream hydraulic geometry. *Water Resources Research*, 27(8):1865–1872, 1991. doi: 10.1029/91wr01363. URL https://doi.org/10.1029/91wr01363.

[482] Peter M. Allen, Jeffrey C. Arnold, and Bruce W Byars. Downstream channel geometry for use in planning-level models. *Journal of the American Water Resources Association*, 30(4):663–671, 1994. doi: 10.1111/j.1752-1688.1994.tb03321.x. URL https://doi.org/10.1111/j.1752-1688.1994.tb03321.x.

[483] Frederick J Kolberg and Alan D Howard. Active channel geometry and discharge relations of us piedmont and midwestern streams: The variable exponent model revisited. *Water Resources Research*, 31(9):2353–2365, 1995. doi: 10.1029/95WR01348.

[484] Barbara A Doll, Dani E Wise-Frederick, Carolyn M Buckner, Shawn D Wilkerson, William A Harman, Rachel E Smith, and Jean Spooner. Hydraulic geometry relationships for urban streams throughout the Piedmont of North Carolina 1. *JAWRA Journal of the American Water Resources Association*, 38(3):641–651, 2002. doi: 10.1111/j.1752-1688.2002.tb00986.x.

[485] Ellen E Wohl and Andrew Wilcox. Channel geometry of mountain streams in New Zealand. *Journal of hydrology*, 300(1-4):252–266, 2005. doi: 10.1016/j.jhydrol.2004.06.006.

[486] Ronald C De Rose, Michael J Stewardson, and Ciaran Harman. Downstream hydraulic geometry of rivers in Victoria, Australia. *Geomorphology*, 99(1-4):302–316, 2008. doi: 10.1016/j.geomorph.2007.11.008.

[487] Sylvain Biancamaria, Kostas M Andreadis, Michael Durand, Elizabeth A Clark, Ernesto Rodriguez, Nelly M Mognard, Doug E Alsdorf, Dennis P Lettenmaier, and Yannick Oudin. Preliminary characterization of SWOT hydrology error budget and global capabilities. *IEEE Journal of Selected Topics in Applied Earth Observations and Remote Sensing*, 3(1):6–19, 2009. doi: 10.1109/JSTARS.2009.2034614.

[488] Núria Catalán, Rafael Marcé, Dolly N Kothawala, and Lars J Tranvik. Organic carbon decomposition rates controlled by water retention time across inland waters. *Nature Geoscience*, 9(7):501–504, 2016. doi: 10.1038/ngeo2720.

[489] J Brasington, BT Rumsby, and RA McVey. Monitoring and modelling morphological change in a braided gravel-bed river using high resolution GPS-based survey. *Earth Surface Processes and Landforms: The Journal of the British Geomorphological Research Group*, 25(9):973–990, 2000. doi: 10.1002/1096-9837(200008)25:9%3C973::AID-ESP111%3E3.0.CO;2-Y.

[490] Robert C Hilldale and David Raff. Assessing the ability of airborne LiDAR to map river bathymetry. *Earth Surface Processes and Landforms*, 33(5):773–783, 2008. doi: 10.1002/esp.1575.

[491] RD Williams, James Brasington, Damia Vericat, and DM Hicks. Hyperscale terrain modelling of braided rivers: fusing mobile terrestrial laser scanning and optical bathymetric mapping. *Earth Surface Processes and Landforms*, 39(2):167–183, 2014. doi: 10.1002/esp.3437.

[492] MS Horritt and PD Bates. Evaluation of 1D and 2D numerical models for predicting river flood inundation. *Journal of hydrology*, 268(1-4):87–99, 2002. doi: 10.1016/S0022-1694(02)00121-X.

[493] Ming-liang Zhang and Yong-ming Shen. Three-dimensional simulation of meandering river based on 3-D RNG κ-ϵ turbulence model. *Journal of Hydrodynamics, Ser. B*, 20 (4):448–455, 2008. doi: 10.1016/S1001-6058(08)60079-7.

[494] Sagy Cohen, Albert J Kettner, and James PM Syvitski. Global suspended sediment and water discharge dynamics between 1960 and 2010: Continental trends and intra-basin sensitivity. *global and planetary change*, 115:44–58, 2014. doi: 10.1016/j.gloplacha.2014.01.011.

[495] K. Schulze, M. Hunger, and P. Döll. Simulating river flow velocity on global scale. *Advances in Geosciences*, 5(nil):133–136, 2005. doi: 10.5194/adgeo-5-133-2005.

[496] Ruh-Ming Li, Michael A Stevens, and Daryl B Simons. Morphology of cobble streams in small watersheds. *Journal of the Hydraulics Division*, 102(8):1101–1117, 1976. doi: 10.1061/JYCEAJ.0004596.

[497] Marshall Nixon, LACEY, and INGLIS. A study of the bank-full discharges of rivers in England and Wales. *Proceedings of the Institution of Civil Engineers*, 12(2):157–174, 1959. doi: 10.1680/iicep.1959.12123.

[498] DB. Simons and ML Albertson. Uniform water conveyance channels in alluvial material. 1963.

[499] William W Emmett. The channels and waters of the upper salmon river area, idaho. Technical report, 1975.

[500] FG Charlton, PM Brown, and RW Benson. *The hydraulic geometry of some gravel rivers in Britain*. Hydraulics Research Station (Great Britain), 1978.

[501] DI Bray. Regime equations for gravel-bed rivers. *Gravel-bed rivers*, pages 517–542, 1982.

[502] Edmund D Andrews. Bed-material entrainment and hydraulic geometry of gravel-bed rivers in colorado. *Geological Society of America Bulletin*, 95(3):371–378, 1984. doi: 10.1130/0016-7606(1984)95%3C371:BEAHGO%3E2.0.CO;2.

[503] Richard D Hey and Colin R Thorne. Stable channels with mobile gravel beds. *Journal of Hydraulic engineering*, 112(8):671–689, 1986. doi: 10.1061/(ASCE)0733-9429(1986)112:8(671).

[504] Gary Parker. Hydraulic geometry of active gravel rivers. *Journal of the Hydraulics Division*, 105(9):1185–1201, 1979. doi: 10.1061/JYCEAJ.0005275.

[505] Howard H Chang. Geometry of gravel streams. *Journal of the Hydraulics Division*, 106 (9):1443–1456, 1980. doi: 10.1061/JYCEAJ.0005504.

[506] Gerald Lacey. Stable channels in alluvium. In *Minutes of the Proceedings of the Institution of Civil Engineers*, volume 229, pages 259–292. Thomas Telford-ICE Virtual Library, 1930. doi: 10.1680/imotp.1930.15592.

[507] Khalid Mahmood, Riaz N Tarar, and Tariq Masood. *Hydraulic geometry relations for ACOP channels*. Environmental & Water Resources Program, Civil, Mechanical and Environmental . . . , 1979.

[508] Larry Allen Rundquist. *A classification and analysis of natural rivers*. PhD thesis, Colorado State University, 1975.

[509] Walter B Langbein. Geometry of river channels. *Journal of the Hydraulics Division*, 90 (2):301–312, 1964. doi: 10.1061/JYCEAJ.0001019.

[510] Laurence A Lewis. Some fluvial geomorphic characteristics of the Manati Basin, Puerto Rico. *Annals of the Association of American Geographers*, 59(2):280–293, 1969. doi: 10.1111/j.1467-8306.1969.tb00671.x.

[511] David N Wilcock. Investigation into the relations between bedload transport and channel shape. *Geological Society of America Bulletin*, 82(8):2159–2176, 1971. doi: 10.1130/0016-7606(1971)82[2159:IITRBB]2.0.CO;2.

[512] AM Harvey. Some aspects of the relations between channel characteristics and riffle spacing in meandering streams. *American Journal of Science*, 275(4):470–478, 1975. doi: 10.2475/ajs.275.4.470.

[513] Garnett P Williams. *Hydraulic geometry of river cross-sections: Theory of minimum variance*, volume 1029. Department of the Interior, Geological Survey, 1978.

[514] Peter A Raymond, Jens Hartmann, Ronny Lauerwald, Sebastian Sobek, Cory McDonald, Mark Hoover, David Butman, Robert Striegl, Emilio Mayorga, Christoph Humborg, et al. Global carbon dioxide emissions from inland waters. *Nature*, 503(7476):355, 2013. doi: 10.1038/nature12760.

[515] Peter A Raymond, Christopher J Zappa, David Butman, Thomas L Bott, Jody Potter, Patrick Mulholland, Andrew E Laursen, William H McDowell, and Denis Newbold. Scaling the gas transfer velocity and hydraulic geometry in streams and small rivers. *Limnology and Oceanography: Fluids and Environments*, 2(1):41–53, 2012. doi: 10.1215/21573689-1597669.

[516] M Gordon Wolman and Lucien M Brush. *Factors controlling the size and shape of stream channels in coarse noncohesive sands*. US Government Printing Office, 1961.

[517] Jiongxin Xu. Comparison of hydraulic geometry between sand-and gravel-bed rivers in relation to channel pattern discrimination. *Earth Surface Processes and Landforms: The Journal of the British Geomorphological Research Group*, 29(5):645–657, 2004. doi: 10.1002/esp.1059.

[518] Laurence C Smith, Bryan L Isacks, Arthur L Bloom, and A Brad Murray. Estimation of discharge from three braided rivers using synthetic aperture radar satellite imagery: Potential application to ungaged basins. *Water Resources Research*, 32(7):2021–2034, 1996. doi: 10.1029/96WR00752.

[519] Petra Döll, Frank Kaspar, and Bernhard Lehner. A global hydrological model for deriving water availability indicators: model tuning and validation. *Journal of Hydrology*, 270(1-2):105–134, 2003. doi: 10.1016/S0022-1694(02)00283-4.

[520] Gary Parker, Peter R Wilcock, Chris Paola, William E Dietrich, and John Pitlick. Physical basis for quasi-universal relations describing bankfull hydraulic geometry of single-thread gravel bed rivers. *Journal of Geophysical Research: Earth Surface*, 112(F4), 2007. doi: 10.1029/2006JF000549.

[521] Tyler V King and Bethany T Neilson. Quantifying reach-average effects of hyporheic exchange on Arctic River temperatures in an area of continuous permafrost. *Water Resources Research*, 2019. doi: 10.1029/2018WR023463.

[522] ES Lindley. Regime channels. In *Proceedings of Punjab Engineering Congress*, volume 7, pages 63–74, 1919.

[523] EW Lane. Stable channels in erodible materials. *Soc. Civil Eng. Trans*, (102):123–194, 1937. doi: 10.1061/TACEAT.0004841.

[524] Emory W Lane. Design of stable channels. *Transactions of the American society of Civil Engineers*, 120(1):1234–1260, 1955. doi: 10.1061/TACEAT.0007188.

[525] Ruh-Ming Li. *Mathematical modeling of response from small watershed*. PhD thesis, Colorado State University, 1974.

[526] Stanley A Schumm. Evolution and response of the fluvial system, sedimentologic implications. 1981. doi: 10.2110/pec.81.31.0019.

[527] Frank Engelund and Eggert Hansen. A monograph on sediment transport in alluvial streams. *Technical University of Denmark 0stervoldgade 10, Copenhagen K.*, 1967.

[528] Terence R Smith. A derivation of the hydraulic geometry of steady-state channels from conservation principles and sediment transport laws. *The Journal of Geology*, 82(1): 98–104, 1974. doi: 10.1086/627939.

[529] William Rodney White, Roger Bettess, and Enio Paris. Analytical approach to river regime. *Journal of the Hydraulics Division*, 108(10):1179–1193, 1982. doi: 10.1061/JYCEAJ.0005914.

[530] TR Davies and AJ Sutherland. Resistance to flow past deformable boundaries. *Earth Surface Processes*, 5(2):175–179, 1980. doi: 10.1002/esp.3760050207.

[531] Timothy RH Davies and Alex J Sutherland. Extremal hypotheses for river behavior. *Water Resources Research*, 19(1):141–148, 1983. doi: 10.1029/WR019i001p00141.

[532] He Qing Huang and Gerald C Nanson. Hydraulic geometry and maximum flow efficiency as products of the principle of least action. *Earth Surface Processes and Landforms: The Journal of the British Geomorphological Research Group*, 25(1):1–16, 2000. doi: 10.1002/(SICI)1096-9837(200001)25:1%3C1::AID-ESP68%3E3.0.CO;2-2.

[533] GR Dou. Hydraulic geometry of plain alluvial rivers and tidal river mouth. *J. Hydraul. Eng*, 2:1–13, 1964.

[534] M Ramette. *A theoretical approach on fluvial processes*. Electricité de France, Direction des Etudes et Recherches, 1980.

[535] Yafei Jia. Minimum froude number and the equilibrium of alluvial sand rivers. *Earth Surface Processes and Landforms*, 15(3):199–209, 1990. doi: 10.1002/esp.3290150303.

[536] Chih Ted Yang. Unit stream power and sediment transport. In *J. Hydr. Div., ASCE*. Citeseer, 1972. doi: 10.1061/JYCEAJ.0003439.

[537] CT Yang. Energy dissipation rate approach in river mechanics. *Sediment Transport*, 1987.

[538] Chih Ted Yang and Charles CS Song. Theory of minimum energy and energy dissipation rate. *Encyclopedia of fluid mechanics*, 1:353–399, 1986. doi: 10.1061/JYCEAJ.0005865.

[539] DIH Barr, JF Riddell, CCS Song, MK Alam, MA Gill, R Manning, A Nishat, CT Yang, and DO Froude. A contribution to regime theory relating principally to channel geometry. *Proceedings of the Institution of Civil Engineers*, 71(3):955–969, 1981. doi: 10.1680/iicep.1981.1834.

[540] Howard H Chang. Geometry of rivers in regime. *Journal of the Hydraulics Division*, 105(6):691–706, 1979. doi: 10.1061/JYCEAJ.0005225.

[541] Howard H Chang. Minimum stream power and river channel patterns. *Journal of Hydrology*, 41(3-4):303–327, 1979. doi: 10.1016/0022-1694(79)90068-4.

[542] Arthur Brebner, Kenneth Charles Wilson, MB Abbott, G Lacey, DIH Barr, JG Herbertson, and TM Prus-Chacinski. Derivation of the regime equations from relationships for pressurised flow by the use of the principle of minimum energy degradation rate. *Proceedings of the Institution of Civil Engineers*, 37(4):775–782, 1967. doi: 10.1680/iicep.1967.8590.

[543] MS Yalin and AM Ferreira Da Silva. Regime channels in cohesionless alluvium. *Journal of Hydraulic Research*, 37(6):725–742, 1999. doi: 10.1080/00221689909498508.

[544] JF Kennedy, PD Richardson, and SP Sutera. Discussion on geometry of river channels. *J. Hydr. Div.(ASCE)*, 90:332–341, 1964.

[545] AD Knighton. Alternative derivation of the minimum variance hypothesis. *Geological Society of America Bulletin*, 88(3):364–366, 1977. doi: 10.1130/0016-7606(1977)88%3C364:ADOTMV%3E2.0.CO;2.

[546] Jeff Dozier. An examination of the variance minimization tendencies of a supraglacial stream. *Journal of Hydrology*, 31(3-4):359–380, 1976. doi: 10.1016/0022-1694(76)90134-7.

[547] SJ Riley. The role of minimum variance theory in defining the regime characteristics of the lower Namoi-Gwydir drainage basin 1. *JAWRA Journal of the American Water Resources Association*, 14(1):1–11, 1978. doi: 10.1111/j.1752-1688.1978.tb02120.x.

[548] Zhiqiang Deng and Kaiquan Zhang. Morphologic equations based on the principle of maximum entropy.

[549] Mohammad N Cheema, Miguel A Mariño, and Johannes J DeVries. Stable width of an alluvial channel. *Journal of irrigation and drainage engineering*, 123(1):55–61, 1997. doi: 10.1061/(ASCE)0733-9437(1997)123:1(55).

[550] Vijay P Singh, Chih Ted Yang, and ZQ Deng. Downstream hydraulic geometry relations: 1. theoretical development. *Water resources research*, 39(12), 2003. doi: 10.1029/2003WR002484.

[551] Vijay P Singh, Chih Ted Yang, and Zhi-Qiang Deng. Downstream hydraulic geometry relations: 2. calibration and testing. *Water Resources Research*, 39(12), 2003. doi: 10.1029/2003WR002498.

[552] Robert Ellsworth Glover and QL Florey. Stable channel profiles. 1951.

[553] Francis M Henderson. Stability of alluvial channels. *Journal of the Hydraulics Division*, 87(6):109–138, 1961. doi: 10.1061/JYCEAJ.0000653.

[554] JC Bathurst. Flow resistance through the channel network. *Channel Network Hydrology*, pages 69–98, 1993.

[555] James D Brown and Gerard BM Heuvelink. Assessing uncertainty propagation through physically based models of soil water flow and solute transport. *Encyclopedia of Hydrological Sciences*, 2006. doi: 10.1002/0470848944.hsa081.

[556] Gerard BM Heuvelink. *Error Propagation in Environmental Modelling with GIS*. CRC press, 1998. doi: 10.4324/9780203016114.

[557] Rui Yao, Kai Sun, and Feng Qiu. Vectorized efficient computation of padé approximation for semi-analytical simulation of large-scale power systems. *IEEE Transactions on Power Systems*, 34(5):3957–3959, 2019. doi: 10.1109/TPWRS.2019.2917583.

[558] Robert F Adler, Guojun Gu, Matthew Sapiano, Jian-Jian Wang, and George J Huffman. Global precipitation: Means, variations and trends during the satellite era (1979–2014). *Surveys in Geophysics*, 38(4):679–699, 2017. doi: 10.1007/s10712-017-9416-4.

[559] Walter W Immerzeel, Ludovicus PH Van Beek, and Marc FP Bierkens. Climate change will affect the Asian water towers. *Science*, 328(5984):1382–1385, 2010.

[560] Michael D Dettinger and Henry F Diaz. Global characteristics of stream flow seasonality and variability. *Journal of hydrometeorology*, 1(4):289–310, 2000. doi: 10.1175/1525-7541(2000)001%3C0289:GCOSFS%3E2.0.CO;2.

[561] Christoff Andermann, Laurent Longuevergne, Stéphane Bonnet, Alain Crave, Philippe Davy, and Richard Gloaguen. Impact of transient groundwater storage on the discharge of Himalayan rivers. *Nature Geoscience*, 5(2):127–132, 2012. doi: doi.org/10.1038/ngeo1356.

[562] Chih-Ping F Hsu and John M Wallace. The global distribution of the annual and semiannual cycles in precipitation. *Monthly Weather Review*, 104(9):1093–1101, 1976. doi: 10.1175/1520-0493(1976)104%3C1093:TGDOTA%3E2.0.CO;2.

[563] Ali Behrangi, Matthew Christensen, Mark Richardson, Matthew Lebsock, Graeme Stephens, George J Huffman, David Bolvin, Robert F Adler, Alex Gardner, Bjorn Lambrigtsen, et al. Status of high-latitude precipitation estimates from observations and reanalyses. *Journal of Geophysical Research: Atmospheres*, 121(9):4468–4486, 2016. doi: 10.1002/2015JD024546.

[564] Bodo Bookhagen and Douglas W Burbank. Toward a complete Himalayan hydrological budget: Spatiotemporal distribution of snowmelt and rainfall and their impact on river discharge. *Journal of Geophysical Research: Earth Surface*, 115(F3), 2010. doi: 10.1029/2009JF001426.

[565] M Rajeevan, Sulochana Gadgil, and Jyoti Bhate. Active and break spells of the Indian summer monsoon. *Journal of Earth System Science*, 119(3):229–247, 2010. doi: 10.1007/s12040-010-0019-4.

[566] Kyung-Ja Ha, Ki-Young Heo, Sun-Seon Lee, Kyung-Sook Yun, and Jong-Ghap Jhun. Variability in the East Asian monsoon: a review. *Meteorological Applications*, 19(2):200–215, 2012. doi: 10.1002/met.1320.

[567] Jiayu Zhou and KM Lau. Does a monsoon climate exist over South America? *Journal of Climate*, 11(5):1020–1040, 1998. doi: 10.1175/1520-0442(1998)011%3C1020:DAMCEO%3E2.0.CO;2.

[568] Adrian Bejan. The constructal law of organization in nature: tree-shaped flows and body size. *Journal of Experimental Biology*, 208(9):1677–1686, 2005. doi: 10.1242/jeb.01487.

[569] Adrian Bejan and Sylvie Lorente. The constructal law of design and evolution in nature. *Philosophical Transactions of the Royal Society B: Biological Sciences*, 365(1545):1335–1347, 2010. doi: 10.1098/rstb.2009.0302.

[570] Adrian Bejan and Sylvie Lorente. Constructal theory of generation of configuration in nature and engineering. *Journal of Applied Physics*, 100(4):5, 2006. doi: 10.1063/1.2221896.

[571] David M Mark and Barry Smith. A science of topography: From qualitative ontology to digital representations. *Geographic information science and mountain geomorphology*, pages 75–100, 2004.

[572] Luna B. Leopold, M. Gordon Wolman, and John P. Miller. *Fluvial Processes in Geomorphology*. Freeman, San Francisco, 1964.

[573] K.D. Woodyer. Bankfull frequency in rivers. *Journal of Hydrology*, 6(2):114–142, 1968. doi: 10.1016/0022-1694(68)90155-8. URL https://doi.org/10.1016/0022-1694(68)90155-8.

[574] Arthur N Strahler. Part ii. quantitative geomorphology of drainage basins and channel networks. *Handbook of Applied Hydrology. McGraw-Hill, New York*, pages 4–39, 1964.

[575] Markley Gordon Wolman and Luna Bergere Leopold. River flood plains: some observations on their formation. 1957.

[576] T Dunne and LB Leopold. Water in environmental planning. wh freeman and company. *San Francisco, California*, 1978.

[577] Luna Bergere Leopold. *A View of the River*. Harvard University Press, 1994.

[578] Stephen Rice. Which tributaries disrupt downstream fining along gravel-bed rivers? *Geomorphology*, 22(1):39–56, 1998. doi: 10.1016/S0169-555X(97)00052-4.

[579] Peter J Whiting, John F Stamm, Douglas B Moog, and Richard L Orndorff. Sediment-transporting flows in headwater streams. *Geological Society of America Bulletin*, 111(3):450–466, 1999. doi: 10.1130/0016-7606(1999)111%3C0450:STFIHS%3E2.3.CO;2.

[580] Chris J Brummer and David R Montgomery. Downstream coarsening in headwater channels. *Water Resources Research*, 39(10), 2003. doi: 10.1029/2003WR001981.

[581] Robert E Horton. Erosional development of streams and their drainage basins; hydrophysical approach to quantitative morphology. *Geological society of America bulletin*, 56(3):275–370, 1945. doi: 10.1130/0016-7606(1945)56[275:EDOSAT]2.0.CO;2.

[582] Stanley A Schumm. Evolution of drainage systems and slopes in badlands at Perth Amboy, New Jersey. *Geological society of America bulletin*, 67(5):597–646, 1956. doi: 10.1130/0016-7606(1956)67[597:EODSAS]2.0.CO;2.

[583] Arthur N Strahler. Quantitative analysis of watershed geomorphology. *Eos, Transactions American Geophysical Union*, 38(6):913–920, 1957. doi: 10.1029/TR038i006p00913.

[584] JT Hack. Studies of longitudinal profiles in Maryland and Virginia. *US Geological Survey Professional Paper B*, 294:45–92, 1957.

[585] Jean-Jacques Flint. Stream gradient as a function of order, magnitude, and discharge. *Water Resources Research*, 10(5):969–973, 1974. doi: 10.1029/WR010i005p00969.

[586] National River Flow Archive, . URL `https://nrfa.ceh.ac.uk/data/station/info/1001`. Accessed: 2017-08-01.

[587] Wendy A Monk, Paul J Wood, David M Hannah, Douglas A Wilson, Chris A Extence, and Richard P Chadd. Flow variability and macroinvertebrate community response within riverine systems. *River Research and Applications*, 22(5):595–615, 2006. doi: 10.1002/rra.933.

[588] Christel Prudhomme and Helen Davies. Assessing uncertainties in climate change impact analyses on the river flow regimes in the uk. part 1: baseline climate. *Climatic Change*, 93(1-2):177–195, 2009. doi: 10.1007/s10584-008-9464-3.

[589] Christel Prudhomme and Helen Davies. Assessing uncertainties in climate change impact analyses on the river flow regimes in the uk. part 2: future climate. *Climatic Change*, 93(1-2):197–222, 2009. doi: 10.1007/s10584-008-9461-6.

[590] Jeffrey J McDonnell and Ross Woods. On the need for catchment classification. *JHyd*, 299(1):2–3, 2004. doi: 10.1016/j.jhydrol.2004.09.003.

[591] Thorsten Wagener, Murugesu Sivapalan, Peter Troch, and Ross Woods. Catchment classification and hydrologic similarity. *Geography compass*, 1(4):901–931, 2007. doi: 10.1111/j.1749-8198.2007.00039.x.

[592] K Sawicz, T Wagener, Murugesu Sivapalan, Peter A Troch, and G Carrillo. Catchment classification: empirical analysis of hydrologic similarity based on catchment function in the eastern USA. *Hydrology & Earth System Sciences Discussions*, 8(3), 2011. doi: 10.5194/hess-15-2895-2011.

[593] Wouter R Berghuijs, Murugesu Sivapalan, Ross A Woods, and Hubert HG Savenije. Patterns of similarity of seasonal water balances: A window into streamflow variability over a range of time scales. *Water Resources Research*, 50(7):5638–5661, 2014. doi: 10.1002/2014WR015692.

[594] Hal Voepel, Benjamin Ruddell, Rina Schumer, Peter A Troch, Paul D Brooks, Andrew Neal, Matej Durcik, and Murugesu Sivapalan. Quantifying the role of climate and landscape characteristics on hydrologic partitioning and vegetation response. *Water Resources Research*, 47(10), 2011. doi: 10.1029/2010WR009944.

[595] Ellen Wohl. Particle dynamics: the continuum of bedrock to alluvial river segments. *Geomorphology*, 241:192–208, 2015. doi: 10.1016/j.geomorph.2015.04.014.

[596] Richard B Alexander, Elizabeth W Boyer, Richard A Smith, Gregory E Schwarz, and Richard B Moore. The role of headwater streams in downstream water quality 1. *JAWRA Journal of the American Water Resources Association*, 43(1):41–59, 2007. doi: 10.1111/j.1752-1688.2007.00005.x.

[597] Ronald L Shreve. Statistical law of stream numbers. *The Journal of Geology*, 74(1): 17–37, 1966. doi: 10.1086/627137.

[598] Ronald L Shreve. Infinite topologically random channel networks. *The Journal of Geology*, 75(2):178–186, 1967. doi: 10.1086/627245.

[599] Ronald L Shreve. Stream lengths and basin areas in topologically random channel networks. *The Journal of Geology*, 77(4):397–414, 1969. doi: 10.1086/628366.

[600] Vijay K Gupta and ED Waymire. Statistical self-similarity in river networks parameterized by elevation. *Water Resources Research*, 25(3):463–476, 1989. doi: 10.1029/WR025i003p00463.

[601] David G Tarboton, Rafael L Bras, and Ignacio Rodriguez-Iturbe. Scaling and elevation in river networks. *Water Resources Research*, 25(9):2037–2051, 1989. doi: 10.1029/WR025i009p02037.

[602] Arthur N Strahler. Hypsometric (area altitude) analysis of erosional topology. *Geol Soc Am Bull*, 63:1117–1142, 1952. doi: 10.1130/0016-7606(1952)63[1117:HAAOET]2.0.CO;2.

[603] Wikimedia Commons. Sinuosity, 2011. URL `https://en.wikipedia.org/wiki/Sinuosity`. [Online. Accessed: 2019-09-24].

[604] Hubert HG Savenije. *Salinity and tides in alluvial estuaries*. Elsevier, 2006.

[605] Jerry Tagestad, Nicholas D Ward, David Butman, and James Stegen. Small streams dominate US tidal reaches and will be disproportionately impacted by sea-level rise. *Science of the Total Environment*, 753:141944, 2021. doi: 10.1016/j.scitotenv.2020.141944.

Index